THEREPI

A THERAPEUTIC EPICARDIAL RESERVOIR FOR THE TREATMENT OF CARDIAC DISEASE

A THESIS PRESENTED

BY

WILLIAM WHYTE

TO

THE DEPARTMENT OF MECHANICAL AND MANUFACTURING ENGINEERING

IN PARTIAL FULFILMENT OF THE REQUIREMENTS

FOR THE DEGREE OF

DOCTOR OF PHILOSOPHY

2019

TRINITY COLLEGE DUBLIN

Declaration

I declare that this thesis has not been submitted as an exercise for a degree at this or any other university and it is entirely my own work. Furthermore, I agree to deposit this thesis in the University's open access institutional repository or allow the Library to do so on my behalf, subject to Irish Copyright Legislation and Trinity College Library conditions of use and acknowledgement.

William Whyte
September 20th, 2018

Abstract

A Therapeutic Epicardial Reservoir for the Treatment of Cardiac Disease
PhD thesis by
William Whyte

The clinical translation of regenerative therapy for the diseased heart, whether in the form of cells, macromolecules or small molecules, is hampered by several factors: the poor retention and short biological half-life of the therapeutic agent, the adverse side effects from systemic delivery, and difficulties with the administration of multiple doses. Here, we report the development, manufacturing processes and pre-clinical application of a therapeutic epicardial device that enables sustained and repeated administration of small molecules, macromolecules and cells directly to the epicardium via a biomaterial-based reservoir connected to a subcutaneous port.

In a myocardial infarct rodent model, we show that repeated administration of cells over a four-week period using the epicardial reservoir provided functional benefits in ejection fraction, fractional shortening and stroke work, compared to a single injection of cells and to no treatment.

Finally, in pursuit of a multimodal delivery system that that can deliver biological therapy with precise spatial and temporal control, we couple the therapeutic reservoir with a pneumatic soft robotic actuator. Using this approach, we demonstrate controlled drug release by altering the compressive stimulus and the biomaterial/cargo interaction.

This work has important practical and translational implications; preclinical use of the system as a research model may elucidate new insights into regenerative cardiac therapy, highlight the synergistic benefits of a holistic multi-modal approach and ultimately progress experimental therapies towards clinical use and improve patient outcomes.

Summary

The heart does not have sufficient regenerative capacity to adequately repair tissue damage following a heart attack. Instead, despite the best efforts of modern medicine, compensatory pathophysiological remodelling often leads to heart failure. Regenerative therapies in the form of cells, proteins, and small molecules have shown considerable success in the treatment of post-myocardial injury and the prevention of ischemic cardiomyopathy in pre-clinical studies. However, although some of these strategies have demonstrated some success in the clinic, their adoption into medical practice has been hindered by low or unpredictable efficacy when tested in large patient populations. The barriers to effective clinical translation including poor retention in the dynamic environment of the beating heart, a short biological half-life, adverse side effects from systemic delivery and difficulty with administering multiple doses.

Motivated by the need for repeat dosing, while simultaneously protecting the fragile cargo post-administration, we developed a new system called "*Therepi*" (***The**rapeutic **epi**cardial reservoir). In our design, a therapeutic reservoir is placed on the border zone of the infarcted heart and connected to a subcutaneous port or self-sealing rubber septum by an indwelling catheter. This system presents numerous advantages including convenient, repeated therapy administration of bioagents of a range of sizes. As a first step towards proving the *Therepi* concept, we developed a representative pre-clinical rodent animal model. In this model, a macroporous gelatin biomaterial was sutured to the epicardial surface of the heart and connected to a subcutaneous port via an implanted conduit. Importantly, the conduit allows for targeted replenishable delivery, without the need for higher systemic doses, while the biomaterial vehicle promotes retention of the delivered cargo and enhances engraftment and viability of cells. We subsequently demonstrated rapid, targeted delivery of small molecules, proteins and cells directly to the heart using this system. We demonstrated delivery of small molecules using the imaging substrate D-Luciferin, proteins using fluorescently tagged bovine serum albumin and cells using luciferase-expressing mouse mesenchymal stem cells. Importantly, cell replenishment significantly increased the cell number or dose at the target site. Finally, we developed a method to accurately monitor cell viability and cardiac function over time in the same animal following myocardial infarction, enabling the mapping of cell dose to disease progression or attenuation.

Next, we designed, optimised and validated an immune-isolating shell to surround the simplified *Therepi* system. Protection from the host immune response is important, as cell and biomaterial systems can be compromised once implanted in the body, with nonspecific protein adsorption and immune/inflammatory cell infiltration impairing the ability of the biomaterial to receive and house therapeutic replenishments. Moreover, the localisation of cells (or other therapeutic cargo) in a distinct, contained environment would be clinically desirable for controlled therapeutic functionality. In our design, a track etched polycarbonate membrane with a sharply defined 0.4-micron pore size separates the biomaterial and the heart. Following optimisation of the manufacturing process, we demonstrated that this membrane could localise transplanted cells in the reservoir, allow for the bi-directional movement of oxygen and nutrients and the sustained release of paracrine factors over an extended period of time. Furthermore, a degree of immune protection was provided *in vivo*, as demonstrated by the histological absence of a large foreign body response around the gelatin-based biomaterial situated inside the membrane. Furthermore, following reservoir implantation on the rat heart, mesenchymal cells remained viable for four weeks, a vast

improvement over the simplified *Therepi* system. This is significant result as the chosen cell was derived from a xenogeneic mouse, which would normally activate a substantial immune response. Improvements in left ventricular function following cell delivery are attributed to the synthesis and secretion of cellular paracrine factors, rather than cell engraftment and differentiation into heart tissue. In line with this mechanism, the optimised *Therepi* replenishment reservoir permits the sustained delivery of cardiac therapy to the infarcted heart, with a bolus release of intracellular contents including cytokines, chemokines, exosomes and paracrine factors following each refill.

Next, we examined the three-dimensional distribution of therapy following *Therepi* delivery and confirmed the ability of multi-sized cargo to diffuse from *Therepi* into heart tissue, even after fibrous capsule formation. A fibrous capsule, generated by foreign materials could compromise the long-term functionality of *Therepi*. Importantly, we demonstrated, despite the formation of a capsule, which hinders but does not impede diffusion, molecules with a range of molecular weights can be transported through the membrane into the tissue, and in the case of adrenaline elicit a potent biological response. With an established pre-clinical model and a device optimised for pre-clinical testing, we assessed the safety and efficacy of repeated syngeneic mesenchymal cell delivery with the *Therepi* system. Following myocardial infarction, we demonstrated that repeated administration of cells over a 4-week period by using *Therepi* provided functional benefits in ejection fraction, fractional shortening and stroke work, compared to a single injection of cells and to no treatment. Interestingly, the acellular *Therepi* provided a sustained benefit across the 28-day study, potentially due to its mechanical reinforcement of the remodelling ventricle or due to an altered healing response caused by the foreign body response.

Finally, in pursuit of a multi-modal delivery system, that can deliver biological therapy with precise spatial and temporal control, we coupled the biomaterial reservoir with a pneumatic soft robotic actuator. For this system, we chose to use an alginate/acrylamide polymer, commonly known as tough gel as the encapsulated biomaterial due to its superior mechanical properties. Importantly for patient safety, our results show that a drug-loaded tough gel can release multiple doses following compression without material rupture, and unwanted drug leakage. First, we demonstrated modulation of drug release by temporarily altering the interaction between the biomaterial and its cargo with compression, thereby causing release of electrostatically coupled and physically entrapped drug. Next, we demonstrated controlled drug release by altering the magnitude, frequency and duration of the compressive stimulus. Finally, we designed and characterised a miniaturised soft robotic actuator, in the form of a hemispherical reservoir, to hold the biomaterial in a passive state, and compress it when pressurised. Using this system, we demonstrated precise temporal control of drug release from the hydrogel, with triggered pneumatic action of the soft robotic actuator.

To conclude, this work has important practical and translational implications. Preclinical use of the system as a research model may elucidate new insights into regenerative cardiac therapy, including the importance of dose, administration frequency and timing of delivery post myocardial injury. Furthermore, the system could highlight the benefits of a holistic multi-modal approach, with precise spatial and temporal control, for the treatment of cardiac disease.

Acknowledgments

Table of Contents

Table of Figures

1   The Delivery of Cardiac Regenerative Therapies

1.1   Preface

In this chapter I review ischemic heart disease, its associated morbidity and mortality, and current treatment regimens. I then assess the promise of cardiac regenerative therapies with a strong focus on their delivery limitations. The latter part of the review examines the synergistic potential of multimodal therapies (cells, growth factors, small molecules, mechanical). The chapter concludes by establishing the central hypothesis and aims of my thesis in context of the current state of the art.

1.2   Clinical Problem

Ischemic heart disease is characterised by the insufficient supply of oxygen rich blood to the heart [1]. An accumulation of atherosclerotic plaque and subsequent narrowing of the coronary arteries can often precipitate a reduction in supply of oxygenated blood. The narrowing can initially present itself as a tightness or discomfort in the chest (angina pectoris), especially upon physical exertion [2]. Further narrowing or total occlusion of the affected coronary artery creates an ischemic, inflammatory environment in the myocardial tissue, leading to extensive cardiac muscle cell death and partial loss of ventricular function. This damage is defined as an acute myocardial infarction, or more commonly termed a heart attack[1] (Figure 1.1a).

A

B

Acute infarct
Inflammation,cell death

Fibrous Scar Formation
Myocyte elongation
Thinning of the infarct area

Adaptive Modelling
Maintenance of pumping function

Spherical Dilation
Myocyte hypertrophy
Interstitial collagen formation

Pathological Modelling
Reduction of pumping function
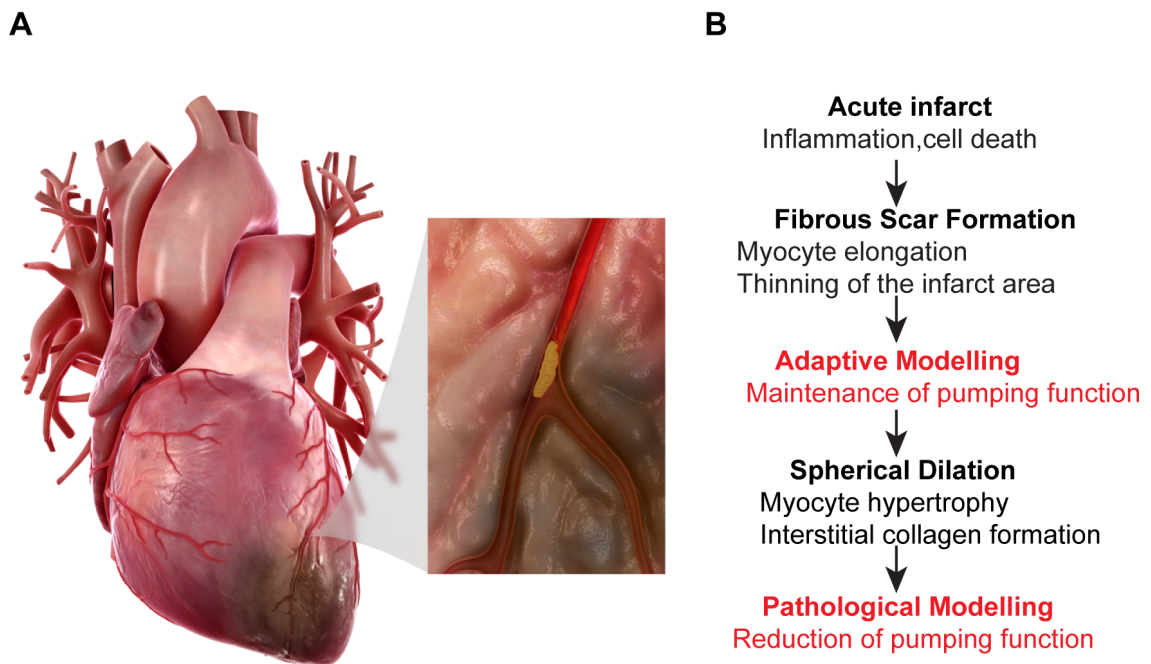
Figure 1.1 Progression to heart failure following a heart attack
(a) Heart attack: Blockage of coronary artery leading to tissue damage. (b) Remodelling process after a heart attack that leads to heart failure.

The regenerative capabilities of the heart are unable to overcome this acute tissue insult. Over time, compensatory pathophysiological remodelling cause fibrous scar formation, thinning of the infarcted tissue and dilation of the affected ventricle [3,4]. Although initially effective in maintaining heart function, these maladaptive processes eventually precipitate to a reduced pumping function and cardiac output. This inability

to pump sufficient blood to satisfy the metabolic needs of the body is termed heart failure, a malignant and progressive disease [3–5] (Figure 1.1b).

Enormous progress has been achieved in the acute treatment of a heart attack, fuelled by advancements in percutaneous revascularisation, accompanying imaging modalities and pharmacotherapy [67]. However, in a paradox of medical success, this improved survival rate has fuelled a heart failure epidemic. Patients are increasingly surviving the initial coronary insult, only to develop heart failure in later life (Figure 1.2[7]). According to the American Heart association, heart disease is the leading cause of death worldwide, claiming 17.3 million deaths annually [8]. In the US alone, 790,000 people have a heart attack each year [8]. Leading on from this, decompensated heart failure is the primary indication for rehospitalisation worldwide with an annual expenditure of \$120 billion and a mean 5-year survival rate of < 50% [9–11]. The disease spectrum of ischemic heart disease, encompassing angina, myocardial infarction and heart failure represents a colossal source of morbidity and mortality worldwide [5]. Consequently, there is an urgent need to develop curative therapies for a vulnerable, ageing, population.
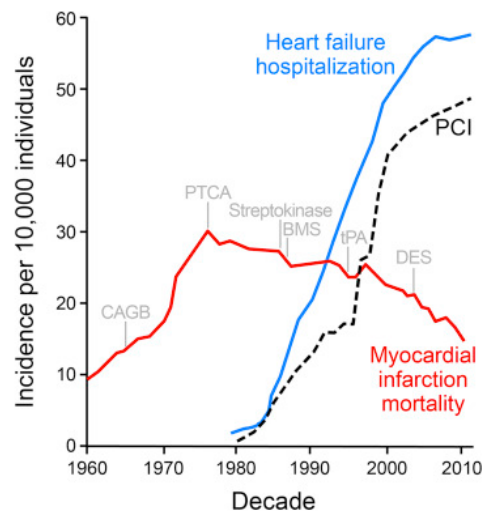
Figure 1.2: The evolution of the heart failure epidemic in context of treatment advancements in acute myocardial infraction. Adapted from Terzic et al 7.

1.3   Current treatment options

Current pharmacological treatments are principally palliative i.e. non regenerative. Modulation of the β-adrenergic receptors (β-adrenergic blockers), renin angiotensin aldosterone system (angiotensin converting enzyme inhibition/aldosterone antagonists), and the natriuretic system (neprilysin inhibitors) reduce clinical symptoms and improve quality of life. Importantly, however, these treatments have been shown to delay disease progression and lower mortality [12,13,22–24,14–21].

Implantable biomedical devices play an integral role as the disease progresses. Cardiac resynchronization therapy, in the form of a pacemaker, is used to monitor and correct irregular heart rate irregularities via tiny pulses of electricity. In patients diagnosed with end stage heart failure, a ventricular assist device can be used to mechanically augment or replace the function of a failing heart. However, the only curative clinical strategy is a heart transplant, and treatment is limited to a lucky few due to scarcity of suitable donor organs.

1.4   Regenerative capacity of the heart

Traditionally, the heart was referred to as a post-mitotic organ, i.e. no cell replication. Histological examination of the prenatal mammalian heart suggests there is an abundance of replicating cells, however these mitotic cells quickly disappear soon after birth, indicating terminal differentiation, and negligible self renewal [25]. This hypothesis is largely supported by clinical observation and epidemiological data, such as the generation of a persistent non-contractile fibrous scar after a heart attack [3,4].

Recent evidence contradicts this post-mitotic view of the heart. Reports that the adult human heart contains mitotic nuclei after both physiological and pathological stressor events, suggests at least low-level cardiomyocyte replication [26,27]. There is, however, much debate on the origin of these new cells and their exact rate of turnover, with reported literature values ranging between <1-10% per year [2628]. Recent evidence suggests that the likely renewal rate is between 1-2% per annum [29]. Nevertheless, we now know the heart has a finite capacity for regeneration. Hence, much research has focused on potential strategies to augment the endogenous cardiac regeneration and repair processes.

1.5   Can stem cells regenerate the heart?

Since 2001, there has been incredible focus and debate on cardiac regeneration mediated through exogenous cell delivery. Initially the field focused mainly on the concept of a regenerative stem or progenitor cell capable of replacing part of the host myocardium [30]. However, lately, this cell-centric "building block" approach has changed, moving away from exogenous cell replacement, towards the current prevailing hypothesis: endogenous cardiac regeneration can be augmented by the release of paracrine factors from transplanted cells [31,32]. Thus far, the field has largely followed two routes of investigation, as a protective therapy following acute myocardial infarction or a restorative therapy in a failing heart.

The next section will detail pivotal pre-clinical research that initially generated momentum in the field. Finally, I will give a brief overview of clinical trial results thus far including the lessons learned and future avenues of exploration.

1.6   Pre-clinical evidence for the regenerative potential of stem cell therapy

In 2001, a seminal paper by Orlic et al originating from the Anversa lab, reported the *de novo* synthesis of myocardium following the injection of Lin−c-kit+ bone marrow cells into the infarcted zone. The study, which showed a 68% regeneration of infarcted heart tissue in a rodent model, challenged the tenet that the heart was a post mitotic organ. Instead, the paper suggested that the heart was highly regenerative, and its regrowth could be driven by a ckit+ cell population, that was readily available in clinic [30].

Numerous studies by independent labs have since failed to replicate these findings. A rigorous assessment by Murray et al, using genetic lineage tracing, concluded that bone marrow cells do not acquire a cardiac phenotype and thus, do not transdifferentiate into cardiac myocytes following an infarct [33], instead adopting a mature haemopoetic state [34]. However, despite conclusive evidence opposing transdifferentiation, some studies have still shown functional benefits [34]. This has led to a new regenerative hypothesis, the release of paracrine factors can lead to endogenous cardiomyocytes proliferation or stimulate the recruitment of endogenous cardiac progenitor cells [32].

In 2003, another highly cited paper was released by the Anversa lab that disputed the perception of the heart as an organ with negligible self-renewal, instead claiming that similar to other organs, the post-mitotic heart contains a small population of stems cells capable of replication in response to physiological and pathological demands. The paper described the discovery of a resident stem cell population in the heart, that similar to a bone marrow stem cell population, had a ckit+ cell surface marker [35]. It was reported that these cardiac progenitor cells could differentiate in to smooth muscle, endothelial and myocyte cells. Finally, these autologous cells, following isolation and expansion, were shown to regenerate 70% of scar tissue in an infarcted rodent heart [35]. These results were replicated for human c-kit+ CSCs, showing substantial generation of labelled cardiomyoctes, endothelial cells and fibroblasts in a mouse model [36].

Similar to the 2001 Orlic paper, controversy has surrounded the proposed mechanism of action of the Lin−c-kit+ stem cells. Two separate research groups were unable to show that c-kit+ CPCs had the ability to differentiate into cardiomyocytes [37][38]. A genetic tracing study conducted by Van Berlo et al confirmed that c-kit+ progenitor cells could produce new cardiac muscle cells, but at very low rate of 0.03%. This study also demonstrated that these cells can differentiate into all three cardiac lineages and give rise to vast amounts of endothelial cells in the heart [39]. In support of their therapeutic potential, regardless of the mechanism of action, Nadal-Ginard and his colleagues showed that c-kit+ CPCs are both necessary and capable of repair and restoration of ventricular function in a diffuse model of cardiomyocyte injury [40].

Similar to ckit+ bone marrow stem cells, positive benefits were attributed to a paracrine effect from the transplanted cells. This paracrine mechanism of action is supported by the extremely poor viability and retention of cells following delivery to the heart muscle. For instance, Hong et al delivered allogeneic cardiac stem cells via the intramyocardial route in a rodent MI model. However, analysis via quantitative PCR revealed almost negligible retention of cells at day 35, with ~1000 transplanted cells detected [41]. To put this number in context, it is estimated that the full integration of ~1 billion mature cardiomyocytes along with supporting cell types would be necessary to replace dead cells and restore full functionality following a heart attack. Despite such poor retention, delivery of CSCs significantly improved left ventricular ejection fraction, and was consistent with positive results demonstrated in other pre-clinical studies following the delivery the same cellular cargo [42–45]. This dissociation between cell number and sustained haemodynamic improvement provides evidence for a paracrine mechanism of action, whereby release of factors (exosomes, miRs, cytokines) modulates the behaviour of nearby cells. Further understanding of the key paracrine factors secreted and molecular mechanisms underpinning this cell population and may lead to ways of augmenting its cardio regenerative potential. Whilst, there is much discussion and controversy regarding the mechanism of action, this has not halted the progression of cardiac progenitor and other stem cell types into clinical trials [46–49].

1.7   Stem cell therapy in clinical trials

The first generation of cardio regenerative stem cells was introduced into clinical practice circa 2002. Lineage-unselected bone marrow mononuclear cells (BMMNCs) was the regenerative cell of choice due to supporting pre-clinical evidence and ease of clinical access [50]. Initial experience with this heterogeneous cell

population were promising, establishing feasibility and safety of the approach [51–53]. Importantly, many of these early small trials reported modest but consistent indicators of functional benefit following a heart attack [54,55], or in congestive heart failure [56]. However, later trials with higher patient numbers such as Time[57], LateTime[58], FOCUS-CCTRN[59], reported no such clinical improvement following the delivery of BMMNCs in the clinical setting post myocardial infarction or in heart failure. Taken on their own, these trials offer conclusive evidence that BMMNCs do not have a beneficial effect in the treatment of acute MI or chronic heart failure. These disappointing results have cast doubt on the field, however the lessons learned have been used to design new trials and to motivate further mechanistic studies.

Close examination of first generation trial protocols revealed considerable variability in procedures for cell isolation, cell incubation time before delivery, delivery vehicle, infusion technique, and cell number [60]. All of these are important variables to consider, and could have a substantial influence on the paracrine secretome of the transplanted cells. Efforts are currently being made to develop standardized operating procedures for cell harvesting, isolation, and expansion and biological assays to anticipate and control for the regenerative potency of the cellular cargo before delivery [60]. Standardized protocols in all these areas will allow a better head to head comparison between trials. In an interesting note, the phase III BAMI trial, involving 3000 patients and the largest trial involving BMMNCs to date, is currently on going. This trial is utilizing the same protocol as the REPAIR-AMI trial, which reported a sustained improvement in LVEF. It is hoped that replicating this successful protocol, and potentially recreating a therapeutic mesenchymal secretome, will lead to a positive clinical improvements [61].

It is important to note that first generation heterogeneous bone marrow populations contained an extremely low percentage of stem cells (0.001-0.01%MSCs). In order to improve the therapeutic effect, efforts are underway to select for cells that display multi-potent traits and eliminate non-regenerative cells [62]. This is typically achieved by selecting for specific cell surface markers. Two of these purified cell populations; human mesenchymal stem cells (hMSC) and endothelial progenitor cells (EPCs) have been assessed in clinical trials for the treatment of cardiac disease. The POSEIDON trial reported a neutral effect on ejection fraction following the administration of autologous and allogeneic bone marrow derived human mesenchymal stem cells [63]. The ACT34-CMI trial reported a reduced incidence of angina following the delivery of a CD34+ endothelial progenitor cell (EPC) population. Interestingly, this was only significant for the lose dose EPC group (1million vs. 5 million), indicating a potential therapeutic window for beneficial effect.

Looking to the future, resident stem cell population in the heart or Cardiac progenitor cells, are currently being tested in the clinical arena. In the phase I trial, SCIPIO, autologous ckit+ cardiac stem cells extracted from the right atrial appendage were expanded and re-delivered via the intracoronary route 4 months after coronary artery bypass graft surgery in MI patients. The trial established safety and feasibility of the approach, while reporting favourable effects on infarct scar dynamics and LV volumes including a large improvement in LVEF at the 12 month time point [64]. Caduceus, a randomized phase I trial, utilised autologous cardiosphere derived cells isolated from an endomyocardial biopsy and reinfused 1.5-3 months post infarct. Again, this approach was shown to be feasible and safe and demonstrated improvements in scar size and

viable myocardium[47]. In addition, the ALLSTAR study is currently active, which will examine the effect of allogeneic cardiosphere cells after acute myocardial infarction[49].

Finally, advances in the regenerative sciences have facilitated the guidance of adult-multipotent stem cells towards a cardiomyogenic fate. Instead of co-administrating growth factors and cells, such as in the ALCADIA trial [48], cells can pre-cultured with a cardiogenic cocktail in the hope of achieving an improved therapeutic effect. Investigators in the C-CURE trial demonstrated that this approach was feasible and clinically safe. Furthermore, the study reports an increase in LVEF of 7%, a decrease in left ventricular end systolic volume and an increase in walking distance during the 6-minute test. All of these results were significant, and substantiated the induction of a phase III trial. This trial (CHART-1[65]) reported significant decreases in end diastolic and systolic volumes at 52 weeks. However, some caution should be used when interpreting these results, as a post-hoc analysis with regards to dosing was used [65]. A follow up trial, CHART-2 is currently being designed.

To conclude, while there has yet to be any conclusive evidence, cell therapy has often demonstrated a modest benefit in some clinical trials. Five meta-analyses and systematic reviews have shown a significant improvement in LVEF ranging from 2-4% following delivery of bone marrow cells [66]. To put this finding into context, established pharmacological treatment regimens such as angiotensin receptor blockers, aldosterone antagonists and β-blockers, reported an LVEF treatment effect of 1.3%, 2%, and 2.9% respectively [66]. However, utmost caution is necessary when interpreting these results. Ejection fraction is a surrogate endpoint and an improvement does not necessarily lead to a reduced mortality rate, or a better quality of life [67]. Moreover, coronary revascularisation and adjuvant pharmacological therapy are established in the clinic to improve clinical outcomes in heart failure [66]. Secondly, while a meta-analysis allows us to overcome the statistical limitations of smaller studies, the grouping of these trials is indeed questionable considering the huge variability in key parameters [66]. Factors that could affect interpretation includes patient enrolment criteria, cell isolation techniques, cell incubation time before injection, choice of delivery vehicle, delivery route and infusion technique, cell number and type of cardiac disease [61]. In summary, although these findings are encouraging, it is far too early to ascertain a positive benefit from stem cell therapy. Major limitations still exist before the promising results seen in pre-clinical tests can become a translational relation. These limitations are likely multifactorial, but include poor cell retention and retention at the injured site, and the method of delivery [5].

1.8   Cell delivery limitations

The issue of cell kinetics, biodistribution and survival is not only limited to cardiac regeneration, but also a critical parameter for the safety and efficacy of all medicinal cell products. Understanding cell fate *in vivo,* and comparing cell dose to efficacy and off target side effects are essential requirements for regulatory approval of any cell product [68]. A study conducted by Schmuck et al demonstrates the extent of cell biodistribution and retention in the body following systemic delivery [69]. In this study, fluorescently labelled human mesenchymal stem cells were infused through the jugular vein of a rodent model, and detected by whole organ 3D cryoimaging, a technique capable of single cell quantification and biodistribution. At 60

minutes post-infusion, 99.7% of detectable cells were distributed in the liver, lungs, and spleen. The remaining 0.3% of detectable cells was found in the heart and other organs (kidney, intestines, testis). The total number of retained cells detected in all organs on day 2 was 0.06% of the original dose, 0.003% of this dose was found in the heart [69]. Delivery of a sufficient number of biologically active cells to a dynamic organ, without causing off target side effects in areas such as the liver or lungs, is a major issue facing the field. In addition, maintaining cell survival following delivery to the organ is a further significant challenge.

Even with direct delivery to the heart muscle, the numbers reported for cell retention and survival are exceedingly low, with <10% of injected cells surviving after 24 hours, and negligible cells remaining after 7 days [70,71]. These bleak statistics sufficiently illustrate one of the major hurdles facing cell therapy. To become a translational reality, a method to deliver and retain cells in the heart tissue, and exert therapeutic effects for sustained periods is necessary. Once this is possible, we can then determine the interplay between cell type, cell dose and remodelling of the injured tissue post MI. Low retention and survival of cells in the heart tissue is likely to be a major reason behind the failure of cell therapies for ischemic cardiomyopathy to demonstrate consistent and clinically significant efficacy to date [72–76]. Numerous reasons have been proposed for this poor retention and survival, including exposure of the living cells to hypoxia and inflammation, mechanical disruption from the incessant beating heart, washout of cells into the systemic blood flow, leakage of the cell suspension at the injection site, and anoikis [5,77–79].

Physiological saline is the current clinical gold standard vehicle for cell delivery to the heart. This vehicle, while simple, and safe, offers little protection to its precious cargo before, during and after delivery. Furthermore, saline lacks the necessary physiochemical properties to locally delivery and retain cells at the pathological site, and provides little biological and mechanical cues for anchorage dependent cells [5].

1.9   Increased cell retention with biomaterial delivery vehicles

Bioengineered materials have the potential to significantly improve retention and survival of cells following transplantation and provide the appropriate mechanical and biological cues to aid cardiac regeneration [80–82]. These materials can act as a surrogate ECM for its cellular payload, thus improving physical protection and enhancing viability at the diseased site. These materials can also provide shelter from insults such as hypoxia and inflammation and reduce cell death resulting from anoikis of anchorage dependent cells [5]. Finally, these cell loaded materials, which are in close contact to the target diseased tissue can locally release therapeutic paracrine factors in a sustained manner. Extensive pre-clinical work by independent laboratories have shown that biomaterial delivery vehicles significantly enhance cell retention and survival in the heart [83,84,93,94,85–92]. These results have been achieved using two main delivery formulations (1) cell encapsulated injectable hydrogels that gelate following delivery into the heart wall or (2) cell-loaded scaffolds that are attached to the outer epicardial surface of the heart wall during surgery [5]. Both of these delivery approaches will be discussed below.

1.9.1   Injectable Hydrogels

Various groups have explored the cell retentive properties and clinical benefits of injectable hydrogels. While it is difficult to make comparisons, due to differences in cell type, animal model, biomaterial and cell

monitoring systems, it is clear that injectable materials increase retention in comparison to saline, and this effect can increase dramatically over time [5]. For instance, Liu et al examined the retention and survival of adipose derived stem cells in a chitosan/β-glycerophosphate/hydroxy-ethyl cellulose delivery vehicle. At 24 hours post delivery the material system showed a 1.5 fold increase in cell number in comparison to a saline control, this increased to an impressive 8 fold at day 28 [95].

1.9.2 Cell seeded scaffold

Epicardial patches offer a promising way to increase retention and consequently improve efficacy of the cellular transplant. A preformed porous scaffold loaded with cells and/or signalling molecules before surgical implantation has been the bedrock of the tissue engineering approach, especially in the orthopaedic field [96,97]. For the purposes of cardiac repair, Collagen has been successfully used as a scaffold for human mesenchymal stem cells[98] and human embryonic cells directed down the mesenchymal lineage [99]. In another example, Leor et al seeding a porous alginate scaffold with foetal cardiac cells before attachment to the infarcted rodent heart. In this study, the scaffolds demonstrated potent neovascularisation and attenuated left ventricular dilation [100].

In a slightly different approach, contractile or engineered heart tissue developed from cell seeded scaffolds show vast potential for cardiac repair. A prominent recent study developed a fibrin based, living cardiac muscle patch composed of cardiomyocytes, smooth muscle and endothelial cells [101]. 28 days post implantation, the strips exhibited robust cardiomyocoyte survival, proliferation, and vascularisation. Furthermore, they demonstrated electromechanical coupling to native heart tissue (in a few cases) and a large functional improvement in ejection fraction compared to before implantation [101].

1.10 Delivery routes

Delivery of a sufficient number of biologically active cells to the dynamic heart, without causing off target side effects in organs such as the lungs and liver, is a major issue facing the field [5]. The intended target is usually the perivascular space or border zone surrounding the site of damage. This can be achieved by systemic delivery via the bloodstream, localised delivery to the coronary circulation or by direct injection into the heart tissue [102].

Targeted or localised delivery confers the advantages of greater control, decreased variability of clinical response, lower necessary therapeutic doses and offer unique opportunities to use biological agents with a short half-life or that are biologically incompatible with the GI tract and blood stream such as cells and growth factors[103–105] (Figure 1.3).
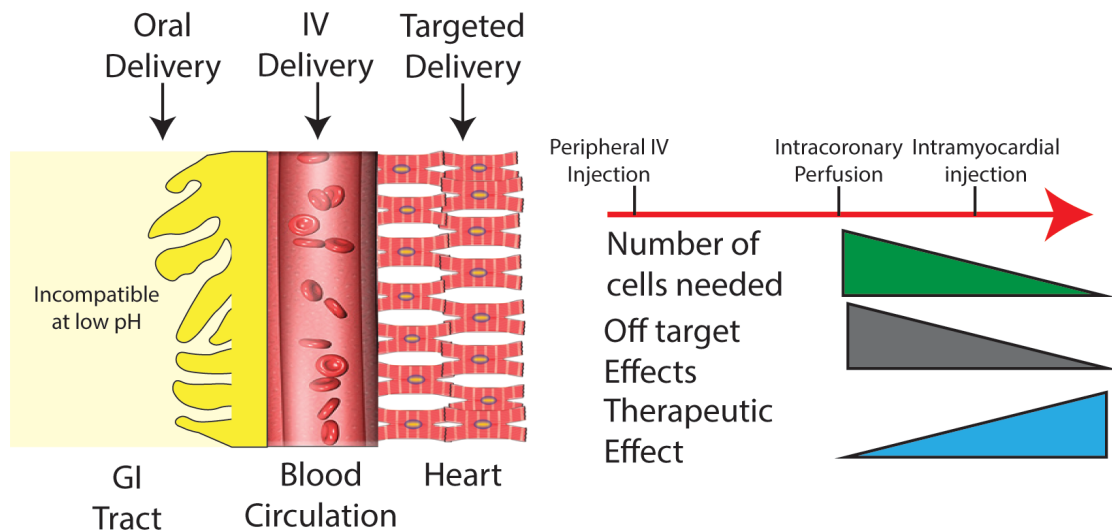
Figure 1.3: Differences in cell delivery by oral, IV or targeted delivery modalities
Targeted delivery (reduction in the number of transport steps) decreases the amount of cells necessary to achieve a therapeutic effect and lowers off-target side effects. Adapted from Rolfes et al[106]

Targeted delivery is usually achieved via percutaneous catheter, however a traditional needle and syringe can be used for direct intramyocardial injection in the case of open-heart surgery [107]. Percutaneous catheters have encountered much innovation over the last 20 years. They are generally composed of thin, flexible, hollow tubing surrounded by a guide wire, which enables manoeuvrability in the vasculature, and a distal tip for administration or injection of the therapy (usually in a saline vehicle). This image guided delivery technique is suitable for diverse patient populations and can facilitate targeted delivery of cells to multiple locations in the heart tissue. Using this approach, cells can be delivered in a targeted manner by infusion through the coronary arteries or coronary veins. Alternatively, a direct intramyocardial injection can be implemented using a transendocardial, or transvenous approach [5,108].

The following section will detail drug and cell delivery methods to the heart. It initially explores current methods for cell delivery in the clinic and finally discusses potential future methods of delivery.

1.10.1 Peripheral Intravenous Delivery

Oral formulations are the most common and patient acceptable method of conventional drug delivery (e.g. tablet, liquid solution or suspension, powder, paste) [103]. However this delivery route is not compatible with cell delivery due to the harsh local conditions of the GI tract (mechanical disruption, low pH, enzymatic breakdown). Even if these conditions were not detrimental to living cells, there is likely to be negligible absorption of such a large cargo through the gastrointestinal mucosa and into the blood stream.

Instead, the intravenous route (IV) is utilised for the systemic delivery of cell therapy. This route is normally accessed via a vein in the hand or arm using a peripheral venous catheter [103,109] (Figure 1.4A). IV administration, while more invasive and less acceptable to the patient, has many delivery advantages over the oral route. Namely, the route bypasses absorption through the gastric mucosa and avoids first pass metabolism by the liver [103]. For this reason, the route is normally chosen for drugs that have poor absorption or

bioavailability when administered orally, potentially making it suitable for cellular cargo [103]. However, IV administration leads to systemic circulation of the cellular cargo both to the desired target site causing therapeutic effects but also to off target sites causing toxic effects [103]. These off-target effects can be enhanced due to entrapment of cells in the microcirculation of organs such as the liver, lungs, and lymphoid tissue [70,71]. Modifications can be applied to the cells or to the intended site of action to improve honing of the therapeutic cargo. For example, in the CELLWAVE study, low energy extracorporeal shock waves were applied to the heart to improve homing of exogenous BM-MSCs and increase expression of growth factors such as SDF-1 and VEGF [110].

1.10.2 Intracoronary Delivery

Coronary Artery infusion: Infusion of stem cells via the coronary artery has been the most consistently used method of delivery in clinical trials thus far [111]. Similar to coronary angioplasty, a guidewire and balloon are positioned in the targeted coronary artery. Inflation of the angioplasty balloon halts blood flow, while the stem cell infusate is delivered at a high pressure into the microvasculature of the infarcted area (Figure 1.4b). The delivery route has a number of advantages to aid clinical adoption (1) previous experience with the safe deployment of devices in the coronary circulation (2) the availability of commercially developed catheter systems for off label use and (3) the potential to achieve a consistent biodistribution in a large portion of the heart from a single infusion, by exploiting the perfusing circulation of coronary vasculature [5]. However extravasation of the transplanted cells into the myocardium is necessary for targeted delivery. This can be a major limiting factor with reported retention rates of 2.6% 1 hour post-delivery [71,108].

Retrograde infusion via the coronary veins: Delivery of stem cells via the coronary venous system has been achieved in pre-clinical and early stage clinical models, demonstrating the safety and feasibility of the approach [112]. In brief, a balloon catheter is advanced via the coronary sinus into the great cardiac vein. Following correct positioning, inflation of the balloon interrupts blood flow in the coronary venous system, and the cell suspension can then delivered in a retrograde fashion under a high pressure. Similar to the coronary arteries this route relies on extravasation of the delivered cargo, representing a major limitation. Further drawbacks with this approach include the potential for blockage by large clumps of cells or a viscous solution. Furthermore, the coronary veins have a variable tortuous anatomy, which can hinder access or make it impossible in some cases. For this reason, the delivery route is normally reserved for cases where there is severe stenosis of the coronary arteries or the [5,108].

1.10.3 Intramyocardial Delivery

Transepicardial Delivery: Transepicardial delivery of cells into the damaged myocardium muscle is typically achieved by the injection of cells through a 27 gauge straight or curved needle, in the setting of open-heart surgery (Figure 1.4c) [5,108]. Due to direct access and easy visualisation of the epicardium surface, transepicardial delivery is considered the most reliable method of delivery, with high rates of cell retention [112]. Hong et al compared the retention and survival of allogeneic cardiac stem cells following intramyocardial or intracoronary delivery [41]. While the results illustrate the poor survival of both delivery routes (each method showing negligible retention at day 35), the study did demonstrate a two-fold increase in retention for the intramyocardial delivery at earlier time points.

However, this approach is more appropriate as an adjunct therapy when surgery is necessary, due to the invasiveness of the method. Innovation in the surgical approach is needed, and much could be learned from other interventional fields such as the replacement of an aortic valve using a transapical delivery approach [5]. In the future, device innovation could enable transepicardial delivery in a less invasive manner, potentially using a lateral mini thoracotomy surgery [5]. Advancement in the area of soft robotic surgical systems holds great promise. For example, the Cell-Fix catheter system consisting of a retractable needle and suction system can access the heart via small incisions. The umbrella shaped polyurethane suction pad can then fix the device against the heart, so the stabilised needle can deliver its cargo in a targeted fashion [113]. The HeartLander robotic crawler, which is capable of navigating and injecting into the epicardial surface of the heart in a minimally invasive fashion, is another pivotal step towards transepicardial delivery [114].

1.10.4 Transendocardial Delivery

Using a percutaneous catheter-based approach, a cell suspension is injected directly into the myocardial tissue from inside the ventricle (Figure 1.4d). The catheter is introduced into the arterial system at the femoral or radial site, and then guided around the aorta in the opposing direction to blood flow, and into the ventricle by way of the aortic valve [5,108]. In theory, this should be the most suitable delivery route for larger cells such as mesenchymal stem cells or for more viscous delivery vehicles, such as hydrogels, which could block the microvasculature in previously mentioned delivery techniques. In addition, the low invasiveness of the procedure extends its use to a high-risk population with the possibility of repeat delivery. A variety of catheters have been developed for this method, and subsequently used in the clinical trial setting [5,108].

Helix Infusion Catheter (BioCardia): The Helix can be identified by its corkscrew shaped hollow needle, which twists into the heart tissue to ensure secure placement before the cell suspension is delivered. A 2D fluoroscopic guidance system is used to direct the user, while a deflectable steering guide allows 3 degrees of freedom [115].

Myocath (Bioheart): The Myocath is a deflectable injection catheter, which enables numerous injections at a pre-specified needle injection depth. Similar to the Helix, it relies on a 2D fluoroscopic guidance system [116].

Myostar (Biologics): In contrast to the Helix and Myocath, the Myostar uses a 3D guidance system (NOGA XP). This system reconstructs an electromagnetic map of the heart that can discriminate between the area of infarct, surrounding border zone and normal tissue. This information can then be used to give precise injections with the steerable catheter and retractable hollow 27-gauge needle [117,118].

1.10.5 Transcoronary Injection

Advances in the design in the design of catheter systems have enabled direct injection to the cardiac tissue via the coronary circulation (Figure 1.4e). Two examples of this approach are discussed below.

TransAccess (Medtronic): The TransAccess, incorporating a phased-array ultrasound tip for guidance, is tracked through the coronary sinus to the targeted coronary vein. Once in the correct position, an extendable nitinol needle is used for venepuncture into the epicardial wall, and the cell suspension can be infused deep into the myocardial tissue using a micro-infusion catheter (Figure 1.4e). The system has two advantages over transedocardial delivery (1) the deep placement of the catheter within the cardiac vein allows for movement

with the dynamic heart tissue (2) the injection is made parallel to the heart wall and thus is unlikely to disrupt a thin infarction scar [119].

Bullfrog (Mercator Medical): The distal tip of the Bullfrog is composed of a balloon with a perpendicular mounted micro-infusion injection needle (35 gauge). This penetrative needle allows the cells to effectively extravasate into the myocardial tissue by bypassing the endothelial layer [120].

1.10.6 Pericardial Delivery

The pericardial sac is a fluid filled sac that surrounds and protects the heart. This lubricating pericardial fluid acts as a shock absorber by reducing friction of the outer membranes against the heart surface. Furthermore, the outermost coat (fibrous pericardium) is a tough, protecting layer that anchors the heart to the sternum and shields it from infections in other organs such as the lungs [121].

Localised delivery to the pericardial fluid has long been recognized as an ideal route for small molecule medicine and drugs with a narrow therapeutic index[106] (Figure 1.4f). Pericardial administration of anti-arrhythmic agents[122,123], angiogenic substances[124], and vasodilators[125] have used in various studies with some success. However, easy reproducible access is a major limiting factor. Disadvantages of the approach include rapid clearance of the cells from the pericardial sac, the potential for pericarditis, pericardial effusion and cardiac tamponade, and the likely occurrence of pericardial adhesions between the heart and lungs. Furthermore, there is a need for a closure device to prevent leakage following delivery [106].
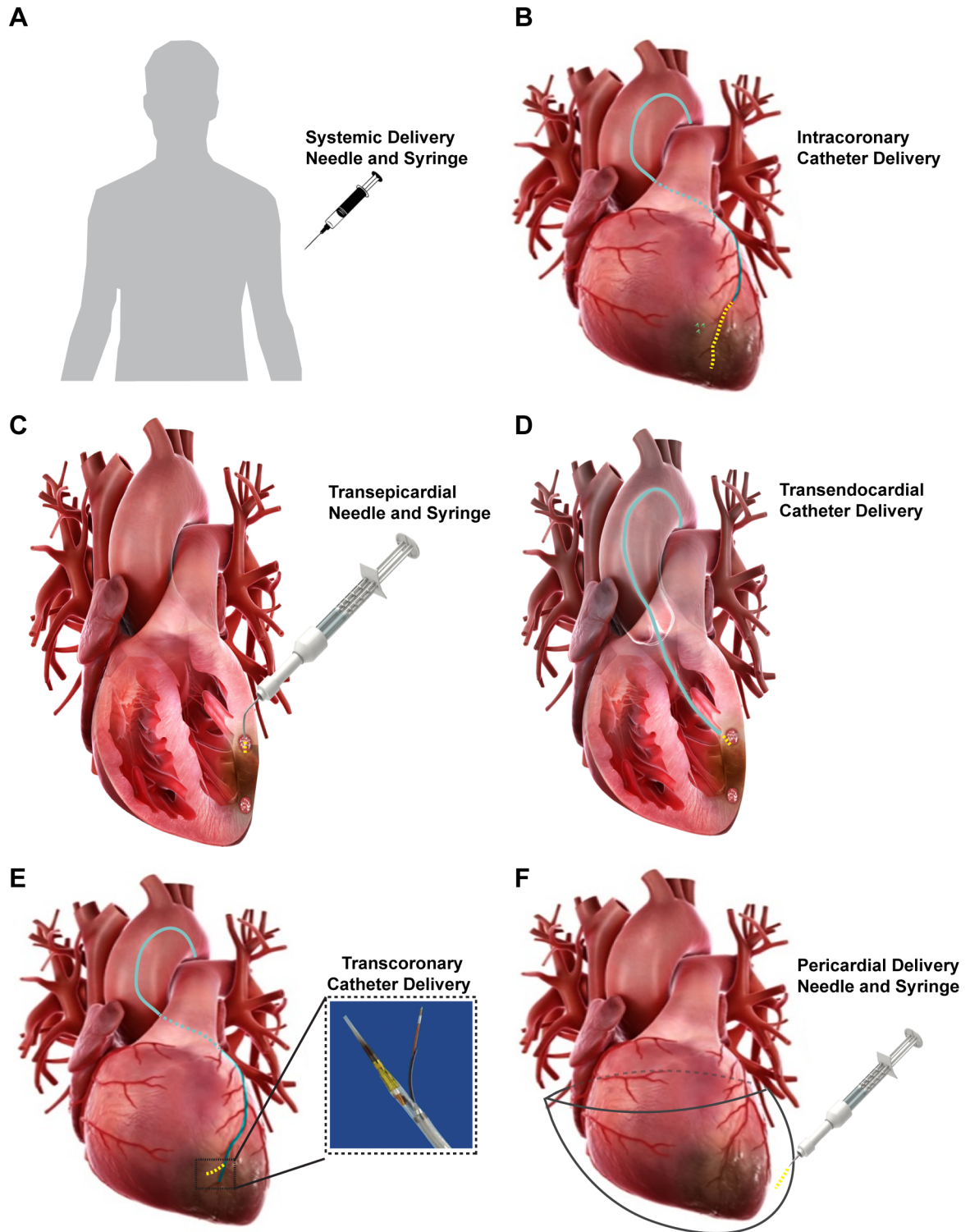
Figure 1.4: Methods of cell delivery to the heart
(a) Systemic delivery to the intravenous blood circulation using a needle and syringe (b) Intracoronary perfusion of a cell suspension to the coronary arteries or vessels using a percutaneous catheter (c) Transepicardial injection to the heart tissue using a needle and syringe, usually during surgery (d) Transendocardial injection to the heart tissue using a percutaneous catheter (e) Transoronary injection into

the heart tissue using a percutaneous catheter system (f) Pericardial delivery using a needle and syringe during surgery.

1.11 Biomaterial Delivery

1.11.1 Patch Delivery

Currently, all patch delivery methods rely on open-heart surgery (Figure 1.5a), which represent a high surgical risk for the chosen patient populations (MI, end stage heart failure). The development of a minimally invasive method of delivery is essential for clinical translation[5].

Attaching an often-fragile biological material to the slippery, dynamic epicardial surface is technically difficulty even with complete visualization and tactile feedback. This is usually accomplished with surgical staples or sutures. The ability to adhere the patch to the epicardial surface without the use of sutures could help facilitate minimally invasive delivery. Advancements in biocompatible glues coupled with minimally invasive methods of on-demand curing could remove this hurdle in the future [126,127].

1.11.2 Hydrogel Delivery

It is envisaged that hydrogels can be delivered via two routes: direct epicardial injection during heart surgery or percutaneous catheter delivery via the endocardium (Figure 1.5 b, c). The epicardial route for biomaterial delivery has been successfully explored in the Augment-HF trial, where alginate alone was investigated for its ability to reverse negative remodelling, by unloading stress in the heart wall [128,129]. The transendocardial route has not yet been explored in the clinic; however, delivery of a biomaterial to the heart in a minimally invasive fashion would negate the need for invasive heart surgery, and be clinically appealing in a large patient cohort [5]. Image guidance with electromechanical mapping or fluoroscopy could give precise spatial control, with the possibility for multiple injections and repeat administrations across different time points [111,130].

A cell-friendly and catheter-compatible hydrogel material will be essential for clinical translation. The mechanism and rate of gelation are one important design criteria. The injected material must cure rapidly (but not too rapidly so as to cause blockage of the delivery tubing) and uniformly at the pathological site, with sufficient structural integrity to avoid the formation of emboli in the bloodstream. A surface eroding material with biocompatible by-products that do not activate the coagulation cascade would be highly desirable [5]. Furthermore, it is important to consider the force required to push a material system through a curved catheter tubing ~1mm in diameter and ~25cm in length, and the effect of this shear stress on its cellular cargo[131]. Despite these challenges, multiple materials have been developed with adaptable rates and mechanisms of curing (shear thinning, PH, temperature)[132]. Furthermore there are vast arrays of commercially available catheter systems, which can be altered and optimised for hydrogel delivery. Several pre-clinical studies have already determined the feasibility of this approach, and more are planned in the cardiovascular and oncology space [93,133–135].

A

Epicardial Patch
Surgical Implantion

B

Injectable Hydrogel
Needle and Syringe

C

Injectable Hydrogel
Catheter Delivery
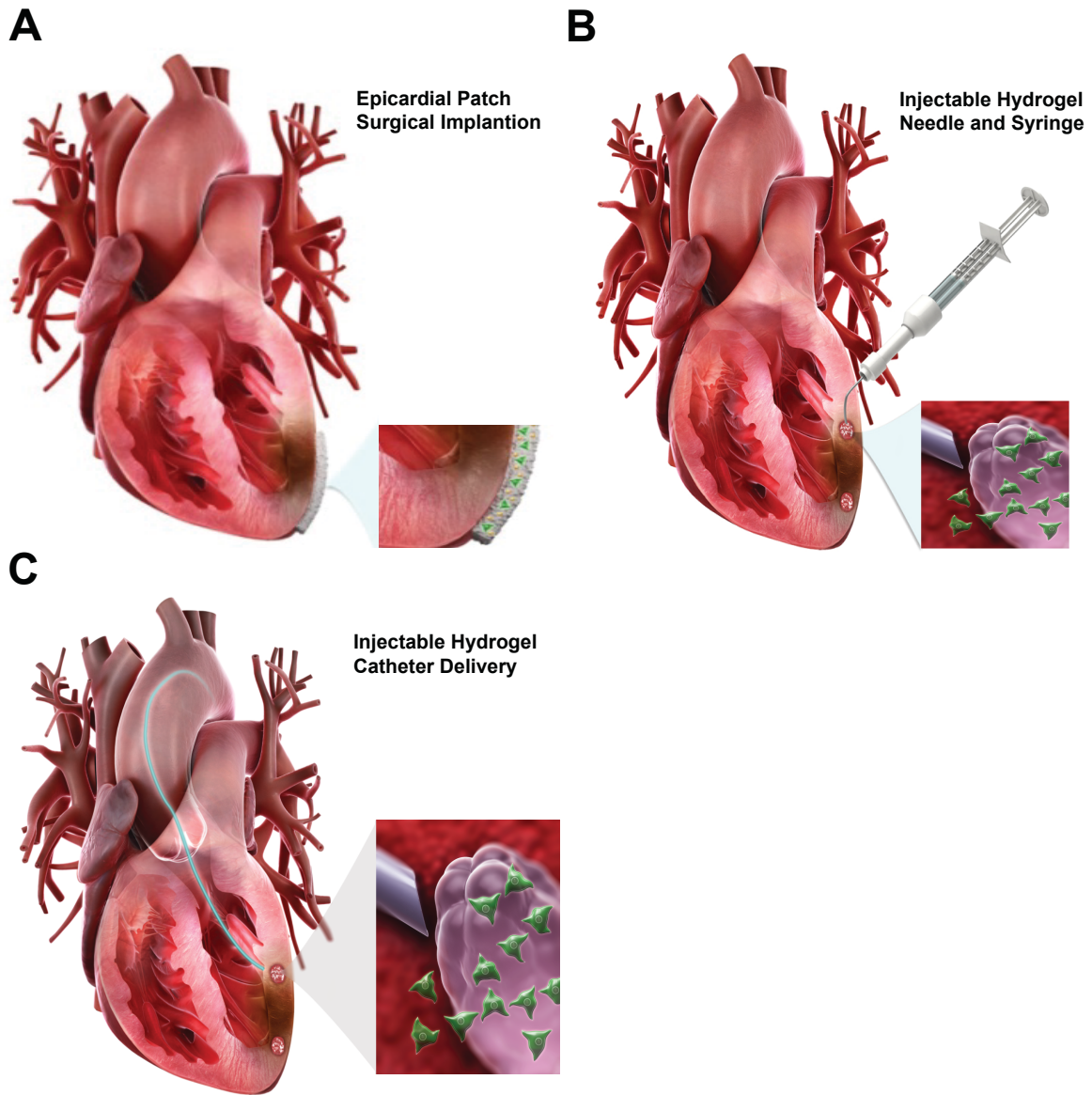
Figure 1.5 Methods of biomaterial delivery to the heart
(a) Epicardial patch delivery during surgery (b) Injectable hydrogel delivery to the endocardium using a percutaneous catheter (c) Injectable hydrogel delivery to the epicardium during surgery

1.12 Sustained Delivery

1.12.1 Bioleonhardt pump

In lieu of prolonging retention and viability, the programmable Bioleonhardt micro-pump enables the sustained delivery of regenerative therapies to the heart. The pump is implanted in the abdomen and connected by a dual pacing and infusion lead to the scar tissue in the heart; a corkscrew tip is used for firm placement into the heart tissue [136]. The pacing/infusion lead serves a dual purpose (1) it is used as a conduit for the sustained delivery of cardiomyogenic and angiogenic cargo stored in the refillable pump (2) The lead provides targeted bioelectric stimulation to the heart muscle. It is proposed that electric signals can cause the controlled endogenous release of growth factors such as SDF-1, VEGF, Follistatin and Hepatocyte Growth Factor. Furthermore, these growth factors can synergistically control the differentiation of exogenous delivered cells into functional heart tissue and mature vasculature [137–139].

1.12.2 Implantable Cell encapsulation devices

Cell encapsulation devices are composed of a biomaterial core with a cellular payload and surrounded by a synthetic non-degradable membrane. The membrane pore size is designed to form an immunological barrier but allow the release cell secreted factors[140]. Furthermore, a secondary membrane with a larger pore size can be incorporated to enable quick vascular in growth [141]. Aptly named "Trojan Horses", these devices can mechanically protect their fragile cargo during transplant/delivery and when exposed to an immunological response [107]. These devices can take many forms such as pouches, beads, and fibres and include any semipermeable, non-degradable material that encapsulates a cellular cargo. For example, Neurotech Pharmaceuticals have developed a cell encapsulation device in the form of an ocular implant that permits the continuous release of therapeutic proteins for the treatment of a range of diseases such as glaucoma or macular telangiectasia [142].

Cell encapsulation devices have attracted a lot of interest for the purposes of islet delivery in the treatment of Type 1 Diabetes. Current approaches involve the use of a thin, flat macro-polymer device, implanted in an anatomical location that is easily accessible for explant/re-implant, such as the subcutaneous space. TheraCyte™ is one example of an encapsulated device undergoing commercial development; a flat, multi-layered membranous pouch, which has demonstrated correction of diabetes and protection against allograft rejection for up to 6 months in a rat model [143].

Seronova Corp had adopted a similar strategy in the design of their Cell pouch system [144]. An acellular pouch is initially implanted subcutaneously, and allowed to incorporate into the host tissue and vasculature. Cells are then seeded as a secondary step onto the scaffold. This approach has many advantages; the accessible subcutaneous site allows for ease of implantation and removal, the pre-vascularised scaffold creates a nourishing environment for the transplanted cells, ensuring high viability. The system is currently undergoing phase I/II clinical trials for type 1 Diabetes (NCT03513939)[145].

Finally, β-Air is another cell encapsulation technology being developed for the treatment of T1D. In addition to a membrane based immune-isolation barrier, oxygen is actively supplied to the cell transplant from a refillable compartment [146]. Insufficient oxygen is one of the reasons given for islet cell deterioration and loss

of insulin independence following the Edmonton protocol, a method of implanting allogeneic islet cells for the treatment of insulin dependent diabetes [140,147]. Impressively, the device recently demonstrated safe xenotransplantation of porcine islets, without immunosuppression, in a primate model of type 1 diabetes [148].

Thus far, cell encapsulation devices have not been exploited for the delivery of cell therapy in cardiovascular disease, however the sustained release of healing paracrine factors from carefully implanted device may overcome the hurdles of associated with cell delivery to the heart.

1.13 Cell Dose

The relationship between cell dose (number of cells surviving in heart) and heart function is currently unclear and at times contradictory. This is likely due to unknown variables such as retention and viability of the transplanted cell cargo. However, based on the paracrine mechanism of action, it is reasonable to assume that sustained cell viability within a suitable therapeutic window will lead to improved therapeutic outcomes [107,131].

The ACT34-CMI trial assessed the intramyocardial injection of autologous CD34^{+}cells in patients suffering from uncontrollable angina [149]. In this trial, 168 patients were allocated to receive placebo, low dose (1 million cells/kg) or a high dos cell injection (5 million cells/kg). While both cell doses decreased the incidence of angina, the high dose was not significant in comparison to the placebo control, suggesting a therapeutic window for an optimum clinical effect [149]. The POSEIDON trial investigated the influence of autologous and allogeneic human mesenchymal stem cells at three separate doses (20, 100 and 200 million cells). At study termination, the low dose group demonstrated a larger reductions in left ventricular volumes and increased ejection fraction [63]. However, each intervention was only tested in 5 individuals.

A dosing response relationship and a therapeutic threshold has also been reported in pre-clinical studies. Dixon et al demonstrated that mesenchymal precursor cells modified indices of left ventricular remodelling in a dose dependent manner, with the greatest effect reported at lower cell concentrations [150]. In a pig pre-clinical model of chronic heart failure, higher concentrations of bone marrow mononuclear cells delivered via endocardial injection demonstrated a higher capillary density [151].

The above pre-clinical and clinical trials suggest that a therapeutic threshold or window exists for cell number. However, caution should be used in when interpreting modulation of the selected endpoints. The use of soft endpoints such as angina in the ACT34-CMI study may be necessary as we currently do not have a full mechanistic understanding of the cell therapies being used; however, this approach limits the clinical applicability of the findings [152]. Indeed, traditional endpoints such as all-cause mortality, major cardiovascular and cerebral events may be more clinically pertinent and robust. Additionally it will be necessary to ensure equivalent potency and cell functionality of the delivered cargo, not just the administered dose [61].

1.14 Cell free therapies

Unlike small molecules or biological agents, which follow the traditional regulatory path of safety and efficacy, cells are living components with physiological and biological functionalities [61]. Rigorous quality control and potency assessments would be necessary for full regulatory approval. It is unclear how feasible such assessments would be for autologous cells, or where this testing would be performed. In principle

allogeneic cells would be less cumbersome. Similar to the traditional manufacturing routes, large batches of cells could be made in a sterile site and subjected to rigorous qualitative assessments, before storage and distribution in a cryobank [61]. This is of course assuming that allogeneic cells are amenable to freezing without losing therapeutic efficacy and do not cause a detrimental immune reaction. The POSEIDON trial, which investigated allogeneic and autologous BM-hMSCs in the treatment of ischemic cardiomyopathy, demonstrated no evidence of immunosensitisation [61,63].

In keeping with the paracrine hypothesis, a more simple and feasible therapeutic strategy would be the delivery of exogenous immunomodulatory and trophic cytokines to the damaged site [61,153]. For example, the phase II VIVA trial demonstrated that vascular endothelial growth factor (VEGF) delivery could improve angiogenesis and reduce incidence of angina in patients suffering from coronary artery disease [154]. Granulocyte-colony stimulating factor (G-CSF) has been shown to modulate the mobilisation of bone marrow progenitor cells *in vitro* and in animal models. Furthermore, safety and feasibility of the approach has been demonstrated in the treatment of acute myocardial infarction and coronary artery disease. However a definitive functional benefit in patients has not yet been proven [153,155,156].

Despite showing promise, no cytokine therapeutic has achieved clinical translation for the treatment of ischemic cardiomyopathy. One potential reason for these failures is the chosen treatment population. The unknown risks associated with novel treatments are generally more acceptable to a high-risk population in an advanced stage of disease. For this reason the majority of these trials have enlisted patients with end stage heart failure, where other therapeutic options were either limited or exhausted. This cohort usually has impaired healing capabilities, even in highly regenerative organs such as the skin. After decades of negative cardiac remodelling, it is doubtful that a single dose could lead to a meaningful improvement. Delivering these therapies, ideally more than once, to a younger population in an earlier stage of disease progression could lead to significant improvements [61].

To date, trials have focused on the delivery of 1-2 biological therapies, however the complex physiological processes in the heart might require activation and inhibition of multiple pathways with precise spatial and temporal control [109]. In an interesting approach, Gnecchi et al demonstrated that a complex combination of growth factors i.e. conditioned media (without cells) was equally effective as Akt modified mesenchymal stem cells in the restoration of heart function in a rodent myocardial infarct model [157,158]. An increased understanding of the mesenchymal stem cell secretome might lead to an elucidation of a cell free, therapeutic cocktail for cardiac regeneration [62]. Harnessing the cell secretome for cardiac repair is an attractive proposition, as multiple possibilities exist to modulate and optimise cytokine release. Gnecchi genetically modified MSCs to overexpress AKT, an integral component of the Wnt signalling cascade, and associated with the regenerative capacity of these cells [157,158]. Other groups have also demonstrated physiological (hypoxic), pharmacological, or growth factor preconditioning, in an effort to express biological components that are not released under basal conditions [62,159,160].

As with cell therapy, delivery challenges exist for the delivery of exogenous cytokines. The cargo is generally unstable *in vivo* and subject to rapid degradation [61]. The preferred delivery route is usually untargeted systemic delivery, thus requiring high doses to achieve efficacy and leading to off target side effects such as

tumorigenesis [161], leaky vessels [162] and hypotension [163]. A method of targeted delivery, and controlled release at the pathological site is critical given these pharmacokinetic and stability issues.

1.15 Mechanical therapy

Providing mechanical support (or unloading) to the diseased heart is possible via a number of therapeutic strategies. Active mechanical support can be provided to the heart by a ventricular assist device. While the design of these devices may vary, their main function is to augment or replace the pumping action of the heart. A common example is the left ventricular assist device (LVAD), which takes blood from the left ventricle, and supplies this to the aorta at a sufficient pressure for recirculation throughout the body [164].

A passive approach to unloading can be provided by a ventricular restraint device (VRD), which wraps around the epicardial surface and help prevent change in ventricular spherical shape and negative remodelling in patients with dilated cardiomyopathy or heart failure. Two of these passive restraint devices have been commercially developed however none are in clinical use. Paracor Medical designed an elastic nitinol mesh (HeartNet) and Acorn Cardiovascular developed a knitted fabric mesh (Corcap) [165].

Injectable hydrogels can be used to increase heart wall thickness and preserve the chamber size. According to Laplace's law, an increase in LV wall thickness ensures a reduction in wall stress. This can lead to a reversal in adverse remodelling and eventually to an improved heart function [166]. An alginate based injectable hydrogels, Algisyl[167], has under undergone commercial development and testing in two separate clinical studies. In the latest AUGMENT trial, Algisyl in combination with the standard treatment regimen led to improved exercise capacity symptoms [128,129]. The product has received regulatory approval in the EU (CE-mark) and received an investigational device exemption from the FDA in order to collect further safety and efficacy data [167].

Cezar and colleagues explored the effects of cyclical mechanical loading and unloading on severely injured skeletal muscle tissue in a murine model [168]. In this study, an implantable biphasic ferrogel or an external pressure cuff was used to apply cyclical compressions to the injured muscle. Impressively, this biological free approach reduced the fibrotic and inflammatory response at the injured site and demonstrated skeletal muscle regeneration and a 3-fold increase in functional capacity after two weeks in comparison to the non-treatment group. While further study is needed, the mechanism of action was likely due to short-term increases in blood perfusion at the injured site due to compression-induced convection currents, rather than increased angiogenesis. These temporary increases in blood flow could then allow increased oxygen transport to the injured site and expedite removal of waste products deleterious to the regenerative process [168].

1.16 Multimodal therapies

1.16.1 The combination of drug and cell therapy

Davis et al investigated the synergistic potential of both cell and biological therapy. Using a self-assembling peptide nanofibre vehicle, they delivered IGF-1 alone, rat CPCs alone, or a combination. Interestingly, the hybrid approach increased cardiomyocyte cross sectional area by 25%, and improved systolic function in a rat myocardial infarct model [169].

The phase I Alcadia trial evaluated a hybrid approach involving autologous cardiac stem cells in conjunction with the sustained release of basic Fibroblast Growth Factor (bFGF), for the treatment for the treatment of ischemic cardiomyopathy [48]. During bypass surgery, cells were administered by intramyocardial injection and a gelatin sheet containing bFGF was attached to the epicardial surface. While no conclusions can be drawn from this trial due to its small size, results indicate a favourable trend in left ventricular function and symptom severity, with no initial safety concerns. Such an approach is enticing as the sustained release of growth factor can act on the delivered cells and exert a therapeutic effect in the target organ[48]. Takehara et al had previously explored this synergistic effect in a porcine model. They demonstrated that co-delivery of human cardiosphere derived cells and bFGF contained in a gelatin sheet significantly enhanced cell engraftment and led to larger increase in ejection fraction as compared to the delivery of each therapy alone [170].

1.16.2 The combination of mechanical and biological therapy

In the recent past, the concept of combining mechanical and biological therapy synergistically has emerged.

It is hoped that this holistic, hybrid approach may have a greater chance of clinical translation than biological therapy alone, and eventually be a realistic alternative to transplantation. These strategies while principally mechanical can have profound effects on the pathophysiological remodelling processes in the heart. In the case of ventricular assist devices, there is increasing evidence to suggest that mechanical unloading can lead to improvements in myocardial structure and function. This improvement is so considerable and sustained in some patients, that they eventually can be weaned off mechanical support altogether [171]. While the molecular underpinnings are not yet understood, some studies have begun to investigate reasons for this therapeutic effect. A study originating from the lab of Hesham A. Sadek hypothesised that the increase in mechanical loading of the heart in the postnatal period, causes an increase in mitochondrial content, with a consequential activation of DNA damage response and permanent arrest of the cardiomyocyte cell cycle. Sadek and colleagues demonstrated that unloaded hearts post LVAD therapy had a 60% reduction in mitochondrial content and a 45% reduction in cardiomyocyte size. Importantly, the study revealed a statistically significant increase in cardiomyocyte replication in the LVAD group, possibly caused by a switch from hypertrophic to hyperplastic cell growth [172].

It has been proposed that delivery of regenerative therapies to a mechanically unloaded heart might have better chance of success than delivery to an organ which is trying to persistently overcome a volume and pressure overload [131]. This idea of combining active mechanical support and cell therapy has been the subject of numerous research studies [173,174]. ASSURANCE is investigating LVAD therapy with Bone Marrow Derived Mononuclear Cells [175]. The MESAD trial is using LVAD therapy with autologous MSCs, with the eventual aim of weaning patients from mechanical assistance [176].

Cell therapy in combination with passive assist devices has also been investigated, with some success. An advantage of this approach is the epicardial placement of the restraint device, which allows for the targeted delivery of cell therapy. In an interesting approach, Shafy et al combined the polyester Corcap restraint device with a cell seeded collagen interface (adipose derived stem cells), in a sheep infarct model, [177]. This partially degradable, cell-device combination demonstrated an increase in ejection fraction, diastolic and systolic function and reduced adverse remodelling and fibrosis.

In the past, ambiguity relating to regulatory strategy for combination products has hindered and discouraged the development of these devices despite the potential for improved clinical outcomes [5]. The formation of the office of combination products by the FDA in 2002 has changed this regulatory landscape [178]. Innovative drug delivery companies such as Microchips Biotech are now following this route, clarifying the path and reducing the burden for future combination therapies [179]. It is hoped that a simpler regulatory route will encourage the development of multimodal technologies for the treatment of cardiovascular disease, and the synergistic potential of such therapies can lead to improved clinical outcomes [131].

1.17   Overarching hypothesis, specific aims and thesis outline

Despite major advances in the acute treatment of a heart attack, mainly achieved through the rapid restoration of blood flow to the damaged ischemic area, residual myocardial scarring often remains [7]. Elimination of this scarring and restoration of full function after a heart attack could halt or delay the progression to heart failure. Regenerative therapies in the form of cells, proteins, and small molecules have shown considerable success in the treatment of post-myocardial injury and the prevention of ischemic cardiomyopathy in pre-clinical studies. However, although some of these strategies have demonstrated some success in the clinic, their adoption into medical practice has been hindered by low or unpredictable efficacy when tested in large patient populations [5,60,131].

The majority of clinical trials have delivered cell therapy in a simple saline vehicle and suffer from similar shortcomings, including low concentration at the diseased site due to untargeted delivery, poor retention in the dynamic environment of the beating heart, a short biological half-life, adverse effects from systemic delivery and the necessity for multiple administrations for best clinical efficacy [180–182]. These limitations equally apply to regenerative growth factor and small molecule therapies. In order for regenerative therapies to achieve tangible clinical success, it likely will be necessary to enhance stem cell viability during delivery and their ability to survive and stay within the harsh environment of the dynamic ischemic heart. Biomaterial delivery vehicles offer one way to enhance retention and provide localised controlled release to the targeted site [83,84,93,94,85-92], but a method to replenish therapy or offer multiple administrations without necessitating invasive surgery has not yet been proven. Finally, the majority of strategies in the clinic have focused on the delivery of one therapeutic agent. This is understandable considering the ethical and regulatory hurdles that need to be overcome [5,61]. However, there is much evidence to suggest the concurrent delivery of multiple therapies, both mechanical and biological, can act in a synergistic manner, enhancing both the efficacy of individual therapies and the overall effect on the target tissue [48,169,170,173–176,183].

To summarise, a common theme underpinning cardiac regenerative studies is the necessity for redelivery or sustained delivery of therapy in a targeted manner to the injured site in a minimally invasive fashion [184]. Furthermore, once delivered there is a need to increase retention and maintain biologically activity of the [5,60,185]. Finally, the ability to co-deliver combination therapies including cell, growth factors and small molecules synergistically with temporal and spatial control may have enhanced clinical efficacy in comparison to the delivery of a single agent [131]. Indeed, a multi-modal strategy may be necessary to mimic or modify the inherently complex physiological and pathological processes in the heart. With these needs in mind, I propose the advanced delivery strategy, *Therepi*, in order to fully realise the potential of regenerative cardiac therapies demonstrated in pre-clinical studies.

The overarching hypothesis of my research is that regenerative cardiac therapies suffer from delivery limitations, restricting their efficacy. A strategy that allows for replenishable targeted delivery, sustained presentation of multi-modal therapies, with the ability for spatial and temporal modification of release, will

23

overcome the hurdles faced by cardiac regenerative therapies, and lead to a new treatment option for heart disease.

The specific aims of my thesis are as follows:
1. **To develop a pre-clinical research model for the targeted, replenishable delivery of multiple types of therapy to a simple, epicardially placed biomaterial.**
2. **To design, optimise and validate *Therepi*; a replenishable, immune-isolated, biomaterial reservoir that allows for sustained release of cardiac therapy.**
3. **To assess the safety and efficacy of *Therepi* following implantation in a rat model of myocardial infarction and explore barriers to clinical translation.**
4. **To functionalise *Therepi* using soft robotic technology for precise spatial and temporal control of drug release.**

Chapter 2 describes how I achieved the first aim of my thesis. In this section, I introduce the *Therepi* concept and describe the development of a representative pre-clinical animal model that permits the targeted and replenishable delivery of cells, small molecule and protein therapies to a biomaterial sutured to the epicardial surface of the heart. This chapter includes a detailed description of the surgical method, and a proof of concept for each therapeutic. This chapter also demonstrates a method to accurately monitor cell viability and cardiac function over time in the same animal following myocardial infarction, and relate disease progression to cell dose and viability.

Chapter 3 focuses on the second aim of my thesis. This chapter details a manufacturing process for a soft flexible, immunoisolatory shell that surrounds the simple catheter implanted biomaterial reservoir developed chapter 2. The shell is designed to maximise transplanted cell retention and survival, enables protection from the host immune response and permits the sustained delivery of therapy to the infarcted heart.

In Chapter 4, we focus on the third aim of my thesis. Initially, the chapter explores and discusses potential barriers to clinical translation including formation of a fibrous capsule, target patient population, and risk of infection. Finally, we assess the safety and efficacy of repeated syngeneic mesenchymal cell delivery with the optimised and validated *Therepi* system (developed in chapter 3) using the pre-clinical research model (developed in chapter 2).

Chapter 5 explores aim 4 of my thesis. The chapter details the addition of a soft robotic element to the *Therepi* Reservoir. Active assist to the biomaterial with a precise actuation stimulus allows us to alter the *in situ* passive release profile with spatial and temporal control, facilitating tuneable pharmacokinetic release of cell and molecular therapies at the pathological site.

2 The development and validation of a pre-clinical model for the targeted, replenishable delivery of multiple types of therapy to a simple epicardially placed biomaterial

2.1 Preface

Chapter 2 describes how I achieved aim 1 of my thesis. In this chapter, I introduce a simplified version of "*Therepi*", a **Ther**apeutic **Epi**cardium, and the development of a representative animal model that enables the replenishable delivery of cells, small and macromolecules to a biomaterial sutured to the epicardial surface of heart. I also discuss a method to monitor cell viability and cardiac function over time in the same animal following myocardial infarction, and relate disease progression to cell dose.

The chapter aims are as follows

1. To develop a simplified delivery system for the targeted and replenishable delivery of therapy to a biomaterial, and a method of implantation of this delivery system on the epicardial surface of the heart, in a pre-clinical rodent model.

2. Validate that the refillable technology also allows the rapid, targeted delivery of small molecules and macromolecules directly to the targeted site

3. To develop and characterise a method for the rapid, accurate longitudinal measurement of cell viability in-vivo.

4. Demonstrate replenishable cell delivery *in-vivo*

5. To develop a method for longitudinally measuring cardiac function in a survival model of the same animal at multiple time points using a pressure-volume micro-conductance catheter.

2.2 Introduction

In a paradox of medical success, patients are increasingly surviving a heart attack, only to develop heart failure later in life [7]. The disease represents an enormous cost to our healthcare systems with an annual expenditure of $120 billion. According to the American Heart Association, 275,000 patients died from heart failure alone in 2009 [9–11]. Consequently, there is an urgent need to develop curative therapies for a vulnerable, ageing, population.

A single dose of cells delivered to the infarcted heart has demonstrated promising regenerative results in a laboratory setting [42–45]. However, improved patient outcomes are limited by poor cell retention and survival at the pathological site, with an acute survival rate of 10% typically reported in the literature regardless of delivery route or cell type[66]. Clinical translation is dependent on new strategies that protect therapeutics within the harsh environment of the infarcted heart and allow them to exert their benefit over extended periods [78,186,187]. Physiological saline is the current clinical gold standard vehicle for cell therapy but offers little protection to its precious cellular cargo [109]. As an alternative, bioengineered materials offer a great deal of promise, with the ability to act as surrogate ECM for anchorage dependent cells, provide shelter from insults such as hypoxia and inflammation, and ultimately increase retention and survival of its cellular payload at the diseased site [83,84,93,94,109,85–92]. In a similar manner, these carrier materials can be utilised for the

enhanced retention and controlled release of small molecules and proteins [188]. Molecular therapies suffer from similar limitations as cells; low concentrations at the desired site due to untargeted delivery and a short biological half-life. However despite inherent pharmacokinetic limitations, they represent a promising and clinically translatable strategy for the treatment of cardiac disease [153–156,189].

Advances in synthetic chemistry has enabled the manufacture of proteins with an enhanced half-life *in vivo* and reduced immunogenicity, paving the way for a new range of therapeutic modalities [190]. Modified protein and peptide bioagents can potentiate cardiac repair through multiple mechanisms including the activation and recruitment of endogenous cardiac progenitor cells at the injured site, the promotion of cardiomyocyte cell cycle re-entry, or the recruitment of calls capable of triggering neovascularization. Studies have been conducted with vascular endothelial growth factor (VEGF)[191], stromal cell derived factor (SDF-1)[192,193] hepatocyte growth factor (HGF)[194] and neuregulin (NRG-1)[195] and insulin-like growth factor (IGF-1)[196]. Furthermore, advances in combinatorial chemistry and high throughput screening means that a library of small molecules can now be synthesized and screened in a representative biological system to determine novel targets and illuminate previously unknown signalling pathways involved in cardiac disease. An increased understanding of the structure activity relationship can permit and guide molecular modifications to enhance stability, target specificity, and ultimately clinical efficacy. Examples of these molecules include prostaglandin E2 (PGE2)[197] or diprotin[5,198].

While biomaterials show great promise for extending and enhancing the benefit of molecular and cellular therapies, they can only be pre-loaded with one dose and exhibit a predetermined release rate and potency. Intriguingly, recent evidence supports a paradigm-shift towards repeated cell administration, demonstrating that multiple administrations are therapeutically superior to single doses in MI and heart failure animal models[181,182]. In addition to cells, it is likely that an improved benefit with repeated dosing could be achieved with other technologies, including small and macromolecules. A method to offer repeat administrations without necessitating repeat invasive surgeries, while simultaneously protecting its cargo post administration, has not yet been demonstrated, motivating the design of this system.

In this chapter, we introduce the initial iteration of "*Therepi*", a **ther**apeutic, **epi**cardially placed biomaterial reservoir that offers a number of advantageous features to address the current limitations for the delivery of cells, macromolecules and small molecules to treat cardiac disease. In our design, a biomaterial is attached to the epicardial surface of the heart and connected to a subcutaneous port through an implanted conduit or catheter, allowing localized, targeted therapy to the diseased tissue, without the need for higher systemic doses. Importantly, replenishable delivery with temporal and potency control is possible with the system and the biomaterial vehicle promotes retention of the delivered cargo and enhanced engraftment and viability of cells [83,84,93,94,85–92]. In this work, we use a methacrylated gelatin cryogel[199], but we foresee this platform system being used with numerous types of biomaterials. We introduce a surgical method of implantation in a rat model that enables repeated replenishment of therapy from a subcutaneous port. We demonstrate delivery of cells using luciferase-expressing mouse mesenchymal stem cells, proteins using fluorescently tagged bovine serum albumin, and small molecules using D-luciferin, an imaging substrate that causes bioluminescence in the presence of the enzyme luciferase and oxygen. We describe a method for longitudinally measuring cardiac

function in a survival model of the same animal at multiple time points using a pressure-volume (PV) micro-conductance catheter with the apical stick or "open chest" method. Previous studies using apical PV catheterization are non-survival studies, and the animal is terminated after the hemodynamic measurements[200–203]. The potential advantages of longitudinal survival studies include reduction of animal numbers while allowing ejection fraction (the percentage of blood leaving each ventricle per contraction) measurements and a full spectrum of cardiac evaluation in a survival model, helping with the study of disease progression and treatment effects.

This work has important practical implications; preclinical use of the system as a research model may elucidate new insights into regenerative cardiac therapy, and progress experimental therapies along the clinical translational path for improved patient outcomes.

2.3 Materials and Methods

2.3.1 Therepi Animal model

Animal preparation and endotracheal intubation: All animal studies were carried out in accordance with the Institute for Animal Care and Use Committee, Harvard University. Female Sprague Dawley rats (225-275g) were anesthetized using isoflurane (1-3% isoflurane in Oxygen). Endotracheal intubation was required to mechanically ventilate the rat. This is described in Figure 2.1 and the following text. A chamber was used for induction of anaesthesia and maintenance with a nose cone was used to maintain anaesthesia during preparation for surgery. The hair between the shoulder blades and on the left side of the chest was removed with an electric razor and hair removal cream. Pre-operative analgesics were administered: buprenorphine (0.05mg/kg IP) and Lidocaine HLC 2% injection USP (100 microliter per injection site, SC). A tilting stand (Hallowell EMC, 000A3467) was used to position the animal for intubation. The arms were taped to the supports on the stand, and an elastic band with Velcro was placed around the two front teeth to hold the animal in place. The animal was tilted at a 45º angle and the glottis area was trans-illuminated with a spotlight placed close to the neck. The tongue was retracted to visualize the opening and closing of the larynx, just above the oesophagus. Lidocaine (10µl of 1%) on tip of intubation tube was used to prevent laryngospasm. A forceps could be inserted into the mouth once the tongue was retracted to keep it open while a 16G, 2.5" catheter (BD angiocath) was inserted into the trachea, timed with the opening of the larynx. Intubation was verified with a dental mirror placed at the end of the catheter. Condensation from breathing was observed at the end of the catheter if correctly placed. The mechanical ventilator (SAR 830P, Harvard Apparatus) was then connected to the catheter via a luer connector on the end of an extension line on the ventilator output, and the chest of the animal was observed to ensure that the lungs were inflating and deflating in time with the ventilator. Settings were adjusted to volume control, flow rate of 200-500cc/min, with an inspiratory time of 0.55 seconds, a respiratory rate of 75 breaths per minute. Pressure was maintained between 12-14cm H_2O on inhalation.
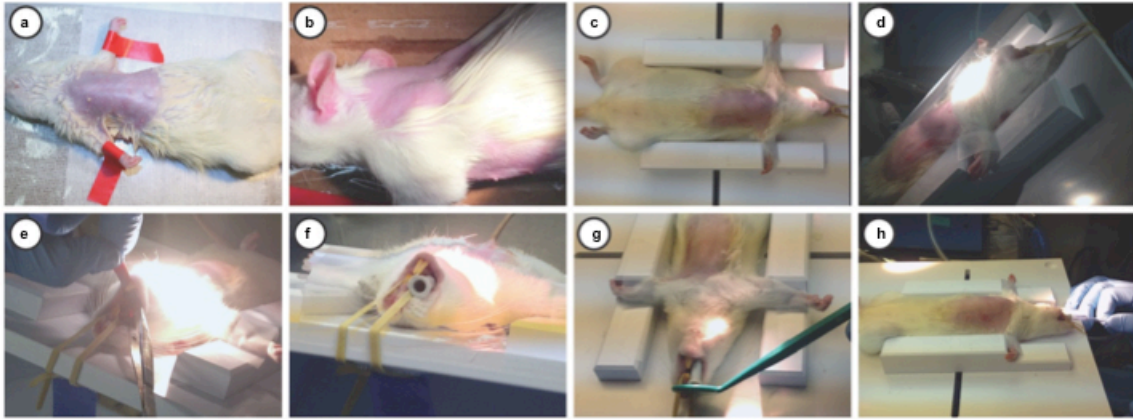
Figure 2.1: Animal preparation and intubation
(a) Hair is removed at the ventral site **(b)** and the dorsal site using an electric shaver and hair removal cream **(c)** The limbs are taped in place, and an elastic band around the incisors is attached to the stand **(d)** The stand is raised, and the glottis is trans-illuminated. **(e)** The stand is positioned so that the operator has a direct view of the larynx. The tongue is retracted and pulled up so that the vocal cords can be visualized. **(f)** A 16G catheter is inserted into the trachea, timed with the opening of the vocal cords. **(g)** Correct insertion is verified by visualizing a small area of condensation on exhalation when a dental mirror is placed at the end of the catheter. **(h)** The ventilator is connected to the intubation catheter with an extension line. The lungs are observed to be moving with the ventilator and settings are adjusted as appropriate.

Subcutaneous catheter tunnelling procedure: Once the animal was intubated, the intubation catheter was tied in place using umbilical tape, and the animal was placed on a sterile drape over a heating pad for the surgery. An indwelling catheter was then tunnelled subcutaneously from a dorsal site between the shoulder blades of the animal to a ventral exit site close to the left fourth intercostal space. This is described in Figure 2.2 and the following text. Briefly, both the dorsal and ventral surgical sites were washed with a 2-step iodine surgical scrub preparation. A small incision was made in the dorsal skin, in between the shoulder blades, and an incision was made at the ventral site, at the area of the fourth intercostal space (usually about the level of the third superior nipple). A forceps was used to tunnel subcutaneously from the dorsal to the ventral site. The forceps was directed through the incision, to grasp a 3Fr catheter (C30PU-RJV1303, Instech Laboratories) and retract it through the tunnel.
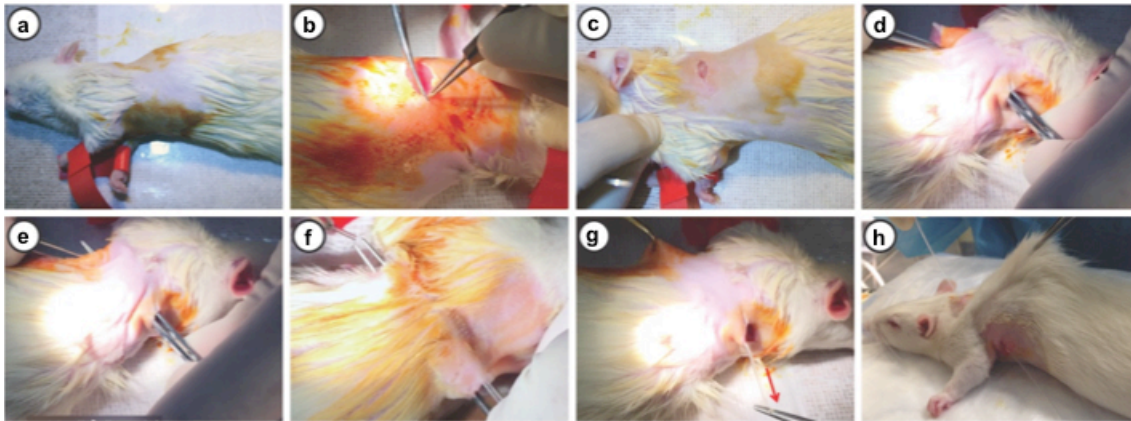
Figure 2.2: Subcutaneous catheter tunnelling procedure
(a) Iodine surgical scrub preparation is applied. **(b)** An incision is created at the ventral and **(c)** dorsal site **(d, e)** A subcutaneous tunnel is created between the dorsal and ventral site using a blunt tweezers **(f)** The forceps are placed through the tunnel so that they exit at the ventro-lateral incision and one end of the catheter is grasped with the forceps **(g)** The catheter is pulled back through the dorsal site **(h)** The catheter can be seen at the tunnel entry and exit points.

Thoracotomy and simplified Therepi placement: Next the access to the heart was established using a thoracotomy and removal of the pericardial sac. The simplified Therepi device was then attached to the heart. This is described in Figure 2.3 and the following text. A thoracotomy was performed by making a small incision parallel to the ribs at the 4th intercostal space, taking care not to cut the catheter at its ventral exit point. The intercostal fascia and muscle was opened using a blunt dissection technique, keeping the instruments parallel to the ribs and taking care to keep the ribs intact. A small chest retractor (Fine Science Tools, 17008-07) was used to spread the ribs and visualize the underlying lungs and heart. The left lung was retracted with a sterile cotton-tipped bud. The pericardium was removed with two fine curved forceps (Fine Science Tools 91197-00). A guide suture (6-0 prolene monofilament, Ethicon 8711) was then placed into the myocardium towards the apex using a spring-loaded needle driver (Castreviejo needle holder, Fine Science Tools 1265-14). Using the guide suture, the heart could be manipulated into position and held there using a haemostat (Fine Science Tools, 91308-12).

The simplified *Therepi* system, consisting of the catheter alone and a methacrylated gelatin cryogel was then attached to the heart. The catheter was positioned by retracting it at the dorsal opening until just enough of the length remained ventrally to be attached to the epicardium. A suture (6-0 prolene, Ethicon 8711) was brought through the tip of the catheter first, and then through the epicardium (on the left ventricle, close to the apex) before securing in place. Then the GelMA cryogel was placed on the heart by first placing a suture through the myocardium, just distal to the end of the catheter. The same suture was then placed through the GelMA and used as a guide to lower the GelMA cryogel on to the surface of heart so that it sat over the end of the catheter. The GelMA was then secured in place with a single suture loop and double knot, ensuring not to tear the GelMA. The guide suture was then removed, and the heart was gently guided back into the thoracic cavity.
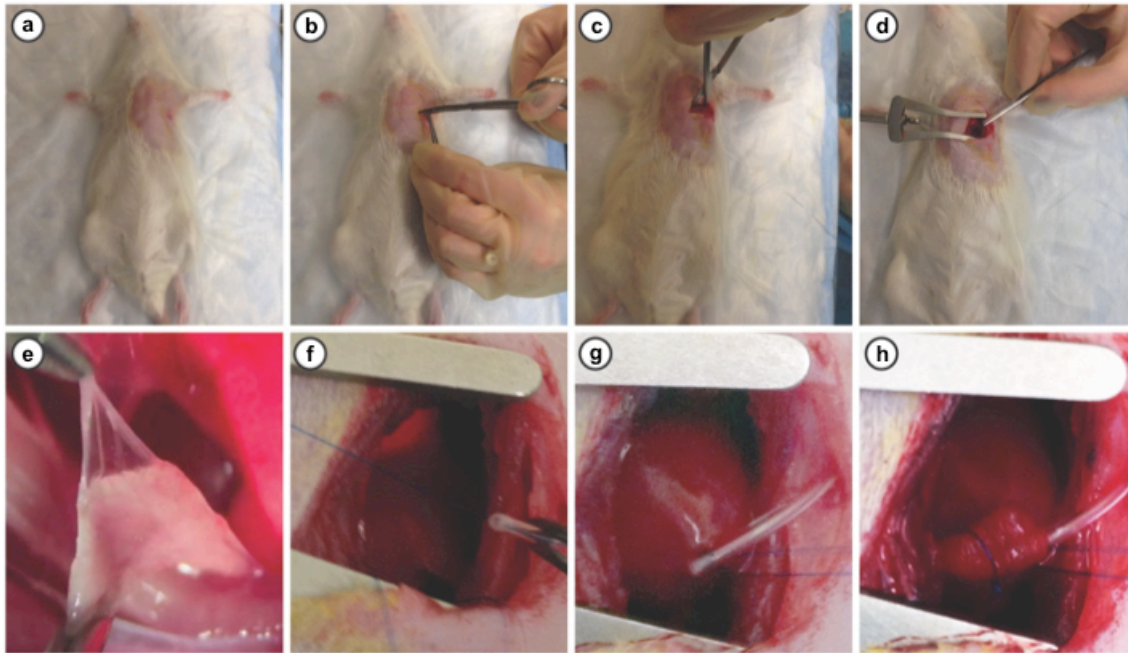
Figure 2.3: *Thoracotomy, simplified Therepi placement and chest closure*
(a) The rat is carefully turned supine, and draped with a clear sterile plastic drape, taking care not to dislodge the intubation catheter or the ventilator connection. **(b)** A small incision is made at the 4th left intercostal space. **(c)** The tissue is dissected bluntly between the ribs to access the thoracic cavity **(d)** A chest retractor is inserted underneath the ribs each side of the incision and opened to visualize the underlying heart **(e)** The lung is gently moved aside with a sterile cotton bud and the pericardium was removed with two fine curved forceps **(f)** The catheter position is adjusted from the dorsal end so that the implanted catheter terminates at the heart. **(g)** The catheter is sutured to the ventricle of the heart, ensuring not to block the catheter. **(h)** The biomaterial is placed on the heart using a pre-placed suture and "parachuting" the biomaterial onto the ventricle then securing it with a single knot so that it is placed at the end of the catheter

Chest closure: Next, the thoracic cavity was closed, and negative pressure was re-established. This is described in Figure 2.4 and the following text. The muscle layers were closed with interrupted sutures, leaving a small opening for the subsequent evacuation step (4-0 coated vicryl polyglactin 910 braided suture, Ethicon J310). A perforated tube connected to a 30cc syringe was placed into the thoracic cavity through a small opening in the muscle layers, and a vacuum was applied while the skin was sealed with fingertips to inflate the lungs and re-establish negative thoracic cavity pressure. A haemostat clamp was immediately placed on the skin, maintaining the airtight seal, and sutures (Ethicon J310) or wound clips (Reflex 9mm) were used to close the wound. Finally, the rat was turned prone, ensuring not to dislodge the intubation catheter or ventilator attachment, animal was re-draped in this position.
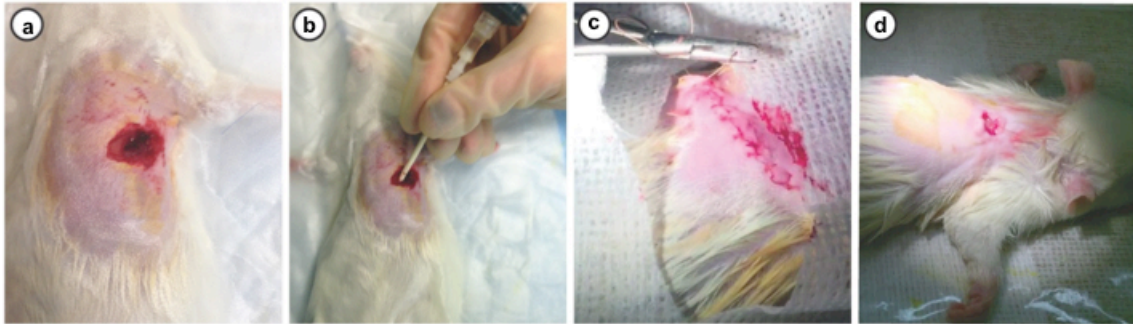
Figure 2.4: Chest closure and reestablishment of negative pressure:
(a) The muscle layer is closed with sutures, leaving a small opening for the next evacuation step. **(b)** A perforated tube connected to a 30cc syringe is placed into the thoracic cavity through a small opening in the muscle layers, and a vacuum was applied while the skin was sealed with fingertips to inflate the lungs and re-establish negative thoracic cavity pressure. A haemostat clamp is immediately placed on the skin, maintaining the airtight seal. **(c)** The skin is closed with wound clips or a suture **(d)** The rat is turned prone, ensuring not to dislodge the intubation catheter or ventilator attachment, animal is re-draped in this position.

Myocardial Infarction: For the hemodynamic study, rats underwent myocardial infarction as previously described [102], immediately prior to Therepi attachment. The left anterior descending artery was permanently ligated with a suture (6-0 prolene, Ethicon 8711) approximately one third of the way from the apex to the base of the heart. Myocardial blanching was apparent after ligation of the LAD, confirming infarction. This procedure is described in Figure 2.5.
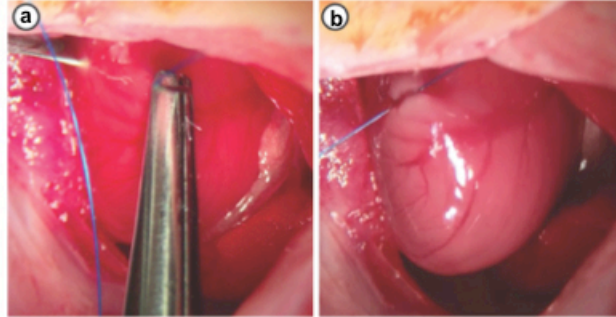
Figure 2.5 Myocardial infarction in a pre-clinical rodent model
(a) The left anterior descending artery is permanently ligated with a suture **(b)** Myocardial blanching is apparent after ligation of the LAD, confirming infarction.

Subcutaneous port placement: Finally, the refill port was placed subcutaneously between the shoulder blades of the rat. This is described in Figure 2.6 and the following text. The animal was carefully moved from the supine to a prone position. The catheter was then trimmed so that 2-3cm of catheter exited the dorsal site. Subcutaneous space sufficient for the vascular access button was then created using forceps. The vascular access button (VAB62BS/22, Instech Laboratories) was then attached and inserted into the subcutaneous pocket, ensuring that the catheter did not kink, but took gradual curves to allow slack for movement. The felt was secured to the underlying fascia using at least two interrupted sutures (Ethicon J310) taking care not to go through the catheter. The skin was then closed with four to five interrupted sutures (Ethicon J310). Finally, the isoflurane was turned off and the animal was ventilated with 100% oxygen on a heated pad until it started breathing on its own. The intubation catheter was then removed. 3ml of warm saline was administered subcutaneously and buprenorphine [0.05mg/kg in 50μl intraperitoneally (IP)] was given every twelve hours for three days post-operatively.
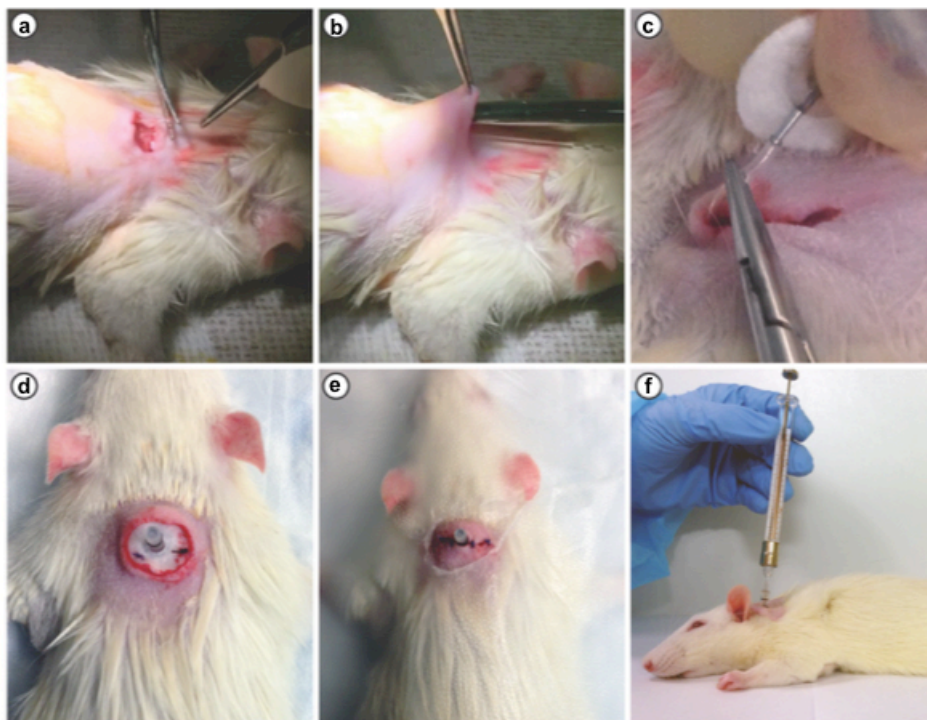
Figure 2.6: Subcutaneous port placement
(a) The catheter is trimmed so that 2-3cm of catheter exits the dorsal site, ensuring there is no kinking in the line but enough slack for movements **(b)** Subcutaneous space sufficient for the vascular access button was then created using a forceps **(c)** The subcutaneous port was then attached to the catheter and inserted into the subcutaneous pocket **(d)** The felt is secured to the underlying fascia using at least two interrupted sutures, taking care not to go through the catheter **(e)** The skin is closed with four to five interrupted sutures and the animal is recovered **(f)** Repeated, minimally invasive delivery is enabled through the port.

2.3.2   14 day longitudinal measurements of hemodynamic cardiac function

Hemodynamic measurements were carried out using the apical stick method as previously described[221]. An average of at least ten cardiac cycles was taken post-calibration for haemodynamic measurements using the Powerlab 8/35 and LabChart Pro software with the PV module. At day 0 a baseline measurement was taken with a pressure-volume (PV) catheter (SP383, AD Instruments), using the apical stick method[221]. With the PV catheter in place, an MI was created as previously described. Another measurement was taken to confirm the MI after ligation of the LAD. IVIS imaging could be carried out at multiple timepoints between implantation and termination, using the port to inject imaging substrate D-luciferin. At day fourteen another thoracotomy was performed at the fifth intercostal space, and hemodynamic measurements and calibration steps were repeated. The animal was then heparinized (10 IU/ml given subcutaneously corresponding to a dose of 40IU/kg) and blood was collected from the ventricle using a 25G needle and a 10cc syringe for cuvette calibration as described[221]. The animal was euthanized by exsanguination while under anaesthesia. Cutting the diaphragm was used as a secondary euthanization method.

A 14- day study was carried out using this hemodynamic analysis. *Therepi*, in this case is a methacrylated biomaterial, encapsulated by a polyurethane backbone, and separated from the heart by a semi-permeable membrane, as described in chapter 3. There were three study groups; (i) No treatment, (ii) *Therepi* with initial cell dose but no refill (*Therepi*+cells) (iii) *Therepi* with initial cell dose and refill on day 4 (*Therepi*+cells+refill). An average of at least ten cardiac cycles was taken post-calibration for ejection fraction and end diastolic volume recording in LabChart Pro software.

2.3.3   Preparation of Materials

Cryogel preparation: Methacrylated gelatin (gelMA) was synthesized as previously described [199]. First, Methacrylic anhydride was reacted with the free amine sites of gelatin to produce pendant methacrylate groups. A 10% w/v solution of type A porcine skin gelatin in Dulbeccos phosphate buffered saline (GIBCO) was prepared. Next, Methacrylic anhydride (Sigma) was added to this solution in a drop wise fashion until a volume ratio of 1:4 was achieved. The resulting solution was stirred at 50°C for 1hour before a 5 fold dilution was performed. Dialysis (12-14 kDa, Spectrum Labs) was then performed for 4 days with frequent distilled water replacement. Finally, the solution was lyophilised and stored at -20°C.

These methacrylate groups were then cross-linked by TEMED/APS initiated free radical polymerization while being frozen (cryopolymerization). Formed ice crystals lead to highly interconnected, micron scale pores. These steps were performed using sterile reagents under aseptic conditions. Cylindrical acrylic moulds (7.5mm diameter, 1.25mm thick) were placed in a freezer at -20°, with direct shelf contact. The lyophilized gelMA was warmed to room temperature. A 137mg/ml ammonium persulfate solution (APS; Bio-Rad) was prepared, and protected from light. A 1% gelatin solution was prepared and placed on a hot plate at 40°C, 500 rpm for 30 minutes, then stored in a 4°C refrigerator for 20 minutes. 4ul tetramethylethylenediamine (TEMED; Bio-Rad) was added to the gelatin solution for every ml of solution, and stirred. The solution was placed in the fridge for three minutes, and then 36μl of APS was added to the gelatin for every ml of solution and stirred. The gelatin solution was pipetted into moulds, filling to excess. An acrylic plate was placed over the mould, ensuring that all air was removed, and the assembly was clamped together with binder clips, and

stored for seventeen hours at -20ºC. The gels were removed by displacing them from moulds with a 7.5mm punch once semi-thawed (30 seconds-1 minute after removing from freezer), and they were stored in distilled sterile water until use.

Cell transfection: Mesenchymal D1 stem cells from BALB/c mice were used. To introduce firefly luciferase to these cells, lentiviral particles were produced containing a vector with mCherry-IRES-Firefly Luciferase driven by the CMV promoter by transfecting the plasmids in HEK-293T cells. The viral particles were then concentrated by centrifugation through an Amicon filter with a 3kDa cut-off. The viral titre was determined by evaluating mCherry signals after transducing MSCs with different concentrations of the particles. MSCs were then incubated with viral particles for 2 days. Cells expressing mCherry were then sorted via flow-activated cell sorting.

Cryogel seeding with cells: Luciferase-expressing mouse mesenchymal stem cells were cultured in the following growth media: Dulbecco's Modified Eagles Medium supplemented with 10% (v/v) bovine serum, 100 U/ml penicillin, and 100 µg/ml streptomycin (Gibco). Cells were stored at 37°C with a 5% CO_2 atmospheric concentration. Trypsin solution (Sigma) was used to separate adherent cells from the adherent tissue culture flask substrate.

GelMa Cryogels were seeded as previously described[46]. Prior to cell seeding, gels were dehydrated using a kimwipe. They were subsequently rehydrated with a cell suspension (1 million cells/12.5µl). Gels were then placed in an incubator (37°C, 5% CO_2) for 60 minutes to allow for cell adhesion. Finally, complete media (as described above) was added and the gels were cultured overnight before implantation.

2.3.4 *In vivo* refills of cells and delivery of small and macromolecules

Cell refills were conducted through the port with 50µl of cell suspension at a concentration of 20×10^6 cells/ml of complete media injected through the port of each animal with a 100µl microsyringe and a PNP-3M injector (Instech Laboratories). The line was then flushed with media to account for the dead volume for each system so that a total of 50µl of cell suspension reached the gel. Small molecules and macromolecules were delivered in the same manner ensuring 50µl of D-luciferin (at 15mg/ml concentration) or 100µl of BSA fluorescently labelled with Vivotag 800 reached the gel. *Therepi*, in the study involving BSA delivery is a methacrylated biomaterial, encapsulated by a polyurethane backbone, and separated from the heart by a semi-permeable membrane, as described in chapter 3. For the IP groups either 150mg/kg of D-luciferin (at 15mg/ml concentration) or 100 µl of BSA/Vivotag 800 was injected IP. Fluorescently labelled BSA was prepared by incubating 3mg/ml of BSA with 100 microgram of Vivotag 800 (Perkin Elmer) for one hour. The non-reacted fluorophore was then separated using size exclusion chromatography (BioSpin P-6, Bio-Rad).

2.3.5 *In vivo* bioluminescence and fluorescence measurements

To measure bioluminescence of F-luc cells *in vivo*, D-luciferin (XenoLight D-Luciferin Potassium Salt, Perkin Elmer) at 15mg/ml was delivered via a refill port or by IP injection, respectively. For the cell refill studies, animals were imaged on day of surgery (day 1), and at multiple days out to day ten for *Therepi*. On day four the refill group was replenished with cells, and imaged two hours before refill and four hours after refill. Animals were anesthetized with 3% isoflurane in oxygen. D-luciferin at 15mg/ml in complete media was injected through the port of each animal with a 100µl microsyringe and a PNP 3M injector accounting for

dead volume so that 50ul of D-luciferin reaching the gel. An IVIS Spectrum Xenogen 5000 (*In Vivo* Imaging System, Perkin Elmer) was used for imaging. Animals were maintained under anaesthesia with 3% isoflurane delivered through a nose cone during imaging. A sequence was acquired with the following settings; luminescent automatic exposure with a target count of 3,000 and a field-of-view set to D (automatic exposure preference range values were set to the following; exposure time: 0.5-170 seconds, binning: 1-8, F-stop: 1, field-of-view D, no delay between images). The sequence was terminated once the signal was seen to drop. The automatic circular region of interest (ROI) tool from Living Image software was used to calculate the total flux of light in areas of interest (photons/sec).

For the fluorescence images (macromolecule delivery) one image was taken for each timepoint at the following settings; automatic exposure, emission 820nm, excitation 745nm (exposure 0.5 seconds for direct injection or 120 seconds for IP injection, binning 8, field of view D, f stop 2). The automatic circular region of interest tool was used to calculate the total flux or radiance at the heart.

2.3.6 Statistical Methods

To choose sample size the following methods were used. A pilot study was performed to determine the mean and standard deviation in bioluminescent measurements at all timepoints for both conditions. This data was used to determine an adequate sample size (n=5) for a sufficiently powered study to show significant difference between the pre-refill and post-refill groups. The following exclusion criteria were pre-established; cells in the simplified *Therepi* were assessed for viability *in vitro* prior to surgery by measuring their bioluminescence with the IVIS spectrum. Devices with bioluminescence less than 10^9 photons/second were excluded. Male rats and rats below 225g or above 275g were excluded. The following rats were also excluded; animals that did not survive the MI surgery, or animals that did not display blanching of the left ventricle on LAD ligation. For the PV loop data, measurement points that did not show a consistent PV loop due to catheter positioning or other reasons were excluded. No formal randomization was used.

2.4 Results

2.4.1 Realisation of the simplified *Therepi* delivery system in an animal model

Here, we introduce the initial prototype of the *Therepi* system, or simplified *Therepi*. Conceptually, this system allows for the targeted and replenishable delivery of biological therapy to a biomaterial in contact with diseased tissue, in this case the heart. In this set-up a macroporous methacrylated gelatin cryogel was used as the chosen biomaterial. It has a large, interconnected pore structure and diffusion would be expected to be unimpeded (Figure 2.7b[199]). Furthermore, the microstructure of preformed GelMA scaffolds have been optimised so they can be that can be introduced in a minimally invasive manner through a conventional needle (i.e. shape memory properties) (Figure 2.7b[199]). Therapy can be pre-loaded onto these scaffolds, before suturing to the epicardium. Alternatively, therapy can then be seeded onto the biomaterial *in situ* through the conduit.

First, a number of subcutaneous ports were investigated and tested. A subcutaneous port (Rat-O-Port, Access Technologies) was initially tested (Figure 2.7c). It could be placed under the skin, making it suitable for multiple housing without risk of damage to the port. However, the dead volume of the system (110μl) was large in comparison to the intended volume of cargo delivery to the heart (~50 μl). Excess volume delivery can cause cardiac complications including pericarditis and pericardial effusion. Next, we tested an externalised pin connecter at the neck of the rat. While this port had minimal dead volume, the animal tended to bite and remove the externalised port (Figure 2.7d). Finally, a mouse vascular access port (Instech) was chosen (Figure 2.7e). This port has a number of advantageous features including (1) a minimal dead volume (3μl) (2) a low profile 14mm disk of polyester mesh surrounding the port, allows for tissue integration and physical stabilization of the port following implantation. Such integration is important in order to avoid displacement of the system due to animal movement and biting (3) the port contains a self-sealing silicone septum, which couples with a specialized injector for facile repeat injections without risk of infection. Polyurethane tubing (C30PU-RJV1303, Instech Laboratories) was chosen as the implantable refill line due to its biocompatibility, resistance to kinking and moderate stiffness. An inner diameter smaller than the outer diameter of the metal barb of the refill port was chosen, so as to achieve a friction fit. It is envisaged that this connection will be suitable for the intended application as the internal diameter of polyurethane tubing narrows on stretching (similar to a Chinese finger trap), thus strengthening the bond.

Next, we implanted this system in a pre-clinical animal model. An overview of the tunnelling and implantation process is described in Figure 2.7f, with a detailed description available in methods section (Figure 2.1, Figure 2.2, Figure 2.3, Figure 2.4, Figure 2.5, Figure 2.6). In brief, a biomaterial was sutured to the epicardial surface of the heart, and a catheter was then sutured to the heart, such that its distal end was in contact with the biomaterial, and its proximal end was connected to a subcutaneous port. Such a configuration allows for replenishable, targeted delivery to the biomaterial and localized release of various cargo including drugs, macromolecules and cells (Figure 2.7a).
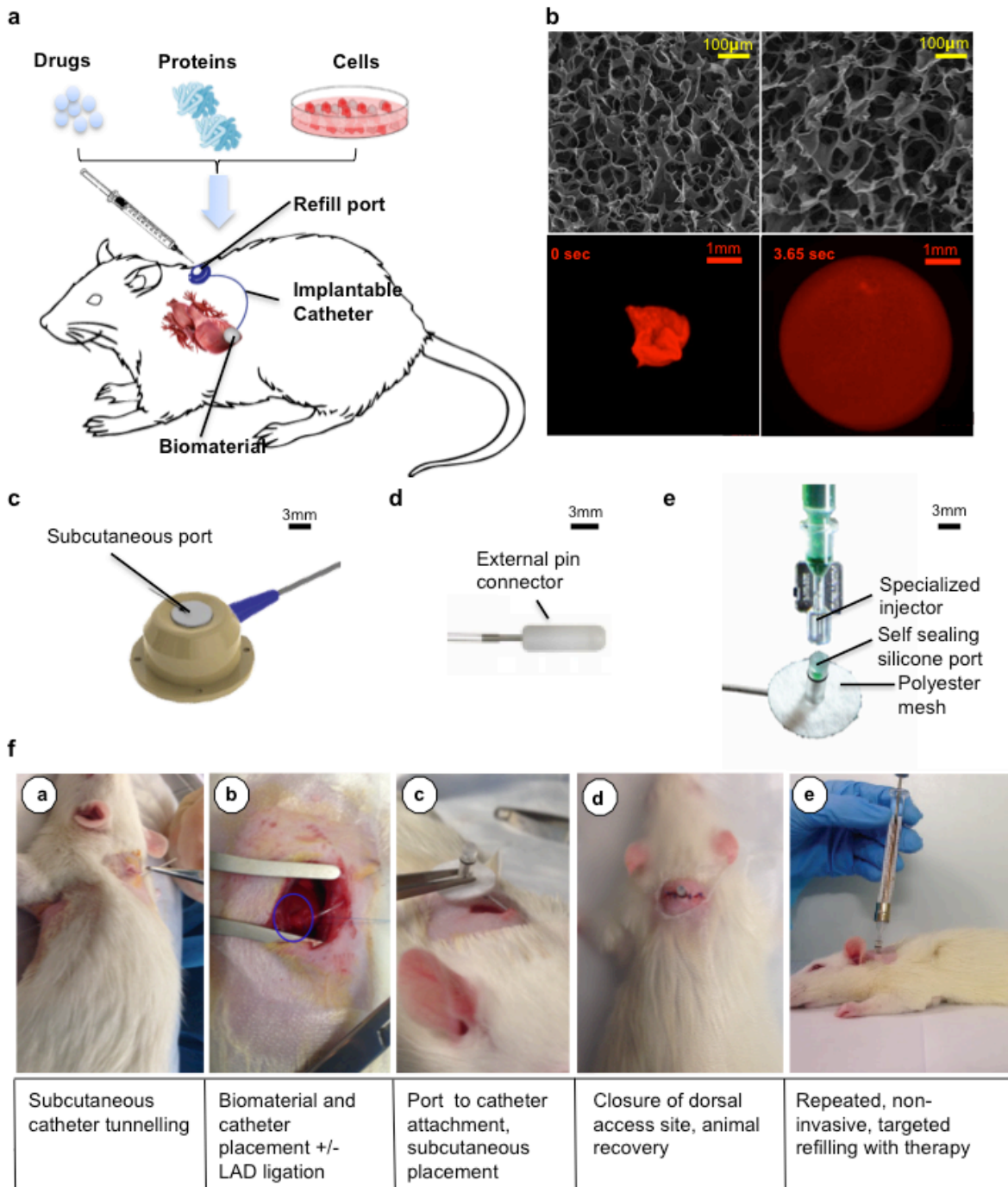
Figure 2.7: Overview of the simplified *Therepi* system
(a) Schematic showing a rat model with a biomaterial on the heart and an implanted catheter leading to the biomaterial that can be refilled with drugs, proteins or cells. **(b)** From left to right (top); surface and cross-section of methacrylated gelatin cryogel, from left to right (bottom), minimally invasive delivery of methacrylated gelatin cryogel using a 16 G needle **(c)** Subcutaneous Rat-O-Port **(d)** External pin-port **(e)** Vascular access button with polyester mesh **(f)** Overview of surgical and refill steps to create animal model.

2.4.2 Targeted delivery of small and macromolecules using *Therepi*.

First, we validated that the simplified *Therepi* system enables delivery of small molecules, and compared the pharmacokinetics of this delivery route to a standard intraperitoneal injection (Figure 2.8a). The imaging substrate D-luciferin was used as an analogue to demonstrate rapid, targeted delivery of small molecules to the heart. The GelMA disc was pre-seeded with luciferase-expressing mouse mesenchymal stem cells (mMSCs) before implantation, such that bioluminescence of the cells indicates the presence of D-luciferin. Direct delivery of the imaging substrate via the port produced a more rapid and intense bioluminescence, as compared to systemic intraperitoneal (IP) delivery (Figure 2.8b). The total dose of delivered substrate via the port was >70-fold less than the amount delivered systemically. However, delivery to the target, as evidenced by the bioluminescence (Figure 2.8c) and calculated by the area under the curve normalized by the dose, was dramatically enhanced with *Therepi* delivery (Figure 2.8d).

Next, we demonstrated that protein therapeutics could be delivered through the *Therepi*. A bovine serum albumin solution tagged with a fluorescent molecule (Vivotag 800) was delivered via the port. After three hours, there was a sustained concentration of the protein at the target site. The same amount of protein was injected IP as a control, but an undetectable quantity of the therapy had reached the target site after three hours; the fluorescence signal at the target was equal to background measurements for IP delivery (Figure 2.8e,f)
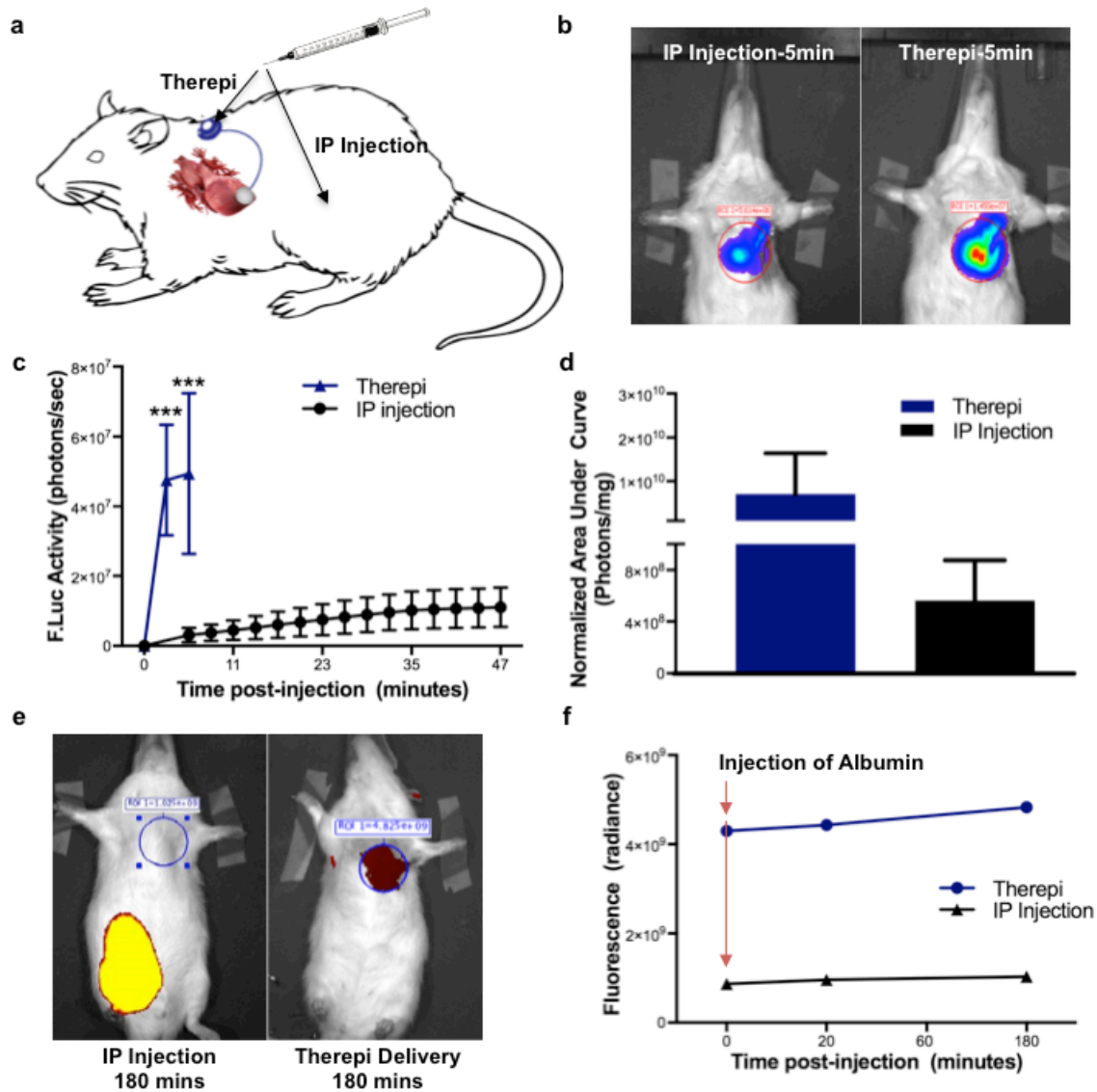
Figure 2.8: Delivery of small and macromolecules using simplified *Therepi*
(a) Schematic of *Therepi* in a small animal model **(b)** Representative bioluminescence of D-luciferin delivery to a simplified *Therepi* system compared to intraperitoneal (IP) injection. **(c)** Quantification of bioluminescence over time post injection of D-luciferin (n=5). ****P*=0.0011, unpaired, two-sided t-test between groups at that timepoint **(d)** Area under the curve, normalized by amount of injected D-luciferin, for IP vs. direct delivery of D-luciferin. *P*=0.2921. **(e)** Demonstration of macromolecule delivery using *Therepi*, Representative images 3 hours after fluorescently-labelled bovine serum albumin was injected using *Therepi* or into the IP space **(f)** Quantification of fluorescence at the heart at specific timepoints following *Therepi* or IP albumin injection.

2.4.3 Measurement of cell viability at multiple time points and demonstration of replenishable cell delivery using simplified *Therepi*.

As demonstrated in Figure 2.8, delivery of the imaging substrate luciferin in the presence of firefly luciferase expressing cells produces a bioluminescent signal. This signal can be directly correlated with cell number [204]. The ability to monitor cell number over time, and replenish cells to the simplified *Therepi* devices placed on an rodent heart was tested, using this system.

Luciferase-expressing mMSCs were pre-seeded on to the methacrylated gelatin biomaterial; this material was subsequently implanted on the rodent heart and connected to the *Therepi* port. The delivery of luciferin via the port directly to the biomaterial produced a rapid, potent signal (as shown in Figure 2.8). In addition, we were able to accurately follow bioluminescence (cell number) over time in the same animal, by precisely delivering luciferin via the port at multiple timepoints (Figure 2.9a). In comparison, systemic delivery of luciferin produced unreliable results when followed over time (data not shown). These inconsistencies can be attributed to a number of factors including (a) unintended intraperitoneal injection of luciferin to the gut, abdominal fat and subcutaneous tissue (b) variable core temperature of the animal under anaesthesia, which can affect luciferase activity and luciferin absorption (c) changeable first pass metabolism by the liver [205]. These inconsistent results demonstrate the inherent pharmacokinetic difficulties associated with systemic delivery.

At day four, one million cells were replenished onto the biomaterial through the subcutaneous port of the refill group, representative images for each time point can be seen in Figure 2.9a. Refilling resulted in a greater than ten-fold increase in the bioluminescence, representing the number of cells at the target site, as compared to non-reloaded gels (Figure 2.9b). The area under the curve for each group was calculated after background subtraction (Figure 2.9c) showing a significant difference between the "dose" of the cell therapy for the refill group.
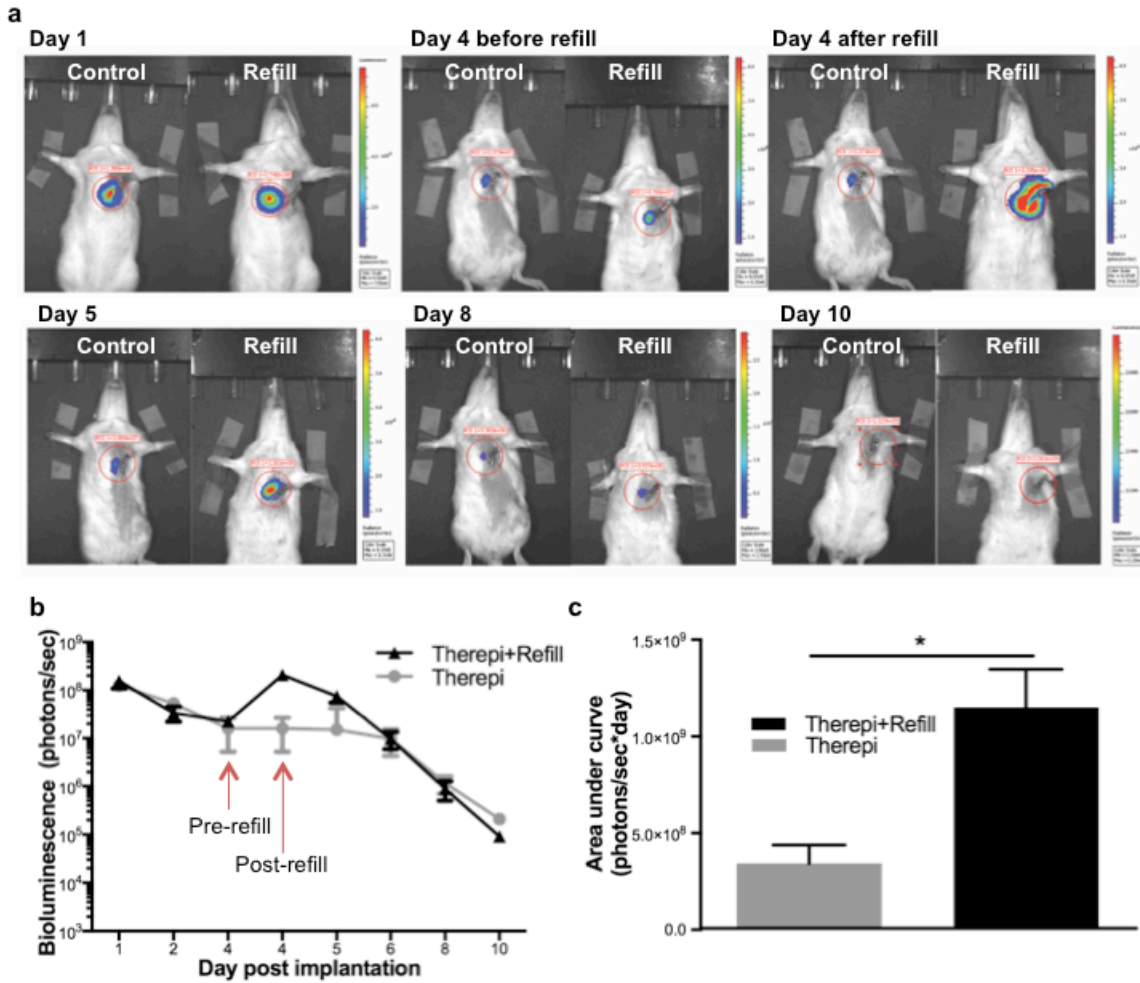
Figure 2.9: Measurement of cell viability at multiple time points and demonstration of cell refill with the simplified *Therepi* system

(a) Representative IVIS images for typical F-luc derived-bioluminescence from days 1 to 10 post implantation for the *Therepi* group without refill (control) and the *Therepi* group with refill at day 4 **(b)** Quantified Bioluminescence for the two groups following delivery of D-Luciferin using *Therepi* (data are mean ± SD, n=5) **(c)** Area under the curve for the group with and without refill; background bioluminescence was subtracted (data are mean ± SD, n=4 or 5, p<0.05 t-test), unpaired, two-sided t-test.

2.4.4 A method for the longitudinal measurement of cardiac function using a pressure-volume micro-conductance catheter.

We next developed a method enabling repeated measurements of cardiac function over time, for individual animals, using a mini-thoracotomy and the apical stick method (Figure 2.10a). This approach allows survival studies, with multiple analyses over time on each animal. Furthermore, the presence of cell therapy could be quantified at multiple days between implantation and as demonstrated in Figure 2.9, allowing us to relate cell dose to disease progression in the same animal.

Animals were not terminated after functional measurements, as is typically reported for the apical stick method (Figure 2.10b). Instead animals were survived for two weeks. At day fourteen another thoracotomy was performed at the fifth intercostal space. The PV catheter was re-inserted into the left ventricle through the apex of the heart, and hemodynamic measurements and calibration steps were repeated. A purse string suture can be placed if needed at the apical puncture suture, and tied after catheter insertion in order to stop excessive bleeding from the fibrous infarcted tissue (Figure 2.10c).

The results of cell refill using mMSC in a rat infarct model were then functionally quantified using this new hemodynamic analysis. Representative pressure volume loops for healthy and infarcted animals are shown in Figure 2.10d,e. There were three groups in this study; (i) in the control group an infarct was created, but no *Therepi* was implanted, (ii) in the second group (*Therepi* – refill), *Therepi* pre-loaded with cells was implanted, but not refilled for the duration of the study, (iii) in the third group (*Therepi* + refill), *Therepi* pre-loaded with cells was implanted and refilled with cells on day 4. The results of the hemodynamic measurements show that there was a tendency for the left ventricular ejection fraction to improve for *Therepi* + refill group. It was maintained constant for the *Therepi*–refill group. In contrast, the ejection fraction was decreased for the control group. This positive result indicates that the delivered cells may prevent early post-MI negative remodelling (Figure 2.10f).

a
— Thoracotomy in 4th IC space
PV catheterization through apical stab
Record baseline
Vena cava occlusion
Hypertonic saline injection
Create infarct
Verify infarct with catheter
Close chest and recover animal

— Thoracotomy in 5th IC space
Placement of purse string suture
PV catheterization through apical stab
Record 2 week data
Vena cava occlusion
Hypertonic saline injection
Heparinize, euthanize and collect blood
Calibrate with cuvette immediately

0d 1d 4d 7d 10d 14d

— Anesthesia, deliver luciferin through port, IVIS image, ± refill of therapy

b

c
Purse-string suture
Catheter Puncture site

d Healthy PV loop
Pressure (mmHg) vs Volume (mL)

e MI PV loop
Pressure (mmHg) vs Volume (mL)

f
Ejection Fraction (%)
Baseline / 2 weeks
No Treatment / Therepi +Cells / Therepi +Cells +Refills

Figure 2.10: Repeated functional measurements in a MI model with the *Therepi* system.
(a) Experimental timeline. Briefly, the infarct creation, device implantation and hemodynamic measurements were conducted at day 0, imaging was conducted at intermediate days, and hemodynamic measurements, experiment termination and calibration were conducted at day 14. **(b)** Schematic of apical stick hemodynamic monitoring method (adapted from Pacher et al[53]). **(c)** Photos from the surgery showing placement of a purse-string suture at the catheter puncture site, to prevent excessive bleeding. **(d)** Representative pressure-volume loop at baseline and **(e)** after MI. **(f)** Ejection fraction (data are mean + SD, n=5 rats, 2-way ANOVA with multiple comparisons and Tukey post-hoc

46

correction). The experiment was completed once each on a total of 15 rats.

2.5 Discussion

In this chapter, we present a delivery system that allows targeted, replenishable and sustained presentation of cellular and molecular therapy to the heart. A biomaterial-based reservoir (gelatin cryogel) initially seeded with luciferase expressing mouse mesenchymal stem cells, was attached to the epicardial surface of the infarcted rat heart. Gelatin, derived from the partial hydrolysis of collagen, contains natural binding motifs to facilitate cell attachment [199]. Due to its biocompatibility, non-toxicity and previous use in the medical fields as a wound dressing and haemostatic device, it is an attractive choice of material for *Therepi* [206]. However, we foresee that this platform can be extended to other biomaterials that have demonstrated an ability to increase cell retention at the heart (e.g., alginate [91], chitosan [89], hyaluronic acid-based gels [84,94], gel foam [83], collagen [5,102]).

An implantable catheter was used as a conduit between this reservoir and a subcutaneous port located at a dorsal site of the rat. The biomaterial reservoir could be refilled with cells through the port at defined time points, increasing the resident cell number 10-fold. Although just one refill was conducted *in vivo*, the possibility for multiple refills and replenishments with similar or different therapies exists. Furthermore, attaching the catheter to a small implanted, refillable pump [207,208] (for example Bioleonheardt's Stem cell pump[136]) would enable a sustained infusion (depicted in Figure 2.11). The ability of the system to allow targeted injection of molecular therapies directly to the biomaterial reservoir in contact with the heart was demonstrated by delivering bovine serum albumin and the imaging substrate D-Luciferin through the subcutaneous port, both indicating a rapid, localized delivery of therapy, which can improve efficiency of drugs and reduce off-target adverse effects.
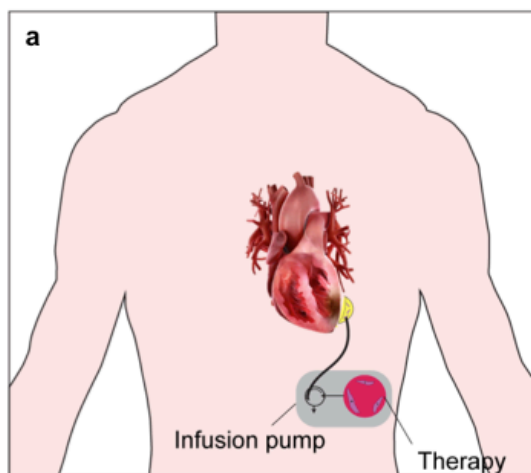
Figure 2.11: Sustained infusion of cell therapy
(a) Implantation of an infusion pump in the abdomen connected to the *Therepi* would allow continuous refill of cells or media of the biomaterial

The pericardium is a fluid filled sac that forms a natural barrier surrounding the heart. Targeting drugs directly to the heart by delivering to the pericardial space or epicardium may be a favourable strategy to obtain higher drug efficiencies, while lessening the side effects. Oral formulations are the most common and patient

acceptable method of drug delivery; however they have many inherent limitations including incomplete absorption through the gastrointestinal mucosa, poor bioavailability and poor compliance [209–211]. IV administration overcomes these issues by bypassing absorption and first pass metabolism. However, for both oral and IV delivery, inter-patient pharmacokinetic variability can cause extensive deviations in the amount of drug that reaches the desired molecular target, and significant quantities of drug reach off target sites, potentially causing side effects [207,212]. This is a particularly important problem for drugs with a narrow therapeutic index, as a high concentration could cause toxic side effects while a low concentration could eliminate any clinical benefit. Localized delivery confers the advantages of greater control over desired tissue exposure, decreased variability of clinical response, lower needed therapeutic doses, and opportunities to use bio-agents with a short half-life or that are biologically incompatible with the gastro-intestinal tract and blood stream (e.g., cells and their secreted paracrine factors). The efficacy of intrapericardial drug delivery to the heart has been studied for angiogenic substances [124] and vasodilators [125] as well as rhythm management drugs (anti-arrhythmic, arrhythmic agents [122,123]). Hermans *et al* [208] used a chronic administration animal model to show pharmacokinetic advantages in the rat with IPC infusion. Van Brakel *et al*, showed that this technique improved the efficacy of β-blockers sotalol and atenolol compared to IV administration [207]. However, easy and reproducible access has been a major limiting factor for IPC delivery. The direct, refillable device demonstrated in this report suggests clinical translation of IPC drug delivery may be readily obtained. In a broader sense, this soft system provides a platform for delivery to other diseased tissues as well, for other therapeutic regimens with a narrow therapeutic index.

In terms of clinical translation, the *Therepi* device and its method of implantation and functional monitoring have potential to prove extremely beneficial for enabling sustained delivery of the paracrine factors released from transplanted cells in close proximity to the diseased tissue of the heart, and for allowing further research studies of the effect of multiple administrations of cells that have previously been impossible due to the prohibitive nature of multiple invasive surgeries. Furthermore the system enables the multimodal localized delivery of different molecular therapies (cells, small molecules, macromolecules) in an attempt to mimic or modify the inherently complex physiological and pathological processes in the heart. In addition to temporal control, multiple reservoirs would enable spatial control, and multimodal treatment regimens to different parts of the heat; for example delivery of pro-regenerative therapy to the left ventricle, and anti-arrhythmic therapy to the left atrium. Finally, the device may be implanted without therapy and filled with its therapeutic cargo non-invasively after a certain amount of time. This is advantageous for previously reported work with autologous stem cells[47], when, for example, a biopsy could be taken at the time of implantation of the *Therepi*, then stem cells would be cultured and expanded and re-implanted through the *Therepi* after a number of weeks or months without the need for an additional surgery.

To maximize potency of cell therapy, systems that can longitudinally monitor viability and function of transplanted cells *in vivo* would be beneficial [107]. The system described in this report addresses this need by having additional utility as an enhanced imaging method for quantifying cell number on the heart. In this case, luciferase-expressing cells are used, and D-luciferin can be injected directly through the *Therepi*, requiring much less substrate, and reducing the duration of time the animal is under anaesthesia. This represents a

considerable advantage in terms of convenience, cost, consistency and time taken to conduct animal imaging. It allows imaging in less than five minutes with 50μl/0.75mg of D-luciferin, compared to IP injection that can require more than 45 minutes for D-luciferin circulation, and up to 3.5ml/52.5mg of D-luciferin. This facilitates more frequent imaging, and a more accurate pharmacokinetic profile. This system can also be used, if desired, for injection of media or nutrients into the reservoir to prolong cell survival. Biosensors could also be injected and retrieved locally to monitor biomarkers indicative of disease. The potential of the system for monitoring and feedback is vast.

Some study limitations should be acknowledged. The functional results shown above, while demonstrating positive trends, are too preliminary to assess if therapeutics delivered in this manner can positively influence cardiac function. A higher-powered study is needed to ensure that the differences in ejection fraction are due to effects of the therapy rather than the natural neovascularization that occurs in varying degrees post-MI. Furthermore, these measurements were taken at 2 weeks and cardiac remodelling is still very active during this time. The results should be compared against the current gold standard treatment, a one-time injection of stems cells in a saline vehicle, which has been shown to improve cardiac function in pre-clinical models[5]. Finally, a cell free Therepi should be included in order to examine the inflammatory/fibrotic response as a result of device implantation. Moreover, mechanical restraint and reinforcement of the infarct zone by the biomaterial could be advantageous, and should be investigated [165,213,214].

MRI and echocardiography are the current clinical gold standard for evaluating cardiac function and subsequent outcomes[215], and though pressure volume loop analysis would be superior in terms of hemodynamic assessment via direct pressure measurement[216], there are some caveats. Echo and MRI allow for repeat assessments of cardiac function in a non-invasive fashion[215]. Pressure/volume measurements via the apical stick method, as described requires additional disruption in the myocardium in order to obtain LV hemodynamic measurement and repeated measurements may potentially confound the detection of myocardial scar depending on the amount of injury. Furthermore, MRI has a significant advantage in visualizing myocardial scar post-MI with high sensitivity and specificity, as well as allowing for serial assessment of transumural myocardial injury and remodelling[217]. Future work will look to use PV measurement in conjunction with Echocardiography and/or MRI in order to corroborate hemodynamic parameters such as ejection fraction and will provide additional data such as wall thickness, mass and chamber size.

In general, implantation of biomaterials, medical devices or prostheses in vascularized tissue leads to the development of fibrous tissue encapsulation, generating a barrier to delivery[218]. This end stage healing response, generated by foreign materials and the friction of the device against the moving epicardial surface could be fatal to the long-term delivery of paracrine factors from the therapeutic reservoir. According to Fick's first law, release of paracrine factors will decrease with an increasing fibrotic capsule or diffusion gradient[219]. While d-luciferin and luciferase bioluminescence is a rapid and accurate method for identifying drug/cell delivery at the desired target site, it does not provide a three-dimensional image of protein or small molecule, penetrating the fibrous capsule and uptake into the heart tissue. Future work will look to examine the 3D distribution of therapy following delivery, and confirm penetration of therapy through the formed

capsule into the heart tissue. It is feasible that fibrous capsule formation will not hinder diffusion initially, when the therapy is most needed. Even, after that time frame, it is reasonable to suggest that small molecule diffusion will not be inhibited. Previous studies have shown that MSC's in some context are anti-inflammatory[220], so they may mediate some adhesions.

We can draw five conclusions from this study; (i) implantation of the biomaterial on the heart with a conduit connecting the reservoir to a subcutaneous access port is possible in a rat model, (ii) the implanted system constitutes a rapid, inexpensive and safe method for bioluminescent quantification of cell number by direct administration of imaging substrate during *in vivo* imaging (iii) the system enables non-invasive replenishment of cells to the Therepi and improves cell number at the site, (iv) the technology also allows rapid, targeted delivery of macromolecules and small molecules directly to the site, (v) a method for longitudinal hemodynamic measurements using a pressure-volume catheter with the apical stick method can be used to quantify cardiac function in a survival animal model.

3 Process development, optimisation and validation for a soft, encapsulated biomaterial reservoir that localises cells and allows for sustained release of cardiac therapy

3.1 Preface

In Chapter 2, we introduced "*Therepi*"(a **Ther**apeutic **Epi**cardium) and developed a representative pre-clinical animal model. In this model, a biomaterial was attached to the epicardial surface of the heart and connected to a subcutaneous port via an implanted refill line. We subsequently demonstrated replenishable delivery of small molecules, proteins and cells using this system.

Chapter 3 focuses on aim 2 of my thesis. The chapter describes design, optimisation and process validation for a biomaterial reservoir. In this design, the biomaterial is encapsulated by a soft flexible shell and is separated from the heart tissue by a semipermeable membrane. As in chapter 2, the reservoir will be connected to a subcutaneous port via a conduit, enabling multiple refills of therapy with temporal and dosage control. This reservoir is designed to maximise transplanted cell retention and survival in comparison to the biomaterial alone, enables protection from the host immune response and permits the sustained delivery of therapy to the infarcted heart. Modifying the membrane pore size can limit the size of therapy diffusion, such as cells, or could be used to control the rate of molecule diffusion into tissue. Finally, we optimised the manufacturing process towards the creation of an "off the shelf" device for pre-clinical testing and towards clinical translation.

The aims of the chapter are as follows

1. Process development for a biomaterial reservoir, comprising a biomaterial surrounded by soft flexible shell and separated from the heart by a semipermeable membrane.
2. Optimisation of the manufacturing process for pre-clinical testing and towards clinical translation
3. Validation of a soft encapsulated biomaterial reservoir that localises cells, provides immune protection and allows for the sustained release of cardiac therapy.

3.2 Introduction

In chapter two, we introduced *Therepi*: a biomaterial connected to a subcutaneous port via an implanted refill line, enabling multiple replenishments with precise control of both timing and dose. A critical component of our approach is the biomaterial, which first receives the delivered cargo, and then locally releases therapy in a sustained manner to the diseased tissue. Phosphate buffered saline is the current clinical gold standard vehicle for regenerative cell therapy in the heart. This vehicle, while simple and safe, offers little protection to its precious cargo before, during and after delivery. Furthermore, saline lacks the necessary physiochemical properties to locally delivery and retain cells at the pathological site, and doesn't provide biological and mechanical cues for anchorage dependent cells [5].

In comparison, biomaterial delivery vehicles significantly enhance cell retention and survival in the heart, as shown by extensive pre-clinical work [83,84,93,94,85–92]. Bioengineered materials can act as a surrogate extra-cellular matrix (ECM) for it's cellular payload[222], and modification of parameters, such as morphology[80],

stiffness [81] or surface chemistry[82] can be used to control cell phenotype and thus paracrine secretome in the biomaterial microenvironment [62]. Furthermore, pore size can be modified to alter release kinetics of small and macromolecules through the matrix [104].

However, the *in vitro* design and functionality of the exogenous cell/biomaterial systems can be compromised once exposed to the body. Nonspecific protein adsorption and immune/inflammatory cell infiltration can impair therapeutic functionality, with the magnitude of response dependent on implant properties such as (1) length of tissue contact, (2) rate of degradation, (3) pore size. (4) shape and morphology, (5) sterility (6) allogeneic or xenogeneic constituents[218,223]. In the case of simplified *Therepi*, infiltration of immune cells such as macrophages, and formation of a fibrous capsule around the biomaterial led to reduced cell viability over time and impaired the replenishment efficiency at later time points. Furthermore, delivering cells to an inflammatory environment such as the failing heart post MI, can limit their reparative efficacy [224]. Mesenchymal stem cells can sense their environment and act accordingly [225,226], with either an anti-inflammatory response that can promote repair, or a pro-inflammatory phenotype which can lead to deleterious tissue remodelling [227,228]. With this in mind, the ability to isolate the biomaterial from the *in vivo* immune response and the localisation of cells (or other therapeutic cargo) in a distinct controlled environment would be clinically desirable.

One promising strategy involving macro-encapsulation is gathering significant interest for the purposes islet delivery in the treatment of diabetes[229]. Aptly named "Trojan Horses", these encapsulation devices are composed of a biomaterial core with a cellular payload surrounded by a synthetic, semipermeable membrane. Membrane pore size can be tuned to form an immunological barrier but allow release of healing paracrine factors. Importantly, the encapsulated biomaterial can be isolated from the inflammatory environment of the infarcted heart and the host foreign body response with this approach. The ability to regulate the interaction between the body and the transplanted cells allows for greater control following delivery and replenishment. Complete immune-isolation could potentially enable the use of allogeneic or xenogeneic cell sources, without the need for immunosuppression. In addition, advances in cellular engineering e.g. induced pluripotent stem cells could be harnessed without fear of tumorigenesis.

This chapter describes the development of a biomaterial reservoir, composed of a biomaterial core, surrounded by an outer impermeable soft shell, and separated from the heart tissue by a synthetic semipermeable membrane. As in chapter 2, this reservoir is connected to a subcutaneous port via a conduit, which enables multiple refills of therapy, exogenous nutrients or imaging substrate for the longitudinal quantification of cell number. The soft impermeable shell is designed to provide structural support while preventing cell loss from mechanical washout. The semipermeable membrane is engineered to allow for the bidirectional movement of oxygen, nutrients, and cellular proteins, but prevent the inward migration of immune cells responsible for the reduced viability of allogeneic cells (Figure 3.1). In a further refinement, the membrane pore size is readily interchangeable in a range of defined pore sizes, thus offering a method to tune the rate of therapy diffusion into tissue, and the size of molecules permitted through the membrane.
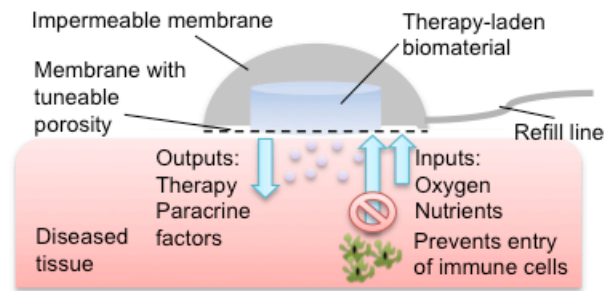
Figure 3.1: *Therepi* **biomaterial reservoir mechanism of action**
Schematic showing how the biomaterial reservoir works. The therapy-laden biomaterial is encapsulated between two layers, allowing selective and controlled diffusion of therapy on to the tissue, and offering mechanical and immunological protection to the therapy.

3.3 Process development for an immunoisolated biomaterial reservoir

3.3.1 Custom membrane manufacture

Initially, we attempted to design an in house thermoplastic membrane with a pore size of 1 micron. To place this size in context, mesenchymal stem cells exhibit a size distribution between ~15-30μm[230]. Initial attempts using a Versa CO_2 laser equipped with a high power density focusing optics lens (HPDFO, Universal laser systems) and a custom designed diode-pumped solid-state laser[231] (Oxford Laser Systems) were unsuccessful due to equipment resolution. Pore size was confirmed via microscopy.

For future work, an elastic thermoplastic membrane with defined pores would be desirable, as it would simplify the manufacturing process, and ensure a robust finished device with homogenous material properties throughout the system.

3.3.2 Assessment of commercially available membranes

Given the difficulty of manufacturing custom-made TPU membranes, we explored the incorporation of commercially available membranes into the device manufacturing process. It was envisaged that an off-the-shelf, optimised membrane would be suitable for initial proof of concept. Membranes (Table 3.1) were initially selected for testing based on the following desirable properties (a) cell biocompatibility, (b) low protein binding, (c) a defined interchangeable pore size and (d) mechanical properties.

Table 3.1: List of commercial membranes used in pull-off testing

Membrane	Manufacturer
Polycarbonate	Cyclopore, Whatman, GE Healthcare Life Sciences
Polyethersulfone (PES)	Sterlitech corporation
Polysulfone (PS)	Acrodisc syringe filter, Sigma-Aldrich
Acrylic copolymer	Versapor membrane, Pall Corporation
PTFE	Corning syringe filter, Sigma-Aldrich
Nylon	Corning bottle top vacuum filter, Sigma-Aldrich

Following initial selection, we assessed each membrane for its ability to thermally bond to thermoplastic polyurethane (TPU), We envisaged that our soft impermeable shell would be composed of TPU. Test membranes were sealed as an intermediate layer between two TPU layers using a heat press (325°F, 10 s) (Figure 3.2a). Peel testing was subsequently performed using a mechanical tester in accordance with a standard test method[232] (Instron 5566 tester, 100N load cell). The unbonded TPU layers were clamped into opposing tensile grips and the Instron was set to extend at a constant rate (25mm/minute) (Figure 3.2b). A polycarbonate membrane (Cyclopore, Whatman) achieved the greatest membrane bond strength and was closest to the TPU control (Figure 3.2c). Given this high bond strength, we proceeded to test this membrane for compatibility with the *Therepi* manufacturing process and the intended end use.

Next, we examined the biocompatibility of the membrane, by seeding both sides of the membrane (shiny/smooth and dull/rough) with mouse mesenchymal stem cells transfected with Firefly Luciferase (Figure 3.2d). The bioluminescent signal of the cells, which can be correlated with cell number [204], tended to increase over time for dull rough side and slightly decreased for the shiny smooth side, however this decrease

was not significant. These results indicate that the membrane is cell compatible, as supported by the literature[233].

To conclude, a polycarbonate membrane (Cyclopore, Whatman) was chosen. It has a sharply defined pore size and distribution created by the targeted irradiation of a thin film followed by chemical dissolution of these weakened areas. This pore size can be easily modified for different release rates or device functionality, with available pore sizes ranging from 0.05μm to 12μm. Furthermore, the membrane is compatible with the *Therepi* manufacturing process and the intended end use.
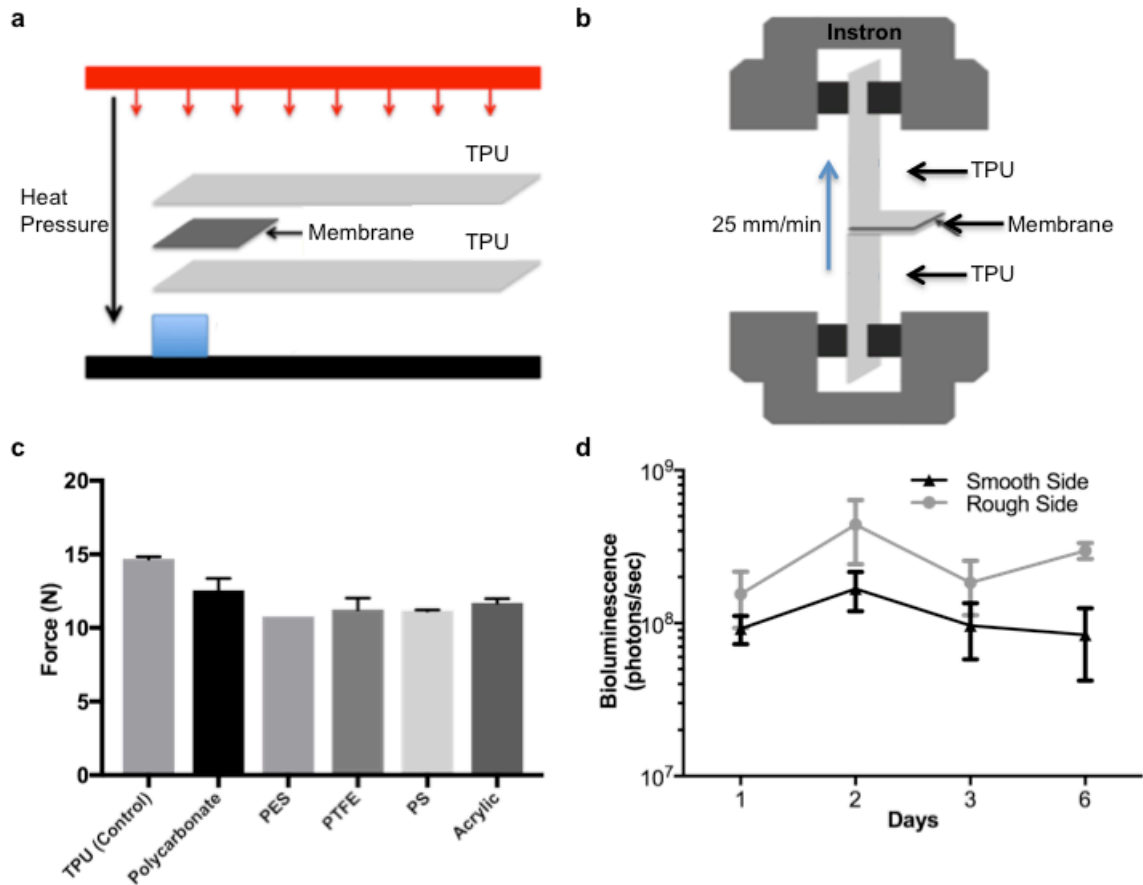
Figure 3.2 Assessment of commercially available membranes
(a) The test membrane was heat sealed between two TPU layers **(b)** Peel testing: TPU strips were clamped into the Instron with the sample membrane situated halfway between the two clamps. **(c)** Average of the maximum force required to delaminate TPU and membrane layers (n=4 for polycarbonate, n=2 for all other samples), data are mean + s.d. **(d)** Biomcompatibility assessment of cell seeded membrane using F.luciferase expressing cells (n=3). Data are mean ± s,d,

3.3.3 Biomaterial reservoir design and fabrication method

Here, we introduce the initial fabrication method for the *Therepi* biomaterial reservoir. In our design, a biomaterial is encapsulated by a soft flexible shell composed of TPU, and is separated from the heart tissue by a semipermeable polycarbonate membrane (Figure 3.3a). The reservoir is connected to a subcutaneous port via a conduit, enabling multiple refills of therapy with temporal control.

The initial fabrication methods for the device are shown in Figure 3.3. Briefly, TPU was used as an impermeable membrane (HTM 8001-M polyether film, 0.003inch thick, American Polyfilm, Inc.). A sheet of TPU was mounted in a vacuum thermal former (EZform SY 1917, Centroform) (Figure 3.3b). A 3-d printed mould (Objet Connex 500) was used as the positive mould and placed on the vacuum platform. The TPU sheet was heated until it sagged in the centre (Figure 3.3c). The heated TPU sheet was then formed over the positive mould. Vacuum was applied to the platform to ensure the sheet fully conformed to the shape of the mould (Figure 3.3d). The formed TPU was then placed in a negative mould. Dehydrated methacrylated gelatin cryogel was placed inside the formed reservoir. A laser cut TPU window (4mm diameter circle cut from a rectangle of 6mmx11mm), a circle of polycarbonate membrane (cylopore polycarbonate membrane, circle, black, 0.4 µm pore size, 14 mm, GE Healthcare Life Sciences) and another laser cut TPU window (4mm diameter circle cut from a rectangle of 6mmx11mm) were aligned and laid on top of each other on the assembly. The dull/rough side of the membrane was orientated to be in contact with the biomaterial and the shiny smooth side of the membrane was orientated to be in contact with the heart tissue. Furthermore, in initial tests, the rough side demonstrated a higher cell biocompatibility. The entire layup was heat-sealed with a heat press (Heat transfer machine QXAi, Powerpress) for 10 seconds at 325°F (Figure 3.3e). Next, a 3Fr polyurethane catheter trimmed to 10cm in length (C30PU-RJV1303, Instech Laboratories) was inserted into the inlet of the device, and UV curable glue (3943 Light Cure Adhesive, Loctite) was used to seal the catheter to the device. The glue was evenly applied around the neck of the catheter-device interface with a P-200 pipette tip. The glue was then cured by exposure to targeted UV light (Bluewave 50AS light curing spot lamp, 340-450nm, 3000mW/cm^2) for two 60-second intervals. The device was flipped between exposures (Figure 3.3f). The device was then sterilised by placement in 70% ethanol for 12 hours, followed by placement in filter-sterilised water for at least 24 hours.

Cells could be loaded in one of two ways. The refill line was used to load or replenish the biomaterial with cells when required (Figure 3.3g). Alternatively, a methacrylated gelatin cryogel preloaded with cells was inserted into the device at the terminal step. A number of changes were made to the manufacturing process in this alternate method. During the heat-sealing step (Figure 3.3e), one side of the device was left unsealed by placement of a Teflon strip in the layered assembly. The catheter was inserted and sealed with UV curable glue as previously described (Figure 3.3f). Next, the device without biomaterial was submerged in 70% ethanol for 12 hours, followed by placement in filter-sterilised water for at least 24 hours. The cell-seeded cryogel was inserted into the device via the unsealed edge in a sterile class II laminar flow hood. This unsealed side of was subsequently sealed using a heat press, in the laminar flow hood.
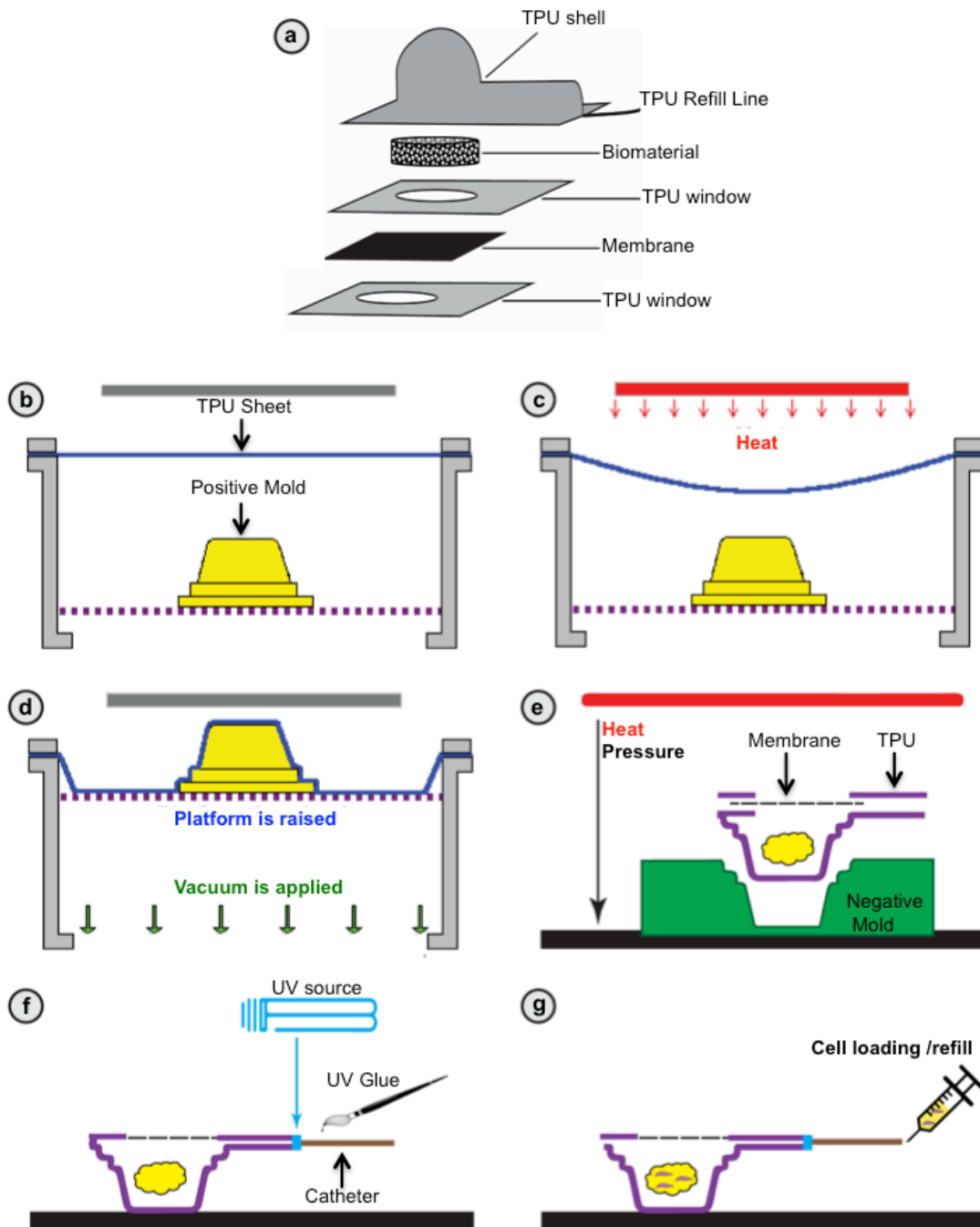
Figure 3.3: Initial manufacturing process for *Therepi biomaterial reservoir*
(a) Biomaterial reservoir design: A biomaterial is encapsulated between an impermeable TPU layer and a membrane with a defined pore size. The membrane is placed in between two TPU windows to secure it in place. **(b-g)** Biomaterial reservoir manufacturing process**: (b)** A thermo-plastic polyurethane sheet is mounted in a thermal former with a vacuum platform and a positive 3-D printed mould was placed on the platform. **(c)** The thermoplastic urethane sheet is heated until it sags in the centre. **(d)** The platform is raised and vacuum is applied so the thermoplastic sheet is formed over the positive mould. **(e)** The formed TPU is placed in a negative mould, and the biomaterial is carefully placed inside. A TPU window, a membrane and another TPU window is placed on top of the assembly and all are sealed together by applying heat and pressure. **(f)** A polyurethane catheter is inserted into the thermoformed channel in the device and is sealed in place with UV curable glue. **(g)** Cells are loaded and replenished

via the refill line

3.3.4   Initial assessment of biomaterial reservoir

First, refilling of cells *in situ* with the *Therepi* system was demonstrated. 10^6 F-luc MSCs were pre-seeded on the GelMA biomaterial and inserted into the *Therepi* system. At days 7 and 14, 10^6 additional cells were added to the system through the refill line, demonstrating the feasibility of multiple cell refills (Figure 3.4 a,b).

Next, we assessed the reservoir in an *in vivo* myocardial infarct rodent model using a xenogeneic mouse cell line. The ability to deliver and replenish cells to the *Therepi* device placed on an infarcted rodent heart was tested (Figure 3.4c). 10^6 F-luc MSCs were pre-loaded into a *Therepi* device, and at day 4, an additional 10^6 cells were refilled onto the biomaterial through the subcutaneous port. This refilling resulted in a greater than ten-fold increase in the bioluminescence, representing the number of cells at the target site, as compared to the devices before replenishment (Figure 3.4d). Representative bioluminescent images are shown for the refill at post-operative time points ((Figure 3.4e). This bioluminescence data demonstrates that that cell survival at the target site is prolonged compared to the simplified device as described previously in chapter 2 (14 days vs. 10 days), however similar decreasing trends in cell viability are shown over time, indicating lack of immune protection. In Figure 3.4d, a transverse slice was taken through both the device and the heart, stained with Haematoxylin & Eosin and analysed by a practicing cardiac/medical device pathologist. There was a significant foreign body response, (including macrophages, giant cells and vascularization) within the *Therepi* reservoir and surrounding the biomaterial. This indicates that the device is not fully sealed, or the seal degraded over time.
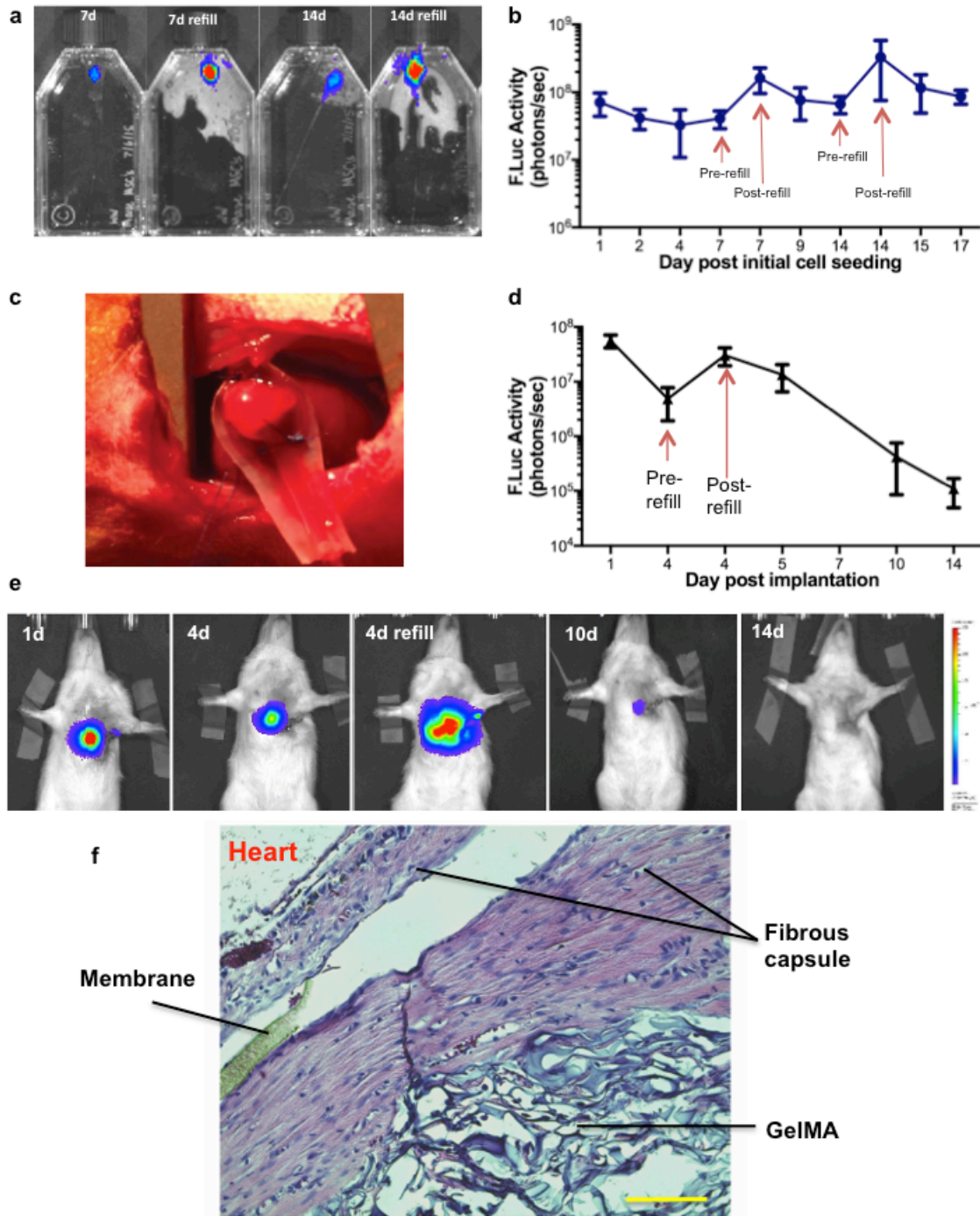
Figure 3.4: Initial assessment of biomaterial reservoir *in vitro* and *in vivo*.
(a) Representative bioluminescence of F-Luc cells in *Therepi* reservoir before and after cell refill at day 7 and day 14. **(b)** Bioluminescence of F-luc cells in *Therepi* reservoir with cell refills at day 7 and day 14. Data are mean ± SD (n=5 devices). **(c)** *Therepi* biomaterial reservoir attached to the heart with a suture. **(d)** Quantified bioluminescence of F-luc cells for *Therepi*+cells+refill, with refill at day 4 (n=5). **(e)**. Representative IVIS images of typical F-luc derived-bioluminescence at time points. **(f)** A histological image from an unsealed *Therepi* device shows a foreign body response (including vascularization, macrophages and giant cells) on the reservoir side of the membrane and surrounding the biomaterial, scale bar is 100µm.

3.4   Identification of manufacturing issues and proposed solutions:

Following *in vivo* assessment, it was apparent that the *Therepi* biomaterial reservoir, while extending cell viability in comparison to the simplified *Therepi,* did not offer immunological protection to the biomaterial and cells encapsulated within. We concluded that the device only offered physical protection to the cell-loaded biomaterial before, during and after surgery.

With the initial biomaterial reservoir design established, we then optimised the manufacturing process to provide both physical and immunological protection. Furthermore, we envisaged that the optimised device would be tested in a pre-clinical study, thus a consistent, reproducible fabrication process, moving towards an industrialized *Therepi* device was desirable. A number of key issues were identified and these are discussed below.

3.4.1   Manufacturing Issue 1: Inconsistent catheter bonding

It was observed during the manufacturing process that the bond at the catheter/reservoir interface was inconsistent. It was hypothesised that the manual process of inserting the catheter, applying the glue, and the UV curing step introduced huge variability to the process.

 To test this hypothesis, devices were manufactured using UV adhesive as shown in Figure 3.3 with one difference, the laser cut window was omitted from one of the TPU layers to form a "balloon" with two impermeable layers. This enabled quantifiable leak testing of the TPU seals. Each balloon was pneumatically pressurised using a custom made pneumatic control system [234], and the following parameters; 150 cycles, frequency of 0.25Hz, period of 2sec, and a pressure of 11psi. During testing, devices were submerged in water and a camera with a high frame rate was used to visualise the location of emerging bubbles and thus the specific site of device failure. An audible pop, evidence of bubbles, or a significant drop in readout pressure was deemed a device failure. In total, 43 devices were tested with 79% showing evidence of leaking. In addition to being inconsistent, the application and curing of UV glue was time intensive. Furthermore, the glue was susceptible to degradation during the ethanol disinfection process, and possibly elicited an enhanced immune response as device seals failed over time.

Implemented process solution: We developed a method of thermally bonding the catheter to the reservoir by applying heat and circumferential pressure to the thermoplastic polyurethane materials. No additive adhesives were necessary to achieve a consistent seal using this method.

3.4.2   Manufacturing Issue 2: Modification to the polycarbonate membrane during the heat-sealing process

The polycarbonate membrane and TPU layers were sealed by the uniform application of heat and pressure using a heat press. However, the glass transition temperature of polycarbonate (293 °F [235,236]) is similar to TPU, so it is difficult to bond the two materials without affecting the pore structure of the membrane. To illustrate this point, Figure 3.5 shows a scanning electron microscopy image of the membrane before and after the heat-sealing process, with the membrane pores exhibiting a heat response.
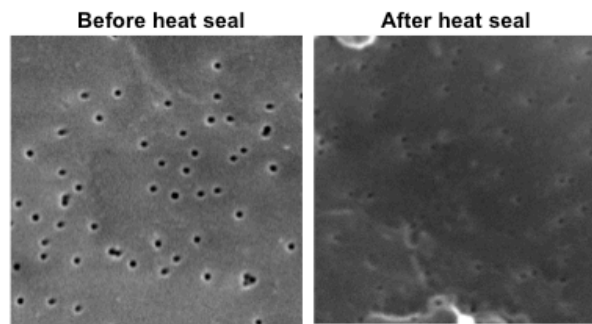
Figure 3.5: Polycarbonate membrane before and after the heat sealing process

Implemented process solution: We designed a method of heat-sealing the polycarbonate and polyurethane layers with greater spatial resolution so that heat and pressure was only applied where polycarbonate interfaced with TPU.

3.4.3   Manufacturing Issue 3: Material failure of membrane at a kink point during device bending

At the terminal point of the catheter, there is a sudden change in stiffness of the overall assembly creating a kink point. Bending of the reservoir (e.g. during attachment to the curved surface of the heart) creates a stress concentration at this point, resulting in material failure of the membrane.

Implemented process solution: We extended the catheter fully into the reservoir, so that the stress was distributed across the catheter and reservoir. Furthermore, we tapered the distal end of the catheter by creating a bevelled tip. This acted as a strain relief and ensured that there was a gradual change in stiffness.

3.4.4   Manufacturing Issue 4:   Challenges producing a sterile, consistently reproducible device suitable for pre-clinical testing

Pre-clinical testing involves device testing in large number of animals over a lengthy period of time.

Implemented process solution: To ensure consistency, and aid with logistics of conducting a pre-clinical trial, we endeavoured to optimise the manufacturing process towards a sterile device that could be stored until required. This optimisation included the following steps (a) use of a lyophilised or dry biomaterial that could hydrated during the cell seeding process (b) use of a suitable terminal sterilisation technique that did not affect the functionality of the device.

3.4.5   Manufacturing Issue 5: Attachment to the heart

Finally, appropriate attachment of the device to the heart was deemed critical to its intended therapeutic efficacy. Incorrect suture placement through the device could puncture the protective seal of the membrane, affecting shielding and isolation from the immune response. Furthermore, differing suture attachment could place different mechanical loads on the heart. Consistency in our approach was critical.

Implemented process solution: With this motivation, we developed a method to precisely place guide suture holes at three points of the device.

3.5 Process optimisation

3.5.1 Process optimisation: Formation of the TPU backbone

Key modifications:

(1) A small dental vacuum thermal former (Yescom Dental Vacuum Former, Generic) was used instead of a larger thermal former (EZform SY 1917, Centroform). A dental thermal former, with its small surface area and high vacuum was much more suitable for the production of small intricate designs, such as our device reservoir structure and catheter inlet.

(2) Holes were created in positive mould, so as to increase distribution of negative pressure during vacuum forming and ensure a consistent accurate thermoforming technique.

(3) A laser cut teflon strip was inserted into the channel to ensure lumen patency during the heat-sealing steps. This was important for two reasons: (1) a flat or planar design was essential to ensure complete sealing with the impulse sealer (later step). A 3D core to maintain patency such as a mandrel would have led to unsealed material near the lumen (2) precisely cut teflon strips (2mmx10mm) allowed us to easily insert the catheter tubing in a later step, without leaving too much space for movement.

Amended manufacturing process

The fabrication process for the formation of the TPU backbone is described in detail below and in Figure 3.6. Thermoplastic polyurethane (TPU) was used as an impermeable membrane (HTM 8001-M polyether film, 0.003 inch thick, American Polyfilm, Inc.). A sheet of TPU was mounted in a vacuum thermal former (Yescom Dental Vacuum Former, Generic). A 3-d printed mould (Objet Connex 500) was used as the positive mould. The positive mould was placed on the vacuum platform and the sheet was heated until it lost all its wrinkles (Figure 3.6a). The heated TPU sheet was then lowered over the positive mould. Vacuum was simultaneously applied to the platform to ensure the sheet fully conformed to the shape of the mould (Figure 3.6b). The formed TPU shape was then placed in a negative mould (Figure 3.6c). A Teflon strip was inserted into grove of the negative mould to keep the channel open during the proceeding heat-sealing steps (Figure 3.6d). A laser cut TPU window (4mm diameter) was placed on top (Figure 3.6e), and the assembly was heat-sealed with a heat transfer machine (Heat transfer machine QXAi, Powerpress) for 4 seconds at 330ºF (Figure 3.6f).
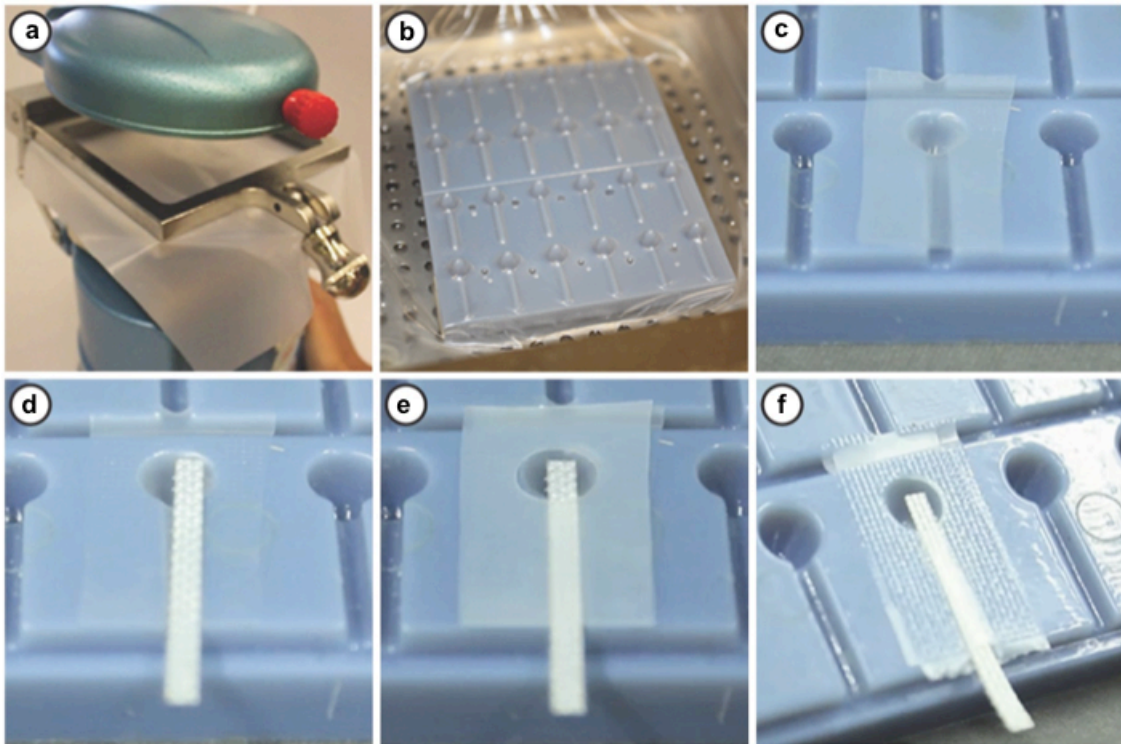
Figure 3.6: Formation of the TPU backbone
(A) A thermo-plastic urethane sheet is mounted in a thermal former with a vacuum platform and a positive 3-D printed mould was placed on the platform. **(B)** The thermoplastic urethane sheet is heated until it sags in the centre. The platform is lowered and vacuum is applied so the thermoplastic sheet is formed over the positive mould. **(C)** The formed TPU is placed in a negative mould. **(D)** A Teflon strip was inserted into grove of the negative mould to keep the channel open during the proceeding heat-sealing steps. **(E-F)** A laser cut TPU window was placed on top and the assembly was heat-sealed with a heat transfer machine.

3.5.2   Process optimisation: Membrane sealing

Key modifications:

(1) In lieu of attaching the membrane with a heat press, which applied uniform heat across the TPU and polycarbonate layers, an impulse sealer was used to attach the membrane. An impulse sealer allows greater spatial control in comparison to the heat press, so that heat and pressure was only applied where polycarbonate interfaced with TPU. Furthermore, the bond achieved by the impulse sealer was much stronger than the bond achieved by the heat press. This was easy to visualize as pull off testing caused material failure of the polycarbonate rather than delamination of both materials.

(2) Aligning the device and membrane with the metallic element of the impulse sealer made a straight-line seal. This was repeated on two other sides, leaving one side open for biomaterial insertion in a later step after terminal sterilisation of the device.   The biomaterial was inserted in an aseptic environment and the final opened side of the device could then be easily sealed using an impulse sealer in a tissue culture hood.

Amended manufacturing process

The fabrication process for the encapsulated device is described in detail below and in Figure 3.7. The TPU backbone was taken out of the negative mould and placed on an impulse heat sealer (H-2065 Deluxe Impulse Sealer, Uline) (Figure 3.7a). A circle of polycarbonate membrane (Cyclopore Track-Etched Membrane Filter, 13mm Diameter, 0.4 Micron, Whatman) was placed under the TPU structure. The assembly was aligned to the metallic element of the impulse sealer, and a piece of tape was used to keep the desired alignment during impulse sealing. Pressure and heat were applied using the impulse sealer by lowering the handle. Care was taken to wait for the assembly to cool before releasing pressure (Figure 3.7b). This was repeated for two other sides of the device, leaving one side open for biomaterial insertion in a later step (Figure 3.7c,d). Excess unsealed material at the perimeter of the reservoir and the inlet lumen was removed using a surgical scissors (Vannas Tübingen Spring Scissors, Harvard Apparatus) (Figure 3.7e). A final version of the reservoir (sealed at 4 sides, and dyed blue for visualisation) is shown in Figure 3.7f.
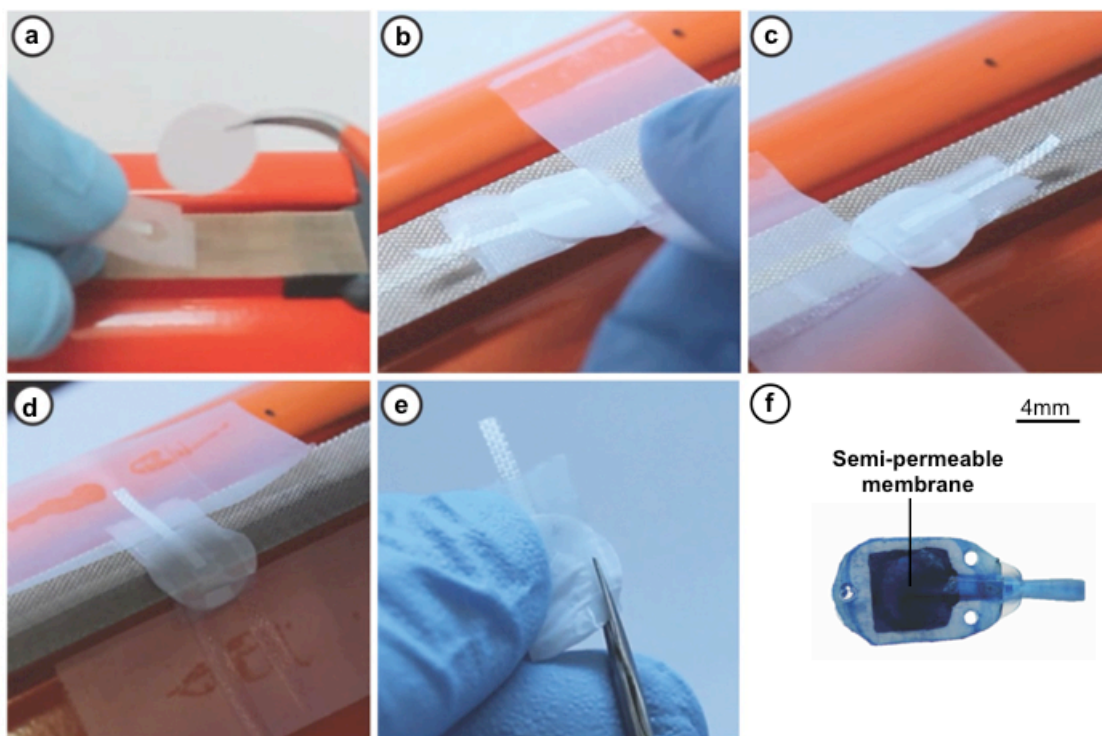
Figure 3.7: Impulse sealing of membrane to TPU backbone
(a) A circular polycarbonate membrane was aligned with the device window and tape was then used to align the assembly with the heat-sealing element of the impulse sealer. **(b-d)** The assembly was sealed at three sides, leaving one side open for biomaterial insertion in a later step **(e)** Excess material was trimmed from the device with a fine scissors **(f)** A finished device, dyed blue for visualisation of the semi-permeable membrane and the sealed edges created by the impulse sealer.

3.5.3 Process optimisation: Fabrication of a bevelled tip at the distal end of the catheter

Key modifications:

(1) The catheter was extended further into the reservoir, so that the tip touched the far wall of the reservoir, thus distributing bending stress cross the catheter and reservoir.

(2) Furthermore, we created a bevelled tip at the distal end of the catheter. This modification was to act as a strain relief and to gradually decrease catheter stiffness, and thus eliminate kink points and increase bendability of the system, so that it could wrap easily around the heart. We also envisaged that a bevelled tip would reduce the risk of catheter blockage.

Amended manufacturing process

The fabrication process for a bevelled catheter is described in detail below and in Figure 3.8. An aluminium block was etched with two lines, placed at a 30º angle to each other. The lines were etched at a depth and width so as to allow the snug placement of the catheter (Micro-Renathane® .040" x .023, Braintee scientific) and the stainless steel single edge razor blade (Accutec Blades, 0.23mm) (Figure 3.8a)

The catheter was placed in an etched line (Figure 3.8b) and held in place using a thumb and index finger (Figure 3.8c). The razor blade was aligned in the adjoining etched line (at a 30º angle to the catheter) and the catheter was cut with the blade (Figure 3.8d). The finished bevelled cut is shown (Figure 3.8e). A magnified view can be seen in Figure 3.8f. (Note, the catheter line has been enhanced by line sketching to improve image clarity against the background). Figure 3.8g demonstrates the *Therepi* reservoir conforming to the heart. In this Micro-CT image, the bevelled tip is extended into the pocket, and nestled in the biomaterial distributing the bending stress evenly.
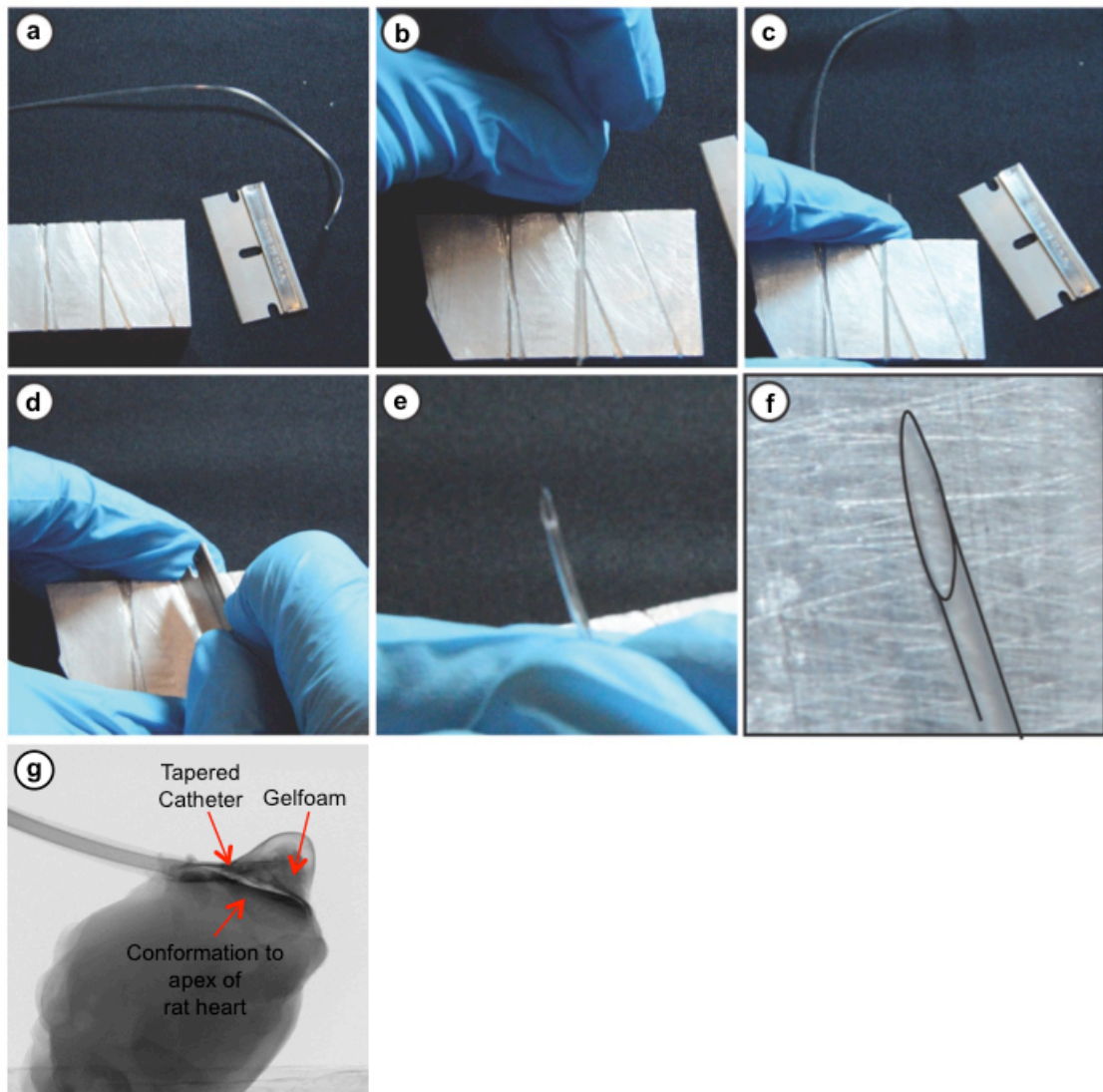
Figure 3.8: Creation of a distal bevelled catheter
(a) Components required for bevelling process: Catheter, single edge razor blade, aluminium block with etched lines for catheter and razor placement **(b)** Catheter is snugly placed in etched line and (c) held in place using thumb and index finger **(d)** the razor blade is aligned in the adjoining etched line, at a 30º angle to the catheter, and the catheter is cut with the blade **(e)** catheter with a reproducible bevelled cut **(f)** close in view of the bevelled cut **(g)** micro-CT of optimised *Therepi* on apex of rat heart, bevelled tip is extended into the pocket, and nestled in the biomaterial, distributing the bending stress across the reservoir.

3.5.4 Process optimisation: Catheter sealing to the biomaterial reservoir

Key modifications:

(1) We developed a method of thermally bonding the catheter to the reservoir. Heat shrink tubing was used to apply consistent circumferential pressure at the interface of the formed channel and the inserted catheter.

(2) A custom made PTFE coated mandrel was inserted into the catheter tubing to retain lumen patency when circumferential pressure was applied by the heat shrink tubing. The PTFE coating, with its low friction coefficient, allowed for easy introduction and removal without material damage.

(3) Heat was discretely applied to the heat shrink tubing via a conductive aluminium block with an opening for catheter insertion. This consistent, targeted application of heat (hot jaw method) would be difficult to achieve with other heating methods such as a heat gun, without damaging the integrity of the adjacent biomaterial reservoir and polycarbonate membrane.

(4) A thermoplastic polyurethane catheter (Micro-Renathane®, Braintee scientific) was used instead of the previous thermoset catheter (C30PU-RJV1303, Instech Laboratories).

Amended manufacturing process

The fabrication process for thermo-sealing the catheter to the reservoir is described in detail below and in Figure 3.9. The laser cut teflon strip was removed from the reservoir. A 10cm thermoplastic polyurethane catheter (Micro-Renathane® .037" x .023, Braintee scientific) with a distal bevelled end was inserted into the formed channel and the catheter was advanced until the distal end touched the wall of the reservoir (Figure 3.9a). A PTFE coated mandrel (0.02196 inch, type 304 S.S/54076, Applied Plastics) was inserted into the catheter to retain patency during the proceeding heal sealing step (Figure 3.9b). Heat shrink tubing (RNF-100-3/64-O-STK, TE Connectivity) was positioned at the unsealed interface between the catheter and the device (Figure 3.9c). The part was inserted into an aluminium block containing a 2.53mm diameter hole and the assembly was heated to 370ºF for 90 seconds with a heat press (Heat transfer machine QXAi, Powerpress) (Figure 3.9d). The part was removed from the aluminium block and the heat shrink tubing was cut away with a Vannas Tübingen Spring Scissors (Harvard Apparatus) (Figure 3.9e). The teflon-coated mandrel was removed, leaving a sealed catheter and reservoir (Figure 3.9f).

Catheter sealing validation

To validate this new heat sealing method, devices were fabricated using the procedure described with the following exception; a fully intact TPU layer was used in lieu of the TPU window and polycarbonate membrane, i.e. a mini TPU balloon was fabricated. Cyclical and burst pressure testing was then used to validate the catheter-balloon seal. A pneumatic control system was set up as previously described [234] (Figure 3.9g). Cyclical testing was initially performed; each device was pressured and then exposed to vacuum at a frequency of 0.66Hz, a period of 1.5sec, and a constant regulator pressure of 3psi for 150 cycles. The balloon was submerged in water. An audible pop, evidence of bubbles, or a significant drop in readout pressure determined device failure. All devices successfully passed cyclical pressure testing (n=6). Finally, the same devices (n=6) were subjected to ramp pressure testing. Pressure was increased at 2psi every 20 seconds until

extensive stretching and material failure. No material failure occurred at the catheter seal. Instead failure occurred at the at the point of thinnest material, where the reservoir had been thermoformed. (Figure 3.9g).
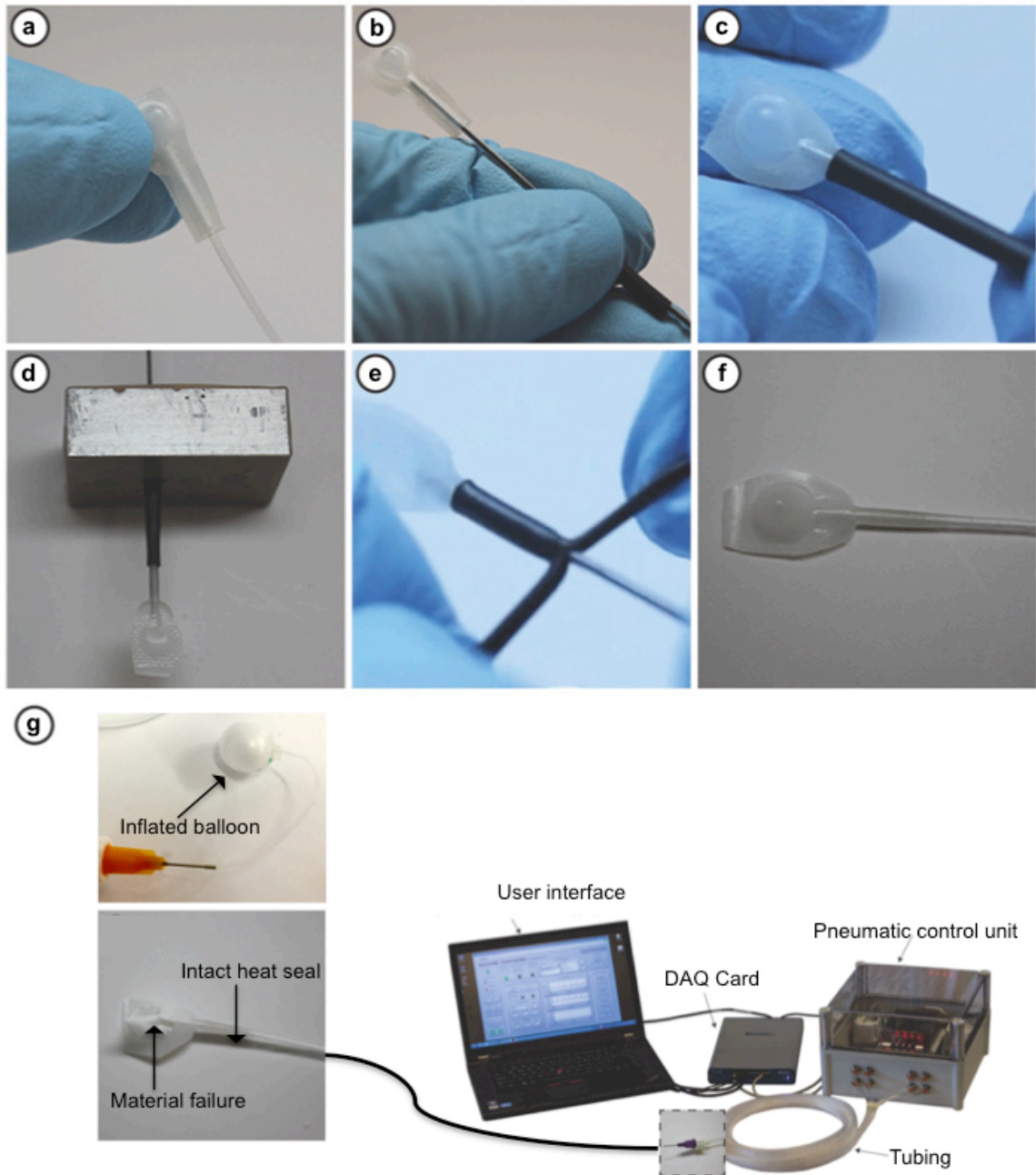
Figure 3.9: Catheter thermo-sealing to biomaterial reservoir
(a) The laser cut teflon strip was removed and a thermoplastic polyurethane catheter with a modified distal bevelled end was inserted into the formed channel. **(b)** A PTFE coated mandrel was inserted into the catheter to retain patency during the catheter healing process. **(c)** Heat shrink tubing was positioned at the unsealed interface between the catheter and the device. **(d)** The parts were bonded in a heated aluminium block, with the heat provided conducted by the block and pressure provided by the contraction of the heat shrink tubing. **(e)** The heat shrink tubing was snipped at the bottom at opposite sides and peeled away. **(f)** The PTFE coated mandrel was removed, leaving a heat-sealed bond **(g)** Left: Image of balloon before and after material failure. Right: pneumatic control system used to actuate the

balloons.

3.5.5 Process optimisation: Creation of guide holes for suture attachment to the heart

Key modifications:

(1) We developed a method to place guide holes for suture placement at the perimeter of the reservoir where TPU is present. This ensures that the suture does not damage the semi-permeable membrane at the centre of the reservoir during attachment, and that attachment to the heart is consistent between devices.

(2) A suture guide hole was placed at three points of the device, so that the semi-permeable is in direct contact with the heart tissue, and that healing paracrine factors can readily diffuse across membrane into heart tissue.

Amended manufacturing process

The process for creating suture guide holes is described in Figure 3.10. In brief, the device was aligned, and a Mazbot ®hole puncher was used to create 0.5 mm guide holes (Figure 3.10a). Holes were placed at three points of the device (Figure 3.10b), and did not damage the semipermeable membrane (Figure 3.10c). Figure 3.10d demonstrates suture attachment of the device to the heart utilising the suture guide holes.
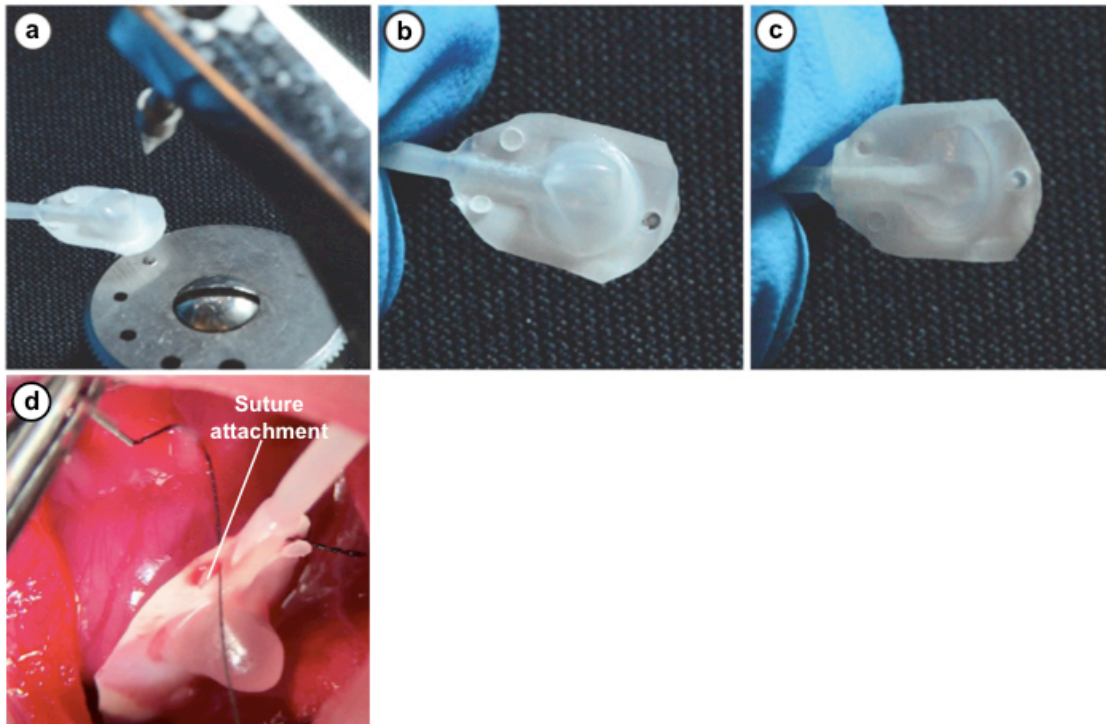
Figure 3.10: Creation of guide holes for suture attachment to the heart
(a) Device was aligned, and a Mazbot ®hole puncher was used to create 0.5 mm guide holes. **(b)** Holes were placed at three points of the device (posterior view of the device). **(c)** Holes did not damage semipermeable membrane (anterior view of the device). **(d)** Suture placement through device guide holes and heart tissue *in vivo.*

3.5.6 Process optimisation: Device sterilisation and biomaterial insertion

Key modifications:

(1) In the initial sterilisation method, the device was sterilised using the following protocol (1) Placement in 70% ethanol for 12 hours (2) Placement in filter-sterilised water for at least 24 hours. In lieu of ethanol, we aimed to terminally sterilise the devices using ethylene oxide, an alkylating gas that disrupts bacterial DNA, preventing reproduction [237]. This low temperature and dry sterilisation process does not affect the material properties of the device, and is a popular method for sterilising medical devices in industry with regulatory approved protocols (ISO 11135) [237]. Ethylene oxide can react with and reside in the porous biomaterial structure for a long period after sterilization. To address this issue, the device was sterilized without the biomaterial (one side of the membrane was left unsealed). After sterilization, the biomaterial was inserted and the remaining polycarbonate-TPU opening was sealed using an impulse heat sealer. These final steps were conduced in an aseptic environment in a class II laminar flow hood.

(2) We replaced the methacylated gelatin hydrogel with a lyophilised gelatin sponge. Importantly, a lyophilised or dry biomaterial can be placed in storage, and subsequently hydrated during the cell seeding process. Gelfoam® is available as off-the-shelf product, and has been approved for implantable use by the FDA (Figure 3.11a). Due to its biocompatibility, non-toxicity and previous use in the medical fields as an implantable haemostatic device, it is an attractive choice of material for *Therepi* [206]. Furthermore, it can be easily modified to an injectable formulation for minimally invasive delivery or replenishment of a biomaterial if needed in future iterations (Figure 3.11b). Gelfoam (like GelMa), contains a large, interconnected pores and diffusion would be expected to be unimpeded through them[199] (Figure 3.11c). Both biomaterials are composed of gelatin, which is derived from the partial hydrolysis of collagen and contains natural binding motifs to facilitate cell attachment [199]. We demonstrate similar long-term cell viability using F-luc expressing mouse MCS's seeded on both Gelfoam and GelMa. Interestingly, GelMa exhibits a drop off in cell viability at earlier time points followed by an increase later. In comparison, Gelfoam exhibits sustained cell viability throughout (Figure 3.11d). Cell seeding to the GelMa scaffold is completed in a dehydrated state, when the pores are collapsed. We hypothesise that a surplus of cells initially attach to the outer perimeter of the gel structure during this step. At earlier time points, some of these cells undergo apoptosis due to contact inhibition and lack of attachment sites. Eventually there is an increase in viability as cells migrate from the perimeter (where the pore size is smaller) to the inner macroporous centre [199]
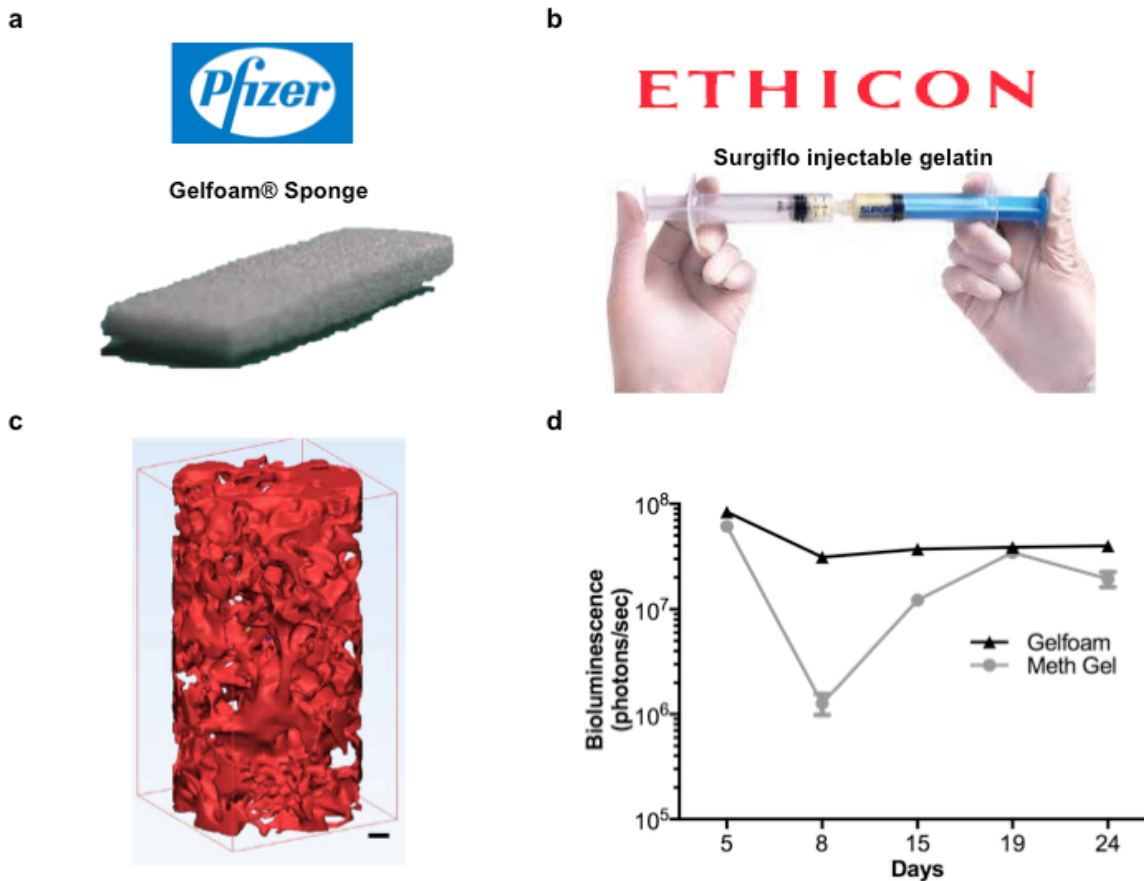
Figure 3.11: Biomaterial selection for *Therepi* reservoir:
(a) Absorbable gelatin sponge (Gelfoam®) sponge manufactured by Pfizer, adapted image[238]. (b) An injectable gelatin matrix (Surgiflo®) manufacture by Ethicon, adapted image[239]. (c) A 3-dimensional reconstruction of a cylindrical sample of Gelfoam® from a micro-computed tomography scan. Scale bar is 100μm (d) Quantified bioluminescence of F-luc cells loaded on GelMa and Gelfoam scaffolds over time.

Amended manufacturing process:

As described in Figure 3.7, the membrane was attached to the TPU backbone at three sides, leaving one side open for biomaterial insertion in a later step. Devices were then sterilised in a low temperature ethylene oxide cycle. Following sterilisation, the remaining steps were conduced in an aseptic environment in a class II laminar flow hood. A cylinder was cut from a gel foam sponge (Gelfoam Haemostatic, Size 12-7mm, Pfizer Pharmaceutical) using a 2mm disposable biopsy punch (Integra Miltex) and inserted into the device. The final polycarbonate-TPU opening was sealed using an impulse heat sealer (H-2065 Deluxe Impulse Sealer, Uline).

3.6 Validation of biomaterial reservoir manufacturing process

As demonstrated in Figure 3.4, the initial *Therepi* biomaterial reservoir design did not confer immunological protection to the encapsulated cell loaded biomaterial, leading to cell death at day 14 following implantation and the formation of a fibrous capsule around the biomaterial (inside the reservoir). A number of design flaws were identified and rectified in the optimisation process. (1) a method to consistently seal the catheter to the reservoir via thermal bonding, (2) a technique to robustly bond the polycarbonate membrane and TPU in a precise manner without damaging the membrane pore structure, (3) fabrication of a bevelled tip at the distal end of the catheter so that it could act as a strain relief when extended into the reservoir, (4) creation of guide holes for consistent and accurate suture attachment to the device and heart without damaging the semipermeable membrane (5) use of a lyophilised biomaterial for an off-the-shelf device, (6) terminal sterilisation using ethylene oxide gas, a dry low temperature technique that is industry recognised and does not affect the material properties of the device. We then validated the optimised *Therepi* reservoir for its ability to encapsulate cells and release healing paracrine factors.

3.6.1 *In vitro* demonstration that cells remain localized within the *Therepi* biomaterial reservoir and release paracrine factors into surrounding media

To demonstrate that seeded cells remain in the *Therepi* reservoir, we delivered 1 million Firefly-luciferase expressing mMSCs to the *Therepi* system on day 0. The system was then submerged in media, in a cell culture flask, with the semi-permeable membrane in direct contact with the surface treated base of the flask (Figure 3.12a). Red firefly luciferase (F-luc) is an intracellular protein (that is not secreted from the cells) and causes bioluminescence in the presence of oxygen and luciferin, thus acting as a proxy for cell number and location. The cells in the reservoir demonstrated F-luc activity over 28 days, quantified by bioluminescence, indicating sustained viability, and therefore transport of nutrients and waste products across the membrane (Figure 3.12b). The addition of D-luciferin to the media demonstrated that cells remained in the *Therepi* reservoir and did not migrate out into the surrounding tissue culture flask over 28 days (Figure 3.12c, "sealed *Therepi*"). We compared this to an earlier iteration of the *Therepi* device, "unsealed *Therepi*" device, which allowed cell migration out into the culture flask by day 28 (Figure 3.12c, "unsealed *Therepi*").

Next, 0.5×10^6 million Gaussia-luciferase expressing mMSCs were seeded along with 0.5×10^6 F-luc mMSCs into the *Therepi* system at day 0 and maintained in a *Therepi* system submerged in media, in a cell culture flask for 28 days. Unlike F-luc, which remains intracellular, Gaussia luciferase (G-luc) is secreted from expressing cells over time (Figure 3.12d). While the F-luc signal confirmed that the transplanted cells remained localized (similar to data shown in Figure 3.12c, "sealed *Therepi*"), a measurement of G-luc activity in media sampled at different timepoints showed a constant increase in paracrine factor activity over time (Figure 3.12e). This finding supports the possibility of implanted cells acting as indwelling paracrine factor sources, releasing factors that diffuse out of the reservoir.
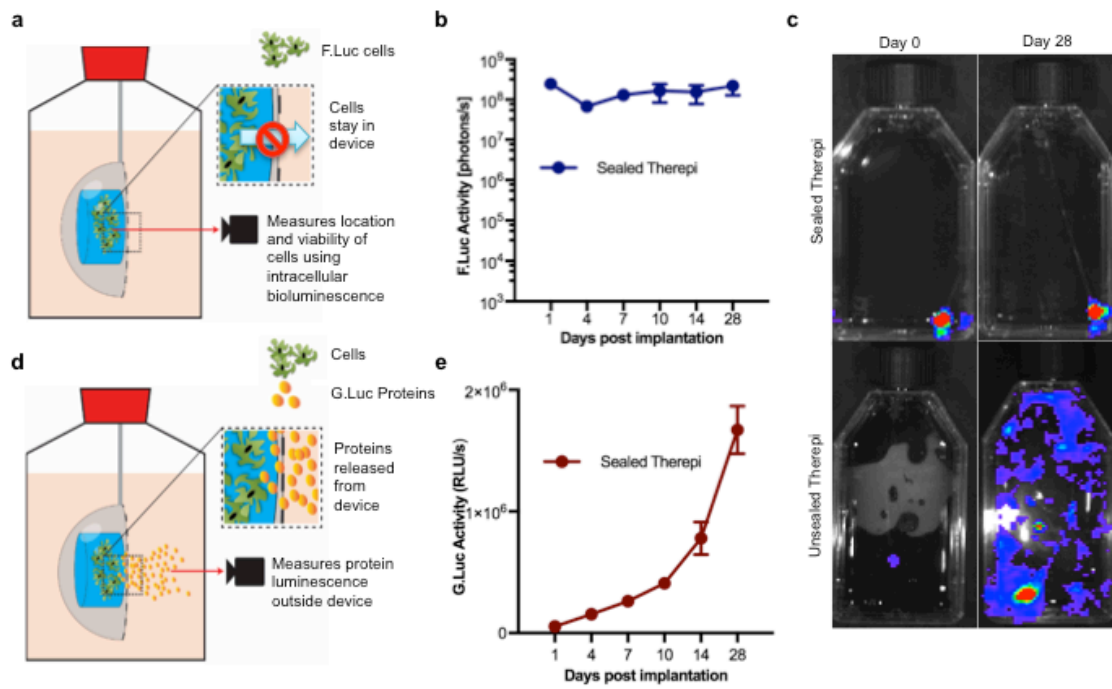
Figure 3.12: The *Therepi* system allows for sustained viability, cell localization, protein release and cell refills *in vitro*.
(a) Schematic of experimental set-up to demonstrate *in vitro* cell localization in the *Therepi* device. **(b)** Luciferase activity in the sealed *Therepi* reservoir showing that implanted cells remain viable in the device for up to 28 days. **(c)** IVIS image showing location of cells via bioluminescence in a sealed and an unsealed *Therepi* device at day 28. **(d)** Schematic of experimental set up to demonstrate *in vitro* protein release. While cells remain inside the device up to 28 days post-implantation, paracrine factors (measured via G-luc bioluminescence) may be released into the surrounding media. **(e)** G-luc activity in the media out to 28 days.

3.6.2 User Testing: Demonstration of immunological protection in a biomaterial reservoir attached to the heart

Finally, in preparation for a pre-clinical trial, we examined the ability of *Therepi* (with an optimised biomaterial reservoir) to confer immunological protection to its cellular cargo in a rodent model. We compared this to the simplified *Therepi system* developed in the previous chapter i.e. a biomaterial connected to a refill line via suture (Figure 3.13a). 1 million firefly-luciferase expressing mouse MSCs was seeded into the *Therepi* reservoir, and implanted on the heart. Bioluminescence, which was used as a surrogate measurement for cell number, was vastly prolonged in the *Therepi* biomaterial reservoir in comparison to simplified *Therepi*, indicating a degree of immune protection.

Finally, the *Therepi* biomaterial reservoir was implanted *in an* MI rat model. After 28 days, the hearts were stopped in diastole and fixed. A transverse slice was taken though the device and heart, stained with Haematoxylin and Eosin and analysed by a cardiac/medical device pathologist. Histological examination of the *Therepi* reservoir in the absence of transplanted cells demonstrates there is no matrix or tissue laid down with the Gelfoam® (Figure 3.13e). Conversely, in the presence of transplanted cells, a cell-derived matrix is laid down by the MSCs in the reservoir (Figure 3.13f). As a control, a histological image from an unsealed *Therepi* device shows a foreign body response, including vascularization, macrophages and giant cells, which is not seen with the intact optimized *Therepi* (Figure 3.13g).
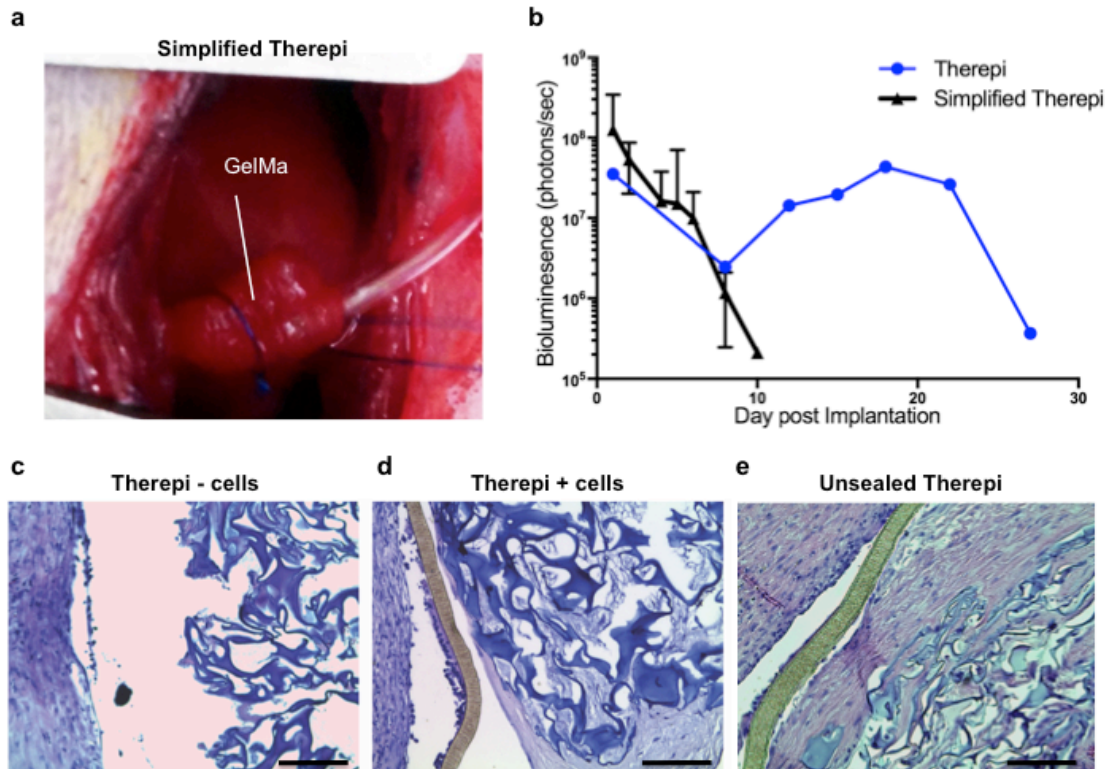
Figure 3.13: Demonstration of immunological protection in a biomaterial reservoir attached to the heart

(a) Simplified *Therepi* consisting of a biomaterial alone sutured to the heart, and connected to a refill line. **(b)** Quantified bioluminescence of F-luc cells seeded in Simplified *Therepi* and optimised *Therepi* over time **(c-e)** Histological images showing a transverse cut through *Therepi* device and heart. **(c)** Image shows optimised *Therepi* without transplanted cells: Image showing very few cells and no cell-derived matrix, foreign response or vascularization in the Gelfoam®, indicating the immune protection imparted by the *Therepi* system. **(d)** Image shows optimised *Therepi* with transplanted cells: In the presence of transplanted cells, a cell-derived matrix is laid down by the MSCs in the reservoir. **(e)** Image shows an unoptimised and unsealed *Therepi* device. The image shows a foreign body response around the biomaterial, including vascularization, macrophages and giant cells. Scale bars are 100μm.

3.7   Discussion

In this chapter, we designed and optimised a protective biomaterial reservoir that builds upon the pre-clinical model developed in chapter two. A soft shell now encapsulates the biomaterial reservoir and a semi-permeable membrane with a precise pore size separates the biomaterial and the heart. The reservoir maximises cell retention, provide protection from the immune response, and allows for the sustained release of therapy. Furthermore, it can wrap around the curvature of the heart, and is of a sufficiently low profile to be safely used in a survival, myocardial infarct rodent model. Importantly, the refill line allows for multiple replenishments.

While the first design iteration offered physical protection to the cell-seeded biomaterial, defects were identified and rectified. Modifications include a method to robustly bond the catheter and semi-permeable membrane without damaging functionality. Moreover, the reservoir was optimised for precise attachment to the heart, without damaging the membrane. To aid with the logistics of implementing a pre-clinical trial, we endeavoured to optimise the manufacturing process towards a device that could be batch manufactured, and then stored until required for testing. To facilitate this, we terminally sterilised the devices with ethylene oxide gas, a low temperature terminal sterilisation process that does not negatively affect the material properties or functionality of the device. Ethylene oxide is a popular method of sterilising devices in industry with ISO approved protocols available[237]. Furthermore, we changed the biomaterial to a lyophilised gelatin sponge, Gelfoam®, that can be hydrated when needed for cell seeding. In a test of cell biocompatibility, Gelfoam performed strongly in a head to head comparison against the original material GelMa. Interestingly, GelMa exhibited a drop off in cell viability at earlier time points followed by an increase later. Cell seeding to the GelMa scaffold is completed in a dehydrated state, when the pores are collapsed. We hypothesise that a surplus of cells initially attach to the exterior of the collapsed gel during cell seeding. At earlier time points, some of these cells undergo apoptosis due to contact inhibition and lack of attachment sites. Eventually there is an increase in viability as cells migrate from the perimeter (where the pore size is smaller) to the inner macroporous centre [199]. In the future, we foresee that this platform can be extended to other biomaterials that have demonstrated an ability to increase cell retention at the heart (e.g., alginate[91], chitosan[89], hyaluronic acid-based gels[84,94], collagen[109,240]).

A track etched polycarbonate membrane with a sharply defined pore size and density was chosen [241]. Importantly, the membrane is available in a range of precise pore sizes, and can be easily interchanged to adjust the type and rate of therapy diffusion if required [242]. Further refinement, such as impregnation of the membrane with a nanoporous biomaterial, such as alginate, could potentially enable a greater degree of protection from the immune response e.g. cytokines [243]. Alternatively, the synthetic semipermeable membrane could be replaced with a mechanically strong nonporous hydrogel [244]. Macroencapsulation devices have attracted significant interest in the treatment of type 1 Diabetes, with multiple devices undergoing commercial development [140,143,245] One interesting approach involves a multi-layered PTFE membrane [141]. The outer later consisting of a 5 micron pore size allows cell infiltration and encourages vascularisation of the implant, while the inner layer with a 0.2 micron pore size immunoisolates the beta cell transplant [143]. This approach might not be suitable for our application, as increased vascularisation could reduce localised bioavailability of

released drug.

To maximize potency of cell therapy, immune protection of transplanted cells would be beneficial. We demonstrated here that *Therepi* loaded with cells could be implanted on the rodent heart, and remain viable for nearly 4 weeks, a common timeframe in pre-clinical studies[246]. This is significant result as the chosen mesenchymal cell was derived from a xenogeneic mouse, which would normally activate an exaggerated immune response [247]. The histological data shown here supports the idea that *Therepi*, when intact, imparts immune protection to the enclosed cargo. The semi-permeable reservoir prevents cell infiltration and a significant foreign body response around the gelatin-based biomaterial, as seen with the unsealed *Therepi* system. An immune response of this nature would likely lead to reduced cell viability at later time points and lessen the efficiency of cell replenishments.

The ability to isolate and study the effect of paracrine factors in a pre-clinical model could be extremely beneficial in the assessment of prospective cardiac regenerative cell therapies and the elucidation of a definitive cardio-regenerative mechanism of action. Gneechi et al conducted numerous studies reporting functional improvements and cardioprotective effects mediated by the delivery of cell conditioned media to the infarcted heart [158,248]. These improvements are attributed to healing paracrine factors released by cells, which is in contrast to earlier trials, where beneficial effects were attributed to cell engraftment[50].

We can draw five conclusions from this study; (i) a consistent and robust thermal bond is formed between the refill line and the reservoir allowing for multiple reproducible therapy replenishments (ii) the semipermeable membrane of the optimised *Therepi* reservoir can localise cells and allow the sustained release of paracrine factors over an extended period of time (iii) suturing of the reservoir to the curved surface of the rat heart is possible without material damage or kinking (iv) the optimised system provides protection from the foreign body response and vastly extends viability of an xenogeneic cell source in comparison to the simplified *Therepi* (v) the system has been optimised for pre-clinical testing.

3.8   Materials and Methods

3.8.1   GelMa

Methacrylated gelatin cyrogels were prepared as described in the previous chapter. A cylindrical acrylic mould (3mm diameter, 1.25mm thick) was used.

3.8.2   Cell transfection

For all studies using the IVIS Spectrum Xenogen 5000 (*In Vivo* Imaging System, Perkin Elmer), clonally derived mesenchymal stem cells from BALB/c mice (D1 ORL UVA [D1] (ATCC® CRL-12424™) were obtained from American Type Culture Collection (ATCC). ATCC cell lines are subjected to comprehensive and repeated authentication and contamination checks including short tandem repeat (STR) profiling, cell morphology, karyotyping and cytochrome C oxidase I (COI) testing. Testing was also completed to ensure that cell cultures were free of mycoplasma or other bacterial or fungal agents, conforming to the mycoplasma-testing stipulations recommended by the FDA "Points to Consider" protocol. To introduce firefly luciferase to these cells, lentiviral particles were produced containing a vector with mCherry-IRES-Firefly Luciferase driven by the CMV promoter by transfecting the plasmids in HEK-293T cells. The viral particles were then concentrated by centrifugation through an Amicon filter with a 3kDa cut-off. The viral titre was determined by evaluating mCherry signals after transducing MSCs with different concentrations of the particles. MSCs were then incubated with viral particles for 2 days. Cells expressing mCherry were then sorted via flow-activated cell sorting. Gaussia Luciferase expressing mouse MSC's were produced using the same approach.

3.8.3   Cell Preparation

Luciferase-expressing mouse mesenchymal stem cells were cultured in the following growth media: Dulbecco's Modified Eagles Medium supplemented with 10% (v/v) bovine serum, 100 U/ml penicillin, and 100 μg/ml streptomycin (Gibco). Cells were stored at 37°C with a 5% CO_2 atmospheric concentration. Trypsin solution (Sigma) was used to separate adherent cells from the adherent tissue culture flask substrate. .

3.8.4   Device cell seeding

Negative pressure was applied to the *Therepi* system, using a syringe. 1 million F-luc cells or 0.5 million G-luc+0.5 million F-luc cells were suspended in 30μl of complete media (as described above) and injected through the refill line into the reservoir. 20μl of media was injected in order to ensure entirety of cell solution volume reached the reservoir, and refill line was free of cells.

3.8.5   *In vivo* studies

Therepi animal model was performed as previously described in chapter 2, with the following exceptions. (i) In lieu of attaching the cryogel and catheter separately to the ventricle, the encapsulated device was secured to the ventricle of the heart with three suture loops (6-0 prolene, Ethicon 8711) as shown in Figure 3.13b (ii) instead of a simple catheter, the catheter part of the encapsulated *Therepi* was tunnelled subcutaneously.

3.8.6   Infarct creation

For the hemodynamic study, rats underwent myocardial infarction as previously described [102], immediately prior to *Therepi* attachment. The left anterior descending artery was permanently ligated with a suture (6-0

prolene, Ethicon 8711) approximately one third of the way from the apex to the base of the heart. Myocardial blanching was apparent after ligation of the LAD, confirming infarction.

3.8.7 Histology

Hearts were arrested in diastole by direct injection of 2-3ml of 1% KCl solution. Hearts were fixed in a 10% neutral buffered formalin solution for 24h. Tissues were then transferred to PBS and stored at 4°C until paraffin embedding. A transverse cut of the heart was made at the device/heart interface. Slices were stained for Haematoxylin & Eosin and analysed by a practicing cardiac/medical device pathologist.

3.8.8 *In vivo* refills of cells

Negative pressure was applied to the *Therepi* system, using a syringe. Cell refills were conducted through the port with 50µl of cell suspension at a concentration of 20×10^6 cells/ml of complete media injected through the port of each animal with a 100µl microsyringe and a PNP-3M injector (Instech Laboratories). The line was then flushed with media to account for the dead volume for each system so that a total of 50µl of cell suspension reached the gel.

3.8.9 *In vivo* bioluminescence measurements

For the cell refill studies, animals were imaged on day of surgery (day 1), and at multiple days out to day fourteen for *Therepi*. On day four the refill group was replenished with cells, and imaged two hours before refill and four hours after refill. Animals were anesthetized with 3% isoflurane in oxygen. D-luciferin (XenoLight D-Luciferin Potassium Salt, Perkin Elmer) at 15mg/ml in complete media was injected through the port of each animal with a 200ul microsyringe and a PNP 3M injector accounting for dead volume so that 50ul of D-luciferin reaching the gel. An IVIS Spectrum Xenogen 5000 (*In Vivo* Imaging System, Perkin Elmer) was used for imaging. Animals were maintained under anaesthesia with 3% isoflurane delivered through a nose cone during imaging. A sequence was acquired with the following settings; luminescent automatic exposure with a target count of 3,000 and a field-of-view set to D (automatic exposure preference range values were set to the following; exposure time: 0.5-170 seconds, binning: 1-8, F-stop:1, field-of-view D, no delay between images). The sequence was terminated once the signal was seen to drop.

3.8.10 Multiple refills *in vitro*

Therepi devices was manufactured as described, and inserted into a T-25 tissue culture flask containing 15ml of media, and placed in an incubator. One million cells were pre-seeded on each of the gels through the catheter. The gels were imaged in the IVIS Spectrum at day 1,2,4,7,9,14,15 and 17. The reservoirs were refilled with 1 million cells in 50 µl of media at day 7 and day 14. For each imaging time point, 50µl of D-luciferin (XenoLight D-Luciferin Potassium Salt, Perkin Elmer) at 15mg/ml was added to each gel and they were imaged in the IVIS Spectrum Xenogen 5000 (In Vivo Imaging System, Perkin Elmer). A sequence was acquired with the following settings; luminescent automatic exposure with a target count of 3,000 and a field-of-view set to D. (automatic exposure preference range values were set to the following; exposure time: 0.5-170 seconds, binning: 1-8, F-stop: 1, delay of 180 seconds between images). The sequence was ended once the signal was seen to drop. The automatic circular region of interest (ROI) tool was used to calculate the total flux per gel (photons/sec), using the same ROI for each gel. The highest value was used for the data.

3.8.11 *In vitro* cell encapsulation

F.Luciferase: Seeded *Therepi* devices were cultured in 10 ml of media, which was changed at suitable intervals. To measure bioluminescence of F-luc cells *in vitro*, D-luciferin (XenoLight D-Luciferin Potassium Salt, Perkin Elmer) at 15mg/ml was added to each tissue culture flask. Flasks or animals were imaged in an IVIS Spectrum Xenogen 5000 (*In Vivo* Imaging System, Perkin Elmer). A sequence was acquired with the following settings; luminescent automatic exposure with a target count of 3,000 and a field-of-view set to C or D (automatic exposure preference range values were set to the following; exposure time: 0.5-170 seconds, binning: 1-8, F-stop:1). The sequence was ended once the signal had reached a plateau or was seen to drop. The highest value was used for the data. The automatic circular region of interest (ROI) tool from Living Image software was used to calculate the total flux of light in areas of interest (photons/sec).

G-luciferase: *In vitro* G-luciferase bioluminescence was measured by transferring 100µl of media from the tissue culture flask to a black 96 well plate. 100 µl of imaging substrate coelenterazine (Rediject, PerkinElmer) at a concentration of 20 µg/ml was auto mixed with samples and imaged using a Spectramax L microplate reader. An integration time of 10 seconds was used. Each biological sample was measured in triplicate and readings were averaged. A cumulative concentration reading was recorded at days 1, 4, 7, 10, 14, 28 while accounting for a G-luc half-life of 6 days[249].

4 Safety and efficacy assessment following Therepi implantation in a rat model of myocardial infarction and exploration of barriers to clinical translation

4.1 Preface

In Chapter 4, I focus on the third aim of my thesis. Initially, I examine the effect of fibrous capsule formation on therapy delivery from the implanted biomaterial reservoir. Next, I assess the safety and efficacy of the optimised and validated Therepi system (developed in chapter 2) using the pre-clinical research model (developed in chapter 1). Finally, this chapter explores and discusses potential barriers to clinical translation including target patient population, minimally invasive delivery capabilities, and risk of infection.

The chapter aims are as follows

1. To examine the ability for small and macromolecules to penetrate fibrous capsule, distribute into myocardial tissue, and produce a biological effect following *Therepi* implantation.
2. To investigate macromolecule diffusivity through fibrous capsule of an acute and chronic nature
3. To assess the safety and efficacy of *Therepi* following repeat cell delivery in a 28-day study in a rodent myocardial infarct model
4. To explore and discuss barriers to clinical translation

4.2 Introduction

Although technological advances in coronary artery revascularization therapies have proven successful at restoring blood flow to the heart after a myocardial infarction (MI) or heart attack, residual myocardial scarring often remains. Elimination of scarring and restoration of full cardiac function post-MI could eliminate or attenuate the cascade of events that lead to ischemic heart failure. While effective clinical therapies in this domain are lacking, simple single deliveries of cells[5,131], growth factors[189–196] or drugs[125,197,207,208,250,251] has shown promise, especially pre-clinically. A common theme underpinning these studies is poor retention, and survival at the diseased site, and the necessity for repeated or sustained delivery for best effiacy[78,186,187].

Stem cells, in particular, have attracted intense interest as a cardiac regenerative therapy. However, modest or inconsistent functional benefits have been reported in clinical trials to date [252]. Synthesis and secretion of paracrine factors is believed to be the main mechanism of action [158,248,253,254] and extending the viability of these transplanted cells within the harsh environment of the post-MI or chronic ischemic heart is likely key to this effect. It is accepted that biomaterials such as alginate enhance cardiac cellular retention and survival in comparison to physiological saline, offering hope for future trials utilizing this delivery vehicle [83,84,93,94,85–92] Furthermore, recent evidence supports a paradigm-shift towards repeated cell administration, demonstrating that multiple administrations are therapeutically superior to single doses in MI and heart failure animal models[181,182,255]. In addition to cells, repeated dosing is likely to improve benefit with other therapeutic technologies, such as growth factors[189–196] and small molecules[125,197,207,208,250,251]. A method to replenish therapy, or offer multiple administrations without necessitating multiple surgeries, has not yet been demonstrated, motivating the design of Therepi as described in chapter 2 and 3.

Therepi enables direct, controlled administration of therapy via a polymer-based reservoir connected to a subcutaneous port. This presents numerous advantages including convenient, repeated therapy administration of bioagents of a range of sizes. Previously, we demonstrated targeted, localized delivery of small molecules, macromolecules and repeat administrations of cells directly to the biomaterial attached to the epicardium, however we failed to examine the effect of fibrous capsule formation, an end stage healing response to foreign material implantation, which could generate a barrier to delivery, and affect the long term functionality of the device[218]. This chapter initially investigates the delivery and penetration of multi-sized of cargo following fibrous tissue encapsulation. Finally, using the animal model and device optimised in chapter 2 and 3, we assess the safety and efficacy of repeated syngeneic mesenchymal cell delivery in a 28-day rodent myocardial infarct model.

4.3 Materials and Methods

4.3.1 Overview of *Therepi* fabrication

The fabrication methods for the *Therepi* system are shown in Figure 4.1 and described here.

Formation of the polyurethane backbone: Thermoplastic polyurethane (TPU) was used as an impermeable membrane (HTM 8001-M polyether film, 0.003inch thick, American Polyfilm, Inc.). A sheet of TPU was mounted in a vacuum thermal former (Yescom Dental Vacuum Former, Generic). A 3-d printed hemispherical mould (Objet Connex 500) with a height of 3.9mm and a diameter of 3.5mm was used as the positive mould. The positive mould was placed on the vacuum platform and the sheet was heated until it was completely smooth. The heated TPU sheet was then lowered over the positive mould. Vacuum was simultaneously applied to the platform to ensure the sheet fully conformed to the shape of the mould. The formed TPU shape was then placed in a corresponding negative mould. A Teflon strip was inserted into grove of the negative mould to keep the channel open during the proceeding heat-sealing steps. A laser cut TPU window was placed on top and the assembly was heat-sealed with a heat transfer machine (Heat transfer machine QXAi, Powerpress) for 4 seconds at 330ºF (Figure 1.4E).

Impulse sealing of the semipermeable membrane: The formed TPU was taken out of the negative mould and aligned in an impulse heat sealer (H-2065 Deluxe Impulse Sealer, Uline). A circle of polycarbonate membrane (Cyclopore Track-Etched Membrane Filter, 13mm Diameter, 0.4 Micron, Whatman) was placed under the assembly and heat-sealed in place. This was repeated for two other sides of the device, leaving one side open for biomaterial insertion in a later step.

Thermo-sealing of the catheter: The laser cut teflon strip was removed from the part. Excess material was trimmed form the device with a fine scissors (Vannas Tübingen Spring Scissors, Harvard Apparatus) (Figure 1.4H). A 10cm, 3Fr, thermoplastic polyurethane catheter (Micro-Renathane® .040" x .023, Braintree scientific) was inserted into the formed channel. A PTFE coated mandrel (0.02196 inch, type 304 S.S/54076, Applied Plastics) was inserted into the catheter to retain patency during the proceeding heal sealing step. Heat shrink tubing (RNF-100-3/64-O-STK, TE Connectivity) was positioned at the unsealed interface between the catheter and the device. The part was inserted into an aluminium block containing a 2.5 mm diameter hole and the assembly was heated to 370ºF for 120 seconds with a heat press (Heat transfer machine QXAi, Powerpress). The part was removed from the aluminium block and the heat shrink tubing was cut away with a Vannas Tübingen Spring Scissors (Harvard Apparatus). After removal of the teflon coated mandrel, the device sent for ETO sterilization (low temperature ethylene-oxide cycle). The remaining steps were conducted in an aseptic environment in a class II laminar flow hood

Biomaterial insertion: A 2mm cylinder cut from a gel foam sponge (Gelfoam Haemostatic, Size 12-7mm, Pfizer Pharmaceutical) using a disposable biopsy punch (Integra Miltex). The final polycarbonate-TPU opening was sealed using an impulse heat sealer (H-2065 Deluxe Impulse Sealer, Uline).
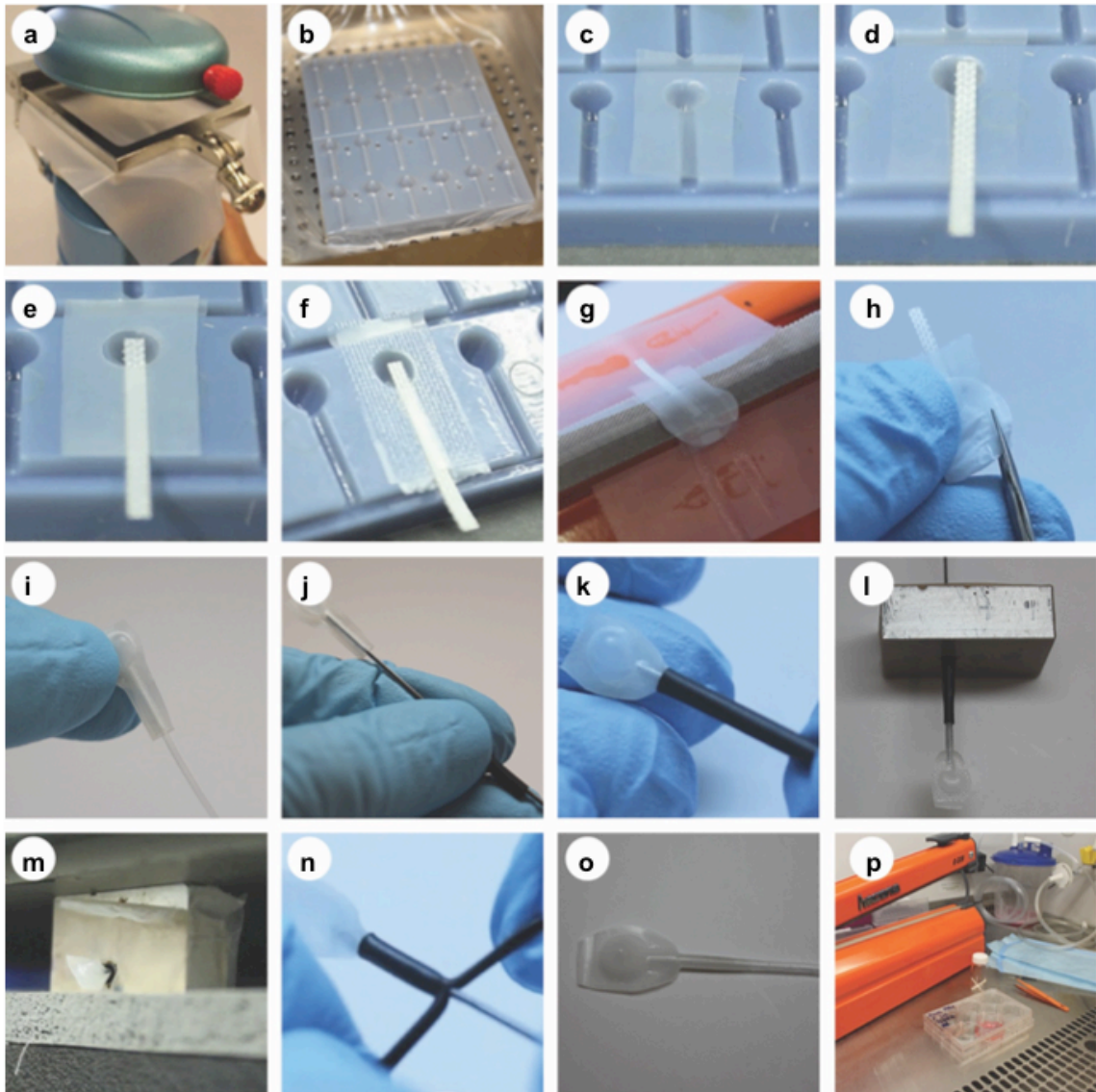
Figure 4.1: Overview of the *Therepi* fabrication method
(a) An exploded view of the layers of the *Therepi* reservoir **(b)** The entire *Therepi* system showing refill line, refill port and reservoir **(c)** A thermo-plastic urethane sheet is mounted in a thermal former with a vacuum platform and a positive 3-D printed mould was placed on the platform **(d)** The thermoplastic urethane sheet is heated until it sags in the centre. The platform is lowered and vacuum is applied so the thermoplastic sheet is formed over the positive mould. **(e)** The formed TPU is placed in a negative mould. **(f)** A Teflon strip was inserted into grove of the negative mould to keep the channel open during the proceeding heat-sealing steps. **(g-h)** A laser cut TPU window was placed on top and the assembly was heat-sealed with a heat transfer machine **(i)** The assembly was aligned in an impulse sealer over a layer of polycarbonate and sealed at three sides, leaving one side open for biomaterial insertion **(j)** Excess material was trimmed from the device with a fine scissors. **(k)** A thermoplastic polyurethane catheter was inserted into the formed channel **(l)** A PTFE coated mandrel was inserted into the catheter to retain patency during the catheter healing process **(m)** Heat shrink tubing was positioned at the unsealed interface between the catheter and the device. **(n-o)** The parts were bonded in a heated aluminium block, with the heat provided conducted by the block and pressure provided by the contraction of the heat shrink tubing **(p)** The heat shrink tubing was snipped at the bottom at opposite sides and peeled away **(q)** The PTFE coated mandrel was removed. At this stage the device was ETO sterilised **(r)** A gel foam cylinder was aseptically inserted into the device. The device was aseptically sealed with an impulse sealer. Cells were injected through the catheter and seeded onto the gel foam

when required for surgery.

4.3.2   Cell preparation and biomaterial seeding

For the 28-day study primary mesenchymal stem cells derived from Sprague Dawley rats were purchased from Cyagen (RASMX-01001). As per manufacturers data, they tested negative for bacteria, fungi, and mycoplasma. Cells at passage 5-7 were used in all groups for the study. Gelfoam® was inserted into *Therepi* devices as a dry cell free material and was subsequently seeded through the *Therepi* refill port. When required, devices were loaded with cells. Negative pressure was applied to the *Therepi* system, using a syringe. 500,000 rat MSC's suspended in media (AlphaMem/Glutamaxm, Gibco, 32561037, with 10% (v/v) bovine serum, 100 U/ml penicillin, and 100 µg/ml streptomycin, Gibco) was injected through the refill line into the reservoir. 20µl of AlphaMem media was injected to clear the refill line of cells. The devices were submerged in a tissue culture flask containing AlphaMem media at 37°C in a 5% CO_2 atmosphere for 3 days. Devices were then transferred to a serum free media, StemPro MSC SFM (Gibco), supplemented with Glutamax (Gibco), 24 hours prior to device implantation.

4.3.3   Intramyocardial Cell Injection

0.5 million cells were suspended in 50µl of StemPro MSC SFM (Gibco) 30 minutes prior to surgery, and stored in ice. 5 separate injection of 10µl were made at the border zone of the infarct. Cells were cultured in AlphaMem/Glutamax (Gibco 32561037) supplemented with 10% (v/v) bovine serum, 100 U/ml penicillin, and 100 µg/ml streptomycin (Gibco) at 37°C in a 5% CO_2 atmosphere for 7 days prior to injection.

4.3.4   Cell Seeding/ Cell Refills

Cell refills were performed on day 4,14 of the 28-day pre-clinical study. Negative pressure was applied to the *Therepi* system, using a syringe, to clear the line. 500,000 rat MSC's suspended in 30µl of serum free StemPro media was injected through the refill line into the reservoir. 20µl of StemPro media (Gibco) was injected to clear the refill line of cells

4.3.5   Functional hemodynamic measurements with Ultrasound

Hemodynamic measurements with echo ultrasound were performed as previously described using a Vevo 2100 Ultrasound machine and a MS200 transducer probe (9-18Mhz)[269]. B-mode measurements were taken using the parasternal long axis view of the heart. M-mode measurements were taken using the parasternal short axis view of the heart, at mid ventricle, with papillary muscles evident. Data was collected and analysed using the Vevolab software (Visualsonics).

4.3.6   Functional hemodynamic measurements with PV catheter

Hemodynamic measurements were carried out using the apical stick method as previously described[221], using the Powerlab 8/35 and LabChart Pro 8 software with the PV module. Pressure and volume were measured using a conductance catheter (SPR-838) in the left ventricle. An average of at least ten cardiac cycles was taken post-calibration for haemodynamic measurements in LabChart Pro software. Volume calibration was determined by inputting max diastolic and systolic volume obtained from ultrasound measurements, as per manufacturer's instructions (PV loop module, Labchart). LabChart Pro 8 (AD Instruments) was also used for PV data analysis.

4.3.7   Histology

Hearts were arrested in diastole by direct injection of 2-3ml of 1% KCl solution. Hearts were fixed in a 10% neutral buffered formalin solution for 24h. Tissues were then transferred to PBS and stored at 4°C until paraffin embedding. A transverse cut of the heart was made at the device/heart interface. Slices were stained for Haematoxylin & Eosin and analysed by a practicing cardiac/medical device pathologist.

4.3.8   Epinephrine delivery and demonstration of functional effect by pressure monitoring

50 μL of epinephrine at a concentration of 1mg/ml (Pfizer) was injected either into the intraperitoneal space or directly into the device's delivery port and changes in blood pressure were monitored. Briefly, either healthy animals or animals with an MI and an implanted device (28 days prior to the experiment) were intubated and anesthetized. A terminal thoracotomy was performed and a PV catheter (Millar SPR-838) was inserted into the left ventricular space via apical stick. After verifying levels of systolic blood pressure were in a physiological range, epinephrine was injected into the intraperitoneal space of healthy animals (n=3) or directly into the device of the animals (n=3). Pressure changes were recorded for up to 2 minutes post-epinephrine injection using the PV catheter (SPR383), Powerlab data acquisition and LabChart 8 software (AD instruments).

4.3.9   Computed tomography imaging for distribution into tissue

An infarcted heart with an acellular *Therepi* device was explanted from a Sprague Dawley rat 26 days after myocardial infarction and *Therepi* implantation. Prior to scanning, a contrast agent phosphomolybdic acid (PMA) at a concentration of 12.5%w/w was used to simulate macromolecule diffusion from the *Therepi* into the *ex vivo* cardiac tissue through the surrounding fibrous capsule. 70μl of PMA was injected into the device and the entire assembly was placed in a humidity chamber. 12 h post PMA injection, a micro computed tomography (µCT) scan of the heart and the attached device was conducted using an XRA-002 X-Tek µCT system. 3D reconstructions were performed using CT-Pro (Nikon Metrology) and the surface renderings were generated using VGStudio Max.

4.3.10   Diffusion chamber for transport of macromolecules across a fibrous capsule

Heart tissue with attached *Therepi* was explanted at various times after placement. Real time measurement of diffusive transport of FITC-dextran through left ventricle tissue with attached polycarbonate membrane from explanted hearts was measured using a diffusion chamber consisting of two compartments, each with a volume of 2 mL. Heart tissue with attached polycarbonate membrane was clamped, using O-rings, between the two compartments of the diffusion chamber. The total exposed tissue area for transport was 0.1257 cm^2. Each compartment was filled with 2 mL of Dulbecco's Phosphate Buffered Saline supplemented with protease inhibitors. At starting time t=0, FITC-dextran of molecular weight 40 kDa or 10 kDa (Sigma-Aldrich) was added to the 'upstream' compartment such that the final upstream concentration of the FITC-dextran was 50 M, allowing for diffusion from the upstream compartment through the tissue into the downstream compartment. The fluorescence at the downstream compartment was continuously measured using a custom fluorescence reader. The baths in both compartments were magnetically stirred to minimize the effects of concentration variations within the compartments. The data from the real-time measurement of

diffusive transport was fitted to the solution of the one-dimensional transient diffusion equation with constant concentration boundary conditions[1] using MATLAB and a diffusion time constant was determined. A partition coefficient of one was assumed.

4.3.11 Penetration of albumin across a fibrous capsule

An acellular *Therepi* device was placed in an MI model Sprague Dawley rat for 26 days. 50 microliters of 1mg/ml cyanine (Cy7, Nanocs) labelled bovine serum albumin was injected through *Therepi*, following heart explantation. Following 24 hours in a humidity chamber, the heart was imaged using epifluorescent microscopy, consisting of a Xenon lamp, Axio Zoom V16 microscope, and a Hamamatsu Flash 4.0 v3. Images showing penetration of fluorescent albumin across a fibrous capsule were generated in Image J using the Fiji image processing package.

4.3.12 Animal surgery: MI model and *Therepi* system implantation

Animal studies were carried out in accordance with the Institute for Animal Care and Use Committee, Harvard University/Brigham and Women's Hospital for the 14-day and 28-day study respectively. All surgical procedures are described in Chapter 2. A shortened summary is also included here. Briefly, Female Sprague Dawley rats (225-250g) were anesthetized using isoflurane (1-3% isoflurane in Oxygen). The hair between the shoulder blades and on the left side of the chest was removed. Pre-operative analgesics buprenorphine (0.05mg/kg subcutaneously) were administered. A regional nerve blocker Lidocaine/Bupivacaine was injected subcutaneously at the surgical sites. Endotracheal intubation was performed. The *Therepi* refill line was then tunnelled subcutaneously from the dorsal site to a ventral exit site close to the left fourth intercostal space. The pericardium was removed using fine forceps. A myocardial infarction was created as previously described[240]. The LAD was permanently ligated with a suture (6-0 prolene) approximately one third of the way from the apex to the base of the heart. Myocardial blanching was apparent after ligation of the LAD, confirming infarction. The *Therepi* reservoir was sutured (8-0 prolene) onto the heart at the infarct border zone using the surgical guided holes placed in the device. Following *Therepi* placement, a vascular access button, or self-sealing port, (VAB62BS/22, Instech Laboratories) was connected to the dorsal end of the catheter and placed subcutaneously between the shoulder blades of the rat .The vascular access button was secured to the underlying fascia using at least two interrupted sutures (Ethicon 4-0 vicryl). The skin was closed and the animal was ventilated with 100% oxygen on a heated pad until autonomous breathing was regained. 3ml of warm saline was administered subcutaneously and buprenorphine [0.05mg/kg in 50μl intraperitoneally (IP)] was given every twelve hours for three days post-operatively.

4.3.13 Statistical Analysis:

Software: Graphpad Prism was used for statistical analysis. Normal distribution was tested for each group using a histogram, and similar variances were checked for groups being compared. For normally distributed data a two-sided, unpaired t-test was used for comparing between two groups with an alpha level of 0.05. A one-way analysis of variance (ANOVA) with Tukey's multiple comparison post-hoc test was used for studies with more than two groups, with an alpha level of 0.05.

Sample size for functional study: A pilot study was initially performed to determine the treatment effect of Therepi following myocardial infraction. This data was used to inform sample size (n=5) for a sufficiently powered study to detect significant differences between treatment and control groups.

Exclusion parameters: Male rats and rats below 225g or above 250g were excluded. The following rats were also excluded; animals that did not survive the MI surgery, animals where the integrity of the device or the subcutaneous line or port was damaged, animals that did not display blanching of the left ventricle on LAD ligation or animals that had an ejection fraction greater than 60% as assessed by echocardiography at day 0. For the PV data, measurement points that did not form a consistent PV loop due to catheter positioning or other reasons were excluded.

Randomization: No formal randomization was used but surgeries were carried out on groups, which were alternated, each group was completed over 2-3 different surgery days.

Blinding: No formal blinding was used, echocardiography imaging was conducted by an independent operator.

4.4 Results

4.4.1 Vision, design and realization of the *Therepi* system

Here we introduce the optimized version of "*Therepi*"; a therapeutic, epicardially placed reservoir that offers many advantageous features to address the current limitations for the delivery of small molecules, macromolecules and cells to treat cardiac disease. The vision for clinical translation is that a therapeutic reservoir is placed on the border zone of the infarcted heart and connected to a subcutaneous port or self-sealing rubber septum by an indwelling catheter, thus enabling multiple minimally invasive replenishments directly to the target site without the need for higher systemic doses (Figure 4.2a).

The system offers a method to tune the rate of therapy diffusion and limit the size of molecules diffusing into tissue by varying the porosity of the semi-permeable membrane (Figure 4.2b). We also incorporated a biomaterial vehicle into the system to promote retention of the delivered cargo and enhance engraftment and viability of cells. In this work, we used Gelfoam®, a commercially available gelatin sponge. However, we foresee this platform system working with a large panel of biomaterials, including, but not limited to alginate[91], chitosan[89], hyaluronic acid-based gels[84,94] and collagen[5,240].

Details of the design and manufacture of the *Therepi* system are summarised in the Materials section (Figure 4.1) and described in detail in chapter 3. Briefly, the biomaterial is encapsulated between two polymer layers – one impermeable and one porous – with the latter interfaced and fixed on the epicardial surface of the heart. The assembled reservoir is then connected to a subcutaneous port through an implanted refill line, allowing for localized, targeted therapy to the diseased tissue (Figure 4.2c).

Next, we summarise the surgical pre-clinical model developed in chapter 2. In brief, in an anaesthetized rat model, the refill line was tunnelled subcutaneously from a dorsal incision to a thoracotomy. Next, an MI model was created by permanently ligating the left anterior descending (LAD) coronary artery. The *Therepi* reservoir was then sutured to the epicardium at the infarct border zone, and the refill line was attached to a subcutaneous, self-sealing port at the dorsal access site and closed. This allowed non-invasive, replenishable, targeted delivery, and localized release of various agents (Figure 4.2 d-e).
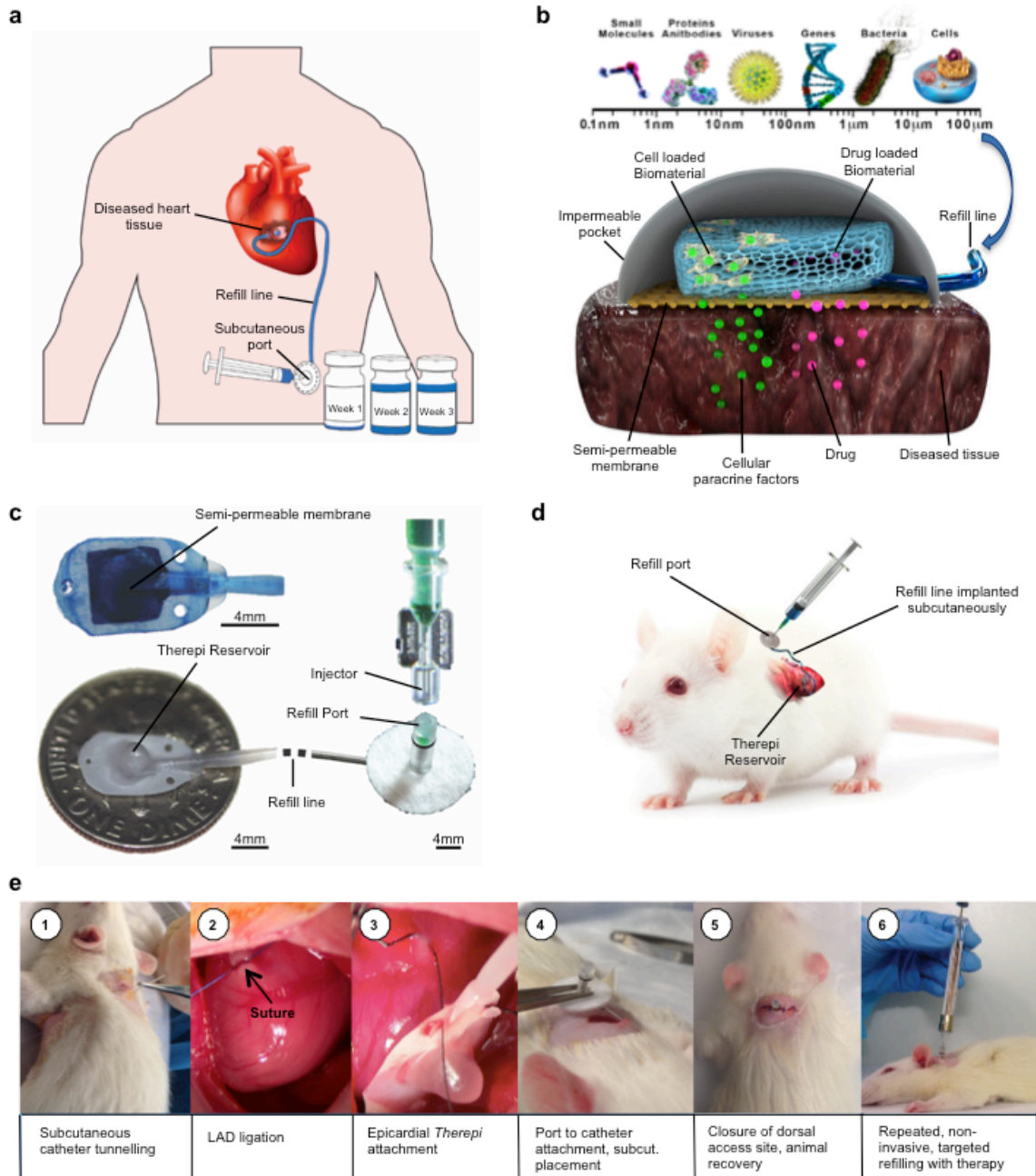
Figure 4.2: Overview of the vision for clinical translation of *Therepi* and its realization for pre-clinical evaluation

(a) Vision for translation of the *Therepi* system to the clinic. Patient is injecting therapy through a subcutaneous port connected to a reservoir at the heart surface via a refill line. **(b)** Overview of *Therepi* system mechanism of action. Release of small molecules/macromolecules or paracrine factors from cells through the semi-permeable membrane. A refill line for targeted replenishment of therapy is shown on the far right **(c)** Pre-clinical realization of *Therepi. Top left:* View of *Therepi* reservoir from tissue-contacting interface, dyed blue to aid with visualization. *Bottom: Therepi* reservoir placed on a dime for size reference and connected to a self-sealing subcutaneous port. *Top right*: Specialized injector for self-sealing port. **(d)** Schematic of *Therepi* in a small animal model **(e)** Surgical procedure for *Therepi* implantation in a rat MI model.

4.4.2 Potential for minimally invasive delivery of Therepi

The resulting device is flexible and foldable and can be guided through a 14G needle or 1.6mm diameter catheter (Figure 4.3 a-b), lending itself to minimally invasive delivery via sub-xiphoid puncture or a mini-thoracotomy for future translation to humans. Re-administration of therapy is achieved non-invasively through the port (Figure 4.3c). Finally, we show compression and recovery of the flexible, soft reservoir with a tweezers (Figure 4.3 d-e).
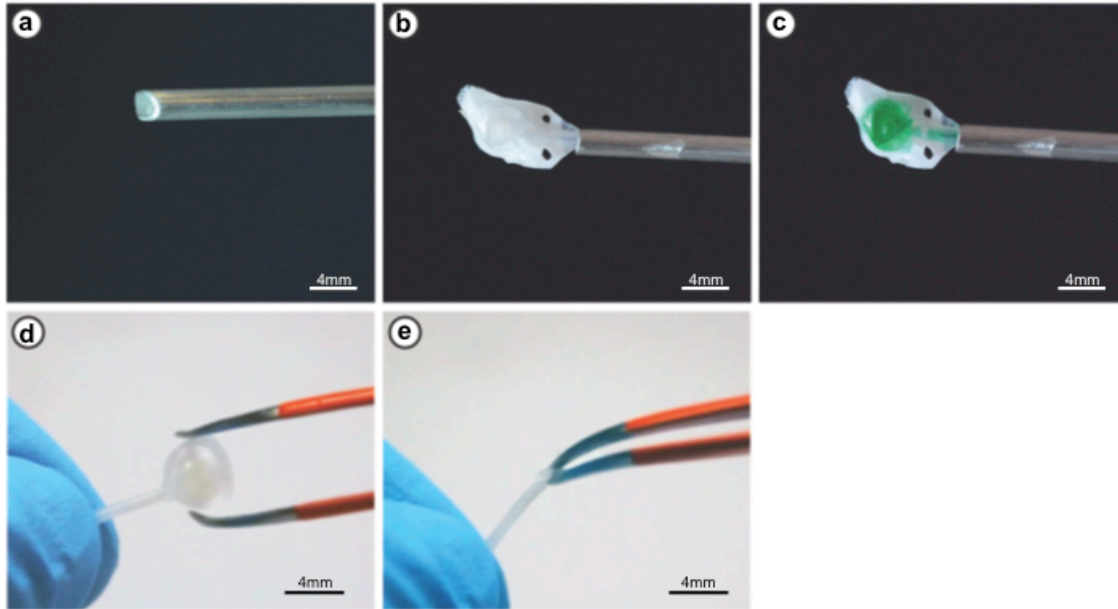
Figure 4.3: Potential for minimally invasive delivery of Therepi
(a-c) Unsheathing of Therepi from a 14G needle **(d-e)** Compression and recovery of the *Therepi* with tweezers showcasing flexibility

4.4.3 Transport of small molecules and macromolecules through *Therepi* system and fibrous capsule into tissue

To illustrate small molecule penetration through the formed fibrous capsule and elicitation of a functional response, epinephrine was delivered through the *Therepi* system 28 days post implantation in an MI model, while recording blood pressure with an apically inserted pressure/volume catheter. Delivery produced a more pronounced and rapid increase in blood pressure as compared to IP delivery, as indicated by the systolic pressure measured over time (Figure 4.4a), and the typical pressure waveforms for the first 100 seconds, recorded in the left ventricle (Figure 4.4b).

To demonstrate that macromolecules delivered via *Therepi* could penetrate myocardial tissue more than 28 days post-implantation in an MI rat model, a micro-computed tomography (μCT) analysis was performed 12 hours after delivery of a drug analogue (the contrast agent phosphomolybdic acid) (Figure 4.4 c-d). The three-dimensional reconstruction of the excised heart enabled visualization of the distribution and penetration of delivered therapy in heart tissue.

Next, the transport of proteins through the *Therepi* and the surrounding fibrous capsule was demonstrated. Fluorescently labelled bovine serum albumin (Cy7 labelled, Nanocs) was delivered through the *Therepi* system, 26 days post-implantation in an MI model, and after formation of a fibrous capsule. 24 hours post administration, fluorescent protein had diffused from the device and penetration through the fibrous capsule into the heart tissue was evident (Figure 4.4e).
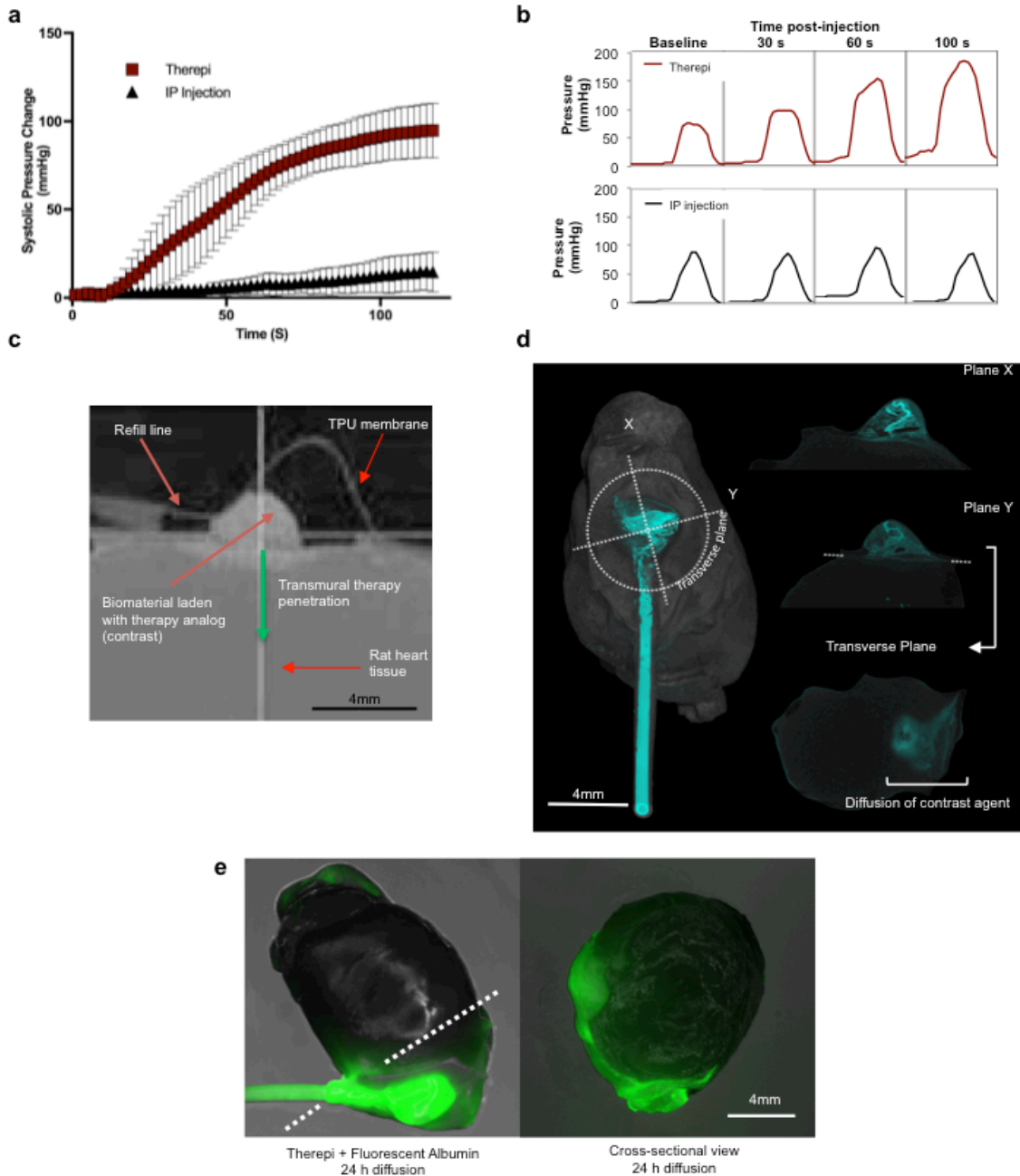
Figure 4.4: Demonstration of fibrous capsule penetration and 3D distribution of macromolecules in the myocardium.
(a) Systolic pressure, as measured by an apically inserted pressure-volume catheter post-injection of epinephrine (n=3 animals). **(b)** Typical intraventricular pressure waveforms seen with each model immediately following epinephrine injection. Data are mean ± SD using a two-sided, unpaired t-test. **(c)** Image from the micro-CT scanner showing the *Therepi* reservoir on the explanted heart and the direction of PMA contrast agent (therapy analogue) penetration. **(d)** 3D reconstruction of entire CT scans at 2 orthogonal planes and transverse plane. **(e)** Diffusion of fluorescent albumin through the fibrous capsule into the heart tissue, 24 h post-delivery of Cy7cyanine labelled albumin. *Left*: Merged fluorescent and bright-field image of the explanted heart+*Therepi* device 26 days after surgical implantation. The heart was cut at the white dotted line. *Right*: Merged fluorescent and bright-field image of cross-section (indicated by white-dotted line).

4.4.4   Assessment of fibrous capsule size and rate of macromolecule diffusivity

Samples of tissues from the *in vivo* MI rat model at 28 days were stained with Haematoxylin and Eosin, and a cardiac/medical device pathologist conducted analysis. The gross appearance of the *Therepi* at day 28 on the heart is shown in Figure 4.5a, with the device conforming to the heart. Histological slices were taken through the device and heart in a transverse slice (Figure 4.5b). A histological overview of the *Therepi* device demonstrates the TPU layer, polycarbonate membrane, enclosed Gelfoam® and reservoir contents, and the fibrous capsule is evident at the device/epicardial interface (Figure 4.5c) (note the breach in the TPU layer here is a processing artefact). The fibrous capsule for the *Therepi* device in the presence or absence of cells and with cell replenishments had a similar appearance and thickness (Figure 4.5 d-f).

Real time measurements of macromolecule diffusivity were obtained using a diffusion chamber consisting of two compartments separated by the tissue of interest, in this case, heart tissue explanted at various time points with a fibrous capsule of acute or chronic nature, and the polycarbonate membrane of the *Therepi* system (Figure 4.5g). Diffusion of 40 kDa FITC-dextran is slower by a factor of ~1.7 once a fibrous capsule has formed around the membrane (Figure 4.5h). After 20 days of *Therepi* placement, the diffusion of 10 kDa FITC dextran through the tissue of interest is 5 -fold faster than the diffusion of 40 kDa dextran, due to the lower molecular weight (Figure 4.5i). Despite the formation of a fibrous capsule, which hinders diffusion to an extent, molecules with a range of molecular weights can be transported through the membrane into the tissue. A summary of this data, including tissue thickness, lag time and the diffusion coefficient is included in **Table 4.1**.

Table 4.1: Diffusion coefficient following formation of fibrous capsule *in vivo (*Figure 4.5*g-i)

Days Post-Implantation	**0**	**20**	**20**
Molecular Weight (kDa)	40	40	10
Tissue Thickness (cm)	0.167	0.225	0.216
Lag time (s)	8909	28750	8172
Diffusion Coefficient (cm²/s)	$3.13*10^{-6}$	$1.76 * 10^{-6}$	$5.71 *10^{-6}$
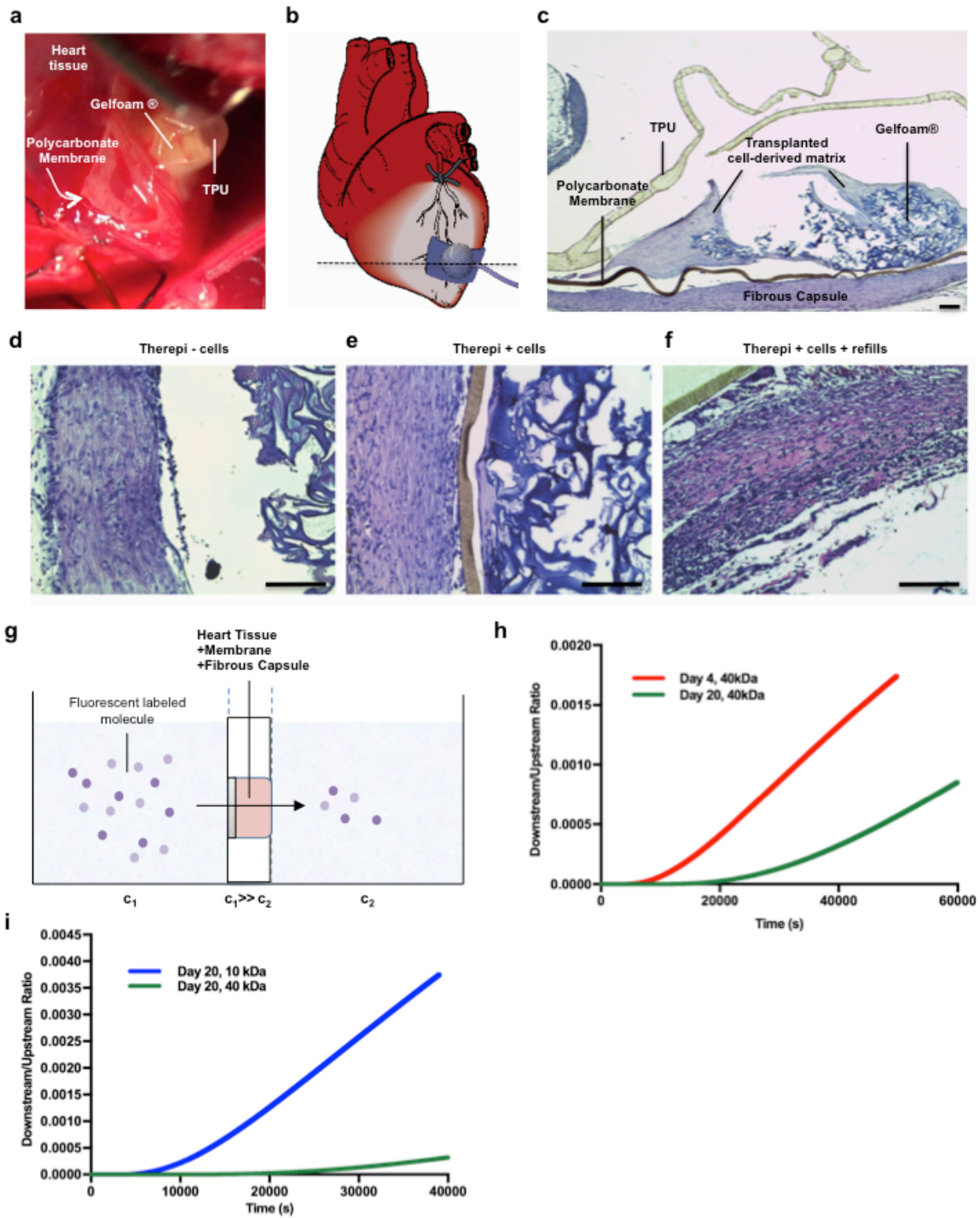
Figure 4.5: Assessment of fibrous capsule size and rate of macromolecule diffusivity.
(a) Appearance of *Therepi* on heart after 28 days. **(b)** Schematic of section through device taken for histology. **(c)** Overview of histological appearance of *Therepi* (TPU and polycarbonate membrane are visible, Gelfoam® with transplanted cells, and fibrous capsule). **(d-f)** Panel of histological images describing device/heart interface showing similar fibrous capsule for each *Therepi* group, regardless of the presence of cells. **(g)** Schematic of the diffusion chamber **(h)** Diffusion of fluorescently labelled 40kDa dextran over time through the diffusion chamber, for devices previously implanted for 4 or 20 days. **(i)** Diffusion of 10kDa and 40kDa dextran across fibrous capsules resulting from implantation for

20 days.

4.4.5   Demonstration of functional improvement with *Therepi*-based cell refilling.

Finally, the impact of *Therepi*-based cell refilling was determined in a 28-day study comparing cardiac function of the following groups over time; sham (MI only), single cell injection, *Therepi* without any cells, *Therepi* with cells, *Therepi* with cells and refills (Figure 4.6a). The delivered cargo was syngeneic bone marrow derived mesenchymal stem cells. Echocardiography was conducted at day 0, 7 and 28 in all groups, and for the refill group, cells were replenished at day 4 and 14 (Figure 4.6b).
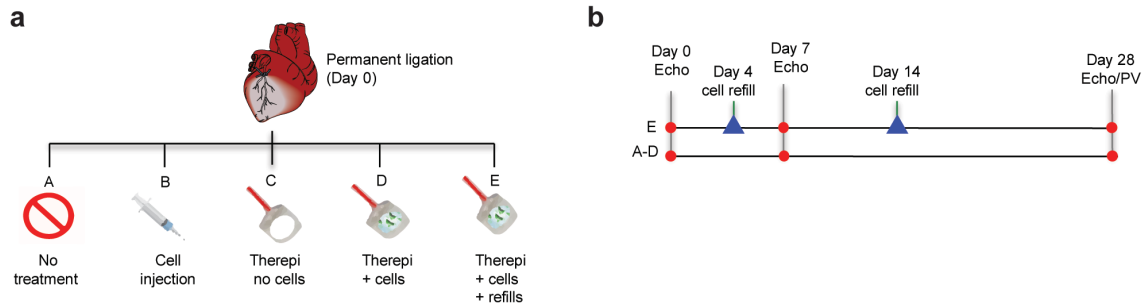
Figure 4.6 Pre-clinical study plan
(a) A description of groups for the 28-day pre-clinical study. (b) A timeline for the pre-clinical study, including timing of cell refills and functional assessment

Systolic and diastolic echocardiographic measurements were used to calculate ejection fraction (Figure 4.7 a-b). Ejection fraction and fractional shortening tended to decrease over time for the MI only and the cell injection group, but increased over time for the acellular *Therepi* device, and significantly for the *Therepi* with cell refill (Figure 4.7 c-e). Additional day 7 and day 28 ejection fraction statistical comparisons are shown in Table 4.2. Hemodynamic measurements of these animals were obtained with a pressure-volume (PV) catheter (AD instruments) at day 28 (Figure 4.7 f-h). Representative PV loops for MI and *Therepi* with cell refill regimen are shown in Figure 4.7f and indicate a leftward shift, and an increase in stroke work (area of PV loop). Ejection fraction measurements agreed with the echocardiographic measurements (Figure 4.7g). Stroke work demonstrated similar trends (Figure 4.7h) with *Therepi* with repeated cell dosing showing superiority to the no treatment group. The finding that cell refills at later time points provided functional benefit suggests therapeutic agents released from the device can diffuse into adjoining cardiac tissue.
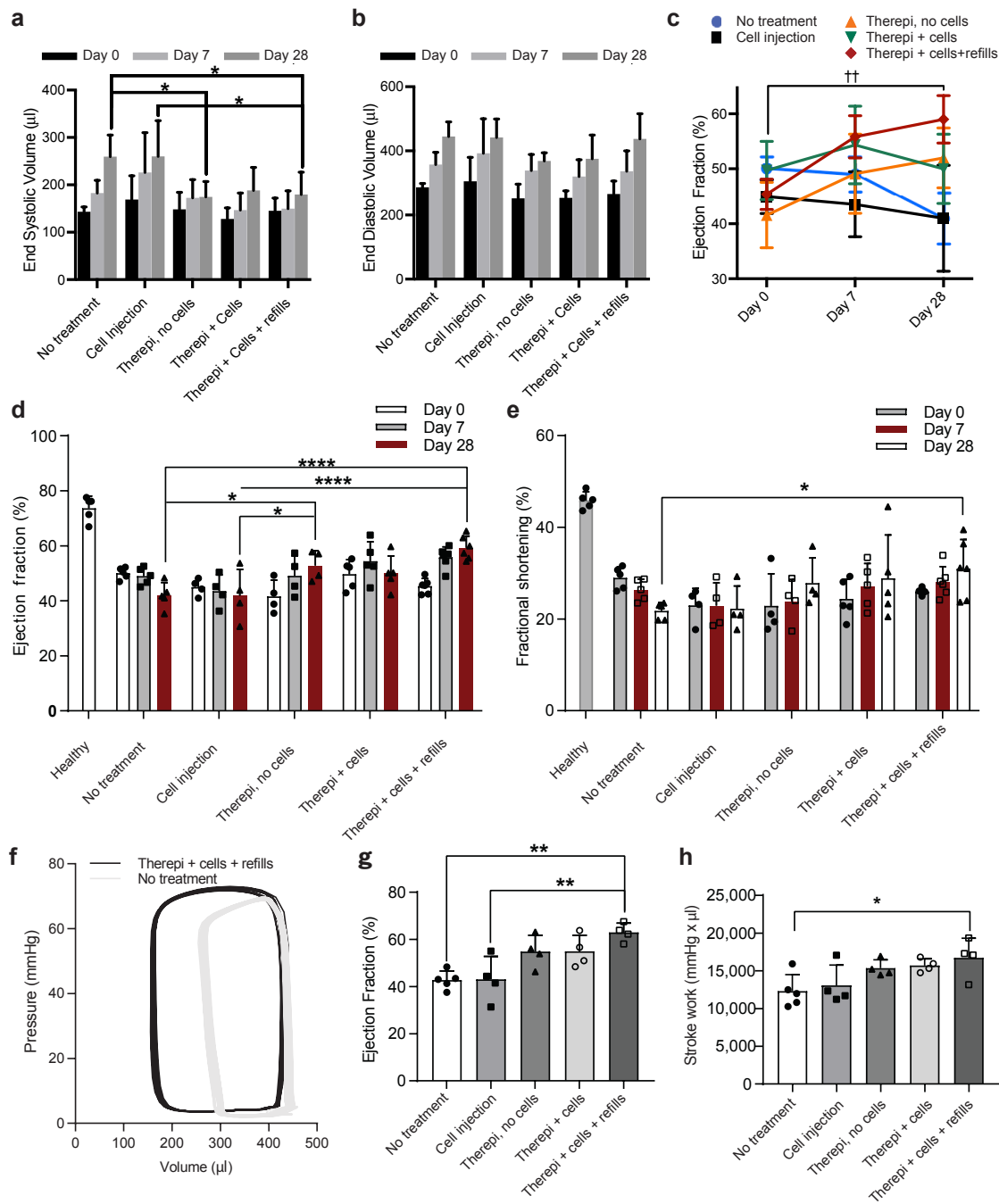
Figure 4.7: Pre-clinical safety and efficacy of *Therepi*. (a-b) End systolic and end diastolic volume for all groups assessed by echocardiography. *P<0.05. Values are mean ± s.d, (n = 4–6), as analysed by a two-way ANOVA, with Tukey's multiple comparisons post-test. **(c)** Ejection fraction over time assessed by echocardiography where ††P = 0.003 is the significance for the Therepi + cells + refill group between days 0 and 28. Values are mean ± s.d. (n = 4–6), as analysed by a two-way analysis of variance (ANOVA) across time points for each treatment group. **(d)** Ejection fraction for all groups as assessed by echocardiography. *P < 0.05, ****P < 0.0001; see Table 2 for exact P values. Values are mean ± s.d. (n = 4–6), as analysed by a two-way ANOVA, with Tukey's multiple comparisons post-test. **(e)** Fractional shortening for all groups assessed by echocardiography. Values are mean ± s.d. (n = 4–6), as analysed by a two-way ANOVA. *P = 0.0228. **(f)** Representative PV Loops for Therepi + cells + refill compared to MI with no treatment. **(g)** Ejection fraction for all groups as assessed by haemodynamic measurements. **P = 0.002 (versus no treatment), **P = 0.0037 (versus cell injection). Values are mean ± s.d. (n = 4 or 5), as analysed by a one-way ANOVA. **(h)** Stroke work for all groups assessed by haemodynamic measurements. *P = 0.0382. Values are mean ±

s.d. (n = 4 or 5), as analysed by a one-way ANOVA, with Tukey's multiple comparisons post-test.

Table 4.2: Multiple comparisons testing for ejection fraction (%) measured by echo (Figure 4.7)					
Tukey's multiple comparisons test	Mean Diff.	95.00% CI of diff.	Significant?	Summary	Adjusted P Value
Day 0					
No Treatment vs. Cell Injection	5.114	-4.84 to 15.07	No	ns	0.6003
No Treatment vs. *Therepi* - cells	8.473	-1.48 to 18.43	No	ns	0.1307
No Treatment vs. *Therepi* + cells	0.3553	-9.029 to 9.74	No	ns	>0.9999
No Treatment vs. *Therepi* + cells + refill	4.696	-4.289 to 13.68	No	ns	0.5843
Cell Injection vs. *Therepi* - cells	3.359	-7.133 to 13.85	No	ns	0.895
Cell Injection vs. *Therepi* + cells	-4.759	-14.71 to 5.195	No	ns	0.6635
Cell Injection vs. *Therepi* + cells + refill	-0.4176	-9.996 to 9.161	No	ns	>0.9999
Therepi - cells vs. *Therepi* + cells	-8.118	-18.07 to 1.836	No	ns	0.1607
Therepi - cells vs. *Therepi* + cells + refill	-3.777	-13.36 to 5.801	No	ns	0.8002
Therepi + cells vs. *Therepi* + cells + refill	4.341	-4.644 to 13.33	No	ns	0.6546
Day 7					
No Treatment vs. Cell Injection	5.449	-4.505 to 15.4	No	ns	0.5401
No Treatment vs. *Therepi* - cells	-0.1212	-10.07 to 9.833	No	ns	>0.9999
No Treatment vs. *Therepi* + cells	-5.326	-14.71 to 4.058	No	ns	0.5043
No Treatment vs. *Therepi* + cells + refill	-6.817	-15.8 to 2.168	No	ns	0.2188
Cell Injection vs. *Therepi* - cells	-5.57	-16.06 to 4.923	No	ns	0.5697
Cell Injection vs. *Therepi* + cells	-10.77	-20.73 to -0.8209	Yes	*	0.0276
Cell Injection vs. *Therepi* + cells + refill	-12.27	-21.84 to -2.688	Yes	**	0.0057
Therepi - cells vs. *Therepi* + cells	-5.205	-15.16 to 4.749	No	ns	0.5839
Therepi - cells vs. *Therepi* + cells + refill	-6.696	-16.27 to 2.882	No	ns	0.294
Therepi + cells vs. *Therepi* + cells + refill	-1.491	-10.48 to 7.494	No	ns	0.9899
Day 28					
No Treatment vs. Cell Injection	0	-9.954 to 9.954	No	ns	>0.9999
No Treatment vs. *Therepi* - cells	-11	-20.95 to -1.046	Yes	*	0.0233
No Treatment vs. *Therepi* + cells	-9	-18.38 to 0.3845	No	ns	0.0661
No Treatment vs. *Therepi* + cells + refill	-18	-26.99 to -9.015	Yes	****	<0.0001
Cell Injection vs. *Therepi* - cells	-11	-21.49 to -0.5078	Yes	*	0.0354
Cell Injection vs. *Therepi* + cells	-9	-18.95 to 0.9538	No	ns	0.0945
Cell Injection vs. *Therepi* + cells + refill	-18	-27.58 to -8.422	Yes	****	<0.0001
Therepi - cells vs. *Therepi* + cells	2	-7.954 to 11.95	No	ns	0.9794
Therepi - cells vs. *Therepi* + cells + refill	-7	-16.58 to 2.578	No	ns	0.2522
Therepi + cells vs. *Therepi* + cells + refill	-9	-17.99 to -0.01498	Yes	*	0.0494

4.5   Discussion

We present an implantable reservoir system that allows targeted, replenishable, and sustained presentation of molecular and cellular therapy to the heart. We have initially demonstrated, despite the formation of a fibrous capsule, which hinders but does not impede diffusion, molecules with a range of molecular weights can be transported through the membrane into the tissue, and in the case of adrenaline elicit a potent biological response. Furthermore, we noted a clear functional effect, through the *Therepi* 28 days after implantation. This functional benefit shown with later refills of cells support that paracrine factors can diffuse through this capsule. Future iterations of the device could use microneedle technology to allow for direct injection into tissue, and further improve delivery [256].

In this study, the delivered cargo was a syngeneic mesenchymal stem cell derived from the bone marrow of Sprague Dawley rats. It was hypothesised that a syngeneic source would induce a modest immune response, in comparison to allogeneic or xenogeneic sources, thus reducing the risk of pericardial adhesions, and the magnitude of fibrous capsule formation. A stem cell originating from bone marrow was chosen for the following reasons: (a) pre-clinical evidence for improving left ventricular function [257–259], (b) extensive use in cardiac regenerative human trials where feasibility of cell isolation and safety of the cells following delivery were established [51–53], (c) attractive cell therapeutics for a range of diseases characterised by chronic inflammation[260]. At the moment in the US, bone marrow stem cells are being investigated in >25 clinical trials for a diverse range of diseases, including Crohns, Multiple Sclerosis, and cancer [261]. We believe that Therepi shows promise as a platform delivery technology for multiple indications; therefore it made sense to initially prove the concept with a platform cell source.

Given the poor survival and rapid clearance of cells post administration, repeated doses are likely needed for best efficacy (like most pharmacological medications)[182]. From a mechanistic point of view, the functional benefit following the intramyocardial injection of bone marrow stem cells was initially attributed to the differentiation of exogenous cells into cardiomyocytes and vasculature[50]. Extensive lineage tracing studies, and extremely poor cell survival, have since disproven that theory[33,34]. It is now widely thought that paracrine release from delivered cells mediates a reparative or regenerative effect[31]. To support this theory, conditioned media from adult stem cells has been shown to generate a similar functional benefit to the cells themselves[32]. Proposed paracrine effects are multi-factorial and include induction of cardiac muscle cell proliferation, immobilisation of resident stem cells, neovascularisation, inhibition of apoptosis, and immunomodulation[31]. It is envisaged that each cell delivery will result in a bolus release of intracellular contents including cytokines, chemokines, exosomes and paracrine factors, followed by a lower sustained release until loss of stemness or cell death. Importantly, a cumulative benefit following repeat delivery has been demonstrated with two different cell types, c-kit[POS] cardiac progenitor cells[181] and cardiac mesenchymal cells[255].

Interestingly, the acellular *Therepi* provided a sustained benefit across the 28-day study, potentially due to its mechanical reinforcement of the remodelling ventricle or due to an altered healing response caused by the foreign body response. Early mechanical restraint of the infarcted left ventricle with polymeric meshed materials or wraps has been demonstrated to be highly effective in reducing infarct expansion and limiting negative remodelling in large animal pre-clinical models[165,213,214]. However, the *Therepi* with one-time cell

delivery had poor results, despite having mechanical reinforcement. While this is surprising, it highlights the importance of cell delivery timing for positive modulation of post-MI healing response. The harsh inflammatory environment of the infarcted heart has been shown to drive delivered MSCs towards a pro-inflammatory phenotype, limiting their reparative efficacy[224]. Cells delivered at the time of MI, and their secretome, would have been subject to this environment, and may even have adversely affected healing and negated any positive effect from the device mechanical reinforcement. If later delivery of cells is favourable, the *Therepi* system can be advantageous in allowing implantation of an acellular device, followed by subsequent cell delivery at a later timepoint, as described for other applications[262]. This approach would compliment delivery with autologous stem cells[47], when, for example, a biopsy could be taken at the time of implantation of the *Therepi*, and stem cells would be isolated, expanded, and then re-implanted through the *Therepi* after a number of weeks or months without the need for an additional surgery

However, there are some potential bottlenecks that need to be overcome before clinical translation is possible. First, the route of clinical access needs to be established. Clinically, our device is intended for percutaneous pericardial access, via sub-xiphoid access and pericardial puncture. Such an approach is increasing as more interventional cardiologists and electrophysiologists have become comfortable with it, presenting opportunities for intra-pericardial drug delivery[263,264]. Current interventional procedures for pericardial diseases include pericardiocentesis and percutaneous balloon pericardiotomy, demonstrating utility of this route for cardiac applications[263,264]. We used sutures for device attachment in this manuscript, however recent innovations in hydrogel adhesion could be used for a less invasive and more uniform adhesion to the heart[127].The procedure could be carried out in hybrid cath labs during reperfusion and would be an additional/adjunct to the current clinical management of a patient with MI. While the intent of this device is not for delivery during open-chest surgery, patients with advanced coronary heart disease, undergoing coronary artery bypass graft surgery could also be a target population.

It should be acknowledged that standard procedures for cell delivery to the heart, including transendocardial and intracoronary catheter delivery (via femoral access) are less invasive in comparison with *Therepi*, and do not require general anaesthesia. However, *Therepi* would be a one-time implantation that allows for multiple therapy administrations, which could be done in an ambulatory setting. Furthermore, the biomaterial reservoir would vastly extend cell survival, and thus potential clinical benefit, in comparison to a cell injection alone. Minimising pericardial adhesions will also be important. Minimally invasive catheter delivery could reduce post-procedural pericarditis, and therefore adhesions, in comparison with open-chest surgery. Alternative methods for reducing pericardial adhesions have also been reported, such as pharmacological control of inflammation (corticosteroids) and enzymatic breakdown of fibrous tissue (fibrinolytics)[265]. Localised delivery of these agents could be possible via Therepi.

Second, catheter associated infections could be a potential issue. It is worth noting, however that a permanent pericardial drainage system connected to a subcutaneous port has previously been safely implanted in patients for up to 5 weeks, with no infection noted[266]. Moreover, a multicentre randomized control trial is currently being undertaken to determine the safety and efficacy of extended pericardial drainage in comparison to a one off pericardiocentesis procedure[267]. A fully subcutaneous port with a self-sealing septum could be used to

minimize the risk, and ports are widely used currently for other applications, for example central venous access for chemotherapy drugs. The catheter tubing could be surface modified with an anti-bacterial, or hydrophilic coating to reduce bacterial adherence. Depending on the length of implantation/use, it is likely that a broad-spectrum prophylactic anti-bacterial regimen will be needed. In the event of disease resulting from the implantation, such as purulent pericarditis, the *Therepi* system itself could be used for the intrapericardial delivery of anti-bacterials and fibrinolytics.

Third, MRI compatibility would be advantageous. Current materials are all MRI compatible, except for the port, which would require modification. Fourth, it is important to design the system with mechanisms to avoid catheter obstruction by therapies, such as cell debris. In this study, cells were removed from the line by following each dose with saline, to clear the line. Other approaches could include enzymatic degradation and mechanical suction. Future versions of *Therepi* could be designed with a dual loop system to aid with these solutions.

Future work, prior to clinical implementation will focus on biodegradable device development, so there is no foreign material remaining on the heart. A permanent version of the device could also be an option, allowing for acute therapy replenishments initially and taking advantage of the long-term passive reinforcement effects[268].

It should be noted that in this pre-clinical study we initiated treatment directly after the time of cardiac injury. This is not directly clinically relevant, as cardiac injury would precede device implantation in the clinic. Future work will involve testing this device subsequent to injury. Furthermore, one type of cell cargo was tested here, a syngeneic mesenchymal cell source. There is a plethora of available cell sources, and other therapeutic cargos available. Determining the correct cargo, dose, and administration frequency, along with an accompanying mechanism of action will be key to advancing this delivery concept to the clinic [182].

We can draw three conclusions from this study; (i) the system enables direct, potent delivery of small molecules, that can penetrate the surrounding fibrous capsule and elicit a functional effect (ii) the system enables localized delivery of macromolecules that penetrate through the fibrous capsule into the myocardial tissue and distribute in three dimensions, (iii) in a 28 day rodent study in an MI model, the *Therepi* device (acellular or with transplanted cells) demonstrates therapeutic superiority compared to no treatment or a single cell injection, and this effect is increased with repeated cell administrations.

5 *RoboTherepi:* A soft robotic assisted hydrogel for precise spatial and temporal control of drug release

5.1 Preface

The previous three chapters focused on the initial development of simplified Therepi, encapsulation of this system in a protective reservoir and finally an assessment of safety and efficacy. Chapter 5 focuses on coupling the encapsulated biomaterial with a soft robotic actuator, which can compress the material on demand, and alter the passive release profile of drug, protein or cell produced paracrine factors with temporal and spatial control.

The aims of the chapter are as follows:

1.   To confirm that a polyacrylamide/alginate tough gel hydrogel is capable of undergoing multiple cycles of gross deformation without fracture

2.   To investigate different methods of modifying drug release from a polyacrylamide/alginate tough gel hydrogel following gross deformation

3.   To design and characterize a miniaturised soft robotic actuator

4.   To develop a method of combining a drug loaded tough gel hydrogel with a pneumatic soft robotic system and demonstrate gross deformation triggered drug release with actuation

5.2 Introduction

Hydrogel drug delivery systems hold vast promise in areas of medicine ranging from tissue engineering to pain management, oncology, and immunology [270]. These implantable systems can spatially and temporally control availability of loaded therapeutics, including cells, small and macromolecules, to the surrounding target tissue[105]. Controlled localized release via hydrogel implants confers many advantages over conventional systemic delivery formulations such as tablets or injections, where high systemic concentrations and lengthy treatment courses are needed to elicit the desired biological effect, leading to off-target side effects, poor patient compliance and reduced clinical efficacy [104]. This poor level of control is particularly detrimental for drugs with a narrow therapeutic index, such as chemotherapy, where a small increase in concentration can lead to toxicity and a small decrease can lead to treatment failure [105].

Composed primarily of water, the physical structure and mechanical properties of a hydrogel are defined by a soluble cross-linked polymer network. Release of drug from this network can be controlled by a number of variables including the space between polymer chains, also known as the mesh size, and chemical or electrostatic interactions between the polymer chains and drug [104]. While great advances have been made in the design of hydrogel systems for the purposes of controlled released, these formulations often exhibits a pre-determined passive release profile, which is initially high, and then tapers quickly [105]. Such a release profile only matches the ideal pharmacokinetic profile of certain drugs. Furthermore, an inflexible release rate does not account for patient, disease or anatomical site variability or preference in the case of pain control [271].

While methods of externally modulating hydrogel drug release have been developed, such as ultrasound waves and magnetic fields, these approaches have shown to be suboptimal due to inconsistent or weak

stimulus application and poor stimulus depth penetration in deeper tissues [272–276]. An ideal system for triggered drug release would predictably and consistently release drug against an applied stimulus in both superficial and deep target organs [104].

While the field of biomaterials is advancing rapidly, medical robotics is also making great strides towards precision drug delivery, i.e. delivering the right treatment at the right time to the right location [211]. Implantable microchip devices have paved the way in this regard [277–281]. Each implant contains 100's of hermitically sealed micro drug reservoirs, which can be opened in response to a programmed schedule, a physiological stimulus, or by wireless communication from the clinician or patient [277]. The delivery platform has undergone clinical testing for the treatment of osteoporosis and shows great promise in conditions with compliance difficulties e.g. psychiatric illness [281]. However these rigid devices have inherent limitations in terms of tissue placement, and are most suitable for subcutaneous implantation [278]. Furthermore, micro-electromechanical manufacturing techniques can limit the type and amount of therapy that can be loaded [277].

We propose to achieve controlled release by coupling a hydrogel component with an inflatable soft robotic actuator. Actuator activation will cause gross deformation of the hydrogel system, accompanied by a temporary increase in mesh size and accelerated transport of drug, protein or cell produced paracrine factors to the local target site. This approach allows us to externally control the timing and magnitude of therapy release from a hydrogel via application of a precise, tuneable soft robotic stimulus, even in deeper dynamic tissues such as the heart. Furthermore, the use of soft components lends itself to safe and minimally invasive device implantation.

In this study, we choose a polyacrylamide/alginate tough hydrogel (TG) due its high fracture energies (up to twice that of conventional hydrogels) and its ability to undergo a high degree of mechanical strain (20 times its original length) [244,282]. Importantly, the ability to undergo high deformation without material failure allows a large design space for tuneable drug release following device actuation. Furthermore, a material that can mechanically deform over multiple cycles without cumulative damage, material failure and unwanted drug release is highly desirable. With this unique coupling of a tough drug-loaded hydrogel and a soft robotic actuator, *RoboTherepi*, we demonstrate controlled release by altering the control strategy and the biomaterial/cargo interaction. This work establishes proof of concept and major progress towards a novel soft robotic assisted hydrogel.

5.3   Materials and Methods

5.3.1   Tough Gel manufacture

Material preparation

Alginate/Acrylamide Solution: A 1:1 ratio of high and low molecular weight Alginate was weighed (KIMICA Alginate 1G, KIMICA Alginate 3G). 0.451g of alginate and 2.704g of acrylamide (A9099 SIGMA) were weighed and dissolved in 20 ml DI water (Acrylamide is toxic, and must be weighed in a closed container and handled in a fume hood). The mixture was then stirred overnight at room temperature until a homogenous viscous solution was produced. Solution was stored at 4°C.

CaSO$_4$ suspension: 2.07g CaSO$_4$.2H$_2$O (255548 SIGMA) was suspended in 10mL DI water and stirred for at least two days.

MBAA solution: 200mg MBAA (M7279 SIGMA) was dissolved in 10mL DI water.

1.5 mM CaCl2 Solution: 500 mg of CaCl2 dihydrate (C7902 SIGMA) was dissolved in 5 mL of calcium and magnesium free HBSS to form a stock solution. 220.5 uL of the stock solution was added to 100 mL of calcium and magnesium free HBSS.

Ammonium persulfate (APS): APS (A3678 SIGMA) solution was prepared just before synthesis by dissolving 330mg into 5mL DI water. The resulting solution was protected from light and kept in closed container.

TEMED: No preparation was needed for TEMED (T7024 SIGMA).

Fluorescein labelled Dextran: FITC-dextran solution (see table below) was prepared just before synthesis by dissolving 3 mg of FITC-dextran into 100 uL of calcium and magnesium free HBSS.

FITC-dextran	FD150S SIGMA	150k
FITC-dextran	FD500S SIGMA	500k
FITC-dextran	FD40S SIGMA	40k
FITC-DEAE-dextran	01649 SIGMA	40k

Materials for syringe mixing: Two 10 mL or 3 mL BD syringes and one luer lock syringe connector are needed for syringe mixing. The luer lock connector was custom printed with an integrated mixer. However, a standard luer lock connector can be used to successfully manufacture TG.

Materials for Tough gel mould: Two teflon coated glass slides, binder clips, and an acrylic mould with the following dimension (7.7 mm diameter, 2.05 mm height) were gathered

TG Synthesis

1.   Alginate-acrylamide solution was degassed before synthesis by placing it under vacuum for 2 hours.
2.   CaSO$_4$ and APS was added to syringe 1. Alginate/AAm mixture, MBAA, TEMED, and FITC-dextran solution were added to Syringe 2. The specific quantities are summarized below under the heading 3ml syringe mixing and 10ml syringe mixing.
3.   Care was taken to ensure that the dead volume of each syringe was full of fluid, and no air was trapped.
4.   A luer lock connector was attached to syringe 2. Alginate mixture was brought up to the tip of the luer lock to avoid a dead volume of air in the subsequent mixing process. Syringe 1 and 2 were connected with the luer lock connector.

5. After connection, solution were promptly and rapidly mixed between the two syringes until distributed evenly (10 times). The resultant mixture was poured into the mould. Glass PDMS coated slides and binder clips were used to make an airtight seal. The assembly was covered with aluminium foil to prevent light exposure, and stored overnight at room temperature until the reaction was completed.

6. Following completion, each gel was taken out of its individual mould. As part of the acrylamide monomer washout process, each gel was soaked in 1 mL of 1.5 mM $CaCl_2$ bath for 30 minutes, followed by three repeated dips in 1mL of calcium and magnesium free HBSS. Gels were then stored in an airtight plastic bag at 4°C and protected from light.

10 mL syringe mixing:

Syringe 1: 95.5 uL $CaSO_4$ and 113 uL APS were added.

Syringe 2: 5 mL Alginate/AAm, 18 uL MBAA, 4 uL TEMED, and 261.6 uL FITC-dextran solution were added.

3 mL syringe mixing:

Syringe 1: 19.1 uL $CaSO_4$ and 22.6 uL APS were added.

Syringe 2: 1 mL Alginate/AAm, 3.6 uL MBAA, 0.8 uL TEMED, and 52.3 uL FITC-dextran were added.

5.3.2 Calculation of total loaded drug

Theoretical loading calculation

$Dextran\ Mass\ (mg) = 1.569;\ Total\ Gel\ Volume\ (uL) = 95.46$

$\text{Drug Concentration}\ \left(\frac{mg}{uL}\right) = \left(\frac{\text{Dextran Mass}}{\text{Total Gel Volume}}\right) = 0.001428$

$Gel\ Diameter\ (mm) = 7.7;\ Gel\ Height(mm) = 2.25;\ Gel\ Volume\ (mm^3) = 95.46$

$Drug\ Loading\ (mg) = Drug\ Concentration * Gel\ Volume = 0.13636$

Experimental loading measurement

A 10-unit/mL solution of Alginate lyase in in calcium and magnesium free HBSS was prepared, and protected from light (A1603 SIGMA). Each gel was submerged in an eppendorf tube containing 1 mL of alginate lyase solution and incubated for 24 hours at 37°C. They were protected from light during this process. Degradation of the nanoporous alginate network caused release of encapsulated drug. To quantify drug recovery of each gel, a sample was taken and measured for fluorescence. A plate reader was used to measure fluorescence at 485nm and 528nm with black 96 well plates. A concentration was calculated from interpolation of a standard curve of known values.

5.3.3 Mechanical tester compression studies

Compression tester: Tough gel mechanical characterization and compressive drug release tests were performed on a Texture analyser with a 5 kg load cell and compression plates (TA.XT Plus, Texture Technologies).

Washout: All gels underwent a washout step of 30 minutes in 1.5 mM CaCl2, followed by three quick dips in calcium and magnesium free HBSS (as previously described)

Rate: The gels were compressed over one minute using the texture analyser (30 s compression, 30 s release). Settings are summarized in the below table

Test mode	Compression
Pre-test speed	0.08 mm/s
Test speeds	0.02, 0.04, and 0.06 mm/s for 25, 50, and 75% respectively
Post-test speed	0.08 mm/s
Target mode	strain
Strain	25, 50, or 75% respectively
Trigger type	Auto (Force)
Trigger force	0.025 N
Advanced options	Off

TG dimensions: 7.7 mm diameter, 2.05 mm height

Compressions Strategy 1:

1. Gels were placed in a 1.5 mM CaCl2 bath for 12 minutes
2. Gels were then compressed at 25, 50 or 75% strain with 1 mL of 1.5 mM CaCl2 surrounding the gel
3. This process was repeated 5 times, every 12 minutes, for each sample.
4. Gels were transferred carefully to a 24 well plate, to allow for diffusion release, between compressions.
5. A 1ml release sample was taken and fully replaced at the following time points: 12 min, 12 min compression, 24 min, 24 min compression, 36 min, 36 min compression, 48 min, 48 min compression, 60 min, 60 min compression.
6. Compression plates were cleaned with 70% isopropanol between each gel test.

Compressions Strategy 2:

1. Gels were placed in 1.5 mM CaCl2 bath for 1 hour.
2. Gels were then compressed at 75% strain with 1 mL of 1.5 mM CaCl2 surrounding the gel
3. This process was repeated 5 times, every hour, for each sample
4. Gels were transferred carefully to a 24 well plate, to allow for diffusion release, between compressions.
5. A 1ml sample was taken and fully replaced at the following time points: 1 h, 1 h compression, 2 h, 2 h compression, 3 h, 3 h compression, 4 h, 4 h compression, 5 h, and 5 h compression.
6. Compression plates were cleaned with 70% isopropanol between each gel test.

5.3.4 Fluorescence measurements

Plate Reader: A SpectraMax M3 plate reader was used to measure Fluorescence at 495 nm (excitation) and 528 nm (emission) for each solution. Fluorescence was measured for three replicates for each solution, and an average reading was calculated. A concentration was calculated from interpolation of a standard curve of known values.

Standard Curve: A standard curve was prepared by diluting the respective FITC-dextran solution that the gels were loaded with. The following concentrations were measured for the standard curve: 1000, 100, 50, 25, 20, 10, 4, 2, 1, 0.5, 0.25, 0.2, 0.1, 0.05, 0.02, 0.01, and 0.004 ug/mL.

5.3.5 Actuator manufacturing process

Outer and inner balloon thermoforming: A 0.0012-inch thick Thermoplastic polyurethane layer (XGD0385, QINGGEN) was used to manufacture the outer balloon. A 0.003-inch thick Thermoplastic

polyurethane layer (HTM 8001-M polyether film, American Polyfilm, Inc.) was used to manufacture the inner balloon layer. A sheet of TPU was mounted in a vacuum thermal former. A positive 3D-printed mould was placed on a platform below the TPU sheet. The TPU sheet was heated until it noticeably sagged at the centre. The TPU was quickly lowered onto the positive mould as a vacuum was applied. As the heated TPU met the positive mould, the TPU sheet formed over the positive mould, with the vacuum ensuring that the sheet fully conformed to the shape of the mould.

Heat-sealing of inner and outer balloon layers: The outer balloon thermoformed TPU layer was placed in a negative mould. A 22G gauge needle was placed in the thermoformed channel to maintain an opening for the catheter tubing to be inserted in a later step. The inner balloon thermoformed TPY layer was placed on top. The assembly was heat-sealed with a heat press (Heat transfer machine QXAi, Powerpress) at 330 °F for 13 seconds. The TPU layers were then sealed together.

Catheter Insertion and sealing: The 22G gauge needle was removed to reveal a thermoformed channel. The TPU catheter tubing was threaded onto a mandrel and the assembly was guided through the channel opening and into the pocket. Heat shrink tubing was placed around the interface between the TPU pocket and the catheter. The device was inserted into the aluminium mould and heated with the heat press at 330 °F for 60 seconds. The device was then turned 180 degrees without removing it from the aluminium block, and heated for another 60 seconds. The device was taken out of the aluminium block and the heat shrink tubing was removed.

Tough gel insertion and sealing of non-rate limiting membrane: The tough gel was placed in the thermoformed pocket. A second sheet of TPU (0.003 inch thick) with 5 evenly distributed laser-cut pores (0.012-inch diameter) was placed over the pocket. The assembly was sealed in place using a heat press at 330 °F for 13 seconds.

Storage: The completed devices was sealed in an airtight container and protected from light until use.

5.3.6   Actuator characterisation studies

Actuator characterisation studies were performed on a Texture analyser with a 5 kg load cell and compression plates (TA.XT Plus, Texture Technologies). The miniaturised actuator was placed in an O-ring, and the force plate of the mechanical tester was lowered until a force was measured. Following force reset, the actuator was pressurised from 1-15psi using two different pneumatic control systems (Figure 5.1). The custom pneumatic control unit was setup was previously described (Figure 5.1a) [234]. The programmable syringe pump (PhD Ultra, Harvard Apparatus) was coupled with a pressure gauge (Figure 5.1b) and moving the syringe backwards and forwards was used to increase or decrease pressure appropriately.
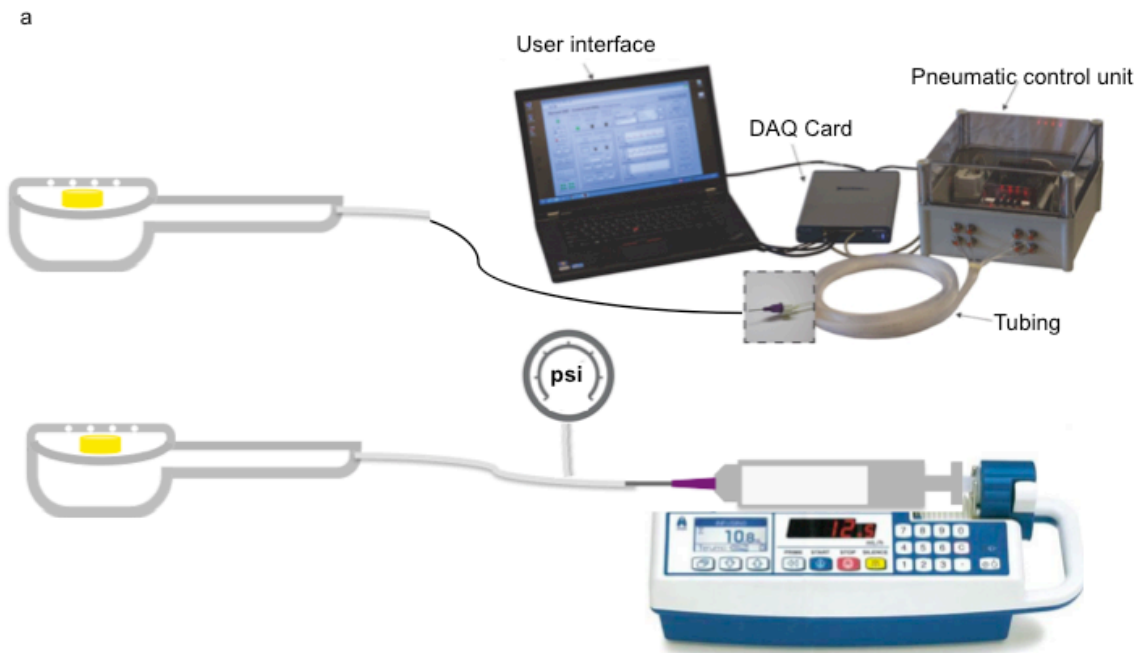
Figure 5.1: Pneumatic control systems for a miniaturized soft robotic actuator
(a) Customised pneumatic control unit **(b)** Programmable syringe pump

5.3.7   RoboTherepi drug release studies

The custom pneumatic control unit was setup was previously described[234], and connected to the devices (Figure 5.1a). The device was submerged in release media to capture drug release. The device was pressurised to 9psi over 30 seconds, followed by depressurisation to 0psi over 30 seconds. This was repeated once every hour for 5 hours. Release samples were taken at the following time points: 1 hour, 1 hour compression, 2 hour, 2 hour compression, 3 hour, 3 hour compression, 4 hour, 4 hour compression, 5 hour, 5 hour compression.

5.4 Results:

5.4.1 *RoboTherepi* vision and mechanism of action

Here we introduce the *RoboTherepi* concept, a replenishable biomaterial reservoir coupled with a soft robotic actuator, which can compress the material on demand, and alter the passive release profile (Figure 5.2a,b). It is envisaged that compression can alter drug release via a number of mechanisms including (a) accelerated convective fluid flow (b) alteration of the biomaterial pore size (c) disruption of chemical or electrostatic interaction between the drug and biomaterial. Clinically, *RoboTherepi* could be placed on the border zone of the infarcted hear, or other damaged tissue. Independent controlled actuation would then be achieved by applying manual or automated pressure to a subcutaneous fluid filled bladder in direct connection with the distal reservoir (via an actuation line). Moreover, minimally invasive therapy replenishments to the biomaterial are possible by injection through a subcutaneous port and fill line (Figure 5.2c).
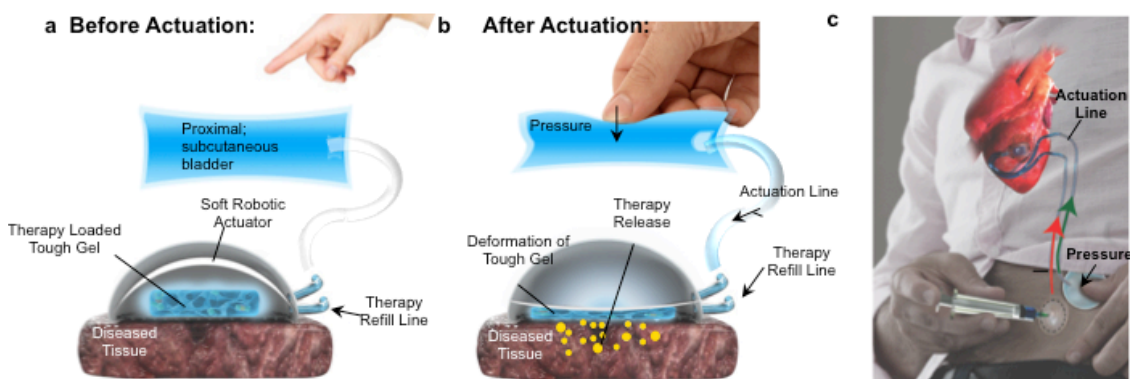
Figure 5.2: Overview of *RoboTherEpi* mechanism of action and vision for clinical translation
(a, b) Overview of the *RoboTherepi* mechanism of action. Application of pressure to a proximal subcutaneous bladder leads to actuation of a distal bladder in contact with a biomaterial-encapsulated reservoir. Subsequent gross deformation of the biomaterial leads to controlled release of therapy to damaged tissue. A catheter line for loading and reloading of therapy is connected to the therapeutic reservoir **(c)** Vision for translation of the *RoboTherepi* system to the clinic. Patient is applying pressure to a subcutaneous fluid filled bladder, connected to a smaller bladder implanted in a deeper tissue. This action leads to actuation of the smaller bladder and subsequent release of biological therapy from the attached therapeutic reservoir. Patient can load and reload therapy to the reservoir by injection through a subcutaneous port and fill line.

5.4.2   A biomaterial capable of undergoing cyclical gross compressive strain

Next, we identified a biomaterial with mechanical properties that could undergo gross deformation without fracture and system failure. Hydrogels in general display poor mechanical properties limiting their potential for clinical application as exhibited by the fracture of covalent linked alginate under a 20% compressive strain (Figure 5.3a)[284]. In contrast, our chosen tough material, can undergo a 90% compressive stain with full recovery (Figure 5.3b)[283]. Here we demonstrate the ability of a drug loaded TG to undergo multiple compressions strain cycles equivalent to 75% of its original height over a period of 5 hours, without fracture or appearance of damage (Figure 5.3c). For this study, the hydrogel was loaded with a drug analogue, 40kDa fluorescently labelled Dextran and stored in calcium supplemented phosphate buffered saline (PBS) between cycles to simulate normal drug loading and release conditions. Furthermore, we show that the force required to compress the biomaterial over multiple cycles remains consistent, even as the biomaterial swells (Figure 5.3d).
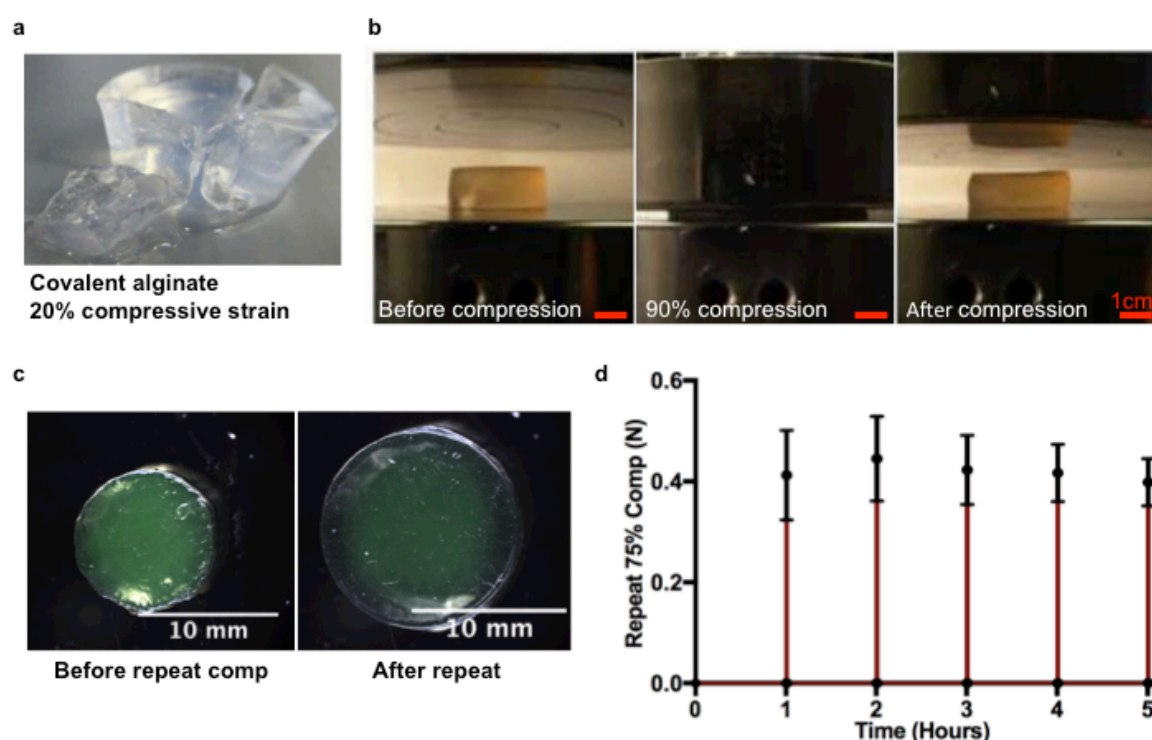
Figure 5.3: A biomaterial capable of undergoing cyclical gross compressive strain
(a) Covalent linked alginate shows material failure under a 20% compressive strain. **(b)** Tough gel shows ability to undergo 90% compressive strain with full recovery. **(c)** Drug loaded TG can undergo multiple cycles of 75% compressive strain in normal release conditions and maintain its mechanical structure (n=4). **(d)** Force required compressing TG by 75% over multiple cycles. In all cases, the gels were compressed over one minute using the texture analyser (30 s compression, 30 s release). (n=4).

5.4.3 Controlled release of drug therapy via compressive deformation, temporary enlargement of hydrogel mesh size, and release of physically entrapped drug

When the drug is smaller than the hydrogel mesh size, release rate is dominated by diffusion, as defined by the Stokes-Einstein equation [285]. According to the equation, diffusivity (D) of the drug through the hydrogel medium is dependent on the radius of the therapeutic agent (which typically scales with molecular weight) and the viscosity of the hydrogel medium (η). Here, T is the absolute temperature, and R is the gas constant.

$$D = \frac{RT}{6\pi\eta r_{drug}}$$

When the drug size is near equivalent or greater than the hydrogel mesh size, steric hindrance by the polymer chains can affect the mechanism of release. In this case, the polymer chains can physically entrap the drug, and dramatically impede diffusion [104]. Here, we investigated a method of controlling drug release by temporarily modifying, via compression, the TG mesh size in comparison to the hydrodynamic radius of the loaded cargo Application of uniaxial compression will cause expansion in normal plane (Figure 5.4 a,b)
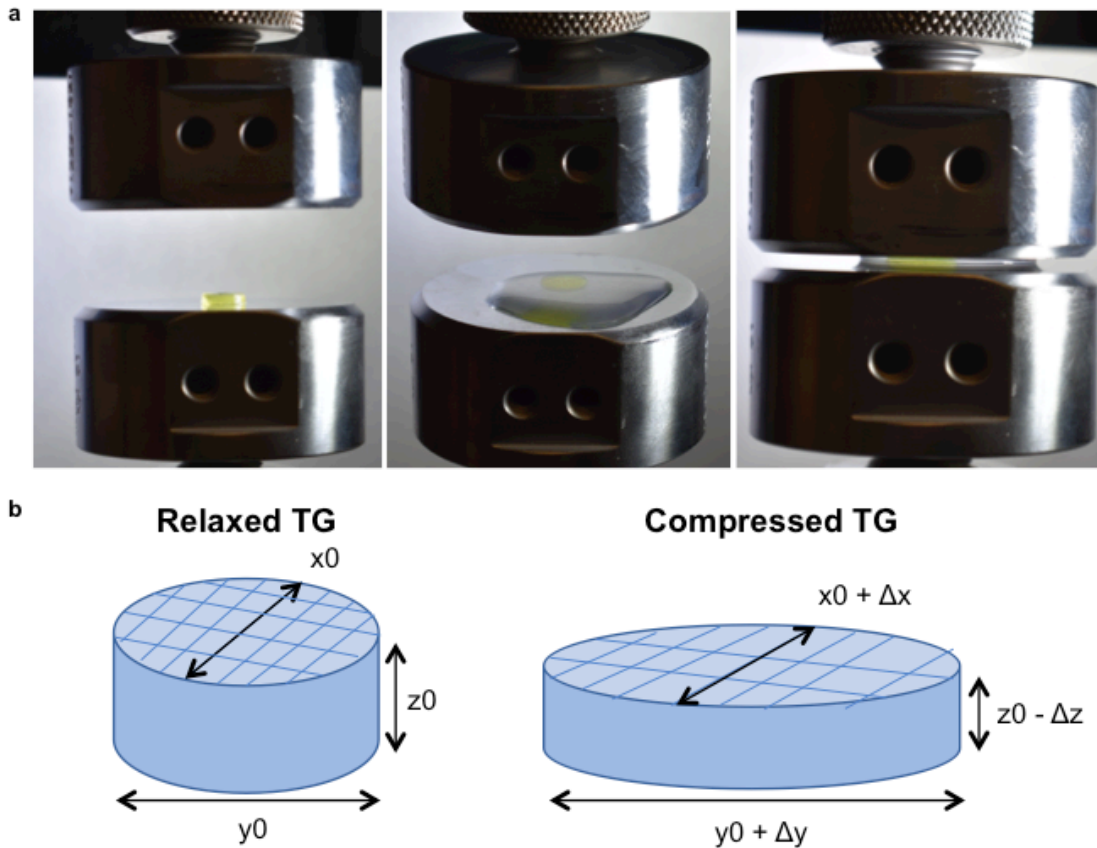
Figure 5.4: Deformation of TG pore size in the x, y, z direction following compression
(a) Compression of tough gel with mechanical tester, surrounding fluid is to capture drug release (b) Application of a force in the z-direction leads to biaxial expansion of pore size in the xy-plane.

We hypothesize that this expansion causes alginate ionic bond breakage and increased pore size in this plane, leading to release of the physically entrapped drug. After release the gel returns to its passive state, and the ionic bonds are reformed (Figure 5.a). First, we validated that increasing molecular weight, hydrodynamic

radius and steric hindrance can affect the diffusion of drug from a tough gel according to the above principles. The polysaccharide Dextran was chosen to demonstrate this, as it is available in a range of well-characterised sizes. [286]. Alginate gels are nanoporous with a mesh size of ~5.8 nanometre [287,288]. 150kDa Dextran has a similar hydrodynamic radius (~6.9 nanometre), so diffusion is impeded by the mesh. 500kDa Dextran hydrodynamic radius (~14.7 nanometre) is almost double the mesh size of alginate, causing significant physical entrapment of the drug (Figure 5.5b).

Next, we investigated the effect of release on compression. A TG loaded with 500kDa dextran was subjected to a 75% compressive cycle every hour for 5 hours, with passive diffusion between cycles. This group was compared to a control, which received no compression. We show a stepwise increase in drug release following each compressive cycle, with cumulative release substantially greater than the control TG, which did not receive any compression (Figure 5.5c). The release rate increased immediately after each compressive cycle, and showed a lower variability than baseline release when decompressed (Figure 5.5c). The average release rate was significantly higher (40 fold) when comparing before and after compression. This shows that we can achieve much higher drug release using compression with a drug whose hydrodynamic radius is close to the mesh size.
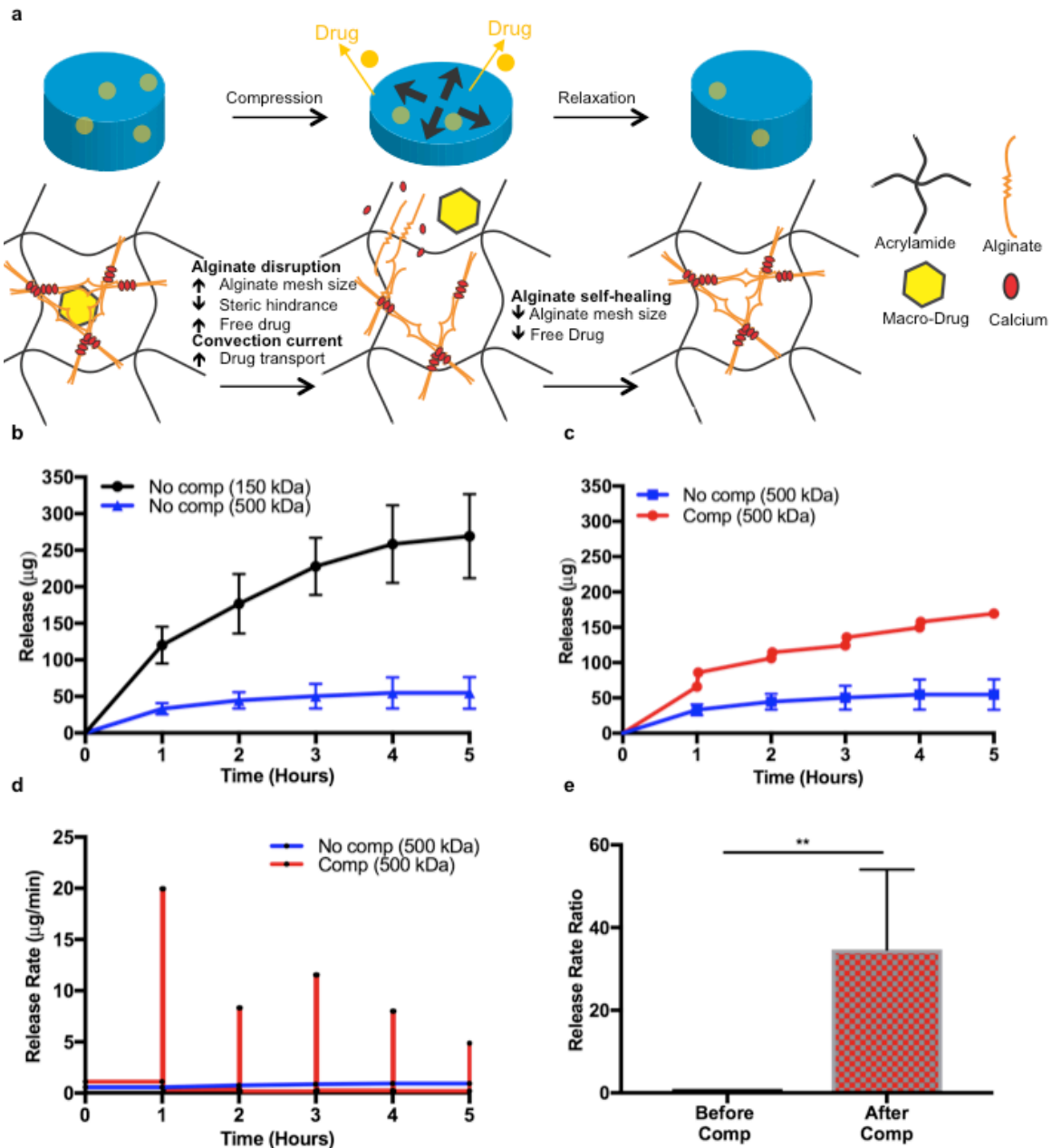
Figure 5.5: Compression induced release of physically entrapped drug
(a) Schematic describing controlled release by altering the size ration between the cargo and the tough gel pore size **(b)** Diffusion release of dextran with two different sizes (n=3) **(c)** Release of 500kDa dextran in response to a 75% compressive strain **(d)** Release rate of 500kDa dextran in response to a 75% compressive strain, and compared to no compression (n=1,3) **(e)** Average release rate ratio for 500kDa dextran before and after a 75% compressive strain (n=5). Significance determined by an unpaired, 2 sided T test, **P=0.0046. Comp=compression

114

5.4.4 Controlled release of drug therapy via compressive deformation, temporary enlargement of hydrogel mesh size, and electrostatic dissociation

Next we investigated a method of controlling drug release by disrupting the electrostatic interaction between the polymer chains of the hydrogel and the drug cargo with compression. In this case, uniaxial compression of the gel will cause expansion in the normal plane (Figure 5.4), leading to alginate network disruption, ionic bond breakage and electrostatic dissociation of bound drug. After release the gel returns to its passive state, and the ionic bonds are reformed (Figure 5.a). Again, we used Dextran as our model drug to study release. To reduce affects caused by steric hindrance we chose a 40kDa Dextran, with a hydrodynamic radius of 4.4 nanometers[286], smaller than the mesh size of common alginate gels (~5.8 nanometre [287,288]). We compared fluorescent dextran with different charge profiles at this size range, a neutral uncharged dextran (FITC–Dextran, sigma) and a positively charged polycationic derivative (FITC-DEAE-Dextran, Sigma).

First, we show that positively charged dextran has a lower release mediated by passive diffusion (Figure 5.b) due to an electrostatic bond formed with the negatively charged alginate polymer chains. Next we investigated the effect of release after compression. A TG loaded with positively charged or neutral dextran was subjected to a 75% compressive cycle every hour for 5 hours, with passive diffusion between cycles (Figure 5.c). The uncharged dextran showed a similar total release both with and without compression over 5 hours. In comparison, there was a clear and significant difference in total release between the compression and non-compression group for the charged dextran (Figure 5.d). The charged and uncharged groups showed similar fold increases in release rate immediately after compression (Figure 5.e). This can be explained by accelerated diffusion of drug, triggered by the compressive force. However, in the 60-minute period after each compressive cycle, the charged group showed significantly greater release than the control non-compression group, suggesting that extra drug molecules had become electrostatically dissociated and available for release. This was not the case for the uncharged neutral dextran (Figure 5.f).
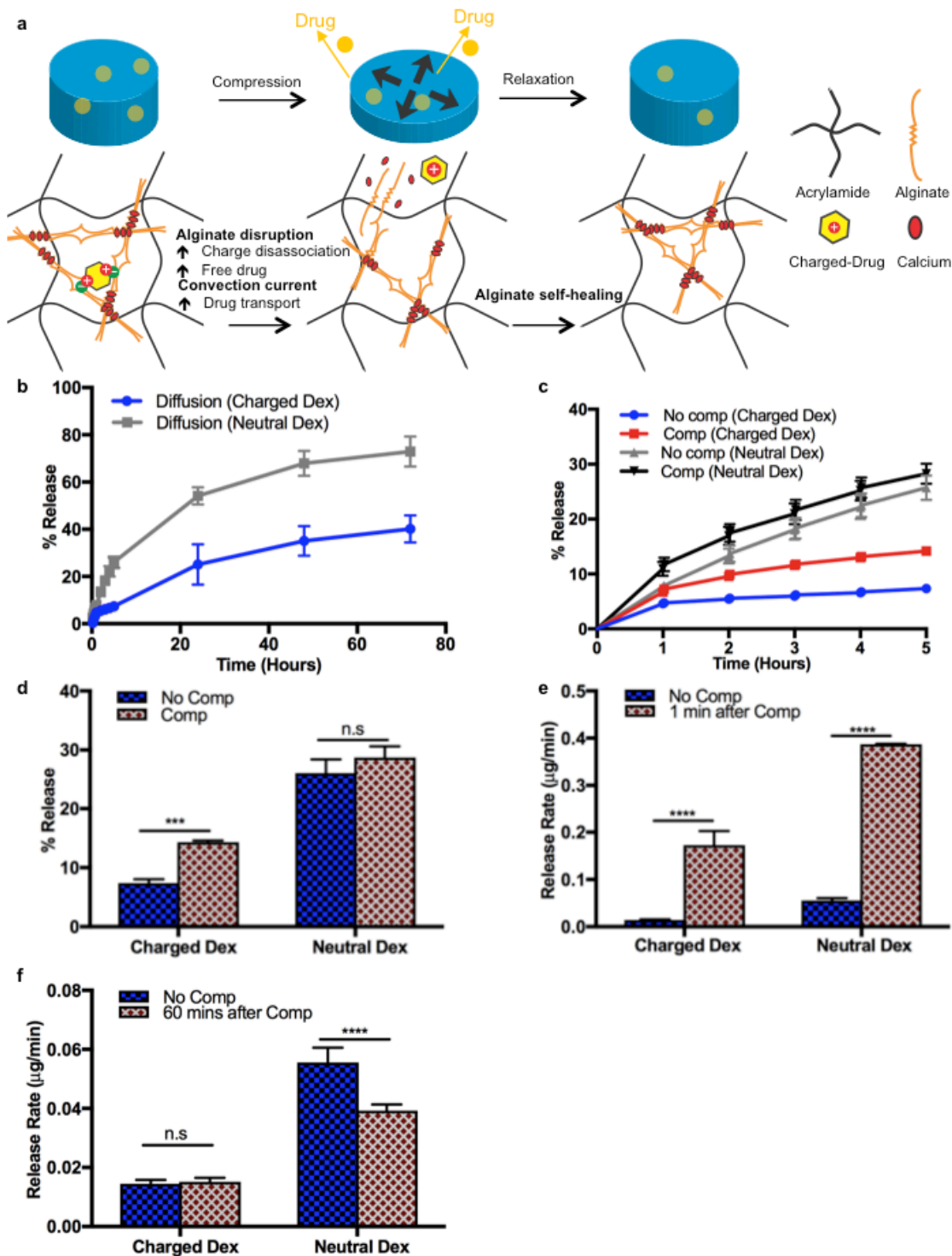
Figure 5.6: Compression induced release of electrostatically coupled drug (a) Schematic describing controlled release by electrostatic dissociation following compression **(b)** Diffusive release of neutral and positively charged dextran **(c)** Release of neutral and positively charged dextran following 75% compressive cycles, (n=4) **(d)** Cumulative release of neutral and positively charged dextran following 75% compressive cycles, significance determined by one way ANOVA with Tukey's, ***P=0.0002 (n=4) **(e)** Release rate of neutral and positively charged dextran 1 minute after compression, significance determined by one way ANOVA with Tukey's, ***P<0.0001 (n=4) **(f)** Release rate of neutral and positively charged dextran 60 minute after compression, significance determined by one way ANOVA with

Tukey's,****P=<0.0001 (n=4). Comp=Compression. Dex=Dextran

5.4.5 Mechanical control strategies for compressive mediated release

Here, we show some of the possible mechanical control strategies that could be used with an implantable soft robotic device. A positively charged 40kDa Dextran molecule loaded into a TG was used to showcase these strategies. First, a TG group underwent varying compressive strain of 25 and 75% every 12 minutes for 1 hour, with passive diffusion between the cycles. A higher compressive strain caused greater cumulative release (Figure 5.7a) and greater release rate following compression (Figure 5.7b). Frequency of compression could also be used to alter release, with greater frequency enhancing release (Figure 5.7c). Finally, we show that compressive duration is another tuneable parameter, with release increasing with the length that the pores are open (Figure 5.7d).
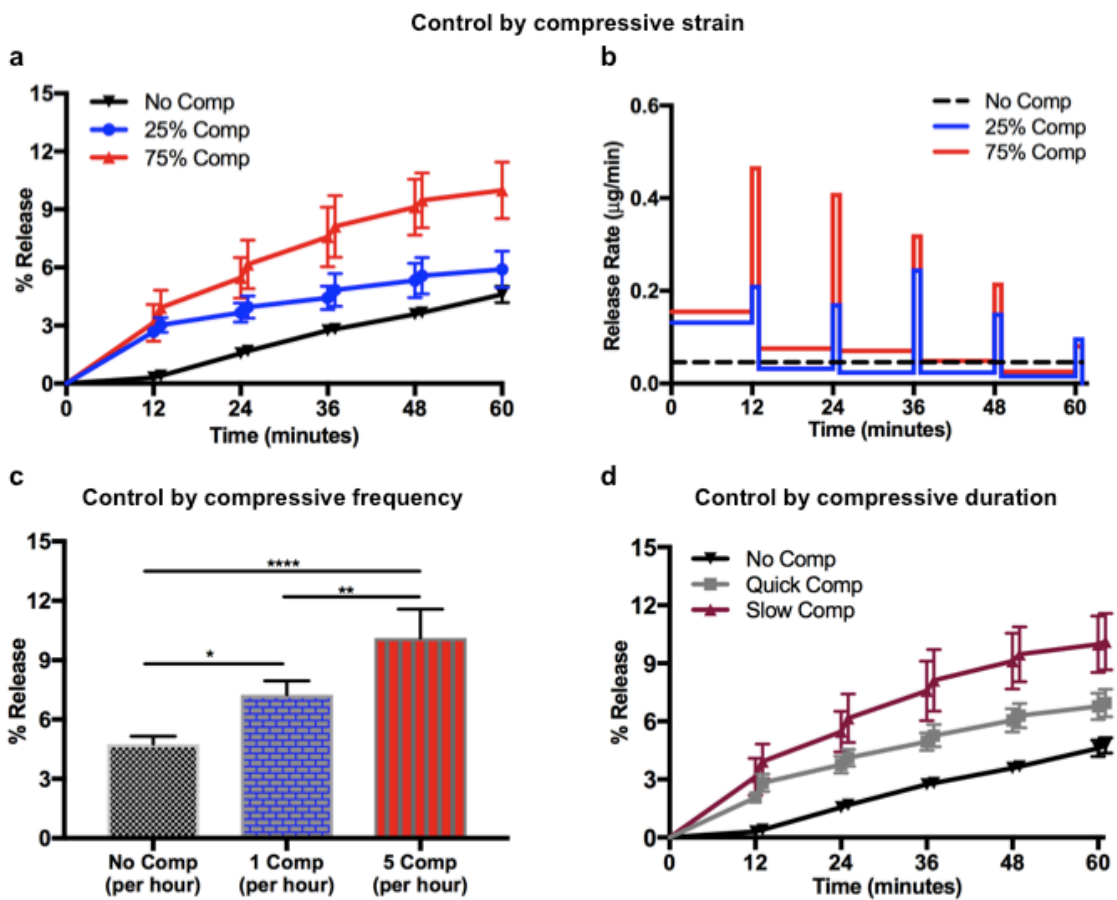
Figure 5.7: Mechanical Control strategies:
(a) Release with varying compressive strain (n=4) **(b)** Release with varying compressive strain **(c)** % Release with varying compressive frequency, significance determined by one way ANOVA with Tukey's, multiple comparisons, *P=0.0127 **P=0.0057 ****P=<0.0001, (n=4) **(d)** Release rate with varying compressive duration (n=4). Comp=Compression.

5.4.6 Realization and characterisation of a miniaturised soft robotic actuator

Here, we show the realisation of a miniaturised soft robotic actuator, in the form of a hemispherical reservoir (4mm diameter, 6mm height,), to loosely hold the tough gel in a passive state, and compress the TG when pressurised. Details of the design and manufacture of the actuator are described in the Methods section. The outer balloon material is thicker (0.0012 inch, polyurethane) than the inner balloon (0.0003 inch) to allow for selective balloon expansion and compression in one direction (Figure 5.8a). Using the compression testing setup shown (Figure 5.8b), we calculated the force generated by the miniaturised actuator at variable pressure (Figure 5.8c). Placing the actuator in an O-ring ensured a consistent area of contact with the measurement plate upon pressurisation. The force generated was theoretically calculated and experimentally tested with two different pressure control systems, a customised pneumatic control system as previously described[234] and a programmable syringe pump coupled with a pressure gauge (Figure 5.1). The forces generated were in the range required to compress a TG disc of 2mm, the diameter of gel that fits in our reservoir without being pre-loaded (Figure 5.8 d, e). The pneumatic control system delivered a less variable pneumatic stimulus due to the presence of a pressure regulator. However, actuation via a programmable syringes pump was more consistent with theoretical calculations, especially at lower pressure.
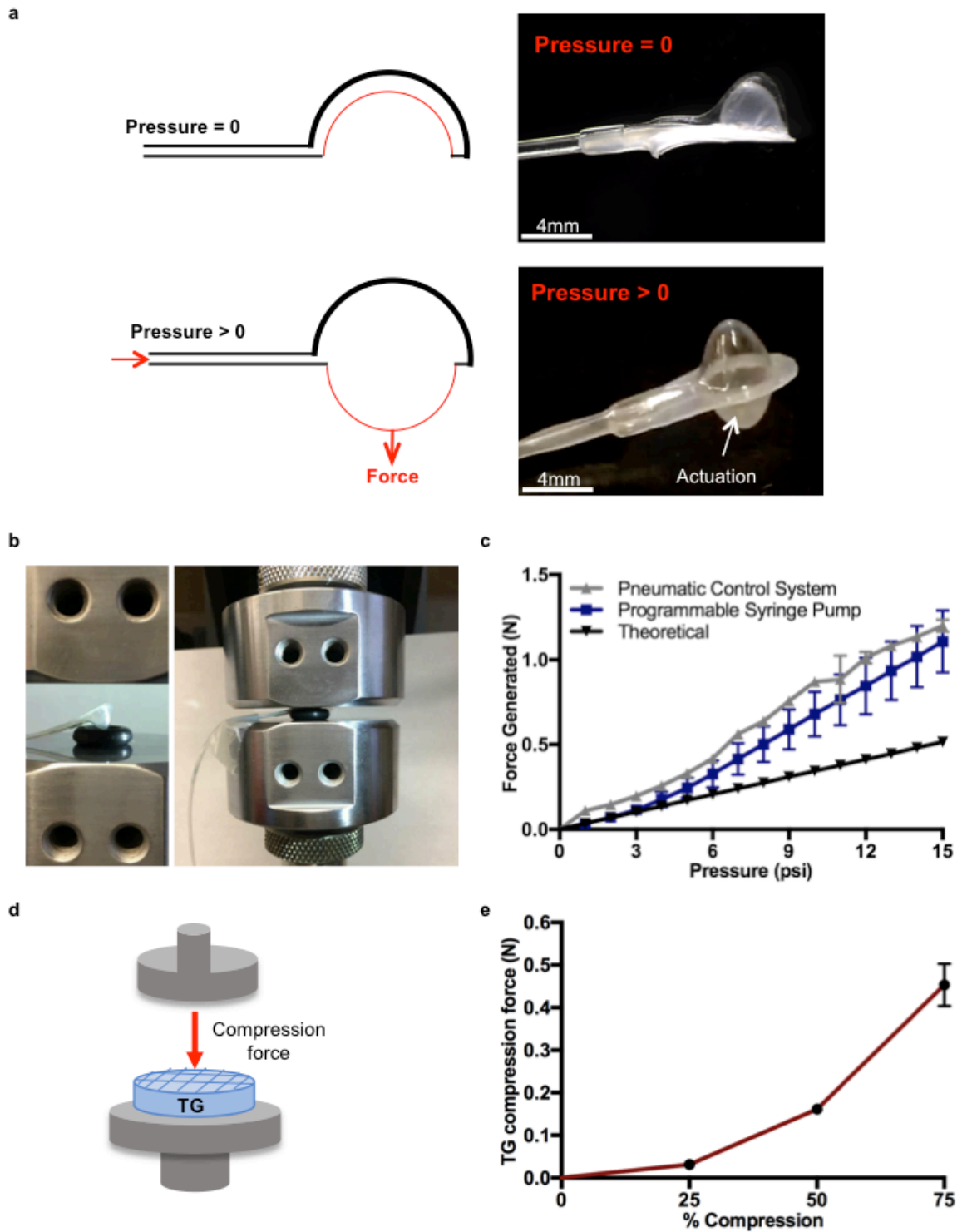
Figure 5.8: Realization and characterisation of a miniaturized soft robotic actuator
(a) Miniaturised soft robotic actuator in a passive and pressurised state **(b)** Texture analyser setup to measure force generation from actuator **(c)** Theoretical and experimental force generation from actuator at varying input pressures) (n=5) **(d)** Texture analyser set up to measure TG compressive force **(e)** Force required to compress tough gel (n=5)

5.4.7 *RoboTherepi*: **Controlled Release of biological therapy with a soft robotic device**

Here, we introduce *RoboTherepi*, a soft robotic actuator physically coupled with a TG biomaterial. Details of the design and manufacture of the actuator are described in the Methods section. As described earlier, the outer balloon material is thicker (0.0012 inch, polyurethane) than the inner balloon (0.0003 inch) to allow for selective balloon expansion and compression of the TG. The TG is physically encapsulated between the actuation layer and a tissue contacting flat layer (0.0003 inch, polyurethane), with 5 evenly distributed laser-cut pores (0.012-inch diameter) to allow for drug release (Figure 5.9a).

In a passive state, the tough gel (2mm diameter, 1mm height) loosely sits in the hemispherical reservoir (4mm diameter, 6mm height). Actuation of the system leads to compression of the TG and release of drug. Once pressure is removed, the system returns to its passive state (Figure 5.9b). To visually demonstrate this concept, we loaded a TG with blue dye, and actuated using *RoboTherepi* (Figure 5.9c).

Finally, we showed drug release from the system, using a TG loaded with 40kDa charged Dextran. Initially, we demonstrated a low baseline release rate, and corresponding cumulative release with no pressure input to the system (Figure 5.9d). Next, using a customised pneumatic control unit[234], we actuated the system at 9 psi once per hour for 5 hours. In response to this actuation stimulus, we show an immediate increase in release rate and a stepwise increase in cumulative release (Figure 5.9e).
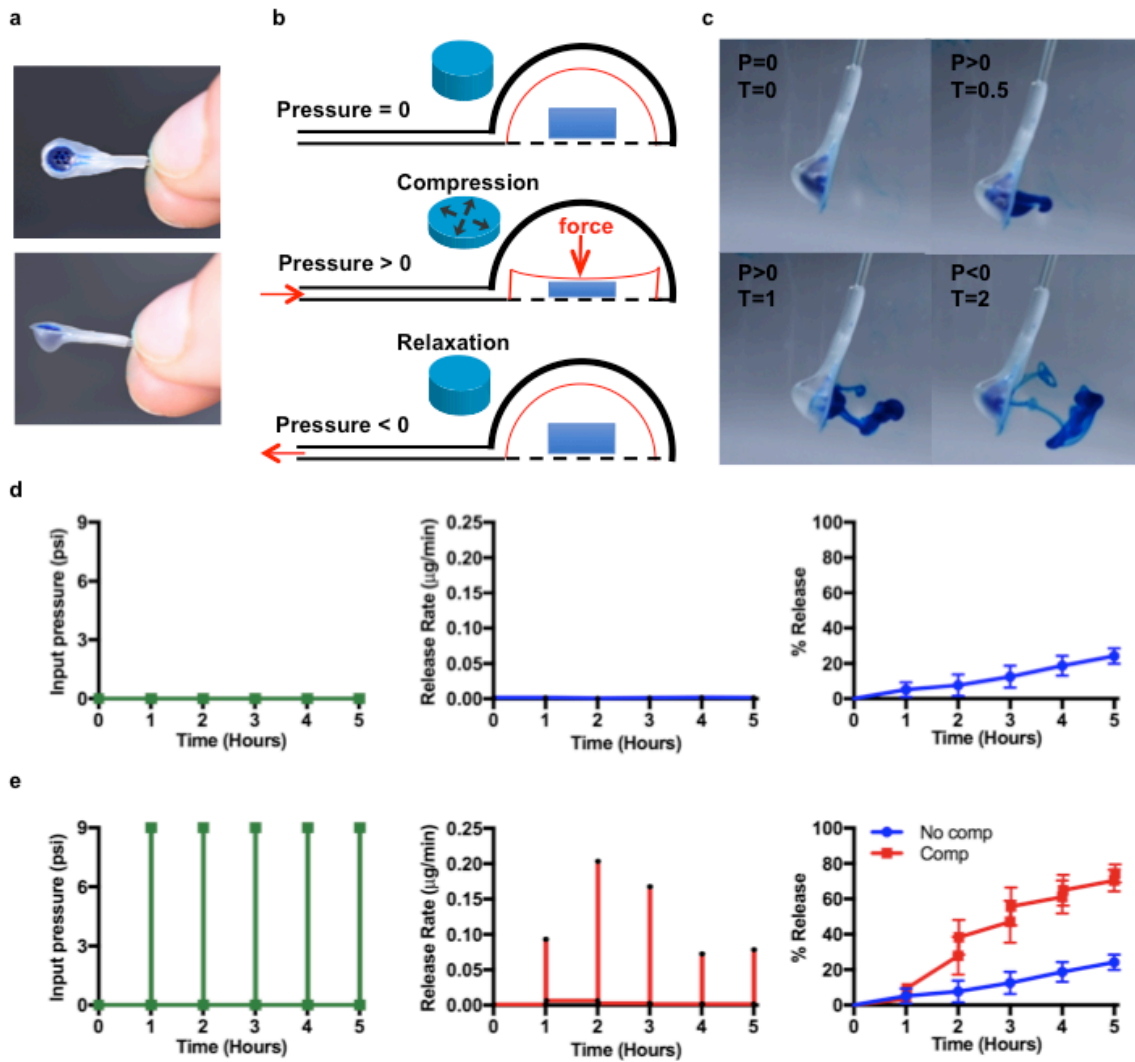
Figure 5.9: *RoboTherepi*: **Controlled Release of biological therapy with a soft robotic device**
(b) Schematic of device before and after actuation **(c)** Release of blue dye from device over one pressure actuation and vacuum cycle **(d)** Release rate and cumulative release of 40kDa charged dextran by simple diffusion from RoboTherepi when the pressure input is o psi **(d)** Release rate and cumulative release of 40kDa charged dextran from RoboTherepi when the pressure input is 9 psi.

5.5   Discussion

Simple hydrogel drug delivery formulations often exhibits a pre-determined passive release profile, which only matches the ideal pharmacokinetic profile of certain drugs and does not account for disease, patient or anatomical site variability [270,271,276]. Here, we present a soft robotic system that can modify release from a hydrogel with precise temporal control using an actuation regime and tailor the treatment course accordingly.

Our chosen hydrogel system, TG, consists of an interpenetrating network of alginate and acrylamide. In a synergistic fashion, both networks combine to achieve high toughness and fracture energy (two orders of magnitude higher than conventional hydrogels) [104,244,282,283]. Unzipping of the densely cross-linked alginate network provides a mechanism of energy dissipation upon deformation, and the long loosely cross-linked polyacrylamide chains bridges cracks and maintains structural integrity once the ionic alginate crosslinks are broken. While a normal alginate hydrogel will rupture at 1.2 times its original length, TG can undergo extensive deformation, up to 20 times its length, without material failure. This creates a large design space for tuneable drug release mediated by gross deformation [244] Importantly for patient safety, our results show that a drug loaded TG can deliver multiple doses without material rupture, and unwanted drug leakage. This is especially important for drugs with a narrow therapeutic index, where a small increase in dose could lead to an adverse drug reaction[289]. These results are consistent with the literature as the alginate network has been show to self heal following deformation, with healing increasing with both time and elevated temperature [244]. Although polyacrylamide is widely used in the biomedical field, it should be noted that its unpolymerised acrylamide monomer is toxic, which is troublesome for clinical translation [290]. A highly efficient polymerisation reaction, and a lengthy washout step would be necessary to ensure safety [283]. Encouragingly, results from the literature suggest that TG is generally not cytotoxic, and induces a mild inflammatory response comparable to biocompatible polymers both subcutaneously[283], and on the heart [127,234].

In addition, to contributing to the materials toughness, the reversibly cross-linked alginate network of the tough gel can also be used as a gate for drug release, which opens upon compression and closes at rest. Enlargement or breaking of these ionic bonds following deformation can release physically entrapped drug or cause electrostatic disassociation of charged drug. In this study we augmented steric hindrance between the hydrogel mesh and drug by increasing the molecular weight of the drug. However, this mechanism could also be applied to smaller molecules if the mesh size of the alginate network was sufficiently reduced. This can be achieved by adjusting polymer concentration and accompanying crosslink density [104]. Alternatively, small molecules could also be conjugated to larger particles for the purpose of additive steric hindrance. As an example, near zero baseline release has been successfully demonstrated by loading BMP conjugated gold nanoparticles ranging from 30-100 nanometre in a ionic cross-linked alginate hydrogel [291]. In future studies, it would be interesting to examine the affect of increasing charge on TG drug release following compression. The efficacy of an ultrasound stimulus in comparison to baseline release declined as the charge ratio increased in a DNA loaded ionic alginate gel [271].

In this study, we initially demonstrate different methods of mechanical control by altering the compressive strain, duration, or frequency of a drug loaded TG, and finally show proof of concept for a soft robotic assisted biomaterial, RoboTherepi, which can achieve these strategies *in vivo*. Intriguingly, the speed of

actuation could be used to determine the velocity and distance in which the drug travels from the implanted reservoir. This method of spatial control has not been previously demonstrated with other drug delivery systems and could prove extremely beneficial in overcoming limitations of implantable drug delivery systems, such as formation of a fibrous capsule, slowing passive diffusion and allowing for drug removal by host vasculature before it reaches its intended clinical target [281,292]. In a broader sense, such an approach could be useful for clinical targets that are poorly vascularised, such as pancreatic tumours [293], and thus need higher levels of spatial targeting, independent of normal vascular-based drug distribution routes.

In clinical applications, temporal control could be achieved by applying manual or automated pressure to a subcutaneous fluid filled bladder in direct connection with a distal actuation reservoir. As demonstrated in the previous chapters, a refill line could also be connected to the reservoir for the minimally invasive replenishment of therapy to the biomaterial. Alternatively, control could be achieved by wireless microchip communication to an on-board actuation system [294]. It should be noted that, a method of storing pneumatic energy would be necessary to power the system [295]. An implantable, fully integrated, soft drug delivery device would have numerous advantages over the current state of the art, a remote controlled microchip containing discrete drug filled reservoirs. [278,281,296,297]. Micro-electromechanical manufacturing techniques can limit the type and amount of therapy that can be loaded into a microchip, with each reservoir limited to lyophilised proteins and small molecules of high potency (up to 1 mg) [298]. In comparison hydrogels can be loaded with multiple types of therapies including living cells[104]. Furthermore, soft compliant materials have distinct advantages over the rigid materials in a microchip: they can be moulded and shaped to the curvature of the targeted area, enabling greater spatial control (Figure 5.10a). A diverse and ever expanding range of soft actuators exist, showing the potential to modify type and degree of therapy dependent on the disease and body part [295]. A recent study by Roche et al, demonstrates an externally actuated soft robotic sleeve, which wraps around the heart. The sleeve is composed of pneumatic actuators oriented in a helical and circumferential pattern in order to mimic the movement and twisting of the myocardial heart fibres [234].

A pneumatic stimulus will cause minimal damage to internal organs, as the actuator contains no rigid components. In fact, a soft controlled biomechanical stimulus may even have a synergistic therapeutic effect with the drug in certain diseases. Cyclical compressions can reduce the fibrotic and inflammatory response at an injured skeletal muscle site and promote muscle regeneration, demonstrating that our therapeutic armamentarium is not just confined to biologics [168]. Beneficial effects were attributed to short-term increases in oxygen transport and waste product removal due to compression-induced convection currents, rather than increased blood vessel formation. [168,299] Coupling mechanical stimulation with a therapeutic designed to promote angiogenesis, such as VEGF, could lead to synergistic activity and enhanced clinical efficacy [300]. While not explored here, *RoboTherepi* allows us co-deliver biological and mechanical stimulation to an injured, ischemic site at will (Figure 5.10b). In a broader sense, the ability to co-deliver therapies including cell, growth factors, small molecules and mechanical therapy synergistically with temporal and spatial control may have enhanced clinical efficacy in comparison to the delivery of a single agent. Indeed, a multi-modal strategy, facilitated by advanced delivery strategies, may be necessary to mimic or modify the inherently complex physiological and pathological processes in the heart [60,185].

In summary, we present an implantable soft robotic drug delivery device that demonstrates controlled release of therapy by inducing gross deformation of an alginate-polyacrylamide tough gel. This exquisite external control of drug release shows considerable promise for enhancing the therapeutic effects of cellular and molecular therapies at the heart, by enabling delivery of a precise dose of the correct cargo at the optimum time. We can draw four conclusions from this study (1) a drug loaded TG can undergo cyclical gross deformation without fracture, and unwanted drug release (2) the ionic alginate network can function as both a drug reservoir and gating mechanism for macro and charged molecules (3) A miniaturised soft robotic actuator can be manufactured and deliver a controlled force by varying the pressure input (4) A soft actuator can be coupled to a TG, where pressurisation of the actuator leads to compression of the TG and controlled release of encapsulated drug.
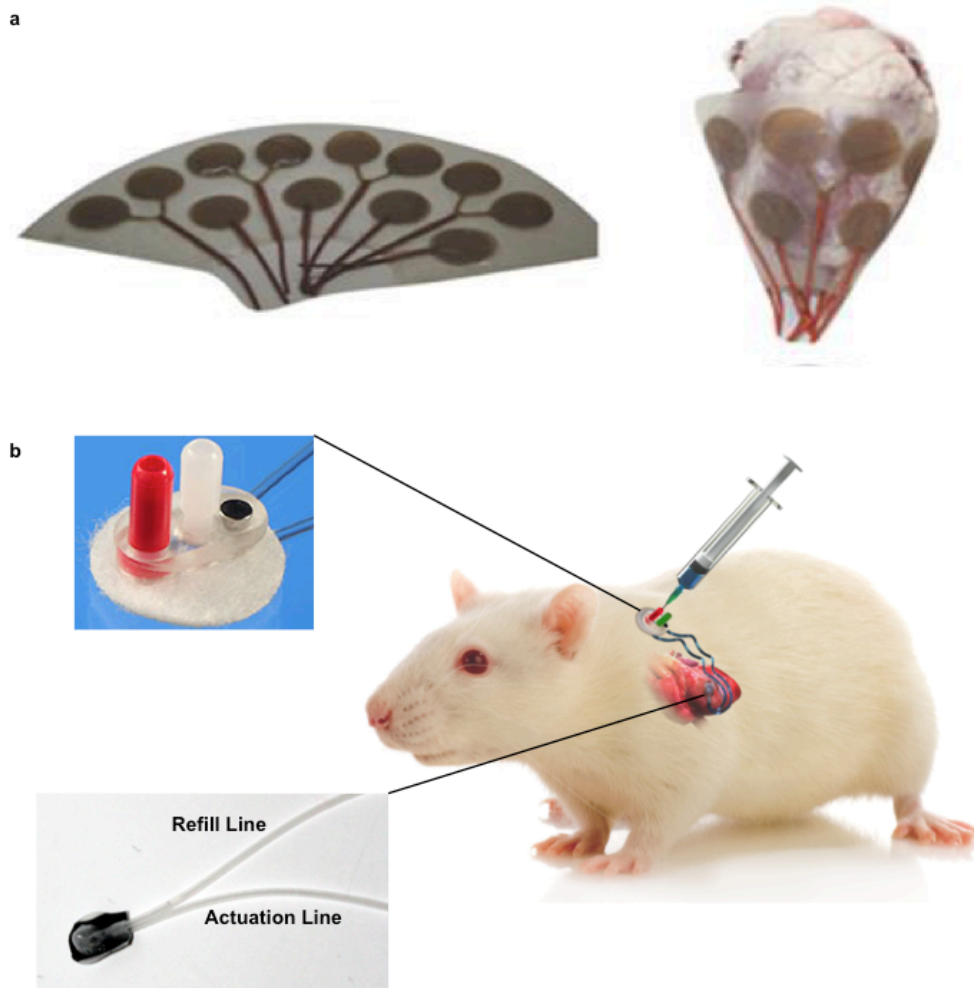
Figure 5.10: Towards pre-clinical testing of *RoboTherepi*
(a) Reservoir arrays for spatial control (b) Top left: Dual self-sealing injection port, red port: delivery of pneumatic/hydraulic pressure, white port: loading and reloading of therapy. Middle right: Representative animal model for *RoboTherepi*. Bottom left: Device with refill and actuation line

6 Conclusion

6.1 Preface

In this chapter, I summarise my previous results and place them in context of my research hypothesis and aims. Finally, I discuss research limitations and future work for *Therepi*.

6.2 Regenerative therapies for the treatment of ischemic heart disease

The spectrum of ischemic heart disease encompassing the initial tissue insult and the chronic long term damage is a leading cause of death worldwide [301]. Accumulation of atherosclerotic plaque and subsequent narrowing or occlusion of the coronary arteries can create an ischemic, inflammatory environment in heart tissue, leading to extensive cardiomyocyte death and reduction in ventricular function. This damage is defined as a myocardial infarction and is more commonly known as a heart attack. The regenerative capacity of the heart is unable to overcome this acute tissue insult, despite surgical and pharmacological treatment, often leading to chronic heart failure [1–4].

Regenerative therapies in the form of cells, proteins, and small molecules have shown considerable success in the treatment of post-myocardial injury and the prevention of ischemic cardiomyopathy in pre-clinical studies. However, although some of these strategies have demonstrated some success in the clinic, their adoption into medical practice has been hindered by low or unpredictable efficacy when tested in large patient populations [78,109,186,187]. The majority of these clinical trials have delivered cell therapy in a simple saline vehicle and suffer from similar shortcomings, including low concentration at the diseased site due to untargeted delivery, poor retention in the dynamic environment of the beating heart, a short biological half-life, adverse effects from systemic delivery and the necessity for multiple administrations for best clinical efficacy [78,186,187]. These limitations equally apply to regenerative growth factor and small molecule therapies.

Advanced delivery strategies have been identified as an important area of research and development in order to fully realize the promise of regenerative therapies [60,185]. Potential improvements include minimally invasive catheter delivery of therapy and the use of a biomaterial carrier vehicle that can be refilled[107] allowing for increased bioavailability of these agents at the pathological site within a suitable therapeutic window. Such an approach could be utilized for the delivery of (i) small bioactive molecules free-loaded into a biomaterial matrix, (ii) protein/macromolecules that could diffuse across a membrane in a controlled fashion, or (iii) a cell payload facilitating release of bioactive molecules that exert therapeutic effects on local tissue for sustained periods.

Finally, simple delivery formulations often exhibit a pre-determined passive release profile of a single therapeutic, which matches the ideal pharmacokinetic profile of only certain drugs and struggles to mimic the *in vivo* biological cascade [105]. There is much evidence to suggest the delivery of multi-modal therapies, both biological and mechanical, with precise temporal and spatial control can act in a synergistic manner, enhancing both the efficacy of individual therapies and the overall effect on the target tissue. For instance, the sequential release of VEGF and PGDF can be used to produce a higher density of mature blood vessels during

angiogenesis [183]. Finally, mechanical stimuli has been shown to optimise bone marrow stromal cell behaviour *in vivo*, positively modulating growth rate, proliferation, migration, and wound healing [302].

6.3   Summary of thesis hypothesis and aims

To conclude, I would like to reiterate my overarching hypothesis and aims, as originally described in chapter one.

Thesis hypothesis:

Regenerative cardiac therapies suffer from delivery limitations, restricting their efficacy. A strategy that allows for replenishable targeted delivery, and sustained presentation of multi-modal therapies, with the ability for spatial and temporal modification of release, will overcome the hurdles faced by cardiac regenerative therapies, and lead to a new treatment option for heart disease.

Thesis Aims:

1. To develop a pre-clinical research model for the targeted, replenishable delivery of multiple types of therapy to a simple, epicardially placed biomaterial.

2. To design, optimise and validate *Therepi*; a replenishable, immune-isolated, biomaterial reservoir that allows for sustained release of cardiac therapy.

3. To assess the safety and efficacy of *Therepi* following implantation in a rat model of myocardial infarction and explore barriers to clinical translation.

4. To functionalise *Therepi* using soft robotic technology for precise spatial and temporal control of drug release.

6.4   Completion of Aim 1:

In chapter two, I introduced the *Therepi* concept and described the development of a representative pre-clinical animal model. *Therepi*, which is short for **Ther**apeutic **epi**cardium, offers a number of advantageous features to address the current limitations of regenerative cardiac therapies; poor cardiac retention, short biological half-life, adverse side effects from systemic delivery and necessity for multiple administrations for best efficacy [102,182].

In our design, a biomaterial is attached to the epicardial surface of the heart and connected to a subcutaneous port through an implanted conduit or catheter, allowing localized, targeted therapy to the diseased tissue, without the need for higher systemic doses. Importantly, replenishable delivery is possible with the system and the biomaterial vehicle promotes retention of the delivered cargo and enhanced engraftment and viability of cells [83,84,93,94,85–92]. A method that offers repeat administrations without necessitating repeat invasive surgeries, while simultaneously protecting its cargo post administration, has not been previously demonstrated, motivating the design of our system.

This chapter includes a detailed method of surgical implantation in a rat model that enables repeated replenishment of therapy from a subcutaneous port and an *in vivo* proof of concept of delivery for three-model therapeutics (small molecules, proteins, cell). In addition, this chapter demonstrates a method to accurately monitor cell viability and cardiac function over time in the same animal following myocardial infarction, and relate disease progression to cell dose and viability. This work has important practical implications; preclinical use of the system as a research model may elucidate new insights into regenerative cardiac therapy, and progress experimental therapies along the clinical translational path for improved patient outcomes.

We draw 5 main conclusion from this study; (i) implantation of the biomaterial on the heart with a conduit connecting the reservoir to a subcutaneous access port is possible in a rat model, (ii) the system enables non-invasive replenishment of cells to the biomaterial and improves cell number at the site, (iii) the technology also allows rapid, targeted delivery of macromolecules and small molecules directly to the site, (iv) the implanted system constitutes a rapid, inexpensive and safe method for bioluminescent quantification of cell number by direct administration of imaging substrate during *in vivo* imaging (v) a method for longitudinal hemodynamic measurements using a pressure-volume catheter with the apical stick method can be used to quantify cardiac function in a survival animal model.

6.5 Completion of Aim 2:

In chapter three, I designed, optimised and validated a manufacturing process for a soft flexible, immunoisolatory shell that surrounds the simplified *Therepi* system developed in chapter 2. An immunoisolated biomaterial reservoir is important, as cell and biomaterial systems can be compromised once implanted in the body, with nonspecific protein adsorption and immune/inflammatory cell infiltration impairing the ability of the biomaterial to receive and house therapeutic replenishments. Moreover, the localisation of cells (or other therapeutic cargo) in a distinct, contained environment would be clinically desirable for controlled therapeutic functionality. Importantly, genetically engineered and xenogeneic cell lines could be utilised with an immunoisolated biomaterial reservoir, without the associated safety issues [140].

In our design, a semi-permeable membrane with a precise pore size separates the biomaterial and the heart. This semipermeable membrane is engineered to allow for the bidirectional movement of oxygen, nutrients, and cellular proteins, but localises transplanted cells in the reservoir and prevents the inward migration of immune cells. Improvements in left ventricular function following cell delivery are attributed to the synthesis and secretion of cellular paracrine factors, rather than cell engraftment and differentiation into heart tissue[50]. In line with this mechanism, the optimised *Therepi* replenishment reservoir permits the sustained delivery of cardiac therapy to the infarcted heart, with a bolus release of intracellular contents including cytokines, chemokines, exosomes and paracrine factors following each refill. In a further advancement, the precise membrane pore size can be easily modified to adjust the type and rate of therapy diffusion if desirable.

We can draw five conclusions from this study; (i) a consistent and robust thermal bond is formed between the refill line and the reservoir allowing for multiple reproducible therapy replenishments (ii) the semipermeable membrane of the optimised *Therepi* reservoir can localise cells and allow the sustained release of paracrine factors over an extended period of time (iii) suturing of the reservoir to the curved surface of the rat heart is possible without material damage or kinking (iv) the optimised system provides protection from the foreign body response and vastly extends viability of an xenogeneic cell source in comparison to the simplified *Therepi* (v) the system has been optimised for pre-clinical testing.

6.6 Completion of Aim 3:

In chapter 4, we examined the three dimensional distribution of therapy following *Therepi* delivery and confirmed the ability of multi-sized cargo to diffuse from *Therepi* into heart tissue, even after fibrous capsule formation. A fibrous capsule, generated by foreign materials and epicardial friction could be fatal to the long-term functionality of *Therepi*. Importantly, we demonstrated, despite the formation of a capsule, which hinders but does not impede diffusion, molecules with a range of molecular weights can be transported through the membrane into the tissue, and in the case of adrenaline elicit a potent biological response.

Finally, we assessed the safety and efficacy of repeated syngeneic mesenchymal cell delivery with the optimised *Therepi* system developed in chapter 3. We show that repeated administration of cells over a 4-week period by using *Therepi* provided functional benefits in ejection fraction, fractional shortening and stroke work, compared to a single injection of cells and to no treatment. The functional benefit shown with refills of cells support that paracrine factors can diffuse through the formed capsule into heart tissue. Interestingly, the acellular *Therepi* provided a sustained benefit across the 28-day study, potentially due to its mechanical reinforcement of the remodelling ventricle or due to an altered healing response caused by the foreign body response [165,213,214].

We draw three conclusions from this study; (i) the system enables direct, potent delivery of small molecules, that can penetrate the surrounding fibrous capsule and elicit a functional effect (ii) the system enables localized delivery of macromolecules that penetrate through the fibrous capsule into the myocardial tissue and distribute in three dimensions, (iii) in a 28 day rodent study in an MI model, the *Therepi* device (acellular or with transplanted cells) demonstrates therapeutic superiority compared to no treatment or a single cell injection, and this effect is increased with repeated cell administrations.

6.7   Completion of Aim 4:

In Chapter 5, we combined a biomaterial reservoir with an inflatable soft robotic actuator, and demonstrated precise temporal control of drug release from the encapsulated biomaterial with a tuneable actuation stimulus. This is important as simple biomaterial drug delivery systems often exhibits a pre-determined passive release profile, which only matches the ideal pharmacokinetic profile of certain drugs and does not account for inter-patient, disease or anatomical site variability [270,271,276]. In contrast, our soft robotic system, *RoboTherepi*, can compress the biomaterial on demand, and alter the passive release profile of drug, protein or cell produced paracrine factors at the epicardial surface of the heart. As in the previous chapters, minimally invasive therapy replenishments to the biomaterial are possible by injection through a refill line. Furthermore, active assist using *RoboTherepi* allows us co-deliver biological and mechanical stimulation to the injured site. Cezar et al demonstrated that cyclical compressions can reduce the fibrotic and inflammatory response at an injured skeletal muscle site and promote muscle regeneration *in vivo* [168]. A soft controlled biomechanical stimulus may also have a beneficial and synergistic therapeutic effect in ischemic heart tissue.

Initially, we confirmed that a drug loaded polyacrylamide/alginate tough gel hydrogel is capable of withstanding multiple cycles of gross deformation without fracture i.e. the expected conditions in our soft robotic system. Then we demonstrated controlled release of drug therapy from this tough gel via compressive deformation and temporary enlargement of hydrogel mesh size. This temporary enlargement of the mesh size can release physically entrapped drug and also cause electrostatic dissociation of charged drug. Next, we designed and characterised miniaturised soft robotic actuator, in the form of a hemispherical reservoir, to loosely hold the tough gel in a passive state, and compress the TG when pressurised. . Finally, we demonstrated controlled release of drug from the hydrogel, with triggered pneumatic action of the soft robotic actuator.

We draw four conclusions from this study (1) a drug loaded TG can undergo cyclical gross deformation without fracture, and unwanted drug release (2) the ionic alginate network can function as both a drug reservoir and gating mechanism for macro and charged molecules (3) A miniaturised soft robotic actuator can be manufactured and deliver a controlled force by varying the pressure input (4) A soft actuator can be coupled to a TG, where pressurisation of the actuator leads to compression of the TG and controlled release of encapsulated drug.

6.8   Research Limitations and future work

The dynamic interplay between the diseased myocardial site, *Therepi* device and loaded cellular cargo will be important to understand, in order to fully realise the potential of the *Therepi*. However, isolating and understanding the physical effects of the device and biological effects of the cells will be difficult to achieve in a small model due to device size relative to the heart. In the present iteration, *Therepi* covers a large proportion of the left ventricle and reducing this size significantly will require a new manufacturing process. In general, Therepi warrants investigation in a larger animal model, that more closely represents the human heart size and disease phenotype. Suggested models include pig or sheep [303].

The pre-clinical study reported in chapter 4 highlights the importance of cell delivery timing for positive modulation of post-MI healing response. In this study, *Therepi* with a one-time cell delivery at day 0 had poor results relative to devices with no cell delivery. The harsh inflammatory environment of the infarcted heart has been shown to drive delivered MSCs towards a pro-inflammatory phenotype, limiting their reparative efficacy[224]. Cells delivered at the time of MI, and their secretome, would have been subject to this environment, and may even have adversely affected healing and negated any positive effect from the device mechanical reinforcement. Future work should examine the timing of cell delivery with *Therepi*. This could easily be achieved by implantation of an acellular device, followed by subsequent cell delivery at a later time point. This approach would compliment delivery with autologous stem cells[47], when, for example, a biopsy could be taken at the time of implantation of the *Therepi*, and stem cells would be isolated, expanded, and then re-implanted through the *Therepi* after a number of weeks or months without the need for an additional surgery.

It should be noted that in this pre-clinical study we initiated treatment directly after the time of cardiac injury. This is not directly clinically relevant, as cardiac injury would precede device implantation in the clinic. Future work will involve testing this device subsequent to injury.

One type of cell cargo was tested here, a syngeneic mesenchymal cell source. However, there is a plethora of available cell sources, and other therapeutic cargos available. Promising candidates include c-kit[POS] cardiac progenitor cells and cardiac mesenchymal cells, which have demonstrated cumulative benefit following repeat delivery using a percutaneous injection technique [181,255]. In terms of clinical translation, it will be important to identify the key cell-secreted factors responsible for cardiac repair, and the accompanying mechanism of action. Cell membrane enclosed vesicles or exosomes are one such promising candidate [304]. Finally, like any pharmacological medication, determining the correct dose and administration frequency will be critical [184].

The data in chapter 3 demonstrates that the optimised *Therepi reservoir* can localise transplanted cells and allow paracrine release *in vitro*. Furthermore, a degree of immune protection was provided *in vivo*, as demonstrated by extended viability of a xenogeneic cell source and histological absence of a large foreign body response around the gelatin based biomaterial. However, reliable and complete immunisolation of the cells in the dynamic environment of the heart was not yet been proven. Further refinement, such as impregnation of the membrane with a nanoporous biomaterial, such as alginate, could potentially enable a greater degree of protection from the immune response e.g. cytokines [243]. Alternatively, the synthetic semipermeable membrane could be replaced with a mechanically strong nanoporous hydrogel [244]. It would be

interesting to examine the effect of membrane material and pore size on the immune response, with particular attention to fibrous capsule size and pericardial adhesions. Finally, a lot of lessons can be learned from the design of macroencapsulation devices for the treatment of type 1 Diabetes [140,141,143,245].

Future work, prior to clinical implementation will focus on biodegradable device development, so there is no foreign material remaining on the heart. While, a permanent version of the device could also be an option, allowing for acute therapy replenishments initially and taking advantage of the long-term passive reinforcement effects[268].

We used sutures for device attachment in this manuscript, however minimally invasive delivery will be difficult to achieve using this attachment method. The recent development of an extremely tough hydrogel adhesive that can form strong bonds with wet tissues could be applied here [127]. Such a method would facilitate a less invasive and more uniform adhesion to the heart. Furthermore, the hydrogel interface at the epicardial surface could reduces the fibrotic, inflammatory response [234].

It is important to design the system with mechanisms to avoid catheter obstruction by therapies, such as cell debris. In this thesis, cells were removed from the line by following each dose with saline, to clear the line. Other approaches could include enzymatic degradation and mechanical suction. Future versions of *Therepi* could be designed with a dual loop system to aid with these solutions. Such a system could also be used for the constant infusion of nutrients to cells, without risk of pericardial effusion. The iPRECIO programmable infusion pump, with refillable reservoir is designed for pre-clinical drug infusion studies in mice and rats, and could be easily coupled with the *Therepi* reservoir [305].

We utilised an alginate acrylamide hydrogel during the development of *RoboTherepi*, due its superior mechanical properties in comparison to conventional hydrogels. It should be noted that the acrylamide monomer is toxic, which is troublesome for clinical translation. A highly efficient polymerisation reaction, and a length washout step would be necessary to ensure safety [283]. Alternatively, the formulation of the TG could be altered to replaced acrylamide with a biocompatible covalent network, which maintains its superior mechanical properties. Such a network should ideally have long polymer chains to bridge cracks and maintain structural integrity once the ionic alginate crosslinks are broken. Furthermore, the ability the form secondary crosslinks with the alginate network would be desirable to allow for force transfer between the two networks [244].

Finally, while not explored here, *RoboTherepi* allows us co-deliver biological and mechanical stimulation to an injured, ischemic site of the heart. Mechanical compression can lead to short-term convective increases in blood and oxygen transport, and waste product removal, from ischemic skeletal tissue [168]. Such a strategy could also be beneficial in heart muscle that has been acutely deprived of blood flow after a heart attack. Rapid advancements in the field of soft robotics has brought about the development of implantable soft devices that can deliver precise force profiles to the heart with spatial and temporal control[295234]. The coupling of mechanical stimulation with therapeutics designed to promote blood vessel formation, such as VEGF and PDGF, could lead to synergistic activity and long term clinical benefits [300].

6.9   Concluding remarks

To conclude, this work has important practical and translational implications. Preclinical use of the system as a research model may elucidate new insights into regenerative cardiac therapy, including the importance of dose, administration frequency and timing of delivery post myocardial injury. Furthermore, the system could highlight the synergistic benefits of a holistic multi-modal approach. The ability to co-deliver therapies including cell, growth factors, small molecules and mechanical therapy synergistically with temporal and spatial control may have enhanced clinical efficacy in comparison to the delivery of a single agent. Indeed, a multi-modal strategy, facilitated by advanced delivery strategies, may be necessary to mimic or modify the inherently complex physiological and pathological processes in the heart.

Ultimately, it is our hope that *Therepi* can help progress experimental therapies towards clinical use and improve patient outcomes.

7 Bibliography

1. Sutton, M. G. S. J. & Sharpe, N. Left Ventricular Remodeling After Myocardial Infarction : Pathophysiology and Therapy. *Circulation* **101,** 2981–2988 (2000).

2. Nabel, E. G. & Braunwald, E. A Tale of Coronary Artery Disease and Myocardial Infarction. *N. Engl. J. Med.* **366,** 54–63 (2012).

3. Burchfield, J. S., Xie, M. & Hill, J. A. Pathological Ventricular Remodeling: Mechanisms: Part 1 of 2. *Circulation* **128,** 388–400 (2013).

4. Azevedo, P. S., Polegato, B. F., Minicucci, M. F., Paiva, S. A. R. & Zornoff, L. A. M. Cardiac Remodeling: Concepts, Clinical Impact, Pathophysiological Mechanisms and Pharmacologic Treatment. *Arq. Bras. Cardiol.* **106,** 62–9 (2016).

5. Hastings, C. L. *et al.* Drug and cell delivery for cardiac regeneration. *Adv. Drug Deliv. Rev.* **84,** 85–106 (2015).

6. Menees, D. S. *et al.* Door-to-Balloon Time and Mortality among Patients Undergoing Primary PCI. *N. Engl. J. Med.* **369,** 901–909 (2013).

7. Terzic, A. & Behfar, A. Stem cell therapy for heart failure: Ensuring regenerative proficiency. *Trends Cardiovasc. Med.* **26,** 395–404 (2016).

8. Benjamin, E. J. *et al.* Heart Disease and Stroke Statistics-2018 Update: A Report From the American Heart Association. *Circulation* **137,** e67–e492 (2018).

9. Braunschweig, F., Cowie, M. R. & Auricchio, A. What are the costs of heart failure? *Europace* **13 Suppl 2,** ii13-7 (2011).

10. Heidenreich, P. A. *et al.* Forecasting the future of cardiovascular disease in the United States: a policy statement from the American Heart Association. *Circulation* **123,** 933–44 (2011).

11. Rohde, L. E., Bertoldi, E. G., Goldraich, L. & Polanczyk, C. A. Cost-effectiveness of heart failure therapies. *Nat. Rev. Cardiol.* **10,** 338–54 (2013).

12. McMurray, J. J. V. *et al.* Angiotensin–Neprilysin Inhibition versus Enalapril in Heart Failure. *N. Engl. J. Med.* **371,** 993–1004 (2014).

13. Granger, C. B. *et al.* Effects of candesartan in patients with chronic heart failure and reduced left-ventricular systolic function intolerant to angiotensin-converting-enzyme inhibitors: the CHARM-Alternative trial. *Lancet (London, England)* **362,** 772–6 (2003).

14. Cohn, J. N. & Tognoni, G. A Randomized Trial of the Angiotensin-Receptor Blocker Valsartan in Chronic Heart Failure. *N. Engl. J. Med.* **345,** 1667–1675 (2001).

15. Packer, M. *et al.* Effect of Carvedilol on the Morbidity of Patients With Severe Chronic Heart Failure. *Circulation* **106,** (2002).

16. Effect of metoprolol CR/XL in chronic heart failure: Metoprolol CR/XL Randomised Intervention Trial in Congestive Heart Failure (MERIT-HF). *Lancet (London, England)* **353,** 2001–7 (1999).

17. The Cardiac Insufficiency Bisoprolol Study II (CIBIS-II): a randomised trial. *Lancet (London, England)* **353,** 9–13 (1999).

18.   Pitt, B. *et al.* The Effect of Spironolactone on Morbidity and Mortality in Patients with Severe Heart Failure. *N. Engl. J. Med.* **341,** 709–717 (1999).

19.   Group, T. D. I. The Effect of Digoxin on Mortality and Morbidity in Patients with Heart Failure. *N. Engl. J. Med.* **336,** 525–533 (1997).

20.   Investigators*, T. S. Effect of Enalapril on Survival in Patients with Reduced Left Ventricular Ejection Fractions and Congestive Heart Failure. *N. Engl. J. Med.* **325,** 293–302 (1991).

21.   Cohn, J. N. *et al.* A comparison of enalapril with hydralazine-isosorbide dinitrate in the treatment of chronic congestive heart failure. *N. Engl. J. Med.* **325,** 303–10 (1991).

22.   Effects of enalapril on mortality in severe congestive heart failure. Results of the Cooperative North Scandinavian Enalapril Survival Study (CONSENSUS). The CONSENSUS Trial Study Group. *N. Engl. J. Med.* **316,** 1429–35 (1987).

23.   Taylor, A. L. *et al.* Combination of Isosorbide Dinitrate and Hydralazine in Blacks with Heart Failure. *N. Engl. J. Med.* **351,** 2049–2057 (2004).

24.   Cohn, J. N. *et al.* Effect of vasodilator therapy on mortality in chronic congestive heart failure. Results of a Veterans Administration Cooperative Study. *N. Engl. J. Med.* **314,** 1547–52 (1986).

25.   Rumiantsev, P. P. (Pavel P. & Carlson, B. M. *Growth and hyperplasia of cardiac muscle cells*. (Harwood Academic Publishers, 1991).

26.   Bergmann, O. *et al.* Evidence for Cardiomyocyte Renewal in Humans. *Science (80-.).* **324,** (2009).

27.   Hsieh, P. C. H. *et al.* Evidence from a genetic fate-mapping study that stem cells refresh adult mammalian cardiomyocytes after injury. *Nat. Med.* **13,** 970–4 (2007).

28.   Senyo, S. E. *et al.* Mammalian heart renewal by pre-existing cardiomyocytes. *Nature* **493,** 433–436 (2012).

29.   van Berlo, J. H. & Molkentin, J. D. An emerging consensus on cardiac regeneration. *Nat. Med.* **20,** 1386–93 (2014).

30.   Orlic, D. *et al.* Bone marrow cells regenerate infarcted myocardium. *Nature* **410,** 701–5 (2001).

31.   Hodgkinson, C. P., Bareja, A., Gomez, J. A. & Dzau, V. J. Emerging Concepts in Paracrine Mechanisms in Regenerative Cardiovascular Medicine and Biology. *Circ. Res.* **118,** 95–107 (2016).

32.   Gnecchi, M. *et al.* Paracrine action accounts for marked protection of ischemic heart by Akt-modified mesenchymal stem cells. *Nat. Med.* **11,** 367–8 (2005).

33.   Murry, C. E. *et al.* Haematopoietic stem cells do not transdifferentiate into cardiac myocytes in myocardial infarcts. *Nature* **428,** 664–668 (2004).

34.   Balsam, L. B. *et al.* Haematopoietic stem cells adopt mature haematopoietic fates in ischaemic myocardium. *Nature* **428,** 668–73 (2004).

35.   Beltrami, A. P. *et al.* Adult cardiac stem cells are multipotent and support myocardial regeneration. *Cell* **114,** 763–76 (2003).

36.   Hosoda, T. *et al.* Clonality of mouse and human cardiomyogenesis in vivo. *Proc. Natl. Acad. Sci. U. S. A.* **106,** 17169–74 (2009).

37.   Zaruba, M.-M., Soonpaa, M., Reuter, S. & Field, L. J. Cardiomyogenic potential of C-kit(+)-

expressing cells derived from neonatal and adult mouse hearts. *Circulation* **121,** 1992–2000 (2010).

38.   Jesty, S. A. *et al.* c-kit+ precursors support postinfarction myogenesis in the neonatal, but not adult, heart. *Proc. Natl. Acad. Sci. U. S. A.* **109,** 13380–5 (2012).

39.   van Berlo, J. H. *et al.* c-kit+ cells minimally contribute cardiomyocytes to the heart. *Nature* **509,** 337–41 (2014).

40.   Ellison, G. M. *et al.* Adult c-kit(pos) cardiac stem cells are necessary and sufficient for functional cardiac regeneration and repair. *Cell* **154,** 827–42 (2013).

41.   Hong, K. U. *et al.* c-kit+ Cardiac stem cells alleviate post-myocardial infarction left ventricular dysfunction despite poor engraftment and negligible retention in the recipient heart. *PLoS One* **9,** e96725 (2014).

42.   Tang, X.-L. *et al.* Intracoronary administration of cardiac progenitor cells alleviates left ventricular dysfunction in rats with a 30-day-old infarction. *Circulation* **121,** 293–305 (2010).

43.   Bolli, R. *et al.* Intracoronary delivery of autologous cardiac stem cells improves cardiac function in a porcine model of chronic ischemic cardiomyopathy. *Circulation* **128,** 122–31 (2013).

44.   Li, Q. *et al.* Intracoronary administration of cardiac stem cells in mice: a new, improved technique for cell therapy in murine models. *Basic Res. Cardiol.* **106,** 849–64 (2011).

45.   Konstandin, M. H. *et al.* Fibronectin is essential for reparative cardiac progenitor cell response after myocardial infarction. *Circ. Res.* **113,** 115–25 (2013).

46.   Bolli, R. *et al.* Cardiac stem cells in patients with ischaemic cardiomyopathy (SCIPIO): initial results of a randomised phase 1 trial. *Lancet* **378,** 1847–57 (2011).

47.   Makkar, R. R. *et al.* Intracoronary cardiosphere-derived cells for heart regeneration after myocardial infarction (CADUCEUS): a prospective, randomised phase 1 trial. *Lancet* **379,** 895–904 (2012).

48.   Yacoub, M. H. & Terrovitis, J. CADUCEUS, SCIPIO, ALCADIA: Cell therapy trials using cardiac-derived cells for patients with post myocardial infarction LV dysfunction, still evolving. *Glob. Cardiol. Sci. Pract.* **2013,** 5–8 (2013).

49.   NCT01458405. Allogeneic Heart Stem Cells to Achieve Myocardial Regeneration (ALLSTAR) - ClinicalTrials.gov. Available at: https://clinicaltrials.gov/ct2/show/NCT01458405.

50.   Orlic, D. *et al.* Bone marrow cells regenerate infarcted myocardium. *Nature* **410,** 701–5 (2001).

51.   Tendera, M. *et al.* Intracoronary infusion of bone marrow-derived selected CD34+CXCR4+ cells and non-selected mononuclear cells in patients with acute STEMI and reduced left ventricular ejection fraction: results of randomized, multicentre Myocardial Regeneration by Intraco…. *Eur. Heart J.* **30,** (2009).

52.   Assmus, B. *et al.* Transplantation of Progenitor Cells and Regeneration Enhancement in Acute Myocardial Infarction (TOPCARE-AMI). *Circulation* **106,** (2002).

53.   Janssens, S. *et al.* Autologous bone marrow-derived stem-cell transfer in patients with ST-segment elevation myocardial infarction: double-blind, randomised controlled trial. *Lancet* **367,** 113–121 (2006).

54.   Wollert, K. C. *et al.* Intracoronary autologous bone-marrow cell transfer after myocardial infarction:

the BOOST randomised controlled clinical trial. *Lancet* **364,** 141–148 (2004).

55. Schächinger, V. *et al.* Intracoronary Bone Marrow–Derived Progenitor Cells in Acute Myocardial Infarction. *N. Engl. J. Med.* **355,** 1210–1221 (2006).

56. Perin, E. C. *et al.* Transendocardial, autologous bone marrow cell transplantation for severe, chronic ischemic heart failure. *Circulation* **107,** 2294–302 (2003).

57. Traverse, J. H. *et al.* TIME Trial: Effect of Timing of Stem Cell Delivery Following ST-Elevation Myocardial Infarction on the Recovery of Global and Regional Left Ventricular FunctionNovelty and Significance. *Circ. Res.* **122,** 479–488 (2018).

58. Traverse, J. H. *et al.* LateTIME: a phase-II, randomized, double-blinded, placebo-controlled, pilot trial evaluating the safety and effect of administration of bone marrow mononuclear cells 2 to 3 weeks after acute myocardial infarction. *Texas Hear. Inst. J.* **37,** 412–20 (2010).

59. Perin, E. C. *et al.* Effect of Transendocardial Delivery of Autologous Bone Marrow Mononuclear Cells on Functional Capacity, Left Ventricular Function, and Perfusion in Chronic Heart Failure. *JAMA* **307,** 1717–26 (2012).

60. Menasche, P. Cardiac cell therapy: lessons from clinical trials. *J. Mol. Cell. Cardiol.* **50,** 258–65 (2011).

61. Behfar, A., Crespo-Diaz, R., Terzic, A. & Gersh, B. J. Cell therapy for cardiac repair—lessons from clinical trials. *Nat. Rev. Cardiol.* **11,** 232–246 (2014).

62. Ranganath, S. H., Levy, O., Inamdar, M. S. & Karp, J. M. Harnessing the mesenchymal stem cell secretome for the treatment of cardiovascular disease. *Cell Stem Cell* **10,** 244–58 (2012).

63. Hare, J. M. *et al.* Comparison of allogeneic vs autologous bone marrow–derived mesenchymal stem cells delivered by transendocardial injection in patients with ischemic cardiomyopathy: the POSEIDON randomized trial. *JAMA* **308,** 2369–79 (2012).

64. Chugh, A. R. *et al.* Administration of cardiac stem cells in patients with ischemic cardiomyopathy: the SCIPIO trial: surgical aspects and interim analysis of myocardial function and viability by magnetic resonance. *Circulation* **126,** S54-64 (2012).

65. Teerlink, J. R. *et al.* Benefit of cardiopoietic mesenchymal stem cell therapy on left ventricular remodelling: results from the Congestive Heart Failure Cardiopoietic Regenerative Therapy (CHART-1) study. *Eur. J. Heart Fail.* **19,** 1520–1529 (2017).

66. Madonna, R. *et al.* Position Paper of the European Society of Cardiology Working Group Cellular Biology of the Heart: cell-based therapies for myocardial repair and regeneration in ischemic heart disease and heart failure. *Eur. Heart J.* **37,** (2016).

67. Anand, I. S., Florea, V. G. & Fisher, L. Surrogate end points in heart failure. *J. Am. Coll. Cardiol.* **39,** 1414–1421 (2002).

68. Fda, Cder & jenkinsj. Good Review Practice: Clinical Review of Investigational New Drug Applications. (2013).

69. Schmuck, E. G. *et al.* Biodistribution and Clearance of Human Mesenchymal Stem Cells by Quantitative Three-Dimensional Cryo-Imaging After Intravenous Infusion in a Rat Lung Injury

Model. *Stem Cells Transl. Med.* (2016). doi:10.5966/sctm.2015-0379

70. Hong, K. U. & Bolli, R. Cardiac stem cell therapy for cardiac repair. *Curr. Treat. Options Cardiovasc. Med.* **16,** 324 (2014).

71. Hou, D. *et al.* Radiolabeled Cell Distribution After Intramyocardial, Intracoronary, and Interstitial Retrograde Coronary Venous Delivery. *Circulation* **112,** (2005).

72. Tang, Y. L. *et al.* Improved Graft Mesenchymal Stem Cell Survival in Ischemic Heart With a Hypoxia-Regulated Heme Oxygenase-1 Vector. *J. Am. Coll. Cardiol.* **46,** 1339–1350 (2005).

73. Laflamme, M. A. *et al.* Formation of human myocardium in the rat heart from human embryonic stem cells. *Am. J. Pathol.* **167,** 663–71 (2005).

74. Reinecke, H., Zhang, M., Bartosek, T. & Murry, C. E. Survival, Integration, and Differentiation of Cardiomyocyte Grafts. *Circulation* **100,** (1999).

75. Toma, C., Pittenger, M. F., Cahill, K. S., Byrne, B. J. & Kessler, P. D. Human Mesenchymal Stem Cells Differentiate to a Cardiomyocyte Phenotype in the Adult Murine Heart. *Circulation* **105,** (2002).

76. Haider, H. K. & Ashraf, M. Strategies to promote donor cell survival: combining preconditioning approach with stem cell transplantation. *J. Mol. Cell. Cardiol.* **45,** 554–66 (2008).

77. Laflamme, M. A. & Murry, C. E. Heart regeneration. *Nature* **473,** 326–35 (2011).

78. Ashraf, M. *et al.* Systems approaches to preventing transplanted cell death in cardiac repair. *J. Mol. Cell. Cardiol.* **45,** 567–581 (2008).

79. Wang, H. *et al.* Injectable biodegradable hydrogels for embryonic stem cell transplantation: improved cardiac remodelling and function of myocardial infarction. *J. Cell. Mol. Med.* **16,** 1310–20 (2012).

80. Xu, Y. *et al.* Cardiac differentiation of cardiosphere-derived cells in scaffolds mimicking morphology of the cardiac extracellular matrix. *Acta Biomater.* **10,** 3449–3462 (2014).

81. Engler, A. J., Sen, S., Sweeney, H. L. & Discher, D. E. Matrix Elasticity Directs Stem Cell Lineage Specification. *Cell* **126,** 677–689 (2006).

82. Lutolf, M. P. *et al.* Synthetic matrix metalloproteinase-sensitive hydrogels for the conduction of tissue regeneration: Engineering cell-invasion characteristics. *Proc. Natl. Acad. Sci.* **100,** 5413–5418 (2003).

83. Hamdi, H. *et al.* Cell delivery: intramyocardial injections or epicardial deposition? A head-to-head comparison. *Ann. Thorac. Surg.* **87,** 1196–203 (2009).

84. Smith, R. R., Marbán, E. & Marbán, L. Enhancing retention and efficacy of cardiosphere-derived cells administered after myocardial infarction using a hyaluronan-gelatin hydrogel. *Biomatter* **3,** (2013).

85. Qian, L. *et al.* Hemodynamic contribution of stem cell scaffolding in acute injured myocardium. *Tissue Eng. Part A* **18,** 1652–63 (2012).

86. Habib, M. *et al.* A combined cell therapy and in-situ tissue-engineering approach for myocardial repair. *Biomaterials* **32,** 7514–7523 (2011).

87. Christman, K. L. *et al.* Injectable fibrin scaffold improves cell transplant survival, reduces infarct expansion, and induces neovasculature formation in ischemic myocardium. *J. Am. Coll. Cardiol.* **44,** 654–60 (2004).

88. Singelyn, J. M. & Christman, K. L. Injectable materials for the treatment of myocardial infarction and heart failure: the promise of decellularized matrices. *J. Cardiovasc. Transl. Res.* **3,** 478–86 (2010).

89. Liu, Z. *et al.* The influence of chitosan hydrogel on stem cell engraftment, survival and homing in the ischemic myocardial microenvironment. *Biomaterials* **33,** 3093–106 (2012).

90. Lu, W.-N. *et al.* Functional improvement of infarcted heart by co-injection of embryonic stem cells with temperature-responsive chitosan hydrogel. *Tissue Eng. Part A* **15,** 1437–47 (2009).

91. Yu, J. *et al.* The use of human mesenchymal stem cells encapsulated in RGD modified alginate microspheres in the repair of myocardial infarction in the rat. *Biomaterials* **31,** 7012–7020 (2010).

92. Wang, T. *et al.* Bone marrow stem cells implantation with α-cyclodextrin/MPEG–PCL–MPEG hydrogel improves cardiac function after myocardial infarction. *Acta Biomater.* **5,** 2939–2944 (2009).

93. Martens, T. P. *et al.* Percutaneous cell delivery into the heart using hydrogels polymerizing in situ. *Cell Transplant.* **18,** 297–304 (2009).

94. Gaffey, A. C. *et al.* Injectable shear-thinning hydrogels used to deliver endothelial progenitor cells, enhance cell engraftment, and improve ischemic myocardium. *J. Thorac. Cardiovasc. Surg.* **19104,** (2015).

95. Liu, Z. *et al.* The influence of chitosan hydrogel on stem cell engraftment, survival and homing in the ischemic myocardial microenvironment. *Biomaterials* **33,** 3093–3106 (2012).

96. O'Brien, F. J. Biomaterials & scaffolds for tissue engineering. *Mater. Today* **14,** 88–95 (2011).

97. Cunniffe, G. M. & O'Brien, F. J. Collagen scaffolds for orthopedic regenerative medicine. *JOM* **63,** 66–73 (2011).

98. Simpson, D., Liu, H., Fan, T.-H. M., Nerem, R. & Dudley, S. C. A tissue engineering approach to progenitor cell delivery results in significant cell engraftment and improved myocardial remodeling. *Stem Cells* **25,** 2350–7 (2007).

99. Simpson, D. L., Boyd, N. L., Kaushal, S., Stice, S. L. & Dudley, S. C. Use of human embryonic stem cell derived-mesenchymal cells for cardiac repair. *Biotechnol. Bioeng.* **109,** 274–283 (2012).

100. Leor, J. *et al.* Bioengineered cardiac grafts: A new approach to repair the infarcted myocardium? *Circulation* **102,** III56-61 (2000).

101. Gao, L. *et al.* Large Cardiac Muscle Patches Engineered From Human Induced-Pluripotent Stem Cell–Derived Cardiac Cells Improve Recovery From Myocardial Infarction in Swine. *Circulation* **137,** 1712–1730 (2018).

102. Roche, E. T. *et al.* Comparison of biomaterial delivery vehicles for improving acute retention of stem cells in the infarcted heart. *Biomaterials* **35,** 6850–8 (2014).

103. Aulton, M. E. & Taylor, K. *Aulton's pharmaceutics : the design and manufacture of medicines.* (Churchill Livingstone/Elsevier, 2013).

104. Li, J. & Mooney, D. J. Designing hydrogels for controlled drug delivery. *Nat. Rev. Mater.* **1,** 16071 (2016).

105. Langer, R. Drug delivery and targeting. *Nature* **392,** 5–10 (1998).

106. Christopher Rolfes, S. H. R. G. and P. A. I. *Current Concepts in General Thoracic Surgery.* (InTech,

2012). doi:10.5772/3070

107.   O'Cearbhaill, E. D., Ng, K. S. & Karp, J. M. Emerging Medical Devices for Minimally Invasive Cell Therapy. *Mayo Clin. Proc.* **89,** 259–273 (2014).

108.   Sheng, C. C., Zhou, L. & Hao, J. Current stem cell delivery methods for myocardial repair. *Biomed Res. Int.* **2013,** 547902 (2013).

109.   Hastings, C. L. *et al.* Drug and cell delivery for cardiac regeneration. *Adv. Drug Deliv. Rev.* **84,** 85–106 (2015).

110.   Khaled, W. *et al.* Clinical results of the cellwave study using novel extracorporeal shock wave application for enhancing the efficacy of cell therapy. in *2012 IEEE International Ultrasonics Symposium* 1–4 (IEEE, 2012). doi:10.1109/ULTSYM.2012.0490

111.   Perin, E. C. & López, J. Methods of stem cell delivery in cardiac diseases. *Nat. Clin. Pract. Cardiovasc. Med.* **3,** S110–S113 (2006).

112.   Dib, N., Khawaja, H., Varner, S., McCarthy, M. & Campbell, A. Cell therapy for cardiovascular disease: a comparison of methods of delivery. *J. Cardiovasc. Transl. Res.* **4,** 177–81 (2011).

113.   CHACHQUES, J. C. *et al.* MRI Evaluation of Local Myocardial Treatments: Epicardial Versus Endocardial (Cell-Fix Catheter) Injections. *J. Interv. Cardiol.* **20,** 188–196 (2007).

114.   Chapman, M. P. *et al.* Application of the HeartLander crawling robot for injection of a thermally sensitive anti-remodeling agent for myocardial infarction therapy. in *2010 Annual International Conference of the IEEE Engineering in Medicine and Biology* **2010,** 5428–5431 (IEEE, 2010).

115.   BioCardia   -   Helix   Biotherapeutic   Delivery.   Available   at: http://www.biocardia.com/product_pipeline/helix.shtml. (Accessed: 26th May 2018)

116.   Haider, H. K., Lei, Y. & Ashraf, M. MyoCell, a cell-based, autologous skeletal myoblast therapy for the treatment of cardiovascular diseases. *Curr. Opin. Mol. Ther.* **10,** 611–21 (2008).

117.   Minguell, J. J., Lorino, R. & Lasala, G. P. Myocardial implantation of a combination stem cell product by using a transendocardial MYOSTAR injection catheter: A technical assessment. *Acute Card. Care* **13,** 40–42 (2011).

118.   Coletta, J. E., Rosenthal, N. & Costa, M. A. Cardiac mapping and stem cell delivery for the damaged myocardium. *Expert Rev. Cardiovasc. Ther.* **6,** 1181–1190 (2008).

119.   *An Essential Guide to Cardiac Cell Therapy - Emerson Perin, James T. Willerson - Google Books.*

120.   Bullfrog®   Micro-Infusion   Device   —   Mercator   MedSystems.   Available   at: http://www.mercatormed.com/bullfrog-micro-infusion-device/. (Accessed: 26th May 2018)

121.   Gray, H. & Clemente, C. D. *Anatomy of the human body.* (Lea & Febiger, 1985).

122.   Ujhelyi, M., Hadsall, K., Euler, D. & Mehra, R. Intrapericardial therapeutics: a pharmacodynamic and pharmacokinetic comparison between pericardial and intravenous procainamide delivery. *J Cardiovasc Electrophsiol* **13,** 605–611 (2002).

123.   Moreno, R., Waxman, S., Rowe, K. & Verrier, R. L. Intrapericardial β-Adrenergic Blockade with Esmolol Exerts a Potent Antitachycardic Effect Without Depressing Contractility. *J. Cardiovasc. Pharmacol.* **36,** 722–727 (2000).

124. Laham, R. J., Hung, D. & Simons, M. Therapeutic myocardial angiogenesis using percutaneous intrapericardial drug delivery. *Clin. Cardiol.* **22,** I6-9 (1999).

125. Baek, S. H. *et al.* Augmentation of intrapericardial nitric oxide level by a prolonged-release nitric oxide donor reduces luminal narrowing after porcine coronary angioplasty. *Circulation* **105,** 2779–2784 (2002).

126. Roche, E. T. *et al.* A light-reflecting balloon catheter for atraumatic tissue defect repair. *Sci. Transl. Med.* **7,** 306ra149 (2015).

127. Li, J. *et al.* Tough adhesives for diverse wet surfaces. *Science* **357,** 378–381 (2017).

128. Lee, L. C. *et al.* Algisyl-LVR^{TM} with coronary artery bypass grafting reduces left ventricular wall stress and improves function in the failing human heart. *Int. J. Cardiol.* **168,** 2022–8 (2013).

129. Mann, D. L. *et al.* One-year follow-up results from AUGMENT-HF: a multicentre randomized controlled clinical trial of the efficacy of left ventricular augmentation with Algisyl in the treatment of heart failure. *Eur. J. Heart Fail.* **18,** 314–325 (2016).

130. Pape, A. C. H. *et al.* An Injectable and Drug-loaded Supramolecular Hydrogel for Local Catheter Injection into the Pig Heart. *J. Vis. Exp.* e52450 (2015). doi:10.3791/52450

131. O'Neill, H. S. *et al.* Biomaterial-Enhanced Cell and Drug Delivery: Lessons Learned in the Cardiac Field and Future Perspectives. *Adv. Mater.* n/a-n/a (2016). doi:10.1002/adma.201505349

132. Hasan, A. *et al.* Injectable Hydrogels for Cardiac Tissue Repair after Myocardial Infarction. *Adv. Sci.* **2,** 1500122 (2015).

133. Singelyn, J. M. *et al.* Catheter-Deliverable Hydrogel Derived From Decellularized Ventricular Extracellular Matrix Increases Endogenous Cardiomyocytes and Preserves Cardiac Function Post-Myocardial Infarction. *J. Am. Coll. Cardiol.* **59,** 751–763 (2012).

134. Kofidis, T. *et al.* Injectable bioartificial myocardial tissue for large-scale intramural cell transfer and functional recovery of injured heart muscle. *J. Thorac. Cardiovasc. Surg.* **128,** 571–578 (2004).

135. Leor, J. *et al.* Intracoronary Injection of In Situ Forming Alginate Hydrogel Reverses Left Ventricular Remodeling After Myocardial Infarction in Swine. *J. Am. Coll. Cardiol.* **54,** 1014–1023 (2009).

136. Bio Leonhardt. Available at: http://www.bioleonhardt.com/.

137. Genovese, J. A., Spadaccio, C., Rivello, H. G., Toyoda, Y. & Patel, A. N. Electrostimulated bone marrow human mesenchymal stem cells produce follistatin. *Cytotherapy* **11,** 448–456 (2009).

138. Spadaccio, C. *et al.* In Situ Electrostimulation Drives a Regenerative Shift in the Zone of Infarcted Myocardium. *Cell Transplant.* **22,** 493–503 (2013).

139. Tan, T., Watts, S. W. & Davis, R. P. Drug Delivery: Enabling Technology for Drug Discovery and Development. iPRECIO® Micro Infusion Pump: Programmable, Refillable, and Implantable. *Front. Pharmacol.* **2,** (2011).

140. Barkai, U., Rotem, A. & de Vos, P. Survival of encapsulated islets: More than a membrane story. *World J. Transplant.* **6,** 69–90 (2016).

141. Brauker, J. H. *et al.* Neovascularization of synthetic membranes directed by membrane microarchitecture. *J. Biomed. Mater. Res.* **29,** 1517–1524 (1995).

142. Neurotech Pharmaceuticals. Available at: http://www.neurotechusa.com/about.html.

143. Kumagai-Braesch, M. *et al.* The TheraCyte™ device protects against islet allograft rejection in immunized hosts. *Cell Transplant.* **22,** 1137–46 (2013).

144. Sernova Corp - Technology. Available at: http://www.sernova.com/technology/. (Accessed: 9th March 2018)

145. A Safety, Tolerability and Efficacy Study of Sernova's Cell Pouch™ for Clinical Islet Transplantation - Full Text View - ClinicalTrials.gov. Available at: https://clinicaltrials.gov/ct2/show/NCT03513939?term=Cell+Pouch&rank=1. (Accessed: 26th May 2018)

146. Beta-O2 Technologies Ltd. Available at: http://beta-o2.com/. (Accessed: 26th May 2018)

147. Shapiro, a. M. J. Islet Transplantation in Type 1 Diabetes: Ongoing Challenges, Refined Procedures, and Long-Term Outcome. *Rev. Diabet. Stud.* **9,** 385–406 (2012).

148. Ludwig, B. *et al.* Favorable outcome of experimental islet xenotransplantation without immunosuppression in a nonhuman primate model of diabetes. *Proc. Natl. Acad. Sci.* **114,** 11745–11750 (2017).

149. Perin, E. C. & Willerson, J. T. CD34+ Autologous Human Stem Cells in Treating Refractory Angina. *Circ. Res.* **109,** (2011).

150. Dixon, J. A. *et al.* Mesenchymal Cell Transplantation and Myocardial Remodeling After Myocardial Infarction. *Circulation* **120,** (2009).

151. Silva, G., Fernandes, M. & Cardoso, C. A dosing study of bone marrow mononuclear cells for transendocardial injection in a pig model of chronic ischemic heart disease. *Texas Hear. Inst.* (2011).

152. Banerjee, S. & Brilakis, E. S. Harnessing the Potential of Human Autologous Stem Cells to Treat Refractory Angina ∗. *JACC Cardiovasc. Interv.* **9,** 1586–1588 (2016).

153. Beohar, N., Rapp, J., Pandya, S. & Losordo, D. W. Rebuilding the damaged heart: the potential of cytokines and growth factors in the treatment of ischemic heart disease. *J. Am. Coll. Cardiol.* **56,** 1287–97 (2010).

154. Henry, T. D. *et al.* The VIVA Trial. *Circulation* **107,** (2003).

155. Zbinden, S., Zbinden, R., Meier, P., Windecker, S. & Seiler, C. Safety and efficacy of subcutaneous-only granulocyte-macrophage colony-stimulating factor for collateral growth promotion in patients with coronary artery disease. *J. Am. Coll. Cardiol.* **46,** 1636–42 (2005).

156. Zohlnhöfer, D. *et al.* Stem Cell Mobilization by Granulocyte Colony-Stimulating Factor for Myocardial Recovery After Acute Myocardial Infarction: A Meta-Analysis. *J. Am. Coll. Cardiol.* **51,** 1429–1437 (2008).

157. Mangi, A. A. *et al.* Mesenchymal stem cells modified with Akt prevent remodeling and restore performance of infarcted hearts. *Nat. Med.* **9,** 1195–201 (2003).

158. Gnecchi, M. *et al.* Evidence supporting paracrine hypothesis for Akt-modified mesenchymal stem cell-mediated cardiac protection and functional improvement. *FASEB J.* **20,** 661–9 (2006).

159. Shi, R.-Z., Wang, J.-C., Huang, S.-H., Wang, X.-J. & Li, Q.-P. Angiotensin II induces vascular

endothelial growth factor synthesis in mesenchymal stem cells. *Exp. Cell Res.* **315,** 10–5 (2009).

160. Kamota, T. *et al.* Ischemic pre-conditioning enhances the mobilization and recruitment of bone marrow stem cells to protect against ischemia/reperfusion injury in the late phase. *J. Am. Coll. Cardiol.* **53,** 1814–22 (2009).

161. Epstein, S. E., Kornowski, R., Fuchs, S. & Dvorak, H. F. Angiogenesis therapy: amidst the hype, the neglected potential for serious side effects. *Circulation* **104,** 115–9 (2001).

162. Carmeliet, P. VEGF as a key mediator of angiogenesis in cancer. *Oncology* **69 Suppl 3,** 4–10 (2005).

163. Henry, T. D. *et al.* Intracoronary administration of recombinant human vascular endothelial growth factor to patients with coronary artery disease. *Am. Heart J.* **142,** 872–80 (2001).

164. Mancini, D. & Colombo, P. C. Left Ventricular Assist Devices. *J. Am. Coll. Cardiol.* **65,** 2542–2555 (2015).

165. Kwon, M. H., Cevasco, M., Schmitto, J. D. & Chen, F. Y. Ventricular restraint therapy for heart failure: A review, summary of state of the art, and future directions. *J. Thorac. Cardiovasc. Surg.* **144,** 771–777.e1 (2012).

166. Lee, L. C., Zhihong, Z., Hinson, A. & Guccione, J. M. Reduction in left ventricular wall stress and improvement in function in failing hearts using Algisyl-LVR. *J. Vis. Exp.* (2013). doi:10.3791/50096

167. LoneStar Heart, Inc. Available at: http://lonestarheartinc.com/. (Accessed: 27th May 2018)

168. Cezar, C. A. *et al.* Biologic-free mechanically induced muscle regeneration. *Proc. Natl. Acad. Sci.* **113,** 1534–1539 (2016).

169. Davis, M. E. *et al.* Local myocardial insulin-like growth factor 1 (IGF-1) delivery with biotinylated peptide nanofibers improves cell therapy for myocardial infarction. *Proc. Natl. Acad. Sci. U. S. A.* **103,** 8155–60 (2006).

170. Takehara, N. *et al.* Controlled Delivery of Basic Fibroblast Growth Factor Promotes Human Cardiosphere-Derived Cell Engraftment to Enhance Cardiac Repair for Chronic Myocardial Infarction. *J. Am. Coll. Cardiol.* **52,** 1858–1865 (2008).

171. Jakovljevic, D. G. *et al.* Left Ventricular Assist Device as a Bridge to Recovery for Patients With Advanced Heart Failure. *J. Am. Coll. Cardiol.* **69,** 1924–1933 (2017).

172. Canseco, D. C. *et al.* Human ventricular unloading induces cardiomyocyte proliferation. *J. Am. Coll. Cardiol.* **65,** 892–900 (2015).

173. Anastasiadis, K. & Antonitsis, P. Cells and pumps: Mechanical support and cellular therapy emerge as a realistic alternative to heart transplantation. *Hippokratia* **16,** 292–3 (2012).

174. Anastasiadis, K. *et al.* Hybrid approach of ventricular assist device and autologous bone marrow stem cells implantation in end-stage ischemic heart failure enhances myocardial reperfusion. *J. Transl. Med.* **9,** 12 (2011).

175. Stem Cell Therapy in Patients With Severe Heart Failure & Undergoing Left Ventricular Assist Device Placement - Full Text View - ClinicalTrials.gov. Available at: https://clinicaltrials.gov/ct2/show/NCT00869024?term=LVAD+stem+cells&rank=2. (Accessed: 23rd October 2015)

176. Bone Marrow-derived Mesenchymal Stem Cells (MSC) Administration in Weaning From Left Ventricular Assist Device - Full Text View - ClinicalTrials.gov. Available at: https://clinicaltrials.gov/ct2/show/study/NCT02460770?term=LVAD+stem+cells&rank=1. (Accessed: 23rd October 2015)

177. Shafy, A. *et al.* Development of cardiac support bioprostheses for ventricular restoration and myocardial regeneration. *Eur. J. Cardiothorac. Surg.* **43,** 1211–9 (2013).

178. Combination Products.

179. Farra, R. & Sheppard, N. First-in-human testing of a wirelessly controlled drug delivery microchip. *Sci. ...* **4,** 1–11 (2012).

180. Collins, S. D., Baffour, R. & Waksman, R. Cell therapy in myocardial infarction. *Cardiovasc. Revasc. Med.* **8,** 43–51 (2007).

181. Tokita, Y. *et al.* Repeated Administrations of Cardiac Progenitor Cells Are Markedly More Effective Than a Single Administration: A New Paradigm in Cell Therapy. *Circ. Res.* **119,** 635–651 (2016).

182. Bolli, R. Repeated cell therapy: a paradigm shift whose time has come. *Circ. Res.* **120,** 1072–1074 (2017).

183. Chen, R. R., Silva, E. A., Yuen, W. W. & Mooney, D. J. Spatio–temporal VEGF and PDGF Delivery Patterns Blood Vessel Formation and Maturation. *Pharm. Res.* **24,** 258–264 (2007).

184. Bolli, R. Repeated Cell Therapy. *Circ. Res.* **120,** 1072–1074 (2017).

185. Malliaras, K. & Marban, E. Cardiac cell therapy: where we've been, where we are, and where we should be headed. *Br. Med. Bull.* 161–185 (2011).

186. Laflamme, M. a, Zbinden, S., Epstein, S. E. & Murry, C. E. Cell-based therapy for myocardial ischemia and infarction: pathophysiological mechanisms. *Annu. Rev. Pathol.* **2,** 307–39 (2007).

187. Gavira, J. J. *et al.* Repeated implantation of skeletal myoblast in a swine model of chronic myocardial infarction. *Eur. Heart J.* **31,** 1013–1021 (2010).

188. Fujita, M. *et al.* Efficacy of photocrosslinkable chitosan hydrogel containing fibroblast growth factor-2 in a rabbit model of chronic myocardial infarction. *J. Surg. Res.* **126,** 27–33 (2005).

189. Jung, D. W. & Williams, D. R. Reawakening atlas: chemical approaches to repair or replace dysfunctional musculature. *ACS Chem Biol* **7,** 1773–1790 (2012).

190. Plowright, A. T., Engkvist, O., Gill, A., Knerr, L. & Wang, Q. D. Heart Regeneration: Opportunities and Challenges for Drug Discovery with Novel Chemical and Therapeutic Methods or Agents. *Angew Chem Int Ed Engl* (2014). doi:10.1002/anie.201307034

191. Segers, V. F. M. & Lee, R. T. Protein Therapeutics for Cardiac Regeneration after Myocardial Infarction. *J. Cardiovasc. Transl. Res.* **3,** 469–477 (2010).

192. Segers, V. F. M. *et al.* Local delivery of protease-resistant stromal cell derived factor-1 for stem cell recruitment after myocardial infarction. *Circulation* **116,** 1683–1692 (2007).

193. Ziegler, M. *et al.* The Bispecific SDF1-GPVI Fusion Protein Preserves Myocardial Function After Transient Ischemia in Mice. *Circulation* **125,** 685-U100 (2012).

194. Urbanek, K. *et al.* Cardiac stem cells possess growth factor-receptor systems that after activation

regenerate the infarcted myocardium, improving ventricular function and long-term survival. *Circ. Res.* **97,** 663–673 (2005).

195. Jabbour, A. *et al.* Parenteral administration of recombinant human neuregulin-1 to patients with stable chronic heart failure produces favourable acute and chronic haemodynamic responses. *Eur. J. Heart Fail.* **13,** 83–92 (2011).

196. Torella, D. *et al.* Cardiac stem cell and myocyte aging, heart failure, and insulin-like growth factor-1 overexpression. *Circ Res* **94,** 514–524 (2004).

197. Hsueh, Y. C., Wu, J. M., Yu, C. K., Wu, K. K. & Hsieh, P. C. Prostaglandin E2 promotes post-infarction cardiomyocyte replenishment by endogenous stem cells. *EMBO Mol Med* **6,** 496–503 (2014).

198. Theiss, H. D. *et al.* Dual stem cell therapy after myocardial infarction acts specifically by enhanced homing via the SDF-1/CXCR4 axis. *Stem Cell Res* **7,** 244–255 (2011).

199. Koshy, S. T., Ferrante, T. C., Lewin, S. a. & Mooney, D. J. Injectable, porous, and cell-responsive gelatin cryogels. *Biomaterials* **35,** 2477–2487 (2014).

200. Clark, J. E., Kottam, A., Motterlini, R. & Marber, M. S. Measuring left ventricular function in the normal, infarcted and CORM-3-preconditioned mouse heart using complex admittance-derived pressure volume loops. *J. Pharmacol. Toxicol. Methods* **59,** 94–99 (2009).

201. Clark, J. E. & Marber, M. S. Advancements in pressure-volume catheter technology - stress remodelling after infarction. *Exp. Physiol.* **98,** 614–21 (2013).

202. Kutty, S. *et al.* Validation of admittance computed left ventricular volumes against real-time three-dimensional echocardiography in the porcine heart. *Exp Physiol* **98,** 1092–1101 (2013).

203. Sato, T. *et al.* ESPVR of in situ rat left ventricle shows contractility-dependent curvilinearity. *Am. J. Physiol.* **274,** H1429-34 (1998).

204. Honma, K. & Ochiya, T. Live-cell luciferase assay of drug resistant cells. *Protoc. Exch.* (2008). doi:10.1038/nprot.2008.169

205. Turner, P. V, Brabb, T., Pekow, C. & Vasbinder, M. A. Administration of substances to laboratory animals: routes of administration and factors to consider. *J. Am. Assoc. Lab. Anim. Sci.* **50,** 600–13 (2011).

206. Yang, G. *et al.* Assessment of the characteristics and biocompatibility of gelatin sponge scaffolds prepared by various crosslinking methods. *Sci. Rep.* **8,** 1616 (2018).

207. van Brakel, T. J. *et al.* Intrapericardial delivery enhances cardiac effects of sotalol and atenolol. *J. Cardiovasc. Pharmacol.* **44,** 50–56 (2004).

208. Hermans, J. J. R. *et al.* Pharmacokinetic advantage of intrapericardially applied substances in the rat. *J. Pharmacol. Exp. Ther.* **301,** 672–678 (2002).

209. Bagnall, A. J. *et al.* Optimal medical therapy for non-ST-segment-elevation acute coronary syndromes: exploring why physicians do not prescribe evidence-based treatment and why patients discontinue medications after discharge. *Circ. Cardiovasc. Qual. Outcomes* **3,** 530–7 (2010).

210. Cutler, D. M. & Everett, W. Thinking Outside the Pillbox- Medication Adherence as a Priority for

Health Care Reform. *N. Engl. J. Med.* **363,** 1–3 (2010).

211. Traverso, G. & Langer, R. Engineering precision. *Sci. Transl. Med.* **7,** 289ed6-289ed6 (2015).

212. O'Sullivan, J. F. *et al.* Potent long-term cardioprotective effects of single low-dose insulin-like growth factor-1 treatment postmyocardial infarction. *Circ. Cardiovasc. Interv.* **4,** 327–35 (2011).

213. Pilla, J. J. *et al.* Early Postinfarction Ventricular Restraint Improves Borderzone Wall Thickening Dynamics During Remodeling. *Ann. Thorac. Surg.* **80,** 2257–2262 (2005).

214. Blom, A. S. *et al.* Ventricular Restraint Prevents Infarct Expansion and Improves Borderzone Function After Myocardial Infarction: A Study Using Magnetic Resonance Imaging, Three-Dimensional Surface Modeling, and Myocardial Tagging. *Ann. Thorac. Surg.* **84,** 2004–2010 (2007).

215. Zhang, S. *et al.* Real-time magnetic resonance imaging of cardiac function and flow-recent progress. *Quant. Imaging Med. Surg.* **4,** 313–29 (2014).

216. Pacher, P. *et al.* Left ventricular pressure-volume relationship in a rat model of advanced aging-associated heart failure. *Am. J. Physiol. Heart Circ. Physiol.* **287,** H2132-7 (2004).

217. Restrepo, C. S., Tavakoli, S. & Marmol-Velez, A. Contrast-Enhanced Cardiac Magnetic Resonance Imaging. *Magn. Reson. Imaging Clin. N. Am.* **20,** 739–760 (2012).

218. Morais, J. M., Papadimitrakopoulos, F. & Burgess, D. J. Biomaterials/tissue interactions: possible solutions to overcome foreign body response. *AAPS J.* **12,** 188–96 (2010).

219. Anderson, J. M. Biological performance of materials-fundamentals of biocompatibility (Vol. 8, Biomedical engineering and instrumentation series), by Jonathan Black, Marcel Dekker, New York, NY, 1981. *J. Biomed. Mater. Res.* **17,** 557–558 (1983).

220. Wang, L.-T. *et al.* Human mesenchymal stem cells (MSCs) for treatment towards immune- and inflammation-mediated diseases: review of current clinical trials. *J. Biomed. Sci.* **23,** 76 (2016).

221. Pacher, P., Nagayama, T., Mukhopadhyay, P., Bátkai, S. & Kass, D. a. Measurement of cardiac function using pressure-volume conductance catheter technique in mice and rats. *Nat. Protoc.* **3,** 1422–34 (2008).

222. Anderson, H. J., Sahoo, J. K., Ulijn, R. V & Dalby, M. J. Mesenchymal Stem Cell Fate: Applying Biomaterials for Control of Stem Cell Behavior. *Front. Bioeng. Biotechnol.* **4,** 38 (2016).

223. Ratner, B. D., Hoffman, A. S., Schoen, F. J. & Lemons, J. E. *Biomaterials Science : an Introduction to Materials in Medicine.* (Elsevier Science, 1997).

224. Naftali-Shani, N. *et al.* Left Ventricular Dysfunction Switches Mesenchymal Stromal Cells Toward an Inflammatory Phenotype and Impairs Their Reparative Properties Via Toll-Like Receptor-4. *Circulation* **135,** 2271–2287 (2017).

225. Bernardo, M. E. & Fibbe, W. E. Mesenchymal Stromal Cells: Sensors and Switchers of Inflammation. *Cell Stem Cell* **13,** 392–402 (2013).

226. Waterman, R. S., Tomchuck, S. L., Henkle, S. L. & Betancourt, A. M. A new mesenchymal stem cell (MSC) paradigm: polarization into a pro-inflammatory MSC1 or an Immunosuppressive MSC2 phenotype. *PLoS One* **5,** e10088 (2010).

227. Zhang, W. *et al.* Necrotic Myocardial Cells Release Damage-Associated Molecular Patterns That

Provoke Fibroblast Activation In Vitro and Trigger Myocardial Inflammation and Fibrosis In Vivo. *J. Am. Heart Assoc.* **4,** e001993–e001993 (2015).

228. Shi, Y. *et al.* How mesenchymal stem cells interact with tissue immune responses. *Trends Immunol.* **33,** 136–43 (2012).

229. Orive, G. *et al.* Engineering a Clinically Translatable Bioartificial Pancreas to Treat Type I Diabetes. *Trends Biotechnol.* **36,** 445–456 (2018).

230. Ge, J. *et al.* The Size of Mesenchymal Stem Cells is a Significant Cause of Vascular Obstructions and Stroke. *Stem Cell Rev. Reports* **10,** 295–303 (2014).

231. Atalay, O. *et al.* A Highly Stretchable Capacitive-Based Strain Sensor Based on Metal Deposition and Laser Rastering. *Adv. Mater. Technol.* **2,** 1700081 (2017).

232. ASTM D1876 - 08(2015)e1 Standard Test Method for Peel Resistance of Adhesives (T-Peel Test). Available at: https://www.astm.org/Standards/D1876. (Accessed: 28th May 2018)

233. Vereshchagina, E., Mc Glade, D., Glynn, M. & Ducrée, J. A hybrid microfluidic platform for cell-based assays via diffusive and convective trans-membrane perfusion. *Biomicrofluidics* **7,** 34101 (2013).

234. Roche, E. T. *et al.* Soft robotic sleeve supports heart function. *Sci. Transl. Med.* **9,** eaaf3925 (2017).

235. Shamim, N., Koh, Y. P., Simon, S. L. & McKenna, G. B. Glass transition temperature of thin polycarbonate films measured by flash differential scanning calorimetry. *J. Polym. Sci. Part B Polym. Phys.* **52,** 1462–1468 (2014).

236. Boedeker Plastics : Polycarbonate Datasheet. Available at: http://www.boedeker.com/polyc_p.htm. (Accessed: 29th May 2018)

237. EtO Sterilization for Medical Devices - ISO 11135 | Sterilization Validation Services. Available at: https://lso-inc.com/sterilization-validation-services/iso11135-eto-sterilization.html. (Accessed: 18th May 2018)

238. How to stop a post-dialysis site bleeding | EMBlog Mayo Clinic. Available at: https://emblog.mayo.edu/2015/04/27/how-to-stop-a-post-dialysis-site-bleeding/. (Accessed: 29th May 2018)

239. SURGIFLO® Hemostatic Matrix Kit | Ethicon. Available at: https://www.ethicon.com/na/products/adjunctive-hemostasis/absorbable-hemostats/surgiflo-hemostatic-matrix-kit. (Accessed: 29th May 2018)

240. Roche, E. T. *et al.* Comparison of biomaterial delivery vehicles for improving acute retention of stem cells in the infarcted heart. *Biomaterials* **35,** 6850–8 (2014).

241. Hernández, A., Calvo, J. I., Prádanos, P. & Tejerina, F. Pore size distributions in microporous membranes. A critical analysis of the bubble point extended method. *J. Memb. Sci.* **112,** 1–12 (1996).

242. Whatman Cyclopore PC Polycarbonate Membrane Filters - GE Healthcare Life Sciences. Available at: https://www.gelifesciences.com/en/af/shop/laboratory-filtration/membranes-and-associated-lab-equipment/track-etched-membranes/whatman-cyclopore-pc-polycarbonate-membrane-filters-p-06309?current=7060-1304. (Accessed: 19th May 2018)

243. Neufeld, T. *et al.* The Efficacy of an Immunoisolating Membrane System for Islet Xenotransplantation in Minipigs. *PLoS One* **8,** e70150 (2013).

244. Sun, J.-Y. *et al.* Highly stretchable and tough hydrogels. *Nature* **489,** 133–6 (2012).

245. Orive, G. *et al.* Cell encapsulation: promise and progress. *Nat. Med.* **9,** 104–7 (2003).

246. Roche, E. T. *et al.* The promise of biomaterial delivery vehicles for improving stem cell retention in the infarcted heart. in *Cardiovascular Research Foundation 9th International Conference on Cell Therapy and Cardiovascular Disease* (2014).

247. Edge, A. S. B., Gosse, M. E. & Dinsmore, J. Xenogeneic cell therapy: current progress and future developments in porcine cell transplantation. *Cell Transplant.* **7,** 525–539 (1998).

248. Gnecchi, M., Zhang, Z., Ni, A. & Dzau, V. J. Paracrine mechanisms in adult stem cell signaling and therapy. *Circ. Res.* **103,** 1204–19 (2008).

249. Tannous, B. Gaussia luciferase reporter assay for monitoring of biological processes in culture and in vivo Bakhos. *Nat. Protoc.* **4,** 582–591 (2009).

250. Saraswati, S. *et al.* Pyrvinium, a potent small molecule Wnt inhibitor, promotes wound repair and post-MI cardiac remodeling. *PLoS One* **5,** e15521 (2010).

251. Waxman, S., Moreno, R., Rowe, K. A. & Verrier, R. L. Persistent primary coronary dilation induced by transatrial delivery of nitroglycerin into the pericardial space: A novel approach for local cardiac drug delivery. *J. Am. Coll. Cardiol.* **33,** 2073–2077 (1999).

252. Clifford, D. M. *et al.* Stem cell treatment for acute myocardial infarction. *Cochrane database Syst. Rev.* CD006536 (2012). doi:10.1002/14651858.CD006536.pub3

253. Kinnaird, T. *et al.* Marrow-derived stromal cells express genes encoding a broad spectrum of arteriogenic cytokines and promote in vitro and in vivo arteriogenesis through paracrine mechanisms. *Circ. Res.* **94,** 678–85 (2004).

254. Wang, X., Zachman, A. L., Haglund, N. A., Maltais, S. & Sung, H. J. Combined usage of stem cells in end-stage heart failure therapies. *J. Cell. Biochem.* **115,** 1217–1224 (2014).

255. Guo, Y. *et al.* Repeated doses of cardiac mesenchymal cells are therapeutically superior to a single dose in mice with old myocardial infarction. *Basic Res. Cardiol.* **112,** 18 (2017).

256. Yang, S. Y. *et al.* A bio-inspired swellable microneedle adhesive for mechanical interlocking with tissue. *Nat. Commun.* **4,** 1702 (2013).

257. Hatzistergos, K. E. *et al.* Bone Marrow Mesenchymal Stem Cells Stimulate Cardiac Stem Cell Proliferation and Differentiation. *Circ. Res.* **107,** 913–922 (2010).

258. Zhang, Z. *et al.* Selective inhibition of inositol hexakisphosphate kinases (IP6Ks) enhances mesenchymal stem cell engraftment and improves therapeutic efficacy for myocardial infarction. *Basic Res. Cardiol.* **109,** 417 (2014).

259. Mathieu, E. *et al.* Intramyocardial Delivery of Mesenchymal Stem Cell-Seeded Hydrogel Preserves Cardiac Function and Attenuates Ventricular Remodeling after Myocardial Infarction. *PLoS One* **7,** e51991 (2012).

260. Klinker, M. W. & Wei, C.-H. Mesenchymal stem cells in the treatment of inflammatory and

autoimmune diseases in experimental animal models. *World J. Stem Cells* **7,** 556–67 (2015).

261. Home - ClinicalTrials.gov. Available at: https://clinicaltrials.gov/. (Accessed: 7th March 2018)

262. http://jdrf.org/press-releases/sernova-corp-announces-collaboration-with-massachusetts-general-hospital-to-develop-novel-diabetes-treatment-with-funding-support-from-jdrf/. Available at: http://jdrf.org/press-releases/sernova-corp-announces-collaboration-with-massachusetts-general-hospital-to-develop-novel-diabetes-treatment-with-funding-support-from-jdrf/. (Accessed: 16th October 2015)

263. Killu, A. M. *et al.* Trends in percutaneous pericardial access during catheter ablation of ventricular arrhythmias: a single-center experience. *J. Interv. Card. Electrophysiol.* **47,** 109–115 (2016).

264. Maisch, B., Ristić, A. D., Pankuweit, S. & Seferovic, P. Percutaneous Therapy in Pericardial Diseases. *Cardiol. Clin.* **35,** 567–588 (2017).

265. Cannata, A. *et al.* Postsurgical intrapericardial adhesions: Mechanisms of formation and prevention. *Ann. Thorac. Surg.* **95,** 1818–1826 (2013).

266. Melfi, F. M. A., Menconi, G. F., Chella, A. & Angeletti, C. A. The management of malignant pericardial effusions using permanently implanted devices. *Eur. J. Cardiothorac. Surg.* **21,** 345–7 (2002).

267. Imazio, M. *et al.* DRainage Or Pericardiocentesis alone for recurrent nonmalignant, nonbacterial pericardial effusions requiring intervention. *J. Cardiovasc. Med.* **15,** 510–514 (2014).

268. Chaudhry, P. A. *et al.* Passive epicardial containment prevents ventricular remodeling in heart failure. *Ann. Thorac. Surg.* **70,** 1275–80 (2000).

269. Bauer, M., Cheng, S., Unno, K., Lin, F. C. & Liao, R. Regional Cardiac Dysfunction and Dyssynchrony in a Murine Model of Afterload Stress. *PLoS One* **8,** 6–11 (2013).

270. Hoare, T. R. & Kohane, D. S. Hydrogels in drug delivery: Progress and challenges. *Polymer (Guildf).* **49,** 1993–2007 (2008).

271. Huebsch, N. *et al.* Ultrasound-triggered disruption and self-healing of reversibly cross-linked hydrogels for drug delivery and enhanced chemotherapy. *Proc. Natl. Acad. Sci.* **111,** 9762–9767 (2014).

272. Qin, J. *et al.* Injectable Superparamagnetic Ferrogels for Controlled Release of Hydrophobic Drugs. *Adv. Mater.* **21,** 1354–1357 (2009).

273. Cezar, C. A. *et al.* Biphasic Ferrogels for Triggered Drug and Cell Delivery. *Adv. Healthc. Mater.* **3,** 1869–1876 (2014).

274. Zhao, X. *et al.* Active scaffolds for on-demand drug and cell delivery. *Proc. Natl. Acad. Sci. U. S. A.* **108,** 67–72 (2011).

275. Kearney, C. J. & Mooney, D. J. Macroscale delivery systems for molecular and cellular payloads. *Nat. Mater.* **12,** 1004–1017 (2013).

276. Brudno, Y. & Mooney, D. J. On-demand drug delivery from local depots. *J. Control. Release* **219,** 8–17 (2015).

277. Microchips Biotech. Available at: http://microchipsbiotech.com/news-pub.php. (Accessed: 15th May

2018)

278. Jr, J. T. S., Cima, M. J. & Langer, R. A controlled-release microchip. 335–338 (1999).

279. Richards Grayson, A. C. *et al.* Multi-pulse drug delivery from a resorbable polymeric microchip device. *Nat. Mater.* **2,** 767–772 (2003).

280. Prescott, J. H. *et al.* Chronic, programmed polypeptide delivery from an implanted, multireservoir microchip device. *Nat. Biotechnol.* **24,** 437–438 (2006).

281. Farra, R. *et al.* First-in-human testing of a wirelessly controlled drug delivery microchip. *Sci. Transl. Med.* **4,** 122ra21 (2012).

282. Naficy, S., Kawakami, S., Sadegholvaad, S., Wakisaka, M. & Spinks, G. M. Mechanical properties of interpenetrating polymer network hydrogels based on hybrid ionically and covalently crosslinked networks. *J. Appl. Polym. Sci.* **130,** 2504–2513 (2013).

283. Darnell, M. C. *et al.* Performance and biocompatibility of extremely tough alginate/polyacrylamide hydrogels. *Biomaterials* **34,** 8042–8 (2013).

284. Cai, S., Hu, Y., Zhao, X. & Suo, Z. Poroelasticity of a covalently crosslinked alginate hydrogel under compression. *J. Appl. Phys.* **108,** 113514 (2010).

285. Young, M. E., Carroad, P. A. & Bell, R. L. Estimation of diffusion coefficients of proteins. *Biotechnol. Bioeng.* **22,** 947–955 (1980).

286. Dextran.

287. Boontheekul, T., Kong, H.-J. & Mooney, D. J. Controlling alginate gel degradation utilizing partial oxidation and bimodal molecular weight distribution. *Biomaterials* **26,** 2455–2465 (2005).

288. Lee, K. Y. & Mooney, D. J. Alginate: properties and biomedical applications. *Prog. Polym. Sci.* **37,** 106–126 (2012).

289. Tamargo, J., Le Heuzey, J.-Y. & Mabo, P. Narrow therapeutic index drugs: a clinical pharmacological consideration to flecainide. *Eur. J. Clin. Pharmacol.* **71,** 549–67 (2015).

290. Exon, J. H. A Review of the Toxicology of Acrylamide. *J. Toxicol. Environ. Heal. Part B* **9,** 397–412 (2006).

291. Kearney, C. J. *et al.* Switchable Release of Entrapped Nanoparticles from Alginate Hydrogels. *Adv. Healthc. Mater.* **4,** 1634–1639 (2015).

292. Anderson, J. M., Niven, H., Pelagalli, J., Olanoff, L. S. & Jones, R. D. The role of the fibrous capsule in the function of implanted drug-polymer sustained release systems. *J. Biomed. Mater. Res.* **15,** 889–902 (1981).

293. Kleeff, J. *et al.* Pancreatic cancer. *Nat. Rev. Dis. Prim.* **2,** 16022 (2016).

294. Eltorai, A. E. M., Fox, H., McGurrin, E. & Guang, S. Microchips in Medicine: Current and Future Applications. *Biomed Res. Int.* **2016,** 1743472 (2016).

295. Rus, D. & Tolley, M. T. Design, fabrication and control of soft robots. *Nature* **521,** 467–475 (2015).

296. Maloney, J. M. *et al.* Electrothermally activated microchips for implantable drug delivery and biosensing. *J. Control. Release* **109,** 244–55 (2005).

297. Nguyen, N.-T., Shaegh, S. A. M., Kashaninejad, N. & Phan, D.-T. Design, fabrication and

characterization of drug delivery systems based on lab-on-a-chip technology. *Adv. Drug Deliv. Rev.* **65,** 1403–19 (2013).

298.   Staples, M., Daniel, K., Cima, M. J. & Langer, R. Application of micro- and nano-electromechanical devices to drug delivery. *Pharm. Res.* **23,** 847–63 (2006).

299.   Lee, K. Y., Peters, M. C., Anderson, K. W. & Mooney, D. J. Controlled growth factor release from synthetic extracellular matrices. *Nature* **408,** 998–1000 (2000).

300.   Silva, E. A. & Mooney, D. J. Effects of VEGF temporal and spatial presentation on angiogenesis. *Biomaterials* **31,** 1235–41 (2010).

301.   Moran, A. E. *et al.* Assessing the Global Burden of Ischemic Heart Disease: Part 1: Methods for a Systematic Review of the Global Epidemiology of Ischemic Heart Disease in 1990 and 2010. *Glob. Heart* **7,** 315–329 (2012).

302.   Suhr, F. *et al.* Cell biological effects of mechanical stimulations generated by focused extracorporeal shock wave applications on cultured human bone marrow stromal cells. *Stem Cell Res.* **11,** 951–964 (2013).

303.   Dixon, J. A. & Spinale, F. G. Large animal models of heart failure: a critical link in the translation of basic science to clinical practice. *Circ. Heart Fail.* **2,** 262–71 (2009).

304.   Sahoo, S. & Losordo, D. W. Exosomes and cardiac repair after myocardial infarction. *Circ. Res.* **114,** 333–44 (2014).

305.   ALZET® - iPRECIO® Programmable Infusion Pump. Available at: http://www.alzet.com/products/iprecio/index.html. (Accessed: 23rd May 2018)